High-order Simple-input Methods for Thick Laminated Composite Straight and Curved Tubes

Hamidreza Yazdani Sarvestani

A Thesis
In the Department
of
Mechanical and Industrial Engineering

Presented in Partial Fulfillment of the Requirements
For the Degree of Doctor of Philosophy (Mechanical Engineering) at
Concordia University
Montreal, Quebec, Canada

September 2016

CONCORDIA UNIVERSITY

SCHOOL OF GRADUATE STUDIES

This is to certify that the thesis prepared

By: **Hamidreza Yazdani Sarvestani**

Entitled: **High-order Simple-input Methods for Thick Laminated Composite Straight and Curved Tubes**

and submitted in partial fulfillment of the requirements for the degree of

Doctor of Philosophy (Mechanical Engineering)

Complies with the regulations of the University and meets the accepted standards with respect to originality and quality.

Signed by final examining committee:

_____ Chair

Dr. Nizar Bouguila

_____ External Examiner

Dr. Larry Lessard

_____ External to Program

Dr. Khaled E. Galal

_____ Examiner

Dr. Martin Pugh

_____ Examiner

Dr. Ramin Sedaghati

_____ Thesis Supervisor

Dr. Mehdi Hojjati

Approved by

_____

Chair of Department or Graduate Program Director

_____ 2016

_____

Dean of Faculty

Abstract

High-order Simple-input Methods for Thick Laminated Composite Straight and Curved Tubes

Hamidreza Yazdani Sarvestani, Ph.D.

Concordia University, 2016

Composites have proven their great potential for many aerospace applications, where high performance justifies high cost. One of the potential applications of composites is helicopter landing gears. Helicopter landing gears consist of straight and curved tubes. A new analysis and design tool is required to consider the manufacturing technology. In this study, high-order analytical methods are proposed to analyze and design thick laminated orthotropic straight and curved tubes subjected to different boundary and loading conditions.

In the first part of this thesis, the elasticity displacement field of thick laminated composite straight tubes is developed. In this investigation, thick composite cantilever tubes under transverse loading are studied using the newly displacement-based method. This method provides a quick, convenient and accurate procedure for the determination of 3D stresses in thick composite straight tubes subjected to both bending and shear loadings. In addition, this method is used to study stress and strain distributions in thick composite straight tubes with different simple and complex lay-up sequences. Note that thick laminated composite straight tubes subjected to cantilever loading conditions are investigated for the first time. Moreover, the developed method is used to analyze thick laminated composite straight tubes subjected to different mechanical loadings such as axial force, torque and bending moment.

In the second part of this thesis, the general displacement field of thick laminated composite curved tubes is developed. By proposing a new high-order displacement-based method, single-layer composite curved tubes are examined. First, a displacement approach of Toroidal Elasticity is chosen to obtain the displacement field of single-layer composite curved tubes. Then, a layer-wise method is employed to develop the most general displacement field

of elasticity for thick arbitrary laminated composite curved tubes. The developed method is used to analyze single-layer and laminated composite curved tubes subjected to pure bending moment. Note that displacement-based Toroidal Elasticity is applied to study thick laminated composite curved tubes for the first time. In addition, the failure analysis on thick composite curved tubes subjected to pure bending moment is conducted. Effects of lay-up sequences of composite curved tubes on stress distributions and failure sequences are investigated, as well.

The accuracy of the proposed methods is verified by comparing the numerical results obtained using the proposed methods against finite element method, experimental data and solutions available in the literature.

The methods that proposed in this thesis do not require meshing. They simplify greatly inputs that the user has to do, once the program for solution is available. This presents a clear advantage over FEM. Therefore, the most important advantage of the proposed methods is that inputs for modeling and analyzing of composite straight and curved tubes with complex lay-up sequences are simple, easy to use and fast to run. In addition, using FEM for the parametric study is cumbersome. By applying the proposed methods, the parametric study for thick laminated composite straight and curved tubes is simple with low computational cost.

Acknowledgements

First of all, I would like to thank my supervisor Prof. Mehdi Hojjati for his unconditional support throughout the period of my studies in Concordia University. He opened many doors for research and scientific aspiration for me and for that, I am forever grateful. Secondly, Prof. Suong V. Hoa that helped me with my research, discussed ideas and gave me directions with this thesis.

I would like to thank all of the administrative staff of Mechanical and Industrial Engineering Department. My special thanks are extended to my current and former lab-mates in Concordia center for Composites for their help and support.

My special thanks to all of my family and friends who always supported and encouraged me.

Dedicated to my parents

Fatemeh & Keramat

Table of Contents

List of Figures

List of Tables

Chapter 1

Introduction, Motivation, Research goals, Methodology and Thesis organization

1.1. Introduction

Composites are one of the most widely used materials in the aerospace industry because of their adaptability to different situations and the relative ease of combination with other materials to serve specific purposes and exhibit desirable properties. This is due to their high strength-to-weight ratio and stiffness-to-weight ratio. However, the stress analysis of a composite structure is often a complex task. Three reasons are mentioned for such a complexity. First of all, the governing equations for composite structures are much more complicated than those of the structures made of isotropic materials. Second, as the material and structure are made at the same time, thus many more parameters are involved. As such, parameters involved in fabrication can play a significant role in the physical and mechanical properties of the material and, as a result, the behavior of the structure. Finally, a major source of intricacy is the layer-wise failure of composite materials. In fact, as soon as a layer fails, a sort of delamination occurs or a crack propagates in plies, and material properties and sometimes governing equations could be different. This readily adds a lot of complexity to the analysis of composite structures. Having mentioned all of the complexities, still analytical and numerical methods are the only reliable sources for a preliminary design. They are well employed to calculate the required dimensions of sections, lay-up sequences and to predict the behavior of the structure at least in the elastic limit.

Composite straight and curved tubes are structures that are frequently used by aerospace, offshore and infrastructure industries. One such structure is a helicopter landing gear. Prediction of the state of stresses and strains in different layers of laminated composite straight and curved tubes within helicopter landing gears are of theoretical interest and practical importance.

1.2. Motivation

Currently, most helicopter landing gears are made of high-grade aluminum alloys and despite their major problems in maintenance and fabrication, as well as failure weakness due to the corrosion, aluminum landing gears have remained the only option for helicopter manufacturing industries. In an effort to develop thermoplastic composite tubes for helicopter landing gears [1], Derisi manufactured composite straight tubes and performed several mechanical tests to determine strains to failure of different balanced laminates. These tubes are relatively thick. Derisi used a procedure called strain-controlled design and based on that, lay-up sequences for composite tubes were developed. This procedure paid particular attention to the strain limit in each of the layers, in order to provide maximum flexibility for the tube, while maintaining good stiffness and strength. However, rigorous analytical methods for the determination of stresses, strains and deformations are not available. Subsequently, there is a need to develop high-order simple-input methods for the stress and failure analyses of thick laminated composite straight and curved tubes subjected to different mechanical loadings.

1.3. Research Goals

Analysis and design of composite helicopter landing gears are challenges. Analytical, numerical and experimental methods may be used in the design and analysis of composite helicopter landing gears. Even though experimental works have been done on developing landing gears, an analytical method does not exist to analyze thick composite straight and curved tubes which are main parts of helicopter landing gears. Concerning the analytical works, most studies on the stress analysis of composite tubes are limited to straight tubes with symmetric loading conditions while, in contrary, landing gears are made of straight and

curved tubes subjected to non-symmetric loadings. In addition, most of the techniques for the stress analysis of curved tubes have been developed for isotropic materials. Concerning the numerical works, one can use finite element method (FEM) to analyze tubes subjected to different types of loadings. However, for structures such as tubes where the geometry is not that complex, the use of FEM is unnecessarily cumbersome. Each time one changes some parameters such as the number of layers, lay-up sequences, length and radius of tube cross section, one has to re-mesh and this is cumbersome.

The main objectives of this thesis are divided in three main categories in the following:

1. Developing a new high-order simple-input method to investigate stress and strain distributions in thick laminated composite straight tubes subjected to mechanical loading conditions. A method, which does not require meshing, simplifies inputs that the user has to do.
2. Developing a new simple-input method to investigate stress and strain distributions in thick laminated composite curved tubes subjected to mechanical loading conditions.
3. The new high-order methods are proposed in order to gain an in-depth and comprehensive understanding of the stress and failure analyses of thick laminated composite straight and curved tubes. Due to the complexity of stress and strain distributions in thick composite tubes, it is not easy to obtain some intuition as to the behavior of the tube under different loading conditions, for the purpose of design. In order to provide some insight into this behavior, the developed methods are used for the parametric study.

1.4. Methodology

The main objective of this study is to develop new analysis and design tools to consider the manufacturing technology (design for manufacturing). The first step in theoretical study is analyzing of a lamina of composite straight and curved tubes. The second step is stress analyzing of laminated composite straight and curved tubes. Next, the analysis will be done to compare the theoretical results with those obtained from tests. Therefore, the work is performed through following steps:

Step 1: The first step in the structural design is to understand the nature of the loads and the working condition. While the loads are known, the designer would be able to select proper materials for the structure; considering other design parameters such as weight, cost, manufacturing and maintenance.

Step 2: The second step of this research is to select a proper composite material, which could properly be employed in the design and manufacturing of helicopter landing gears. Accordingly, Carbon AS4/PEKK was selected as the material to be used in manufacturing [1].

Step 3: The third step is the stress and failure analyses of the structure and finding out the appropriate cross sections and lay-up sequences while the material is known. The analytical methods for stress and failure analyses of composite straight and curved tubes subjected to different boundary and loading conditions are developed and the advantages of the proposed methods are highlighted.

1.5. Thesis Organization

This thesis has nine chapters which are briefly described as following:

Chapter 1 provides a brief introduction to composite materials and their applications such as helicopter landing gears. The motivation, research goals and methodology of this thesis are also presented in this chapter.

Chapter 2 includes a comprehensive literature review on different methods used to investigate the behavior of composite straight and curved tubes under different types of boundary conditions and mechanical loadings.

Chapter 3[1] starts with developing a new high-order simple-input method to obtain stresses and strains in thick arbitrary laminated composite straight tubes. The most general displacement field of elasticity for a thick laminated composite straight tube is developed. A layer-wise method is employed to analytically determine local displacement functions and

[1] Chapter 3 is published as: H. Yazdani Sarvestani, S.V. Hoa, and M. Hojjati, "Stress analysis of thick orthotropic cantilever tubes under transverse loading," *Advanced Composite Materials,* 2016:1-28.

stresses under transverse loading. The accuracy of the proposed method is verified by comparing the theoretical results with experimental data, FEM and Lekhnitskii solution.

In Chapter 4[2], by using the new simple-input displacement-based method developed in the previous chapter, the behavior of stress distributions in thick laminated composite straight tubes with different lay-up sequences considering effects of the shear load part of the cantilever loading condition is studied. Knowledge is extracted from the parametric study showing effects of the orientations of different layers on stresses.

In Chapter 5[3], the developed analytical method is used to study thick laminated composite straight tubes subjected to combined axial force, torque and bending moment. The accuracy of the proposed method is subsequently verified by comparing the numerical results obtained using the proposed method with finite element method (FEM) and experimental data. The proposed method provides advantages in terms of computational time compared to FEM.

Chapter 6[4] proposes a new method to investigate single-layer composite curved tubes subjected to pure bending moment by employing a displacement approach of Toroidal Elasticity. The governing equations are developed in three toroidal coordinates system. The method of successive approximation is used to find the general solution. The accuracy of the proposed method is assessed by comparing the numerical results obtained using the present method with FEM, stress-based Toroidal Elasticity and Lekhnitskii solution.

In Chapter 7[5], the displacement field of single-layer composite curved tubes obtained in the previous chapter is used to develop the most general displacement field of elasticity for

[2] Chapter 4 is published as: H. Yazdani Sarvestani, S.V. Hoa, and M. Hojjati, "Effects of shear loading on stress distributions at sections in thick composite tubes," *Composite Structures*, 2016;140:433-445.

[3] Chapter 5 is published as: H. Yazdani Sarvestani, and M. Hojjati, "A high-order analytical method for thick composite tubes," *Steel & Composite Structures*, 2016;21(4):755-773.

[4] Chapter 6 is published as: H. Yazdani Sarvestani, S.V. Hoa, and M. Hojjati, "Three-dimensional stress analysis of orthotropic curved tubes-part 1: single-layer solution," *European Journal of Mechanics - A/Solids*, 2016.

[5] Chapter 7 is published as: H. Yazdani Sarvestani, and M. Hojjati, "Three-dimensional stress analysis of orthotropic curved tubes-part 2: laminate solution," *European Journal of Mechanics - A/Solids*, 2016.

thick arbitrary laminated composite curved tubes. The principle of minimum total potential energy is applied to calculate stresses in thick composite curved tubes under pure bending moment. The accuracy of the proposed method is evaluated by comparing the numerical results obtained from the developed method against FEM, experimental data and a solution available in the literature.

Chapter 8[6] presents failure analysis on thick laminated composite curved tubes subjected to pure bending moment. By employing results of the proposed method, the progressive failure analysis is performed using Tsai-Wu criterion. Effects of lay-up sequences of thick composite curved tubes on stress distributions and failure sequences are investigated.

Chapter 9 summarizes the conclusions and contributions of this study and presents a list of recommendations for future works.

[6] Chapter 8 will be shortly published as: H. Yazdani Sarvestani, and M. Hojjati, "Failure analysis of thick composite curved tubes," *Composite Structures*, 2016.

Chapter 2

Literature review

2.1. Helicopter Landing Gears

The conventional Bell helicopter landing gears consist of two parallel curved cross tubes, which are connected by two longitudinal skid tubes (*see Figure 2.1*). Cross tubes of helicopter landing gears consist of straight tubes at the middle and curved tubes at the sides. In the present chapter, the works which have been performed by researchers to study stress and strain behavior of composite tubes are reviewed in two main following categories including composite straight and curved tubes.

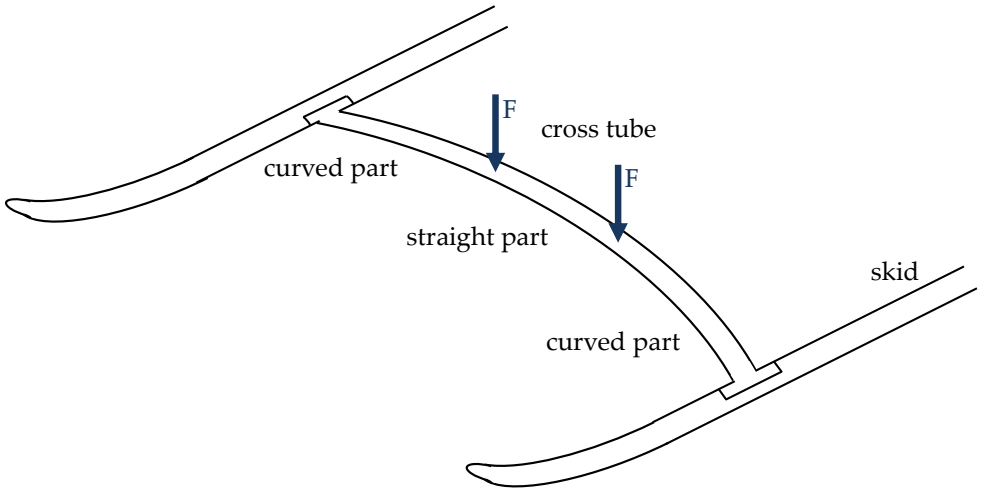

Figure 2.1: Helicopter landing gear.

2.2. Composite Straight Tubes

Composites have many applications due to the properties, which they provide with the essential advantages over other materials. In many examples, composite materials are the

correct answer if designed, manufactured and used properly. Composites have specific advantages in many areas when their properties are designed into the ultimate product. One type of composite structures is a straight tube that is frequently used in many engineering applications. Although thin tubes have been the thrust of the initial applications, more attention is now being paid to thick tubes. In addition, stress analysis of thick composite tubes is often a complex task. A few reasons are responsible for such a complexity. The governing equations of composite tubes are complicated. In addition, a major source of intricacy is the layer-wise failure of composite materials. In fact, as soon as a layer fails, a sort of delamination occurs or a crack propagates in the plies, material properties and sometimes the governing equations could be different. Above all, tube geometries are a lot more complicated than flat geometries. Therefore, it is necessary to review different methods, which have been used to analyze a thick composite straight tube to find out gaps in developing a simple method to investigate complex phenomena in such a structure. The following two sections are a literature review of composite straight tube analyses based on whether methods are analytical or numerical.

2.2.1. Analytical Methods

Lekhnitskii [2] was one of the first researchers who developed elasticity solutions for monolithic homogeneous orthotropic cylindrical shells subjected to different mechanical loadings including cantilever loading conditions. By using stress functions, Lekhnitskii assumed out-of-plane stress components equal to zero. Vibration behavior of circular cylindrical shells were analyzed by Sheinman and Weissman [3] to study effects of the extension-shear elastic couplings. Kollár and Springer [4] studied the stress analysis of composite cylinders and cylindrical segments subjected to hygrothermal and mechanical loads. The case of uniform external pressure and orthotropic homogeneous material was developed by Kardomateas [5]. Miki and Sugiyama [6] proposed a method to optimum designs for required in-plane stiffness, maximum bending stiffness, buckling strength and natural frequency of laminated plates by using lamination parameters as fundamental design variables. The three-dimensional stress and displacement analyses of transversely loaded of composite hollow cylinders with cross-ply laminates were investigated [7]. To obtain a prediction of structural response, a third-order shell theory was proposed by Huang [8] based

on Reddy's parabolic shear strain distribution. Jolicoeur and Cardou [9] developed a general analytical solution for stresses and displacements of a composite cylinder subjected to bending, tensile and torsion loads. Di and Rothert [10] calculated stress fields of orthotropic cylindrical shells using a higher-order shear deformation theory. Their formulations were derived to present displacement and transverse shear stresses for bending of a thin cross-ply composite straight tube with the simply-supported boundary condition at one end. Basar and Ding [11] investigated the theoretical fundamentals based on a layer-wise theory. Their solutions included transverse shear and transverse normal strains. Based on the three-dimensional theory of elasticity, Kardomateas [12] developed benchmark solutions for the buckling problem of orthotropic cylindrical shells. He assumed that the shell was under external pressure or axial compression. Brank and Carrera [13] investigated multilayered composite plates and shells based on a piece-wise linear variation of the displacement field through-thickness using a shell theory. The analysis of a three-layered cross-ply laminated square plate and shell panel with simply supported boundary conditions was performed. The method was presented for a case of a square plate loaded by bi-sinusoidal transverse pressure and buckling of a cylindrical panel under a point load. By extending solutions for monolithic structures, closed form elasticity solutions for sandwich shells under external and/or internal pressure were developed [14]. Khare et al. [15] analyzed thermo-mechanical behavior of simply supported cross-ply laminated composite and sandwich cylindrical shell panels. By using three-dimensional (3D) elasticity, shell theory and ABAQUS; the buckling of a sandwich cylindrical shell under uniform external hydrostatic pressure was analyzed by Han et al. [16]. IJsselmuiden et al. [17] used Tsai-Wu failure criterion into the lamination parameter design space in the most general setting to derive a conservative failure envelope that guarantees a failure-free region of the lamination parameter space. Silvestre [18] developed a formulation to study shear and material coupling effects on the linear structural behavior of composite straight cylinders and tubes. Bending modes and deformed configurations of the cross section for thin composite tubes under different boundary conditions were investigated. His formulation was presented only for the variation of thin tube cross sections along the length; not for stress distributions of thick composite tubes within layers. A multi-step framework for a design of composite panels was presented by using a guide-based genetic algorithm to avoid lay-up sequence mismatch [19]. Derisi et al. [20, 21]

proposed lay-up sequences to manufacture thick composite straight tubes that exhibit large deformation. Three-point and four-point bending tests were performed to assess results obtained from experimental data with those obtained from a finite element method. A composite tube that shows the same strength and stiffness as a high-grade aluminum tube for helicopter landing gear applications was designed, fabricated and tested (*see Figure 2.2*). They showed that aluminum straight tubes for helicopter landing gears are replaced by the lighter manufactured composite straight tubes. Note that the investigation was only conducted on straight tubes. In addition, they did not investigate stress distributions of the whole composite landing gear to modify the presented lay-up sequence.

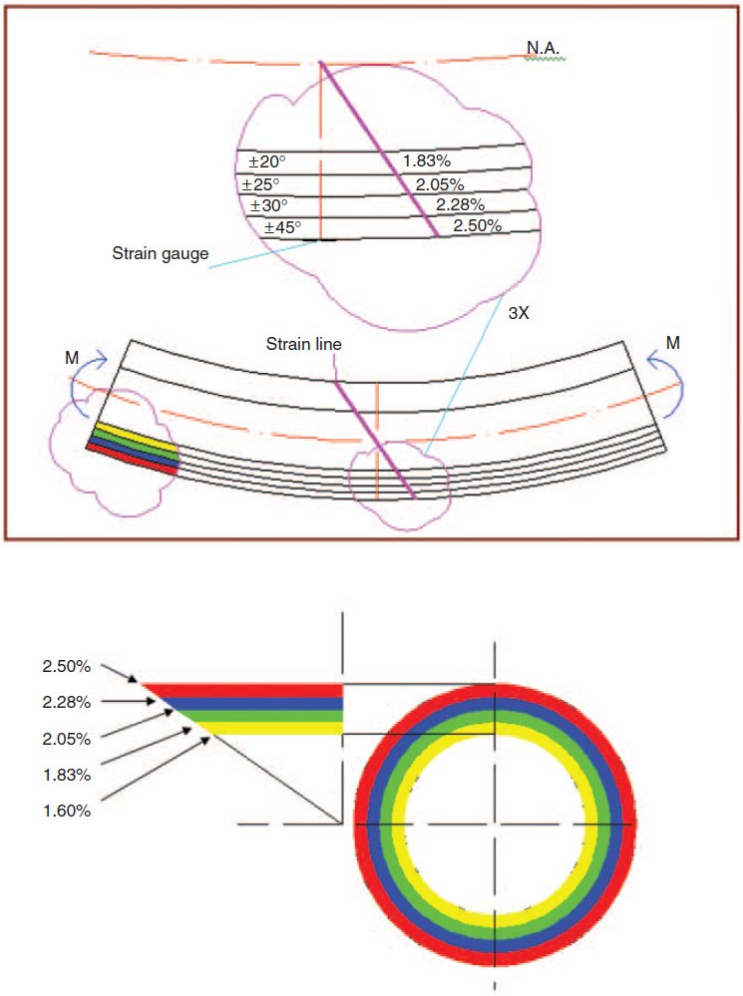

Figure 2.2: Axial strain distribution across thickness of a composite tube under bending [20].

Shadmehri et al. [22] developed theoretical formulations by using a three-dimensional laminate theory to obtain the stiffness of composite tubes. They compared theoretical formulations and experimental results. In addition, the mechanical behavior of straight tubes subjected to bending was examined in their work. To find out the energy absorption capabilities of glass-fiber straight tubes, a study was performed by Pickett and Dayal [23]. Effects of the tube geometry, ply orientations, number of plies and tube thickness on the specific energy absorption in composite tubes were studied and compared with results obtained by experiments. Recently, a method was developed to investigate pure bending of laminated composite straight tubes. Stress distributions for thin composite tubes with simple lay-up sequences were presented. In addition, a formula to calculate the flexural stiffness for composite straight tubes was derived. They used NASTRAN to evaluate theoretical results [24] (*see Figure 2.3*).

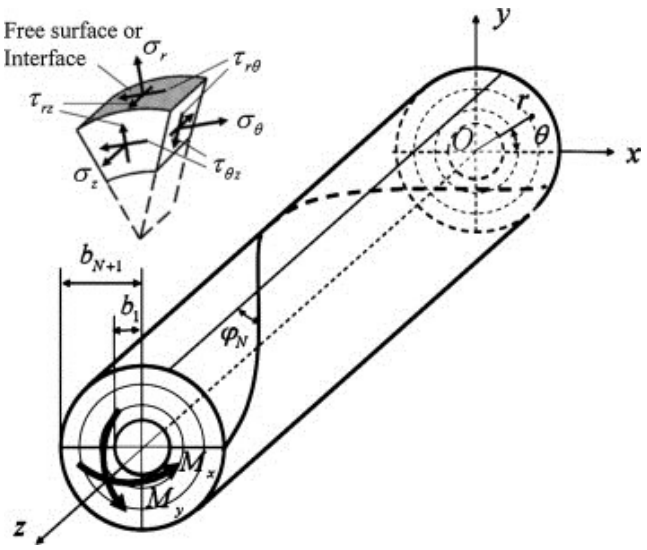

Figure 2.3: Pure bending of a composite tube [24].

The stress analysis of composite hollow straight tubes subjected to pressure, axial force, torsion, shear and bending was performed by Sun et al. [25]. The stress analysis follows Lekhnitskii formulation, which was based on stress functions. They provided solutions for a homogenized tube and a composite tube with a single-layer. Consequently, their method was efficient for thin hollow composite tubes. The results obtained from the proposed method were compared with those obtained from FEM. Menshykova and Guz [26] performed the

stress analysis on thick laminated composite tubes subjected to bending loads. They found stresses as a function of the material properties, thickness, lay-up sequence and the magnitude of the bending load (*see Figure 2.4*). Capela et al. [27] investigated the fatigue behavior of composite tubes under bending/torsion dynamic loadings. Effects of the torsion stress on the fatigue strength and failure mechanisms were shown. The static analysis of carbon nanotube-reinforced composite cylinders under thermo-mechanical was studied [28]. Radial and circumferential stress distributions were presented and influences of ply orientations and volume fraction of carbon nanotubes on stress distributions were analyzed.

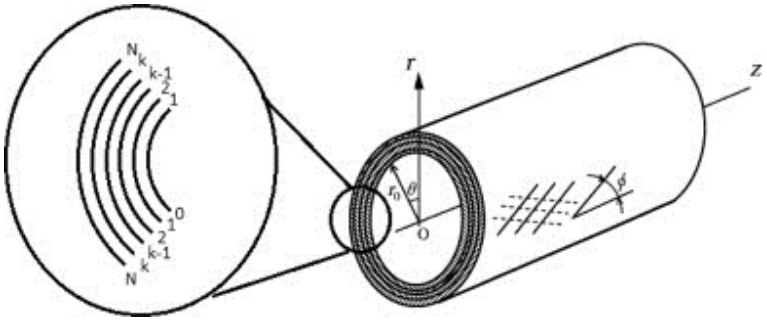

Figure 2.4: Multi-layered filament-wound pipe in cylindrical coordinates [19].

Nowak and Schmidt [29] presented a model to study fiber metal laminated cylinders under an axisymmetric load. A developed theoretical model was validated by FEM results. Jonnalagadda et al. [30] investigated bend-twist coupling effects on composite tubes by proposing an analytical model for thin straight tubes subjected to combined bending and torsion loading conditions. In addition, a formula was developed to obtain the shear center distance (*see Figure 2.5*). They found out that the shear center distance was independent of the radius of the tube cross section but proportional to the tube length. They verified the theoretical results with FEM analysis.

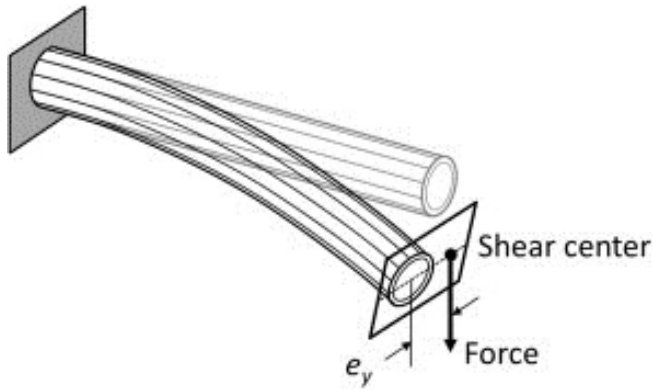

Figure 2.5: A composite tube with shear center away from the tube axis [30].

2.2.2. Numerical Methods

Mackerle [31] reported a recent comprehensive review of finite element formulations for tubes. Hinrichsen and Palazotto [32] investigated a nonlinear thick composite shell element to impose a cubic spline function on the thickness deformation. Hamdallah and Engblom [33] analyzed moderately thick laminated composite shells by using plate-type element formulations. Hossain [34] studied the stress of anisotropic moderately thick composite doubly curved shells and shell panels using a finite element model. The first-order shear deformation shell theory was employed to propose the finite element model. In addition, a simply supported composite spherical shell panel subjected to uniformly distributed and sinusoidal transverse loads was investigated. Kress et al. [35] proposed a finite element model, which diminishes the number of free parameters for each layer, to determine interlaminar stress distributions in laminated singly curved structures. By using the third-order shear deformation theory of Reddy with a meshless numerical method, the deformation of composite plates and shells was analyzed [36]. Salahifar and Mohareb [37] presented a finite element model based on a thin shell theory to study circular cylinders under harmonic forces. Based on the proposed method using shape functions, an element was designed to capture warping, ovalization and radial extensibility. By using the Taylor series of expansion, a limit-based approach was presented to study stresses of composite tubes under bending moments [38]. Their solution is only limited to provide solutions for the cases where the layers are oriented at 0° or 90° with respect to the cylinder axis. Bai et al. [39] investigated the mechanical behavior of moderately thick thermoplastic tubes under combined bending and tension based on the nonlinear ring theory using the principle of virtual work. Only axial,

hoop and shear stresses were considered to study buckling responses. They verified formulations with FEM results obtained using ABAQUS.

Even though many analytical and numerical works have been performed for analyzing composite straight tubes subjected to different types of mechanical loadings, no work has been found to investigate stress distributions of thick laminated composite straight tubes under cantilever loading conditions. In addition, above review shows that there is a need to propose a simple analytical method to develop design guidelines for lay-up sequences of cantilever thick composite straight tubes. Although finite element methods are used, it is necessary to do the meshing for each structure every time some dimensions and/or lay-up sequences are changed. Therefore, it is desired to have a method where inputs to obtain the solution are simple. In order to develop the desired method to study the mechanical behavior of thick composite straight tubes, layer-wise theory is employed in this research.

2.2.3. Layer-wise Theory

Several displacement-based methods have been developed to study behavior of laminated composite structures. In general, these methods may be divided into two groups: the equivalent single-layer theories (ESL) and layer-wise theories, which are based on variation of the displacement field through thickness. For some applications, ESL theories provide a sufficiently accurate behavior of the global laminate response (e.g. deflection, vibration frequency and buckling load); however, ESL theories are mostly insufficient to determine 3D stress and strain fields at the ply level. This weakness is perceptible in relatively thick laminated composite structures such as thick laminated tubes (*see Figure 2.6*). However, layer-wise theory (LWT) allows each layer of the laminate to act like a real three-dimensional layer being able to present accurate results for the local quantities such as interlaminar stresses [40]. Briefly, different methods are reviewed in the following to get a better idea of advantages of layer-wise methods in comparison with other methods.

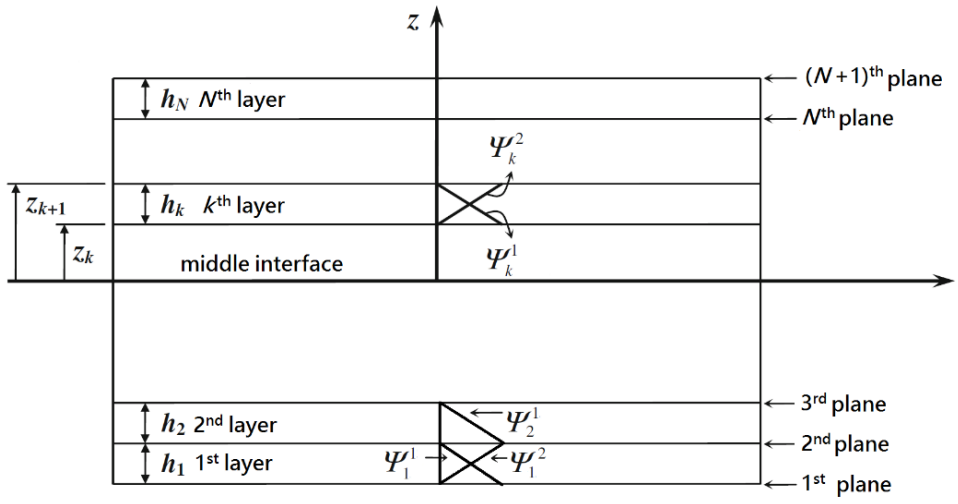

(a)

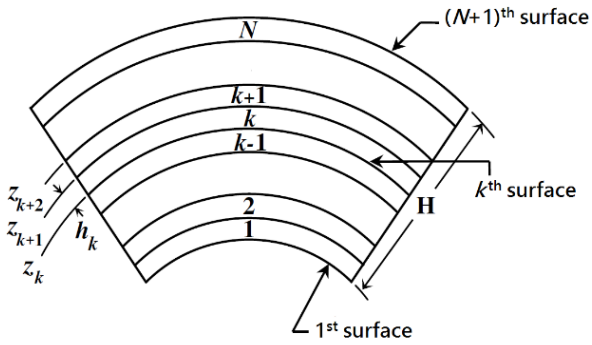

(b)

Figure 2.6: **(a)** Local Lagrangian linear interpolation functions, **(b)** a lay-up in a laminated composite tube.

Basic characteristics of interlaminar stresses in a double-layered circular cylindrical shell with simply supported ends and under a uniform pressure were investigated by Li et al. [41]. Then, Hinrichsen and Palazotto [32] developed a nonlinear thick composite shell element to impose a cubic spline function on the thickness deformation. Out-of-plane thermo-mechanical stresses were investigated in [42] for a simply supported cross-ply cylindrical shell with different ending boundary conditions. Fraternali and Reddy [43] used a penalty-based numerical procedure to cover the stretching of the transverse normal in a spherical shell. Huang [8] presented a third-order shell theory based on Reddy's parabolic shear strain distributions to get a better prediction of structural responses. Similarly, the stress field was calculated in orthotropic cylindrical shells [10], where an effective piece-wise linear function was utilized (*see Figure 2.7*).

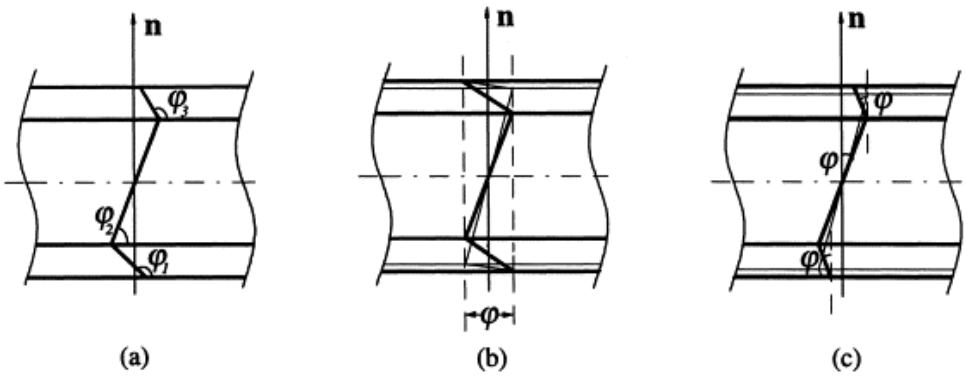

Figure 2.7: Piece-wise linear through-thickness functions [10].

A post-process method based on a higher-order theory was used in order to estimate interlaminar stresses in a simply supported cylindrical shell [44]. Superimposing a cubic global displacement field on a zig-zag linearly varying field, a higher-order shell theory was presented in [45] for cylindrical bending of simply supported laminated composite shells. Rao and Ganesan [46] used three-dimensional models to study interlaminar stresses in clamped cross-ply spherical shells. Accuracy of layer reduction techniques on the analysis of interlaminar shear stresses in laminated cylindrical shells was assessed through a combination of the typical single-layer and multiple-layer shell theories [47]. Wu and Chi [48] performed three-dimensional analyses for laminated composite doubly curved shells subjected to transverse loads by using separation of variables and a state-space approach. Brank and Carrera [49] developed a refined shell theory based on a zig-zag variation of displacement field through-thickness to analyze multilayered composite shells. Through-thickness distributions of transverse normal stresses were added to the formulation of the first and higher-order shear deformable shell elements in [50]. A global-local higher-order model was also proposed in [51] to determine through-thickness stress distributions in laminated shells under cylindrical bending. Roque and Ferreira [36] studied the deformation of plates and shells using the third-order shear deformation theory. Reddy's layer-wise theory was employed to study stresses of composite plates subjected to different types of mechanical loadings by using the elasticity displacement field for long laminates [52-54].

2.3. Composite Curved Tubes

Composite curved tubes are structures that are frequently used in the aerospace, offshore and infrastructure industries. These structures usually are thin or thick and are subjected to certain load conditions such as tension, torsion, shear and bending loads. One such application is the helicopter landing gear. Prediction of the state of stress and strain in different layers of composite curved tubes is of theoretical interest and practical importance. Note that the analysis of a curved tube structure is a lot more complicated than a straight tube structure. Analytical and/or numerical methods have been used to study mechanical behavior of curved tubes by many researchers. At the following section, different methods used to study curved structures are reviewed to find an appropriate method for our purpose.

2.3.1. Analytical and Numerical Methods

Qatu [55] analyzed thin and moderately thick laminated composite curved beams to find natural frequencies. The theoretical modelling of laminated composite shells of arbitrary shapes was developed to estimate shear stresses and avoid shear correction factors [56]. Zhang et al. [57] presented an analytical method to obtain interlaminar stresses at curved boundaries of symmetric composite shells under in-plane loadings based on the zeroth order approximation of a boundary-layer theory. Khare et al. [15] analyzed thermo-mechanical behavior of simply supported cross-ply laminated composite and sandwich doubly curved cylindrical and spherical shell panels. Kress et al. [35] proposed a finite element model, which diminished the number of free parameters for each layer, to determine interlaminar stress distributions in laminated singly curved structures. Shearing and radial stresses in curved beams were derived based on satisfying both equilibrium equations and static boundary conditions on the surfaces of beams [58]. Dryden [59] obtained stress distributions across a functionally graded circular beam subjected to pure bending by using stress functions. Oktem and Chaudhuri [60] used a higher-order shear deformation theory to obtain an analytical solution for the deformation of a finite-dimensional cross-ply doubly-curved panel (*see Figure 2.8*).

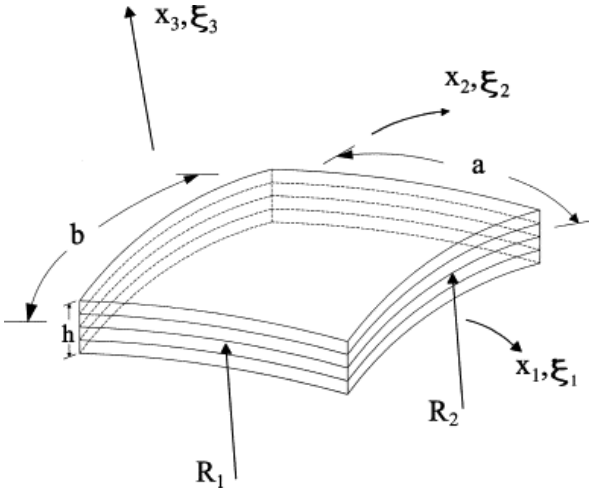

Figure 2.8: Geometry of a laminated doubly-curved panel [60].

Interlaminar normal stress distributions in moderately thick singly curved laminates were obtained to predict critical delamination loads observed in experiments [61]. Unidirectional and cross-ply laminated specimens were designed and tested under tensile and compressive loads to compare with results. Interlaminar shear stresses were considered in equilibrium equations to improve their model. They found out that the interlaminar normal stress leads specimens to delaminate in tensile load conditions and the interlaminar shear stress made specimens to fail in compression conditions. In the other work by the same authors in [62], moderately thick doubly curved laminates were investigated based on the through-the-thickness equilibrium equations for arbitrary shells. Interlaminar normal stresses obtained by their method were verified with finite element model results for simple lay-up sequences [62]. The free vibration analysis was performed on functionally graded beams with curved axis by using a finite element method to discretize the motion equations [63]. The first-order shear deformation theory was used to study static and free vibration behavior of laminated curved beams. The exact solution for simply supported boundary conditions was presented. Shear deformation, curvature complexity and material couplings, which affect the analysis of thick composite curved beams, were investigated in [64]. Analytical models were proposed using Timoshenko beam model to study the stress response of functionally graded curved bars under pure bending conditions in elastic states and plane stress assumptions [65]. Wang and Liu [66] presented elasticity solutions for curved beams with functionally graded layers subjected to a uniform load on the outer surface using Airy stress function method. A

mathematical model was developed to analyze behavior of laminated curved beams [67]. Coupled partial differential governing equations were developed in polar coordinates by applying variational and energy principles to model behavior of the structure. Experiment and finite element data were utilized to verify the theoretical model [67]. Arefi [68] proposed an analytical solution for a functionally graded curved beam subjected to pure bending. Arefi employed the linear theory of elasticity to obtain the general relation for distributions of radial and circumferential stresses. Flexural behavior of functionally graded doubly curved shell panels were studied numerically under thermal and/or mechanical loads using a higher-order shear deformation theory [69]. Their analysis was included the linear and non-linear terms in the mathematical model to obtain the exact flexure of the structure. The variational principle was used to derive governing equations of the panel structure.

The above review shows that most of researchers have worked on inhomogeneous curved bars which have rectangular cross sections (*see Figure 2.9*). Therefore, there is a need to develop a method that can provide the displacement field and subsequently stresses for thick laminated composite curved tubes subjected to different types of mechanical loadings based on simple inputs. Since displacement and stress fields are required to be obtained through the desired method, displacement-based of Toroidal Elasticity is utilized for this propose.

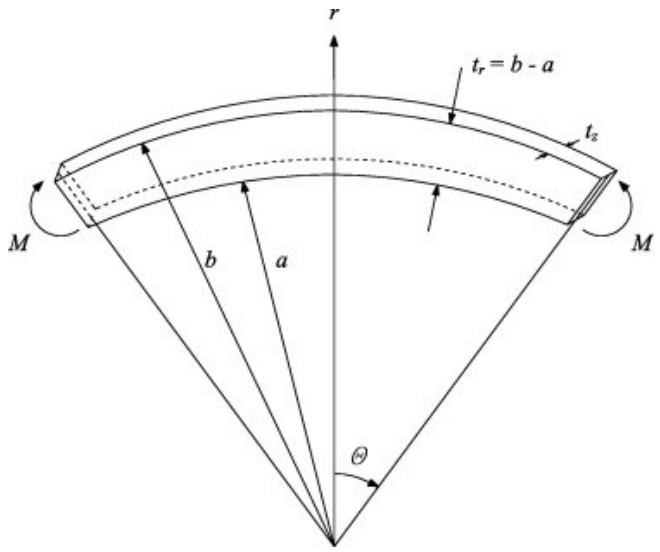

Figure 2.9: The geometry of the curved bar under pure bending [65].

2.3.2. Theory of Toroidal Elasticity

Theory of Toroidal Elasticity (TE) is employed to determine stress and displacement fields in toroidal rings, elbows and tubes where are used in different applications in industries. Gohner [70] was the first researcher to develop TE theory to study an isotropic curved solid circular ring sector under pure twist and bending moments. Figure 2.10 presents the coordinate system used in Gohner works to obtain the solution. The progress made by Gohner on TE was only on axisymmetric cases. In addition, the coordinate system used in Gohner works only is applied for the boundary conditions of a solid circular cross-section.

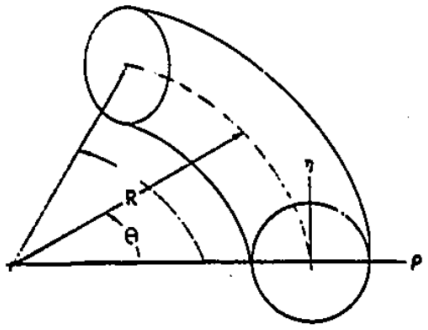

Figure 2.10: Gohner coordinate system [11].

In 1911, Von Karman [71] developed a theoretical description to explain why a curved tube has more flexibility in bending than a straight one. His works provided the fundamentals for the further isotropic curved tube analysis. In general, Toroidal Elasticity is divided in two major methods. Some researchers have been using stress-based TE to describe mechanical behavior of isotropic curved tubes and other researchers have been using displacement-based TE.

2.3.2.1. Stress-based Toroidal Elasticity (SBTE)

The stress-based Toroidal Elasticity (SBTE) is used to obtain the stress field in a thick curved tube. A constant thickness curved tube is represented by Toroidal coordinate system r, Φ and θ where r and Φ are polar coordinates in the plane of the curved tube cross section and θ defines the position of the curved tube cross section as shown in Figure 2.11. Kornecki [72] and McGill [73] developed the theory of Toroidal Elasticity by extending Gohner works.

Kornecki [72] used the method of successive approximation to solve governing equations. The finite difference method was employed by McGill [73]. Both of the studies were based on the assumption of axisymmetric condition.

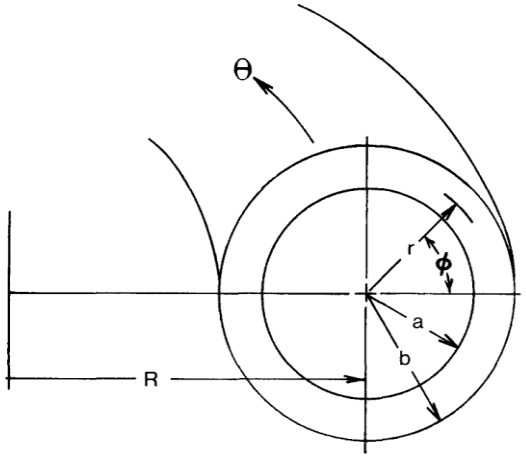

Figure 2.11: Geometry and coordinate system [85].

The method of successive approximation or perturbation method is a useful and powerful method to obtain solutions to equations. The solution for each component of the displacement is assumed to be a series in terms of a small parameter.

A significant contribution to the theory of Toroidal Elasticity was made by Lang [74]. The stress-based Toroidal Elasticity (SBTE) was studied comprehensively by Lang since 1984 [74]. He summarized previous research works [75-84] and developed the stress-based Toroidal Elasticity in the Toroidal coordinate system. He recast the three equilibrium equations and six compatibility equations into the Toroidal coordinate system. The method of successive approximation was used to develop solutions. This theory is employed to solve either axisymmetric problems or non-axisymmetric problems. In Lang's works, the stress approach method was used, subsequently, he did not obtain displacement fields directly.

Lang [75-84] performed comprehensive studies on thick isotropic curved tubes under different types of loadings. The problem of an isotropic curved tube subjected to internal and external pressure was studied by Lang [75, 76]. The zeroth, first and second order fields of stress series were developed. He obtained one set of numerical results for a thick isotropic curved tube under internal pressure. Lang [77] obtained stresses for an isotropic toroidal tube subjected to end bending moments, as well. The stress-based Toroidal Elasticity was

employed so that the solution satisfied compatibility equations. The solution was developed up to the first-order state using the method of successive approximation. The solution was extended to the second order in [78]. A thick 90° curved tube subjected to torsion [84], out-of-plane bending by end shear forces [83], in-plane end shear forces [79] and end normal forces [80] were subsequently investigated. For these four load conditions, the zeroth and first order stress fields were developed, and no numerical results were presented. The solution of the torsion problem was developed up to the third order using successive approximation method.

2.3.2.2. Displacement-based Toroidal Elasticity (DBTE)

Displacement-based Toroidal Elasticity (DBTE) is employed to develop the displacement field within a thick curved tube. This method has the advantage of yielding immediately the displacements as well as the stresses as compared with SBTE. Moreover, the zeroth order displacement functions required for starting the method of successive approximation are easily set up based on the general mechanical knowledge. Note that the displacement components are important information for considering special restriction and for a fracture analysis.

The works of Lang have been extended by Redekop [85]. Redekop selected the displacement components u_r, u_Φ and u_θ as the basic variables (*see Figure 2.12*) and developed the governing Navier equations in this coordinate system. Solutions were found by the method of successive approximation.

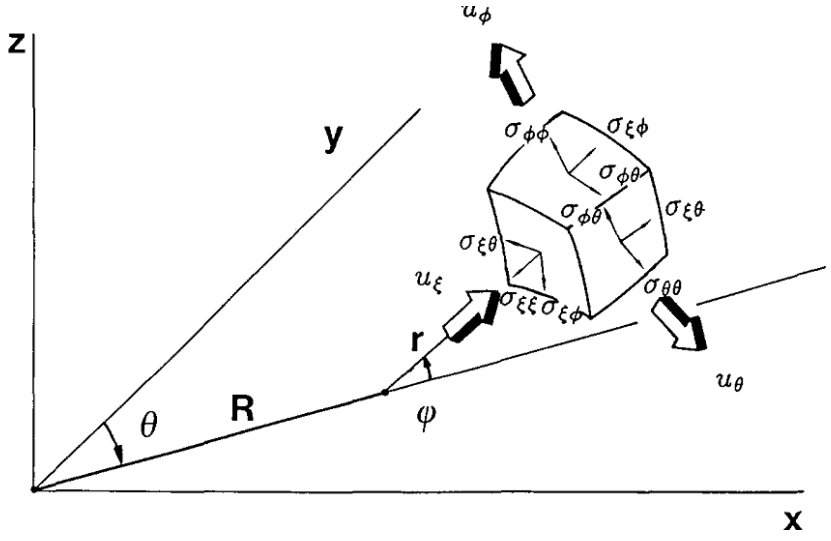

Figure 2.12: Displacement and stress components [85].

Redekop [85] investigated isotropic curved tubes under in-plane loading by the displacement-based Toroidal Elasticity. Numerical solutions for thick curved tubes subjected to internal pressure loads were given as well. The stress and displacement fields were given up to the third order. The numerical solutions obtained for this case were verified with finite element results. Redekop and Zhu [86] provided a computer program based on displacement-based Toroidal Elasticity to obtain stresses for a thick isotropic curved tube spanning a curved segment of 90° subjected to five different loading conditions including internal pressure, in-plane couple bending, out-of-plane couple bending, torsion and out-of-plane shear force. A displacement-based solution for an isotropic curved tube under out-of-plane loading condition was presented by Zhu and Redekop [87] using DBTE. The method of successive approximation was used again to obtain the solution. They provided the governing Navier equations up to the third order in toroidal coordinates system. An analytical solution was proposed using displacement-based Toroidal Elasticity theory to obtain the displacement components and stress field of the band loading of a thick isotropic curved tube as shown in Figure 2.13 [88]. Results obtained using the analytical solution were compared with results obtained from the finite element method.

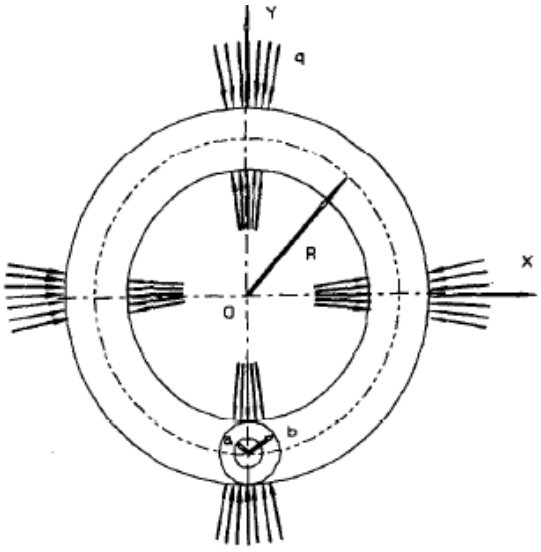

Figure 2.13: Geometry and loading [88].

For the first time, the theory of displacement-based Toroidal Elasticity has been adapted in this study to investigate the behavior of thick laminated orthotropic curved tubes subjected

to mechanical loadings; as opposed to isotropic materials as have been investigated by the other researchers reviewed in this chapter.

Chapter 3

This chapter starts with developing a new high-order simple-input method to obtain stresses and strains in thick arbitrary laminated composite straight tubes. The most general displacement field of elasticity for a thick laminated composite straight tube is developed. A layer-wise method is employed to analytically determine local displacement functions and stresses under transverse loading. The accuracy of the proposed method is verified by comparing the theoretical results with experimental data, FEM and Lekhnitskii solution.

Stress Analysis of Thick Orthotropic Cantilever Tubes under Transverse Loading

Hamidreza Yazdani Sarvestani, Suong V. Hoa and Mehdi Hojjati

Department of Mechanical and Industrial Engineering, Concordia University, Montreal, Quebec H3G 1M8, Canada

Abstract

In this chapter, a new high-order displacement-based method is proposed to investigate stresses and strains in thick arbitrary laminated orthotropic cantilever straight tubes under transverse loading. The most general displacement field of elasticity for an arbitrary thick laminated orthotropic straight tube is developed. A layer-wise method is employed to analytically determine the local displacement functions and stresses under transverse loading. The accuracy of the proposed method is subsequently verified by comparing the theoretical results with experimental data, finite element method (FEM) and Lekhnitskii solution. The results show good agreement. In addition, high efficiency in terms of computational time is shown when the proposed method is used as compared with FEM. Finally, several numerical examples for stress and strain distributions in various thick cantilever straight tubes subjected to transverse loading are discussed.

Keywords: Displacement field; Thick orthotropic cantilever straight tube; Displacement-based method; Layer-wise theory; Stress analysis; Transverse loading.

3.1. Introduction

Composite tubes are structures that are frequently used in the aerospace, offshore and infrastructure industries. Prediction of the state of stress and strain in different layers of composite tubes is of theoretical interest and practical importance. Although thin shell structures have been the thrust of the initial applications, more attention is now being paid to

thick tube structures. In all applications, accurate design and inclusive analysis are important to guarantee safety. It should be noted that stress analysis of cylindrical composite structures is often a complex task. A few reasons are responsible for such a complexity. The governing equations of composite tubes are complicated. In addition, a major source of intricacy is the layer-wise failure of composite materials. In fact, as soon as a layer fails, a sort of delamination happens or a crack propagates in the plies, material properties and sometimes the governing equations could be different. Above all, the composite tube geometry is a lot more complicated than flat geometries.

Mackerle [31] reported a recent comprehensive review of finite element formulations for tubes. Hinrichsen and Palazotto [32] investigated a nonlinear thick composite shell element to impose a cubic spline function on the thickness deformation. Hamdallah and Engblom [33] analyzed moderately thick laminated composite shell structures by using plate-type element formulation. Kardomateas [5] developed the case of uniform external pressure and orthotropic homogeneous material. Elasticity solutions for other types of loading of homogeneous composite shells were summarized in [12]. Lekhnitskii [2] developed elasticity solutions for monolithic homogeneous orthotropic cylindrical shells. To obtain a prediction of structural response, a third-order shell theory was proposed by Huang [8] based on Reddy's parabolic shear strain distribution. In a similar way, Di and Rothert [10] calculated stress fields in orthotropic cylindrical shells. Basar and Ding [11] investigated the theoretical fundamentals based on a layerwise theory. Their solutions included transverse shear and transverse normal strains. By properly extending the solutions for monolithic structures, elasticity solutions for sandwich shells were developed [14]. Sheinman and Weissman [3] studied the effect of the extension-shear elastic couplings to analyze vibration behavior of circular cylindrical shells. Silvestre [18] developed a formulation of Generalized Beam Theory (GBT) to study the non-classical effects on the structural behavior of fiber reinforced polymer composite circular hollow members. To find out the energy absorption characteristics of glass-fiber circular crush tubes, a study was developed by Pickett and Dayal [23]. Brank and Carrera [13] investigated some aspects of refined analysis for multilayered composite plates and shells based on a piece-wise linear variation of the displacement field through-thickness. Khare et al. [15] analyzed thermo-mechanical behavior of simply supported cross-ply composite and laminated sandwich doubly curved cylindrical and spherical shell panels. Hossain [34]

investigated the stress of anisotropic doubly curved thick composite shells and shell panels using a finite element model. Kress et al. [35] proposed a finite element model, which diminishes the number of free parameters for each layer, to determine interlaminar stress distribution in singly curved laminated structures. Roque and Ferreira [36] studied the deformation of plates and shells by using third-order shear deformation theory of Reddy. In addition, to obtain the shape parameters an optimization technique was applied. By using three dimensional (3D) elasticity, shell theory and ABAQUS, the buckling of a sandwich cylindrical shell under uniform external hydrostatic pressure was analyzed by Han et al. [16] in three ways. Salahifar and Mohareb [37] presented a finite element model based on thin shell theory to study the circular cylinders under general harmonic forces. Recently, a method was developed to analyze the pure bending of arbitrary laminated composite tubes. They used NASTRAN to compare with theoretical results [24].

The above review shows that little work has been done to address the analysis for stresses and strains in thick composite cantilever straight tubes under transverse loading. Although finite element methods are used for analyzing such structures, it is necessary to do the meshing for each structure every time some dimensions are changed. Therefore, it is desired to have a method where inputs for the solution are simple; i.e. one only needs to enter in the actual dimensions and lay-up sequences without the meshing work. The present chapter is devoted to develop an analytical high-order method that can provide stresses, strains and deformations for thick laminated composite straight tubes subjected to cantilever loading with simple inputs. The layer-wise method, which includes the full three-dimensional constitutive relations, is employed to calculate the three-dimensional stress distributions within the aforementioned tube. Then, comparison is made between results obtained for the proposed analytical method with experimental data, FEM (ANSYS) and Lekhnitskii solution. Good agreement is obtained. Finally, the stress and strain distributions in tube cross sections are studied through a number of examples. In addition, the stresses and strains are investigated at different cross sections and for different applied force values.

3.2. Motivation

In an effort to develop thermoplastic composite tubes for helicopter landing gears [1], Derisi designed and manufactured composite straight tubes and performed three-point bending tests to determine the strains to failure of different balanced laminates. These tubes are relatively thick (more than 100 layers giving thickness of more than 11 mm). Derisi used a procedure called strain-controlled design and based on that, lay-up sequences for composite tubes were developed. This procedure paid particular attention to the strain limit in each of the layer, in order to provide maximum flexibility for the tube, while maintaining good stiffness and strength. However, rigorous analytical techniques for the determination of stresses, strains and deformations are not available. In this study, a simple-input method for the stress analysis of thick composite tubes subjected to cantilever loading is developed.

3.3. Formulation

3.3.1. *Strain-Displacement Relations*

A thick laminated orthotropic cantilever straight tube with mean radius R and thickness h is subjected to the transverse loading F as shown in Figure 3.1. The cylindrical coordinates (x, θ, r) are placed at the one of the composite tube's end so that x and r are the axial and radial coordinates, respectively. Within the kth layer of an orthotropic straight tube, the infinitesimal strain-displacement relations of elasticity in cylindrical coordinate system (x, θ, r) are given by [89] (*see Figure 3.1*):

$$\varepsilon_{xx}^{(k)}(\theta,r)=\frac{\partial u_1^{(k)}(x,\theta,r)}{\partial x} \tag{3.1}$$

$$\varepsilon_{\theta\theta}^{(k)}(\theta,r)=\frac{1}{r}\frac{\partial u_2^{(k)}(x,\theta,r)}{\partial \theta}+\frac{u_3^{(k)}(x,\theta,r)}{r} \tag{3.2}$$

$$\varepsilon_{rr}^{(k)}(\theta,r)=\frac{\partial u_3^{(k)}(x,\theta,r)}{\partial r} \tag{3.3}$$

$$\gamma_{\theta r}^{(k)}(\theta,r)=\frac{1}{r}\frac{\partial u_3^{(k)}(x,\theta,r)}{\partial\theta}+\frac{\partial u_2^{(k)}(x,\theta,r)}{\partial r}-\frac{u_2^{(k)}(x,\theta,r)}{r} \tag{3.4}$$

$$\gamma_{xr}^{(k)}(\theta,r)=\frac{\partial u_3^{(k)}(x,\theta,r)}{\partial x}+\frac{\partial u_1^{(k)}(x,\theta,r)}{\partial r} \tag{3.5}$$

$$\gamma_{x\theta}^{(k)}(\theta,r)=\frac{\partial u_2^{(k)}(x,\theta,r)}{\partial x}+\frac{1}{r}\frac{\partial u_1^{(k)}(x,\theta,r)}{\partial\theta} \tag{3.6}$$

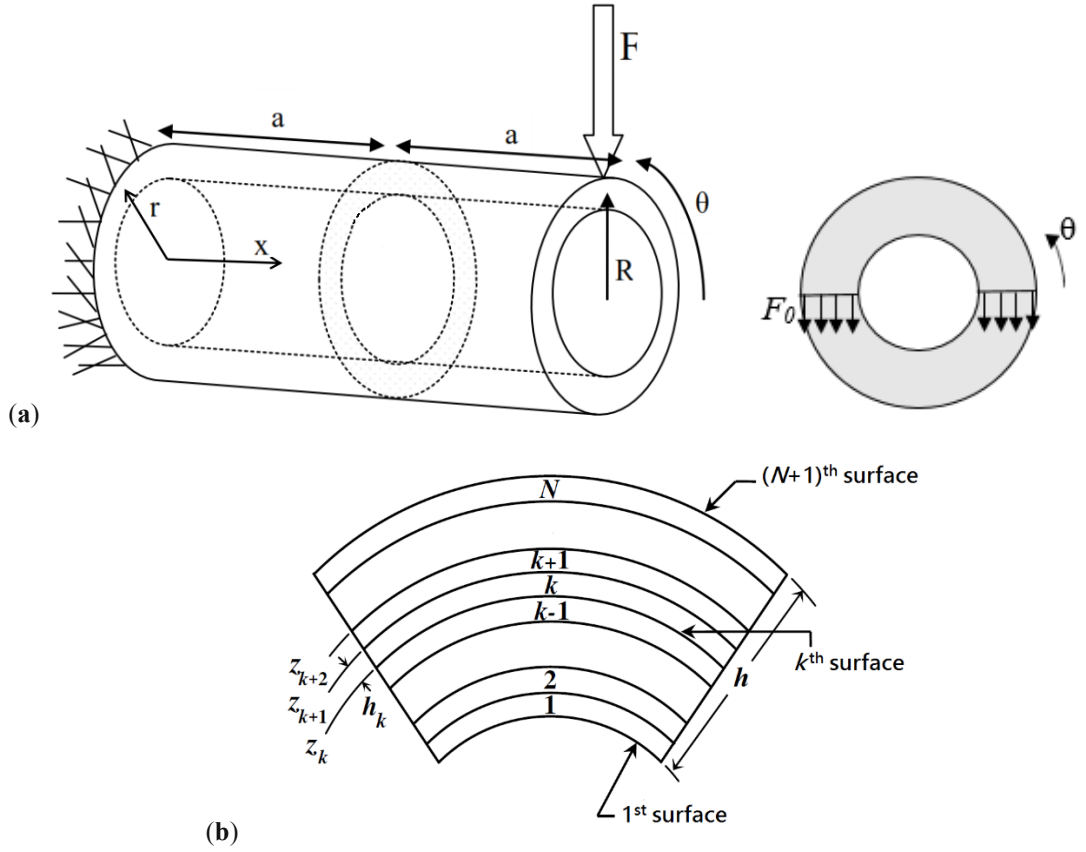

Figure 3.1: **(a)** The geometry of a straight tube and the coordinate system. **(b)** The lay-up sequence in a laminated composite tube.

where $u_1^{(k)}(x,\theta,r)$, $u_2^{(k)}(x,\theta,r)$ and $u_3^{(k)}(x,\theta,r)$ represent the displacement components in the x, θ and r directions, respectively, of a material point located at (x, θ, r) in the kth ply of a composite straight tube in Figure 3.1. Next, by taking integration, one can determine the most general form of the displacement components for composite straight tubes as explained in the detailed in the following. Integrating Eq. (3.1) yields;

$$u_1^{(k)}(x,\theta,r)=x\,\varepsilon_{xx}^{(k)}(\theta,r)+u^{(k)}(\theta,r) \tag{3.7}$$

Substituting Eq. (3.7) into Eq. (3.5) yields;

$$\gamma_{xr}^{(k)}(\theta,r)=\frac{\partial u_3^{(k)}(x,\theta,r)}{\partial x}+x\,\frac{\partial \varepsilon_{xx}^{(k)}(\theta,r)}{\partial r}+\frac{\partial u^{(k)}(\theta,r)}{\partial r} \tag{3.8}$$

Integrating Eq. (3.8) yields:

$$u_3^{(k)}(x,\theta,r)=x\left(\gamma_{xr}^{(k)}(\theta,r)-\frac{\partial u^{(k)}(\theta,r)}{\partial r}\right)-\frac{1}{2}x^2\frac{\partial \varepsilon_{xx}^{(k)}(\theta,r)}{\partial r}+w^{(k)}(\theta,r) \tag{3.9}$$

Substituting Eq. (3.9) into Eq. (3.3) yields;

$$\varepsilon_{rr}^{(k)}(\theta,r)=x\,\frac{\partial}{\partial r}\left(\gamma_{xr}^{(k)}(\theta,r)-\frac{\partial u^{(k)}(\theta,r)}{\partial r}\right)-\frac{1}{2}x^2\frac{\partial^2 \varepsilon_{xx}^{(k)}(\theta,r)}{\partial r^2}+\frac{\partial w^{(k)}(\theta,r)}{\partial r} \tag{3.10}$$

From Eq. (3.10), we conclude that;

$$\gamma_{xr}^{(k)}(\theta,r)-\frac{\partial u^{(k)}(\theta,r)}{\partial r}=f_1^{(k)}(\theta);\quad \varepsilon_{xx}^{(k)}(\theta,r)=rf_2^{(k)}(\theta)+f_3^{(k)}(\theta) \tag{3.11}$$

Substituting Eq. (3.11) back into Eqs. (3.7) and (3.9) yields;

$$u_1^{(k)}(x,\theta,r)=x\left(rf_2^{(k)}(\theta)+f_3^{(k)}(\theta)\right)+u^{(k)}(\theta,r) \tag{3.12}$$

$$u_3^{(k)}(x,\theta,r)=xf_1^{(k)}(\theta)-\frac{1}{2}x^2f_2^{(k)}(\theta)+w^{(k)}(\theta,r) \tag{3.13}$$

Next, we substitute Eq. (3.12) into Eq. (3.6) to have;

$$\gamma_{x\theta}^{(k)}(\theta,r)=\frac{\partial u_2^{(k)}(x,\theta,r)}{\partial x}+x\left(\frac{\partial f_2^{(k)}(\theta)}{\partial \theta}+\frac{1}{r}\frac{\partial f_3^{(k)}(\theta)}{\partial \theta}\right)+\frac{1}{r}\frac{\partial u^{(k)}(\theta,r)}{\partial \theta} \tag{3.14}$$

Integrating Eq. (3.14) yields;

$$u_2^{(k)}(x,\theta,r)=x\,\gamma_{x\theta}^{(k)}(\theta,r)-\frac{1}{2}x^2\left(\frac{\partial f_2^{(k)}(\theta)}{\partial \theta}+\frac{1}{r}\frac{\partial f_3^{(k)}(\theta)}{\partial \theta}\right)-x\,\frac{1}{r}\frac{\partial u^{(k)}(\theta,r)}{\partial \theta}+v^{(k)}(\theta,r) \tag{3.15}$$

By substituting Eq. (3.15) and Eq. (3.13) into Eq. (3.4), the following is obtained:

$$\begin{aligned}\gamma_{\theta r}^{(k)}(\theta,r)=x\Bigg(&\frac{1}{r}\frac{\partial f_1^{(k)}(\theta)}{\partial \theta}+\frac{1}{r^2}\frac{\partial u^{(k)}(\theta,r)}{\partial \theta}+\frac{\partial \gamma_{x\theta}^{(k)}(\theta,r)}{\partial r}-\frac{\gamma_{x\theta}^{(k)}(\theta,r)}{r}-\frac{\partial}{\partial r}\left(\frac{1}{r}\frac{\partial u^{(k)}(\theta,r)}{\partial \theta}\right)\Bigg)\\&+x^2\left(\frac{1}{r^2}\frac{\partial f_3^{(k)}(\theta)}{\partial \theta}\right)-\frac{v^{(k)}(\theta,r)}{r}+\frac{\partial v^{(k)}(\theta,r)}{\partial r}+\frac{1}{r}\frac{\partial w^{(k)}(\theta,r)}{\partial \theta}\end{aligned} \tag{3.16}$$

From Eq. (3.10), we conclude that;

$$\frac{1}{r^2}\frac{\partial f_3^{(k)}(\theta)}{\partial \theta}=0 \qquad (3.17a)$$

$$\frac{1}{r}\frac{\partial f_1^{(k)}(\theta)}{\partial \theta}+\frac{1}{r^2}\frac{\partial u^{(k)}(\theta,r)}{\partial \theta}+\frac{\partial \gamma_{x\theta}^{(k)}(\theta,r)}{\partial r}-\frac{\gamma_{x\theta}^{(k)}(\theta,r)}{r}-\frac{\partial}{\partial r}\left(\frac{1}{r}\frac{\partial u^{(k)}(\theta,r)}{\partial \theta}\right)=0 \qquad (3.17b)$$

From Eq. (3.17a), it is concluded that;

$$f_3^{(k)}(\theta)=C_6^{(k)} \qquad (3.18)$$

Combination of Eq. (3.15), Eq. (3.13) and Eq. (3.2) yields;

$$\varepsilon_{\theta\theta}^{(k)}(\theta,r)=\frac{x}{r}\left(\frac{\partial \gamma_{x\theta}^{(k)}(\theta,r)}{\partial \theta}-\frac{1}{r}\frac{\partial^2 u^{(k)}(\theta,r)}{\partial \theta^2}+f_1^{(k)}(\theta)\right)-\frac{x^2}{2r}\left(\frac{\partial^2 f_2^{(k)}(\theta)}{\partial \theta^2}+f_2^{(k)}(\theta)\right)$$
$$+\frac{1}{r}\frac{\partial v^{(k)}(\theta,r)}{\partial \theta}+\frac{w^{(k)}(\theta,r)}{r} \qquad (3.19)$$

From Eq. (3.19), it is concluded that;

$$\frac{\partial \gamma_{x\theta}^{(k)}(\theta,r)}{\partial \theta}-\frac{1}{r}\frac{\partial^2 u^{(k)}(\theta,r)}{\partial \theta^2}+f_1^{(k)}(\theta)=0 \qquad (3.20a)$$

$$\frac{\partial^2 f_2^{(k)}(\theta)}{\partial \theta^2}+f_2^{(k)}(\theta)=0 \qquad (3.20b)$$

Therefore, from Eq. (3.20b), we have:

$$f_2^{(k)}(\theta)=C_5^{(k)}\cos\theta+C_4^{(k)}\sin\theta \qquad (3.21)$$

By substituting derivative of Eq. (3.20a) with respect to r into derivative of Eq. (3.17b) with respect to θ while considering Eq. (3.20a) at the same time, the following is obtained:

$$\frac{\partial^2 f_1^{(k)}(\theta)}{\partial \theta^2}+f_1^{(k)}(\theta)=0 \qquad (3.22a)$$

Therefore;

$$f_1^{(k)}(\theta)=C_1^{(k)}\sin\theta+C_2^{(k)}\cos\theta \qquad (3.22b)$$

From Eq. (3.20a), we have:

$$\gamma_{x\theta}^{(k)}(\theta,r)=\frac{1}{r}\frac{\partial u^{(k)}(\theta,r)}{\partial \theta}+C_1^{(k)}\cos\theta-C_2^{(k)}\sin\theta+h_1^{(k)}(r) \qquad (3.23a)$$

By combination of Eq. (3.22) and Eq. (3.17b), it is concluded that;

$$h_1^{(k)}(r) = C_3^{(k)} r \qquad (3.23b)$$

Finally, substituting Eqs. (3.18), (3.21), (3.22b) and (3.23b) into Eqs. (3.12), (3.13) and (3.15) yields;

$$u_1^{(k)}(x,\theta,r) = xr\left(C_4^{(k)}\sin\theta + C_5^{(k)}\cos\theta\right) + C_6^{(k)}x + u^{(k)}(\theta,r)$$

$$u_2^{(k)}(x,\theta,r) = x\left(C_1^{(k)}\cos\theta - C_2^{(k)}\sin\theta - C_3^{(k)}r\right) - \frac{1}{2}x^2\left(C_4^{(k)}\cos\theta - C_5^{(k)}\sin\theta\right) + v^{(k)}(\theta,r)$$

$$u_3^{(k)}(x,\theta,r) = x\left(C_1^{(k)}\sin\theta + C_2^{(k)}\cos\theta\right) - \frac{1}{2}x^2\left(C_4^{(k)}\sin\theta + C_5^{(k)}\cos\theta\right) + w^{(k)}(\theta,r) \qquad (3.24)$$

$u_1^{(k)}$, $u_2^{(k)}$ and $u_3^{(k)}$ present the displacement field within composite straight tubes. However, the unknown functions and constants have to be determined.

3.3.2. *Elasticity Displacement Field*

A thick laminated orthotropic cantilever straight tube with mean radius *R* and thickness *h* is subjected to the transverse loading *F* as shown in Figure 3.1. The cylindrical coordinates (*x*, *θ*, *r*) are placed at the one of the composite tube's end so that *x* and *r* are the axial and radial coordinates, respectively. The appropriate integration of the linear strain-displacement relations of elasticity, within cylindrical coordinate system, as derived in the previous section, yields the displacement field for the *k*th layer (Eq. (3.24)). In order to satisfy the interfacial continuities of the displacement components, it is necessary for the integration constants appearing in Eq. (3.24) to be the same for all layers. It is therefore concluded that the most general form of the displacement field for the *k*th layer of laminated composite straight tubes is given as:

$$u_1^{(k)}(x,\theta,r) = xr\left(C_5\cos\theta + C_4\sin\theta\right) + C_6x + u^{(k)}(\theta,r)$$

$$u_2^{(k)}(x,\theta,r) = x\left(C_1\cos\theta - C_2\sin\theta - C_3r\right) - \frac{1}{2}x^2\left(C_4\cos\theta - C_5\sin\theta\right) + v^{(k)}(\theta,r)$$

$$u_3^{(k)}(x,\theta,r) = x\left(C_1\sin\theta + C_2\cos\theta\right) - \frac{1}{2}x^2\left(C_5\cos\theta + C_4\sin\theta\right) + w^{(k)}(\theta,r) \qquad (3.25)$$

3.3.3. *Layer-wise Theory (LWT)*

The equivalent single-layer theories are not able to precisely find stresses and strains in laminated composites. However, layer-wise theory (LWT) allows each layer of the laminate

to act like a real three-dimensional layer while being able to present good results for the local quantities. In LWT, the displacement components of a generic point in the laminate are assumed as [53, 54]:

$$u_1(x,\theta,z) = u_k(x,\theta)\Omega_k(z)$$
$$u_2(x,\theta,z) = v_k(x,\theta)\Omega_k(z)$$
$$u_3(x,\theta,z) = w_k(x,\theta)\Omega_k(z) \qquad (k = 1,2,...,N+1) \qquad (3.26)$$

with *k*, here and in what follows, being a dummy index implying summation of terms from *k*=1 to *k*=*N*+*1*. The variable *N* corresponds to the total number of numerical layers within the laminated orthotropic tube. In Eq. (3.26), u_1, u_2 and u_3 denote the total displacement components in the *x*, θ and *z* directions, respectively. Also, $u_k(x,\theta)$, $v_k(x,\theta)$ and $w_k(x,\theta)$ represent the displacements of the points initially located at the *k*th plane (defined by $z=z_k$, *see Figure 3.2*) within the composite straight tube in the *x*, θ and *z* directions, respectively. The variable *N* in Eq. (3.26) corresponds to the total number of numerical layers within the laminated orthotropic tube. Furthermore, $\Omega_k(z)$ is the global Lagrangian interpolation function associated with the *k*th plane. It is used for the discretization of the displacement through-thickness coordinate *z* (note that *r* which is thickness coordinate used in the previous section has the following relation with *z, r*=*R*+*z*). Depending upon the polynomial order of the interpolation function, Eq. (3.26) exhibits piecewise polynomial variation. It is noted that the accuracy of LWT is enhanced by subdividing each physical layer into a finite number of numerical layers. Clearly, as the number of subdivisions (*p*) through-thickness is increased, the number of governing equations and the accuracy of the results are increased.

To find unknown local functions, $u_k(x,\theta)$, $v_k(x,\theta)$ and $w_k(x,\theta)$, the LWT displacement field (Eq. (3.26)) is applied. Therefore, the elasticity displacement field in Eq. (3.25) is rewritten in a simpler form as:

$$u_1(x,\theta,z) = x(R+z)\left(C_5\cos\theta + C_4\sin\theta\right) + C_6 x + U_k(\theta)\Phi_k(z)$$
$$u_2(x,\theta,z) = x\left(C_1\cos\theta - C_2\sin\theta - C_3(R+z)\right) - \frac{1}{2}x^2\left(C_4\cos\theta - C_5\sin\theta\right) + V_k(\theta)\Phi_k(z)$$
$$u_3(x,\theta,z) = x\left(C_1\sin\theta + C_2\cos\theta\right) - \frac{1}{2}x^2\left(C_5\cos\theta + C_4\sin\theta\right) + W_k(\theta)\Phi_k(z) \qquad (3.27)$$

It is pointed out here that, by employing through-thickness linear interpolation functions (*see*

Figure 3.2), the continuity of displacement components through the thickness of the laminate is identically satisfied. On the other hand, the transverse strain components remain discontinuous at the interfaces that will subsequently amplify the possibility of having continuous interlaminar stresses at the interfaces of adjacent layers by increasing the number of numerical layers through the physical laminate. The linear global interpolation function is defined as:

$$\Phi_k(z)=\begin{cases} 0 & z \le z_{k-1} \\ \psi^2_{k-1}(z)=\dfrac{1}{h_{k-1}}(z-z_{k-1}) & z_{k-1}\le z \le z_k \\ \psi^1_k(z)=\dfrac{1}{h_k}(z_{k+1}-z) & z_k \le z \le z_{k+1} \\ 0 & z \ge z_{k+1} \end{cases} \tag{3.28}$$

where $\psi^j_k\ (j=1\text{and}\,2)$ are the local Lagrangian linear interpolation functions (*see Figure 3.2*), with h_k is the thickness of the kth layer.

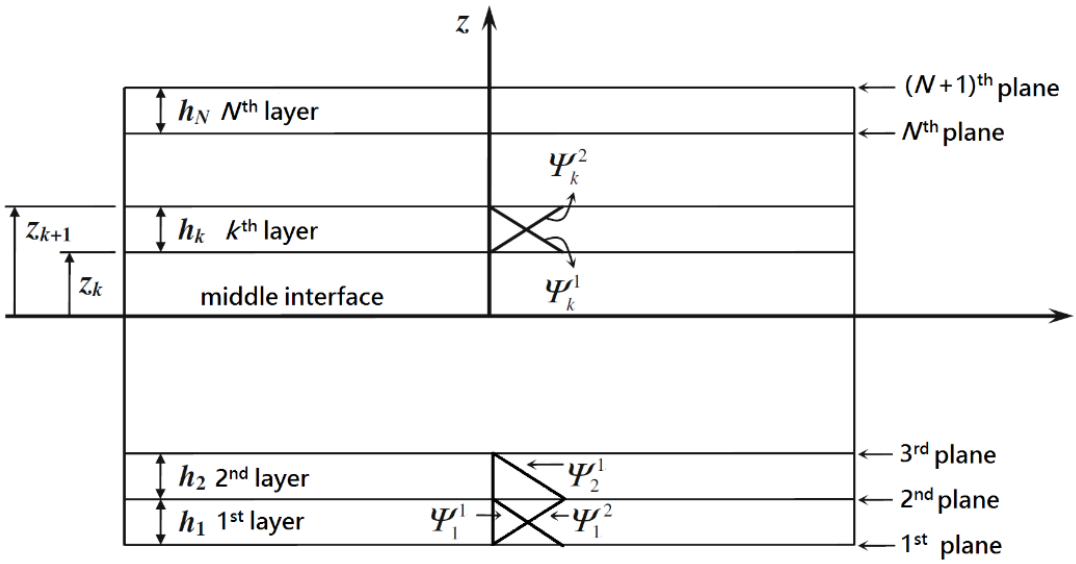

Figure 3.2: Local Lagrangian linear interpolation functions.

By introducing $r=R+z$, the strain-displacement relations are as given as:

$$\varepsilon_{xx}=\frac{\partial u_1}{\partial x},\qquad \varepsilon_{\theta\theta}=\frac{1}{R+z}\frac{\partial u_2}{\partial \theta}+\frac{u_3}{R+z},\qquad \gamma_{x\theta}=\frac{\partial u_2}{\partial x}+\frac{1}{R+z}\frac{\partial u_1}{\partial \theta}$$

$$\gamma_{\theta z}=\frac{1}{R+z}\frac{\partial u_3}{\partial \theta}+\frac{\partial u_2}{\partial z}-\frac{u_2}{R+z},\qquad \gamma_{xz}=\frac{\partial u_3}{\partial x}+\frac{\partial u_1}{\partial z},\qquad \varepsilon_{zz}=\frac{\partial u_3}{\partial z} \tag{3.29}$$

Substitution of Eq. (3.27) into the strain-displacement relations (3.29) yields the following results:

$$\varepsilon_{xx}=(R+z)\left(C_5\cos\theta+C_4\sin\theta\right)+C_6,\qquad \varepsilon_{\theta\theta}=\frac{V_k'+W_k}{R+z}\Phi_k,\qquad \varepsilon_{zz}=W_k\Phi_k'$$

$$\gamma_{\theta z}=\frac{W_k'-V_k}{R+z}\Phi_k+V_k\Phi_k',\qquad \gamma_{xz}=U_k\Phi_k'+\left(C_1\sin\theta+C_2\cos\theta\right),$$

$$\gamma_{x\theta}=\left(C_1\cos\theta-C_2\sin\theta-C_3\left(R+z\right)\right)+\frac{U_k'\Phi_k}{R+z} \tag{3.30}$$

In Eq. (3.30) and what follows, a prime indicates an ordinary differentiation with respect to an appropriate variable (*i.e.,* either θ or z). The equilibrium equations of a laminated orthotropic straight tube with N numerical layers are obtained by employing Eq. (3.30) in the principle of minimum total potential energy [90]. The results are, in general, *3(N+1)* local equilibrium equations corresponding to *3(N+1)* unknown functions U_k, V_k and W_k and six global equilibrium equations associated with the six parameters C_1, C_2, C_3, C_4, C_5 and C_6.

According to the principle of minimum total potential energy [90] at the equilibrium configuration of a body the variation of the total potential energy Π of the body must vanish. That is:

$$\delta\Pi\equiv\delta U+\delta V=0 \tag{3.31}$$

where δU is the variation of total strain energy of the body, i.e.,

$$\delta U=\int_0^{2a}\int_{-h/2}^{+h/2}\int_{-\pi}^{\pi}\left(\sigma_{xx}\delta\varepsilon_{xx}+\sigma_{\theta\theta}\delta\varepsilon_{\theta\theta}+\sigma_{zz}\delta\varepsilon_{zz}+\sigma_{\theta z}\delta\gamma_{\theta z}+\sigma_{xz}\delta\gamma_{xz}+\sigma_{x\theta}\delta\gamma_{x\theta}\right)\mathrm{d}\theta\mathrm{d}z\mathrm{d}x \tag{3.32}$$

and V is negative of the work done on the body by the specified external forces. Here,

$$V=-F.u_2\left(x=2a,\theta=0^\circ \text{ and } 180^\circ, r=R+z\right)=-\int_{-h/2}^{+h/2}F_0.u_2\left(at\ \theta=0^\circ\right)dz-\int_{-h/2}^{+h/2}F_0.u_2\left(at\ \theta=180^\circ\right)dz$$

$$=\int_{-h/2}^{+h/2}4F_0C_3a\left(R+z\right)dz=4F_0C_3Rah \tag{3.33}$$

and therefore, $\partial V=4F_0Ra\,h\,\partial C_3$. Note that F_0 is the shear load that is uniformly distributed

on lines aligned on radius as shown in Figure 3.1a. In addition, the variations of strains in Eq. (3.30) are found as:

$$\delta\varepsilon_{xx} = (R+z)\left(\delta C_5 \cos\theta + \delta C_4 \sin\theta\right) + \delta C_6, \qquad \delta\varepsilon_{\theta\theta} = \frac{\delta V_k' + \delta W_k}{R+z}\Phi_k, \qquad \delta\varepsilon_{zz} = \delta W_k \Phi_k'$$

$$\delta\gamma_{\theta z} = \frac{\delta W_k' - \delta V_k}{R+z}\Phi_k + \delta V_k \Phi_k', \qquad \delta\gamma_{xz} = \delta U_k \Phi_k' + \left(\delta C_1 \sin\theta + \delta C_2 \cos\theta\right),$$

$$\delta\gamma_{x\theta} = \left(\delta C_1 \cos\theta - \delta C_2 \sin\theta - \delta C_3 (R+z)\right) + \frac{\delta U_k' \Phi_k}{R+z} \tag{3.34}$$

Upon substituting $\partial V = 4F_0 R\, a\, h\, \partial C_3$ into Eq. (3.31), carrying out the necessary integrations, and employing the fundamental lemma of calculus of variations the equilibrium equations and the associated boundary conditions of a laminated composite straight tube subjected to transverse force are obtained as:

$$\delta U_k : Q_x^k - \frac{dM_{x\theta}^k}{d\theta} = 0$$

$$\delta V_k : Q_\theta^k - \frac{dM_\theta^k}{d\theta} - R_\theta^k = 0$$

$$\delta W_k : M_\theta^k - \frac{dR_\theta^k}{d\theta} + N_z^k = 0 \qquad (k = 1,2,...,N+1) \tag{3.35}$$

$$\delta C_1 : \int_{-\pi}^{\pi}\int_{-h/2}^{+h/2} R\left(\sigma_{xz}\sin\theta + \sigma_{x\theta}\cos\theta\right) dz\, d\theta = 0$$

$$\delta C_2 : \int_{-\pi}^{\pi}\int_{-h/2}^{+h/2} R\left(\sigma_{xz}\cos\theta - \sigma_{x\theta}\sin\theta\right) dz\, d\theta = 0$$

$$\delta C_3 : \frac{1}{h}\int_{-\pi}^{\pi}\int_{-h/2}^{+h/2} R\,\sigma_{x\theta}(R+z)\, dz\, d\theta = -2F_0$$

$$\delta C_4 : \int_{-\pi}^{\pi}\int_{-h/2}^{+h/2} R\,\sigma_{xx}(R+z)\sin\theta\, dz\, d\theta = 0$$

$$\delta C_5 : \int_{-\pi}^{\pi}\int_{-h/2}^{+h/2} R\,\sigma_{xx}(R+z)\cos\theta\, dz\, d\theta = 0$$

$$\delta C_6 : \int_{-\pi}^{\pi}\int_{-h/2}^{+h/2} R\,\sigma_{xx}\, dz\, d\theta = 0 \tag{3.36}$$

where the generalized stress and moment resultants are defined as:

$$\left(N_z^k, Q_x^k, Q_\theta^k\right) = \int_{-h/2}^{+h/2} \left(\sigma_{zz}, \sigma_{xz}, \sigma_{\theta z}\right) \Phi_k' \, dz$$

$$\left(M_\theta^k, M_{x\theta}^k, R_\theta^k\right) = \int_{-h/2}^{+h/2} \frac{1}{R+z} \left(\sigma_{\theta\theta}, \sigma_{x\theta}, \sigma_{\theta z}\right) \Phi_k \, dz \qquad (3.37)$$

The following boundary conditions must be satisfied at the ends of the composite straight tube:

$$R_\theta^k = Q_x^k = N_z^k = 0 \qquad \text{at}\left(\text{z}=\pm\text{h}/2\right) \qquad (3.38a)$$

$$u_1^{(k)} = u_2^{(k)} = u_3^{(k)} = 0 \qquad \text{at}\left(\text{x}=0\right) \qquad (3.38b)$$

Note that in Eq. (3.35) the superscript *k* refers to the *k*th interface in the laminated orthotropic tube. The three-dimensional constitutive law within the *k*th layer of a laminated orthotropic tube given as follows [91]:

$$\begin{pmatrix} \sigma_{xx} \\ \sigma_{\theta\theta} \\ \sigma_{zz} \\ \sigma_{\theta z} \\ \sigma_{xz} \\ \sigma_{x\theta} \end{pmatrix}^{(k)} = \begin{bmatrix} \bar{C}_{11} & \bar{C}_{12} & \bar{C}_{13} & 0 & 0 & \bar{C}_{16} \\ \bar{C}_{12} & \bar{C}_{22} & \bar{C}_{23} & 0 & 0 & \bar{C}_{26} \\ \bar{C}_{13} & \bar{C}_{23} & \bar{C}_{33} & 0 & 0 & \bar{C}_{36} \\ 0 & 0 & 0 & \bar{C}_{44} & \bar{C}_{45} & 0 \\ 0 & 0 & 0 & \bar{C}_{45} & \bar{C}_{55} & 0 \\ \bar{C}_{16} & \bar{C}_{26} & \bar{C}_{36} & 0 & 0 & \bar{C}_{66} \end{bmatrix}^{(k)} \begin{pmatrix} \varepsilon_{xx} \\ \varepsilon_{\theta\theta} \\ \varepsilon_{zz} \\ \gamma_{\theta z} \\ \gamma_{xz} \\ \gamma_{x\theta} \end{pmatrix}^{(k)} \qquad (3.39)$$

where $\bar{C}_{ij}^{(k)}$ represent the off-axis stiffnesses. By substituting Eq. (3.30) into Eq. (3.39) and the subsequent results into Eq. (3.37), the stress resultants are given the following relations:

$$\begin{aligned} \left(N_z^k, M_\theta^k, M_{x\theta}^k\right) = {} & \left(B_{36}^{jk}, H_{26}^{kj}, H_{66}^{kj}\right) U_j' + \left(B_{23}^{jk}, H_{22}^{kj}, H_{26}^{kj}\right) V_j' \\ & + \left(B_{23}^{jk} + A_{33}^{kj}, H_{22}^{kj} + B_{23}^{kj}, H_{26}^{kj} + B_{36}^{kj}\right) W_j \\ & + \left(A_{36}^k, F_{26}^k, F_{66}^k\right)\left(C_1 \cos\theta - C_2 \sin\theta\right) - \left(\bar{B}_{36}^k, B_{26}^k, B_{66}^k\right) C_3 \\ & + \left(\bar{B}_{13}^k, B_{12}^k, B_{16}^k\right) C_4 \sin\theta + \left(\bar{B}_{13}^k, B_{12}^k, B_{16}^k\right) C_5 \cos\theta + \left(A_{13}^k, F_{12}^k, F_{16}^k\right) C_6 \end{aligned}$$

$$\begin{aligned} \left(Q_x^k, Q_\theta^k, R_\theta^k\right) = {} & \left(A_{55}^{kj}, A_{45}^{kj}, B_{45}^{kj}\right) U_j + \left(A_{45}^{kj} - B_{45}^{jk}, A_{44}^{kj} - B_{44}^{jk}, B_{44}^{kj} - H_{44}^{kj}\right) V_j \\ & + \left(B_{45}^{jk}, B_{44}^{jk}, H_{44}^{kj}\right) W_j' + \left(A_{55}^k, A_{45}^k, \text{F}_{45}^k\right)\left(C_1 \sin\theta + C_2 \cos\theta\right) \end{aligned} \qquad (3.40)$$

where the laminate rigidities in Eq. (3.40) are defined as:

$$\left(A_{pq}^{kj},\bar{B}_{pq}^{kj},D_{pq}^{kj}\right)=\sum_{i=1}^{N}\int_{z_i}^{z_{i+1}}\bar{C}_{pq}^{(i)}\left(\phi_k'\phi_j',\phi_k\phi_j',\phi_k\phi_j\right)\mathrm{dz}$$

$$\left(B_{pq}^{kj},H_{pq}^{kj},G_{pq}^{kj}\right)=\sum_{i=1}^{N}\int_{z_i}^{z_{i+1}}\bar{C}_{pq}^{(i)}\left(\frac{\phi_k\phi_j'}{R+z},\frac{\phi_k\phi_j}{\left(R+z\right)^2},\frac{\phi_k\phi_j}{R+z}\right)\mathrm{dz}$$

$$\left(A_{pq}^{k},B_{pq}^{k},\bar{B}_{pq}^{k}\right)=\sum_{i=1}^{N}\int_{z_i}^{z_{i+1}}\bar{C}_{pq}^{(i)}\left(\phi_k',\phi_k,\phi_k'\left(R+z\right)\right)\mathrm{dz}$$

$$\left(D_{pq}^{k},F_{pq}^{k},E_{pq}^{k}\right)=\sum_{i=1}^{N}\int_{z_i}^{z_{i+1}}\bar{C}_{pq}^{(i)}\left(\frac{\phi_k}{\left(R+z\right)^2},\frac{\phi_k}{R+z},\frac{\phi_k'}{R+z}\right)\mathrm{dz} \qquad (3.41)$$

$$\left(k,j=1,2,...,N+1\right)$$

The local displacement equilibrium equations are obtained merely by substituting Eq. (3.40) into Eq. (3.35):

$$\begin{aligned}
\delta U_k:&-H_{66}^{kj}U_j''+A_{55}^{kj}U_j-H_{26}^{kj}V_j''-B_{45}^{jk}V_j-\left(H_{26}^{kj}+B_{36}^{kj}-B_{45}^{jk}\right)W_j'=B_{16}^{k}\left(C_4\cos\theta-C_5\sin\theta\right)\\
&-\left(A_{55}^{k}+F_{66}^{k}\right)\left(C_1\sin\theta+C_2\cos\theta\right)\\
\delta V_k:&-H_{26}^{kj}U_j''+\left(A_{45}^{kj}-B_{45}^{kj}\right)U_j-H_{22}^{kj}V_j''+\left(A_{44}^{kj}-B_{44}^{kj}-B_{44}^{jk}+H_{44}^{kj}\right)V_j\\
&-\left(H_{22}^{kj}+B_{23}^{kj}-B_{44}^{jk}+H_{44}^{kj}\right)W_j'=B_{12}^{k}\left(C_4\cos\theta-C_5\sin\theta\right)-\left(A_{45}^{k}-\mathrm{F}_{45}^{k}+F_{26}^{k}\right)\left(C_1\sin\theta+C_2\cos\theta\right)\\
\delta W_k:&\left(-B_{45}^{kj}+H_{26}^{kj}+B_{36}^{jk}\right)U_j'+\left(H_{44}^{kj}-B_{44}^{kj}+H_{22}^{kj}+B_{23}^{jk}\right)V_j'-H_{44}^{kj}W_j''\\
&+\left(H_{22}^{kj}+B_{23}^{jk}+B_{23}^{kj}+A_{33}^{kj}\right)W_j=\left(\bar{B}_{36}^{k}+B_{26}^{k}\right)C_3-\left(\bar{B}_{13}^{k}+B_{12}^{k}\right)\left(C_4\sin\theta+C_5\cos\theta\right)-\left(A_{13}^{k}+F_{12}^{k}\right)C_6\\
&+\left(A_{36}^{k}+F_{26}^{k}-\mathrm{F}_{45}^{k}\right)\left(C_2\sin\theta-C_1\cos\theta\right)\\
&k=1,2,...,N+1 \qquad (3.42)
\end{aligned}$$

In addition, the global equilibrium equations of the composite straight tube are expressed in terms of displacement functions by substituting Eq. (3.30) into Eq. (3.39) and the subsequent results into Eq. (3.36). The results present as:

$$
\begin{aligned}
\delta C_1 &: \int_{-\pi}^{\pi} R \begin{pmatrix} \mathrm{F}_{45}^{k}\left(W_j' - V_j\right)\sin\theta + A_{45}^{k} V_j \sin\theta + A_{55}^{k} U_j \sin\theta + \bar{A}_{55}\left(C_1\sin\theta + C_2\cos\theta\right)\sin\theta + \\ \bar{A}_{16}\,\mathrm{C}_6\cos\theta + \bar{B}_{16}\left(C_5\cos\theta + C_4\sin\theta\right)\cos\theta + \mathrm{F}_{26}^{k}\left(V_j' + W_j\right)\cos\theta \\ + \mathrm{B}_{36}^{k}\mathrm{W}_j\cos\theta + \bar{A}_{66}\left(C_1\sin\theta + C_2\cos\theta\right)\cos\theta - \bar{\mathrm{B}}_{66}\mathrm{C}_3\cos\theta + \mathrm{F}_{66}^{k}\mathrm{U}_j'\cos\theta \end{pmatrix} d\theta = 0 \\
\delta C_2 &: \int_{-\pi}^{\pi} R \begin{pmatrix} \mathrm{F}_{45}^{k}\left(W_j' - V_j\right)\cos\theta + A_{45}^{k} V_j \cos\theta + A_{55}^{k} U_j \cos\theta + \bar{A}_{55}\left(C_1\sin\theta + C_2\cos\theta\right)\cos\theta - \\ \bar{A}_{16}\,\mathrm{C}_6\sin\theta - \bar{B}_{16}\left(C_5\cos\theta + C_4\sin\theta\right)\sin\theta - \mathrm{F}_{26}^{k}\left(V_j' + W_j\right)\sin\theta \\ - \mathrm{B}_{36}^{k}\mathrm{W}_j\sin\theta - \bar{A}_{66}\left(C_1\sin\theta + C_2\cos\theta\right)\sin\theta + \bar{\mathrm{B}}_{66}\mathrm{C}_3\sin\theta - \mathrm{F}_{66}^{k}\mathrm{U}_j'\sin\theta \end{pmatrix} d\theta = 0 \\
\delta C_3 &: \frac{1}{h}\int_{-\pi}^{\pi} R \begin{pmatrix} \bar{B}_{16}C_6 + \bar{D}_{16}\left(C_5\cos\theta + C_4\sin\theta\right) + B_{26}^{k}\left(V_j' + W_j\right) + \bar{B}_{36}^{k}W_j - \bar{D}_{66}C_3 + A_{66}^{k}U_j' \\ + \bar{B}_{66}\left(C_1\cos\theta - C_2\sin\theta\right) \end{pmatrix} d\theta = -2F_0 \\
\delta C_4 &: \int_{-\pi}^{\pi} R \begin{pmatrix} \bar{B}_{11}C_6\sin\theta + \bar{D}_{11}\left(C_5\cos\theta\sin\theta + C_4\sin^2\theta\right) + B_{12}^{k}\left(V_j' + W_j\right)\sin\theta + F_{13}^{k}W_j\sin\theta \\ -\bar{D}_{16}C_3\sin\theta + B_{16}^{k}U_j'\sin\theta + \bar{B}_{16}\left(C_1\cos\theta - C_2\sin\theta\right)\sin\theta \end{pmatrix} d\theta = 0 \\
\delta C_5 &: \int_{-\pi}^{\pi} R \begin{pmatrix} \bar{B}_{11}C_6\cos\theta + \bar{D}_{11}\left(C_5\cos^2\theta + C_4\sin\theta\cos\theta\right) + B_{12}^{k}\left(V_j' + W_j\right)\cos\theta \\ + F_{13}^{k}W_j\cos\theta - \bar{D}_{16}C_3\cos\theta + B_{16}^{k}U_j'\cos\theta + \bar{B}_{16}\left(C_1\cos\theta - C_2\sin\theta\right)\cos\theta \end{pmatrix} d\theta = 0 \\
\delta C_6 &: \int_{-\pi}^{\pi} R \begin{pmatrix} \bar{A}_{11}C_6 + \bar{B}_{11}\left(C_5\cos\theta + C_4\sin\theta\right) + F_{12}^{k}\left(V_j' + W_j\right) \\ + B_{13}^{k}W_j - \bar{B}_{16}C_3 + F_{16}^{k}U_j' + \bar{A}_{16}\left(C_1\cos\theta - C_2\sin\theta\right) \end{pmatrix} d\theta = 0
\end{aligned}
\tag{3.43}
$$

where the extra laminate rigidities appearing in Eqs. (3.43) are defined as:

$$
\begin{aligned}
\left(\bar{A}_{pq}, \bar{B}_{pq}, \bar{D}_{pq}\right) &= \sum_{i=1}^{N}\int_{z_i}^{z_{i+1}} \bar{C}_{pq}^{(i)}\left(1, R+z, \left(R+z\right)^2\right)\mathrm{dz} \\
\left(\bar{F}_{pq}, \bar{E}_{pq}\right) &= \sum_{i=1}^{N}\int_{z_i}^{z_{i+1}} \bar{C}_{pq}^{(i)}\left(\frac{1}{R+z}, \frac{1}{\left(R+z\right)^2}\right)\mathrm{dz}
\end{aligned}
\tag{3.44}
$$

3.4. Analytical Solution *(State-space Method)*

The system in Eqs. (3.42) shows *3(N+1)* coupled ordinary differential equations with constant coefficients which may be displayed in a matrix form as follows:

$$[M]\{\eta''\}+[K]\{\eta\}=\{F_1\}(C_5\sin\theta-C_4\cos\theta)+\{F_2\}C_3\theta+\{F_3\}C_6\theta$$
$$+\{F_4\}(C_1\sin\theta+C_2\cos\theta) \qquad (3.45)$$

where

$$\{\eta\}=\left\{\{U\}^T,\{V\}^T,\{\bar{W}\}^T\right\}^T$$
$$\{U\}=\{U_1,U_2,...,U_{N+1}\}^T$$
$$\{V\}=\{V_1,V_2,...,V_{N+1}\}^T$$
$$\{\bar{W}\}=\{\bar{W}_1,\bar{W}_2,...,\bar{W}_{N+1}\}^T \qquad (3.46a)$$

and

$$\bar{W}_j=\int^{\theta}W_j\,\mathrm{d}\theta \qquad (3.46b)$$

The coefficient matrices [M], [K], $\{F_1\}$, $\{F_2\}$, $\{F_3\}$ and $\{F_4\}$ in Eq. (3.45) are defined in *Appendix A*. It is confirmed that the general solution of Eq. (3.45) may be presented as:

$$\{\eta\}=[\psi]\left[\sinh(\lambda\theta)\right]\{k\}+[K]^{-1}\{F_1\}(C_5\sin\theta-C_4\cos\theta)+[K]^{-1}\{F_2\}C_3\theta$$
$$+[K]^{-1}\{F_3\}C_6\theta+[K]^{-1}\{F_4\}(C_1\sin\theta+C_2\cos\theta) \qquad (3.47)$$

and [sinh ($\lambda\theta$)] is a *3(N+1)×3(N+1)* diagonal matrix. That is:

$$\left[\sinh(\lambda\theta)\right]=diag\left(\sinh(\lambda_1\theta),\sinh(\lambda_2\theta),...,\sinh\left(\lambda_{3(N+1)}\theta\right)\right) \qquad (3.48)$$

Also [ψ] and $\left(\lambda_1^2,\lambda_2^2,\ldots,\lambda_{3(N+1)}^2\right)$ are the modal matrix and eigenvalues of $(-[M]^{-1}[K])$, respectively. Vector $\{k\}$ is an unknown vector representing *3(N+1)* integration constants. The constants *Cj* (j=1, 2, 3, 4, 5 and 6) could be calculated within LWT analysis. Therefore, the boundary conditions in Eq. (3.39) are first imposed to find the vector $\{k\}$ in terms of the unknown parameters *Cj* (j=1, 2, 3, 4, 5 and 6). These constants are then determined in terms of the specific shear force F_0 by the satisfaction of the global equilibrium equations in Eq. (3.43). For completeness, the steps details involved in computing unknown parameters are displayed in *Appendices B & C*.

3.5. Lay-up Sequence Selection

As it is mentioned, Derisi [1] developed a lay-up sequence to be used for making composite landing gears for helicopters that may provide large deformation and gradual fracture. A composite tube with the $[(90°_{10}/0°_{10})_3/\pm45°_{25}]$ lay-up was manufactured and tested to study the behavior of orthotropic tubes subjected to bending load [1, 20]. Table 3.1 shows the different types of lay-up sequences considered. First, the [0°] composite tube is selected to compare with Lekhnitskii solution. Composite tubes with lay-up sequence of the $[(90°_{10}/0°_{10})_3/\pm45°_{25}]$ lay-up are studied for comparison with experimental data. Finally, in spite of the complex experimental lay-up considered, the simple lay-up sequence of the $[0°_{55}/90°_{55}]$ laminated composite tube is selected in order to gain an in-depth and comprehensive understanding of stress and strain distributions. The number 110 is obtained based on the availability of experimental data for the composite tubes with 110 layers, for comparison purpose.

Table 3.1: Lay-up sequence number.

Laminate number	Lay-up sequence	Purpose
1	[0°]	Comparison with Lekhnitskii solution
2	$[(90°_{10}/0°_{10})_3/\pm45°_{25}]$	Comparison with experimental data
3	$[0°_{55}/90°_{55}]$	Stress and strain distributions

3.6. Results and Discussion

Numerical results are presented and discussed for various arbitrary laminated composite cantilever tubes subjected to the shearing load. All physical layers are modeled as being made up of *p* numerical layers. The mechanical properties of the composite tube are given in Table 3.2.

Table 3.2: Characteristics of the composite tube [1, 20].

Properties	E_1 (GPa)	$E_2=E_3$ (GPa)	$G_{12}=G_{13}= G_{23}$ (GPa)	$\upsilon_{12}=\upsilon_{13}$	υ_{23}
Carbon AS4/PEKK	140	10	5.56	0.31	0.33

Furthermore, the stress and strain components are normalized as $\bar{\sigma}_{ij}=\sigma_{ij}/\sigma_0$ and $\bar{\varepsilon}_{ij}=\varepsilon_{ij}/\varepsilon_0$, respectively, where $\sigma_0=(F.x.r)/(\pi/64*(OD^4-ID^4))$ and $\varepsilon_0=\sigma_0/E_1$ with the outer diameter *OD* and the inner diameter *ID* of the composite straight tube. In the present cases, the composite tube section has an internal diameter of 56 mm and an external diameter of 78 mm, i.e. a wall thickness of 11 mm. In addition, the length of the composite tube is 405 mm. All physical layers have equal thickness (=0.1 mm) [1].

3.6.1. *Comparison of the Proposed Method and Lekhnitskii Solution*

Since Lekhnitskii [2] proposed the elasticity method for monolithic homogeneous orthotropic cylindrical shells with $\sigma_{zz}=\sigma_{\theta\theta}=\sigma_{z\theta}=0$ assumptions, the [0°] composite tube is considered to compare the results between the proposed method and Lekhnitskii solution for the cantilever tube. Figures 3.3 and 3.4 show σ_{xx}, σ_{zx} and $\sigma_{\theta x}$ distributions at the middle cross section of the [0°] composite tube at $x=a$ under the shear force. Good agreement is seen between the results obtained by two methods.

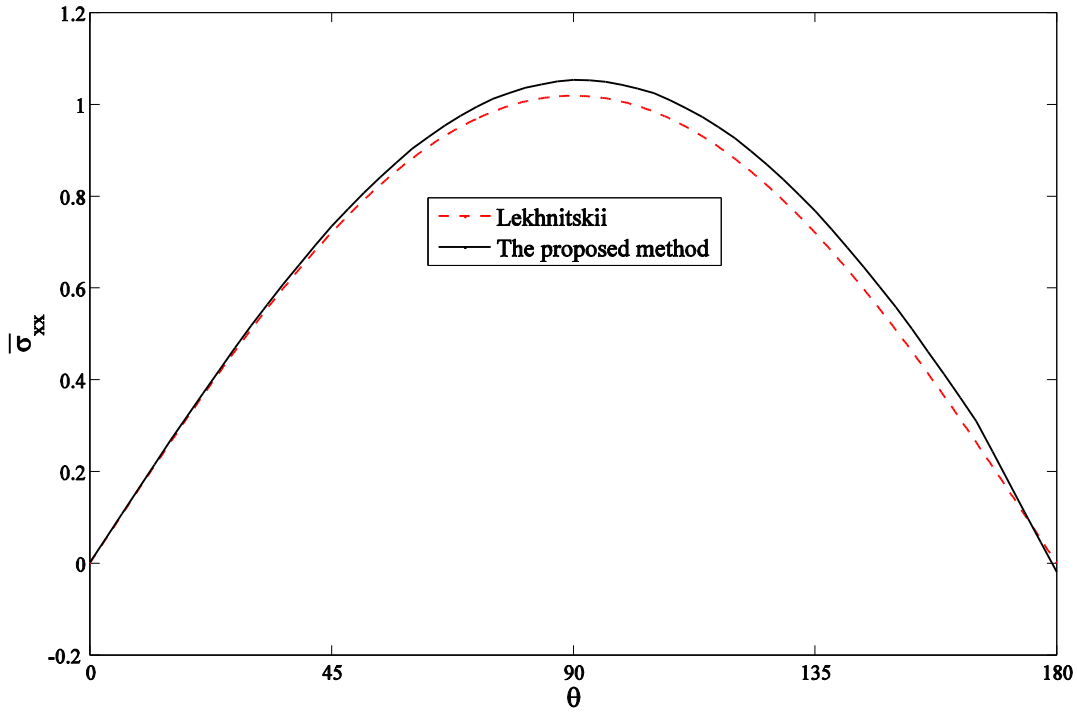

Figure 3.3: Distribution of the axial stress for the [0°] laminate at $x=a$.

3.6.2. *Comparison of the Proposed Method and FEM*

The radial stresses, σ_{zz}, at the 0°/90° interface of the $[0°_{55}/90°_{55}]$ laminated orthotropic straight tube at $x=a$ obtained by the present method and FEM (ANSYS) are compared in Figure 3.4. Good agreement between the analytical analysis and FEM (ANSYS) results is obtained. The present method results are obtained for p= 6, 10, 12 and 15 (numerical layers within LWT=p). It is seen that the results for p=12 and 15 are the same. Therefore, p=12 is selected to achieve the other results for the present method (in all the subsequent calculations, p is set equal to 12). Note that the accuracy of LWT method is improved by increasing the number of numerical layers (p) in each lamina. The mesh-independency study is performed for ANSYS. Mesh refining is performed two times while the element aspect ratio is kept constant. It is noted that for the initial mesh, 46200 elements (*15axial× 28circumferential× 110thickness directions*) are used to model the structure. For the 1st refined mesh, the thickness and circumferential directions are refined twice as much as the initial mesh (*184800 elements totally*). In addition, for the 2nd refined mesh, the axial and circumferential directions are refined twice as much as the initial mesh and the thickness direction is refined 4 times as much as the initial mesh to model the orthotropic straight tube (*739200 elements totally*). Also, modeling and analyzing of the laminated orthotropic straight tube with simple lay-up (0° and 90°) and the initial mesh take around 7200 seconds while they take around 10800 and 18000 seconds for the 1st and 2nd refined meshes, respectively. In addition, modeling and analyzing complex lay-up composite structures (*see experimental lay-up*) take so much longer, around 21600 and 25200 seconds for the 1st and 2nd refined meshes, respectively. While the modeling and analyzing of the same structure (*same complex lay-up*) using the developed method take 600 seconds (with using *p=12* in the proposed method).

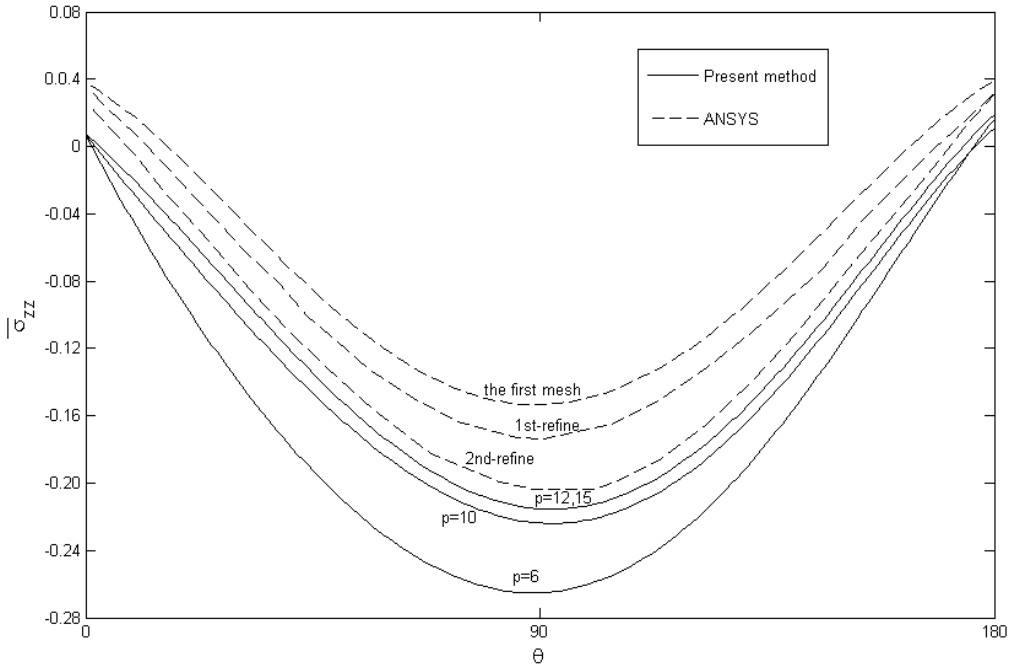

Figure 3.4: Comparison of the radial stress obtained by the present method and ANSYS at the 0°/90° interface of the $[0°_{55}/90°_{55}]$ laminated straight tube at $x=a$.

3.6.3. *Comparison of the Proposed Method with Experimental Data*

In this part, the proposed method results are compared with experimental data. A composite tube with the $[(90°_{10}/0°_{10})_3/\pm45°_{25}]$ lay-up was manufactured and tested to study the behavior of composite tubes subjected to bending loads [1, 20]. The properties of that composite tube are given in Table 3.2. In the experimental case, the tube section has an internal diameter of 56 mm and an external diameter of 78 mm. The composite tube has 110 layers in total. The tube was made using a fiber placement machine. Three-point bending test was carried on a few composite tubes [1, 20]. Since, here, the cantilever composite tube is studied, three-point bending test situation is considered as two cantilever straight tubes connected at one end (*x=0)* and *F=P/2* applied at the other end (*x=2a)* (*P* is force considered in [1, 20]) as shown in Figure 3.5.

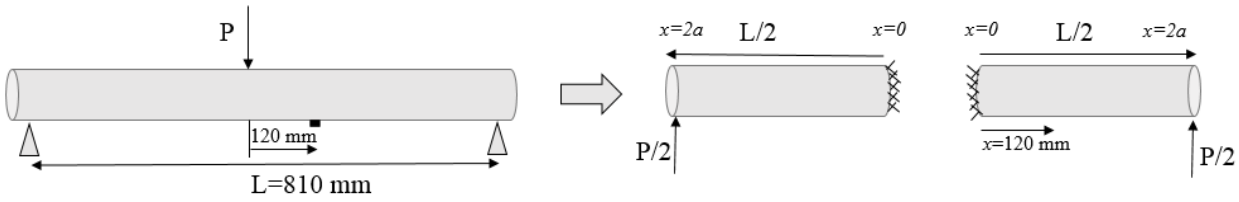

Figure 3.5: Three-point bending test and consideration as two cantilever composite tubes.

To compare, the results are taken from strain gauges installed on the composite tube to measure axial and hoop strains at 120 mm offset from the midpoint at the bottom line of the composite tube (*see Figure 3.5*). The tube was loaded (the maximum applied load was 20 KN) until maximum axial strain at the midpoint reached to 0.003 which was well in the elastic zone of all layers. The comparison of the proposed method results at $x=120$ *mm* and $\theta=90°$ while the composite tube length is 405 mm (*2a=405 mm, see Figure 3.5*) with experimental data is shown in Figure 3.6 showing the force variation versus axial strains and hoop strains, respectively. Good agreement between the analytical analyses and experimental results is obtained. In addition, FEM (ANSYS) results are shown in Figure 3.6 to present the accuracy of the proposed method. It is seen that the proposed method results are closer to the experimental data than those of FEM. In addition, with increasing load, the present method is more accurate than FEM. Note that the 2nd refined mesh is used to get FEM results here.

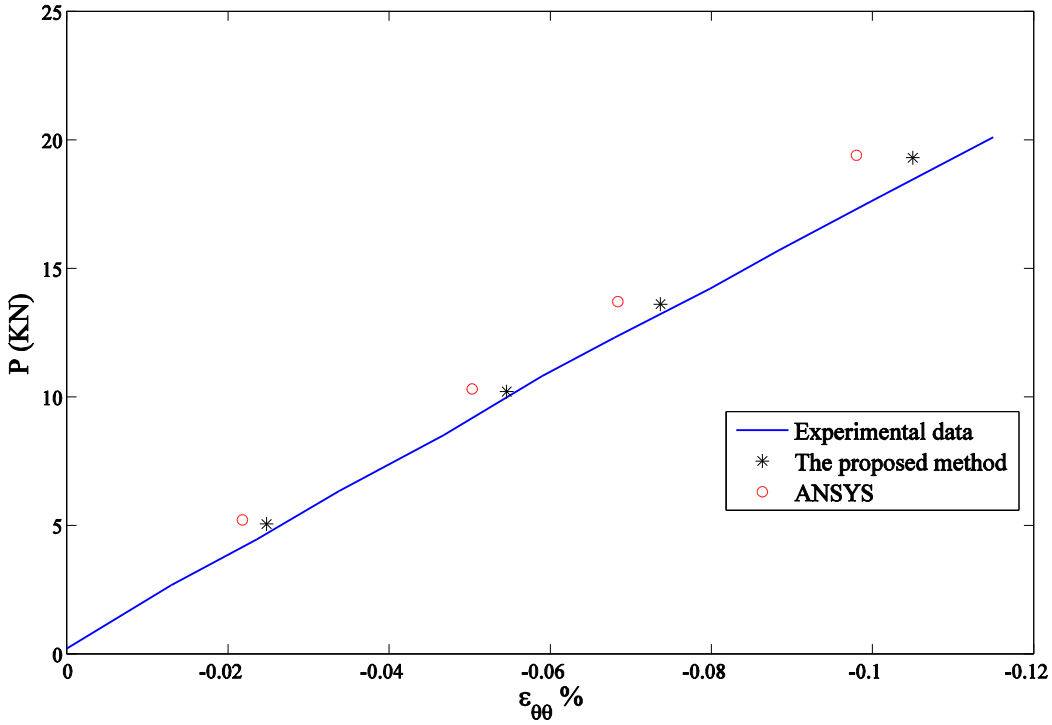

Figure 3.6: Load-hoop strain at 120 mm offset.

3.6.4. *Advantages of the Proposed Method*

The most important advantage of the proposed method is that the inputs for the modeling of composite structures with complex lay-up sequences (*see the experimental lay-up*) are simple, easy to use and fast to run. Contrary, to model complex lay-up composite structures in FEM, it is necessary to create several parts individually, mesh every part separately, and assign every lay-up sequence to the attributed part of structures. However, through using the proposed method, one just needs to simply define dimensions and lay-up sequences at the beginning of the program. Therefore, it is obvious that the modeling of complex lay-up orthotropic structures using FEM takes much longer than using the developed method. In addition, using FEM for parametric study is cumbersome. For example, to study the thickness effect on stress and strain distributions by using FEM, it is necessary to model the geometry for different thicknesses and obviously it takes longer than using the proposed method. By applying the proposed method, the parametric study of thick composite tubes is simple with low computational cost.

In addition, in FEM, to keep the aspect ratio between different directions of the element reasonable, one has to use a large number of elements. However, that is almost impossible for the real composite structures including thick composite tubes in engineering applications since there are so many layers with small thicknesses. Therefore, the laminated approximation in the thickness direction has to be employed not only for laminated shell elements but also for composite solid elements. For this reason, researchers are always interested in the theoretical methods for real composite structures. LWT is a popular candidate to obtain the solution with more accuracy for composite structures. However, for general composite structures subjected to different loading conditions, LWT can only be used in the thickness direction together with the company of FEM in other directions. For this sense, LWT can only be considered as a better laminated approximation in the thickness direction than CLT (Classical Lamination Theory). In this chapter, the more accurate solution for composite cantilever tubes is obtained not only by using LWT in the thickness direction (*i.e.,* the radial direction) as general case but also by using the theoretical approaches in other directions, including the longitudinal direction as well as the circumferential direction. To add to the advantages, high efficiency in terms of computational time is obtainable when the proposed method is used as compared with FEM.

3.6.5. *Stress and Strain Distributions*

A discussion performed here is on the cantilever orthotropic straight tube subjected to the transverse force. The stress and strain distributions are discussed through several numerical examples based on the proposed method at *x=a (i.e., x=202.5 mm)*, unless otherwise mentioned.

The variations of the interlaminar radial stress, σ_{zz}, the shear stress, $\sigma_{\theta z}$, and the hoop stress, $\sigma_{\theta\theta}$, at the 0°/90° interface of the $[0°_{55}/90°_{55}]$ laminated orthotropic straight tube are presented in Figure 3.7a. It is seen that the radial stress, σ_{zz}, and the hoop stress, $\sigma_{\theta\theta}$, have negative values from 0° to 180° (the upper region of the tube cross section). In addition, the results show anti-symmetric behavior for the lower region of the tube cross section (180°-360°). Therefore, the positive maximum value of σ_{zz} occurs at θ=270°. Note that the positive interlaminar radial stress, σ_{zz}, can cause delamination failure in the composite tube. It is observed that the maximum positive value of σ_{zz} occurs at θ=270°, while the maximum

positive value of $\sigma_{\theta z}$ occurs at $\theta=0°$ of the composite tube cross section. The distributions of the radial, σ_{zz}, hoop, $\sigma_{\theta\theta}$, and shear stresses, $\sigma_{\theta z}$, at three different sections (*x=50 mm, x= 202.5 mm and x=355 mm*) are shown in Figures 3.7b, 3.7c and 3.7d, respectively. It is observed that the values of all stresses at *x=50 mm* are greater than those at the other cross sections (*x= 202.5 mm and x=355 mm*). However, the increase rates for these stresses are different. The hoop stress, $\sigma_{\theta\theta}$, increases more than the other stresses and the shear stress, $\sigma_{\theta z}$, increases less than the others at *x=50 mm*. In addition, the shear stress, $\sigma_{\theta z}$, decreases less than the other stresses at *x=355 mm* and the hoop stress, $\sigma_{\theta\theta}$, decreases more than the others at *x=355 mm*.

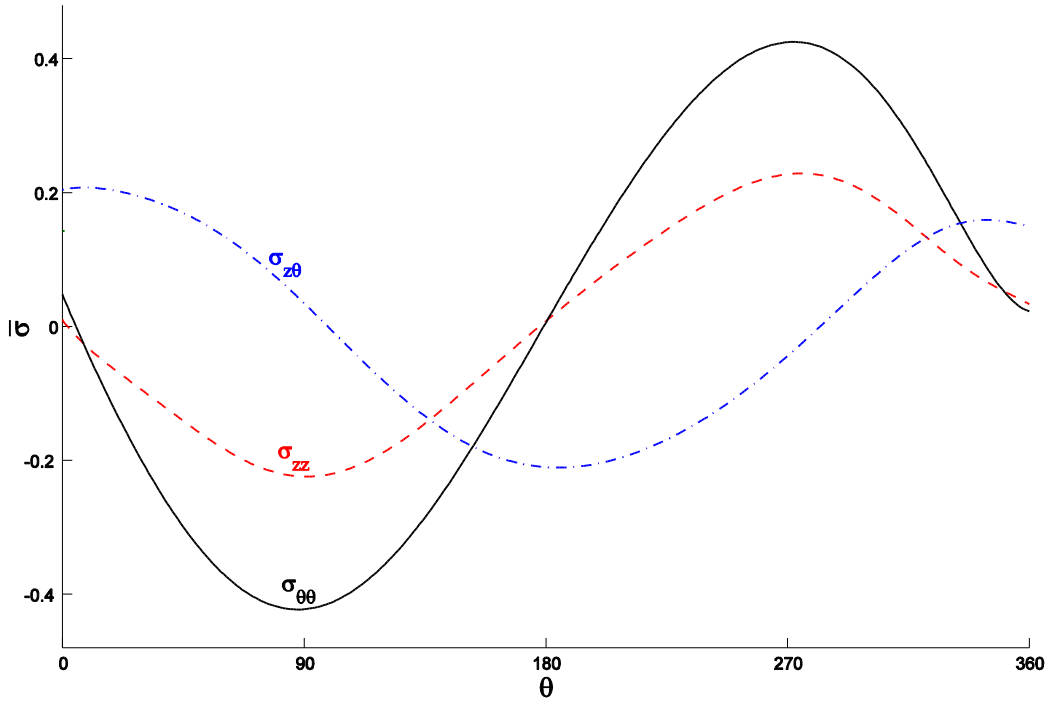

Figure 3.7a: Distribution of the stresses at the 0°/90° interface of the [$0°_{55}$/$90°_{55}$] laminated straight tube at *x=a*.

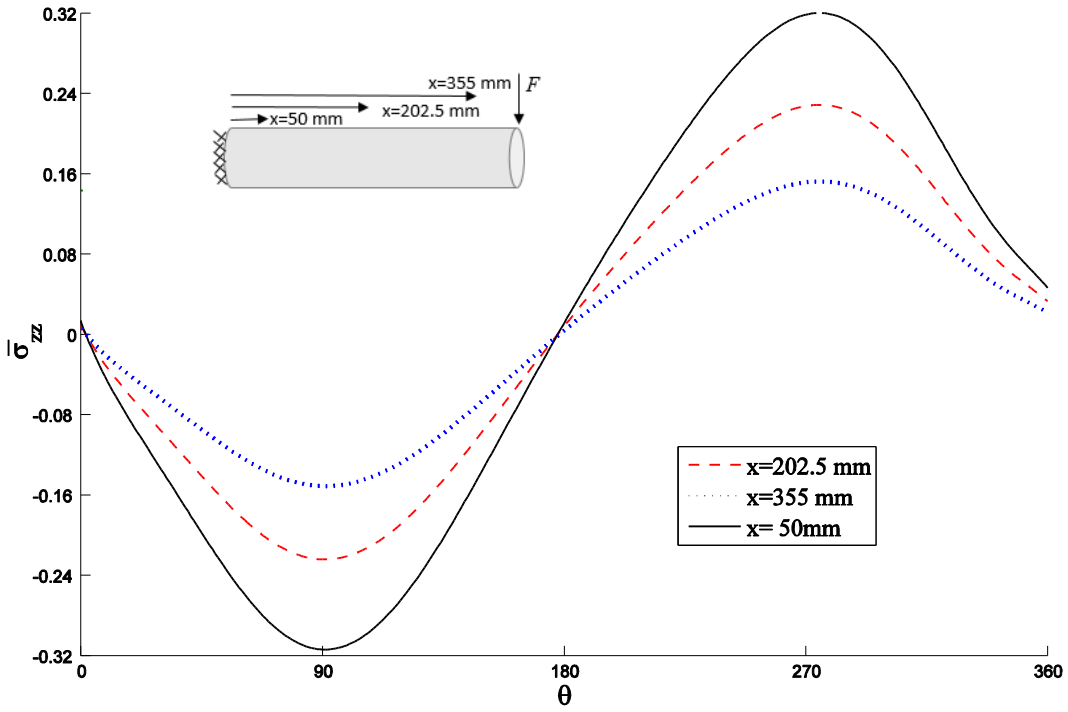

Figure 3.7b: Distribution of the radial stress, σ_{zz}, at the 0°/90° interface of the $[0°_{55}/90°_{55}]$ laminated straight tube at different cross sections.

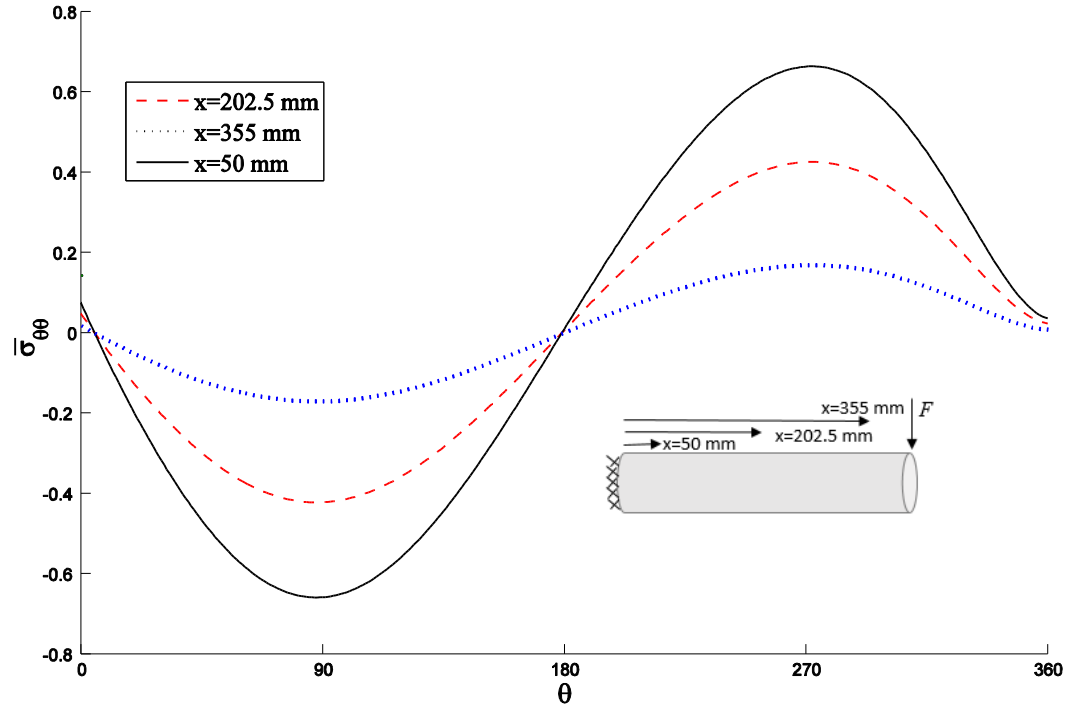

Figure 3.7c: Distribution of the hoop stress, $\sigma_{\theta\theta}$, at the 0°/90° interface of the $[0°_{55}/90°_{55}]$ laminated straight tube different cross sections.

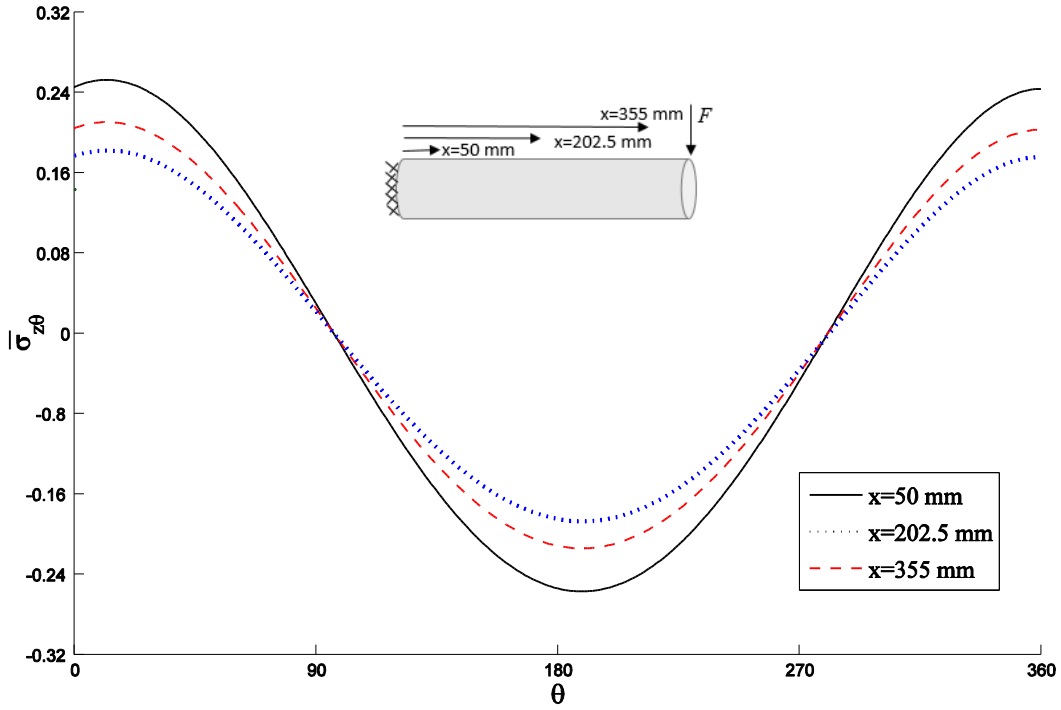

Figure 3.7d: Distribution of the shear stress, $\sigma_{\theta z}$, at the 0°/90° interface of the [$0°_{55}$/$90°_{55}$] laminated straight tube different cross sections.

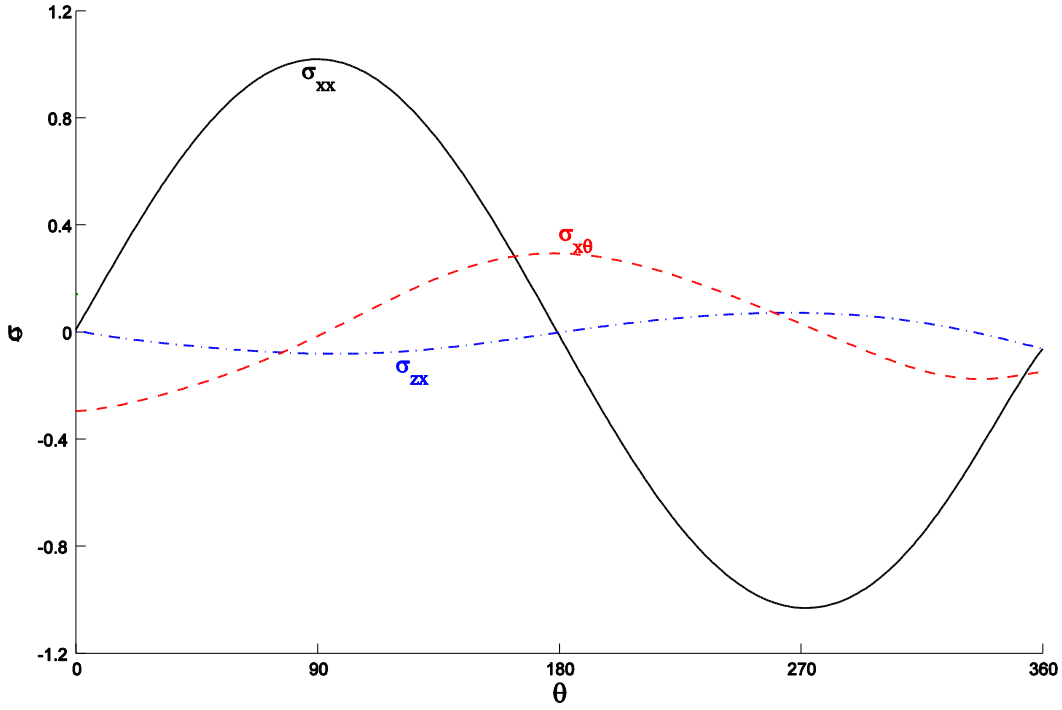

Figure 3.8: Distribution of the stresses at the 0°/90° interface of the [$0°_{55}$/$90°_{55}$] laminated straight tube at $x=a$.

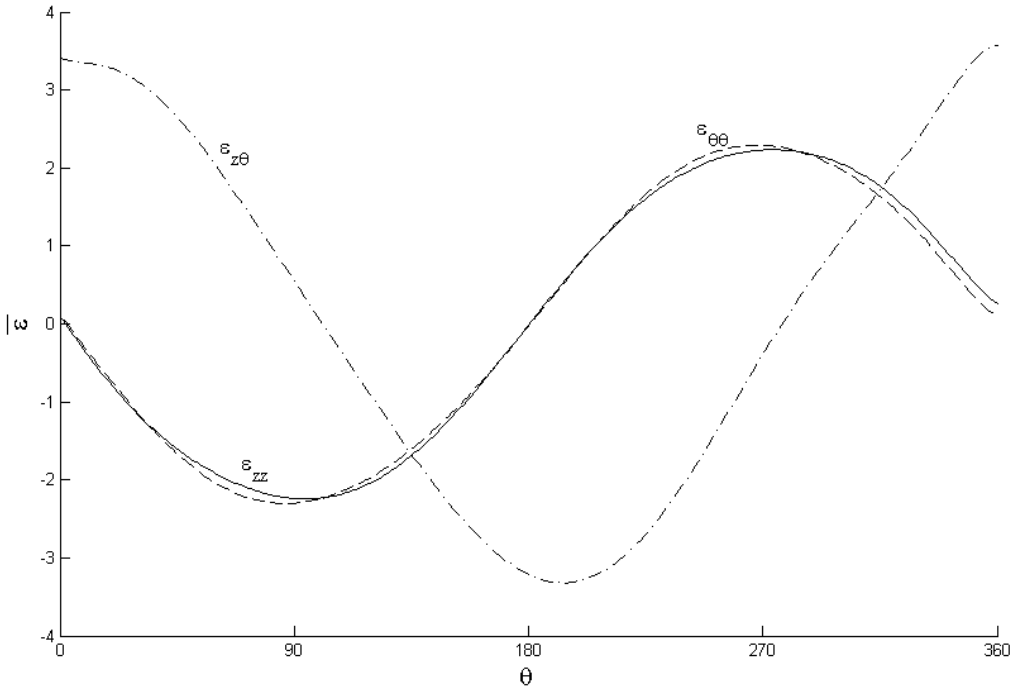

Figure 3.9a: Distribution of the strains at the 0°/90° interface of the [$0°_{55}/90°_{55}$] laminated straight tube at *x=a*.

The variations of the axial stress, σ_{xx}, and the shear stresses, σ_{xz} and $\sigma_{x\theta}$, at the 0°/90° interface of the [$0°_{55}/90°_{55}$] composite tube, in whole tube cross section with respect to θ are shown in Figure 3.8. It is observed that the magnitude of the axial stress, σ_{xx}, is greater than those of shear stresses σ_{xz} and $\sigma_{x\theta}$. It is further observed that whereas the sign of shear stresses, σ_{xz} and $\sigma_{x\theta}$, is changed in the half upper region (0°-180°), the axial stress, σ_{xx}, retains its sign in this region.

The variations of the strains ε_{zz}, $\varepsilon_{z\theta}$ and $\varepsilon_{\theta\theta}$ at the 0°/90° interface of the [$0°_{55}/90°_{55}$] cantilever laminated orthotropic tube are displayed in Figure 3.9a. It is seen that the strains, $\varepsilon_{z\theta}$ and $\varepsilon_{\theta\theta}$, have the same trend in the tube cross section. It is also observed that the shear strain, $\varepsilon_{z\theta}$, decreases toward θ=90° and increases toward θ=180° at the upper region of the tube cross section. Figures 3.9b, 3.9c and 3.9d represent the distribution of the radial, ε_{zz}, hoop, $\varepsilon_{\theta\theta}$, and shear strains, $\varepsilon_{z\theta}$, at three different sections (*x=50 mm, x= 202.5 mm and x=355 mm*), respectively. It is seen that the values of all strains at *x=355 mm* are less than those at the

other cross sections (*x= 50 mm and x=202.5 mm*). However, the increase rates of these strains are different. The hoop strain, $\varepsilon_{\theta\theta}$, increases more than the other strains and the shear strain, $\varepsilon_{z\theta}$, increases less than the others at *x=50 mm* while the shear strain, $\varepsilon_{z\theta}$, decreases less than the other strains at *x=355 mm* and the hoop strain, $\varepsilon_{\theta\theta}$, decreases more than the others at *x=355 mm*.

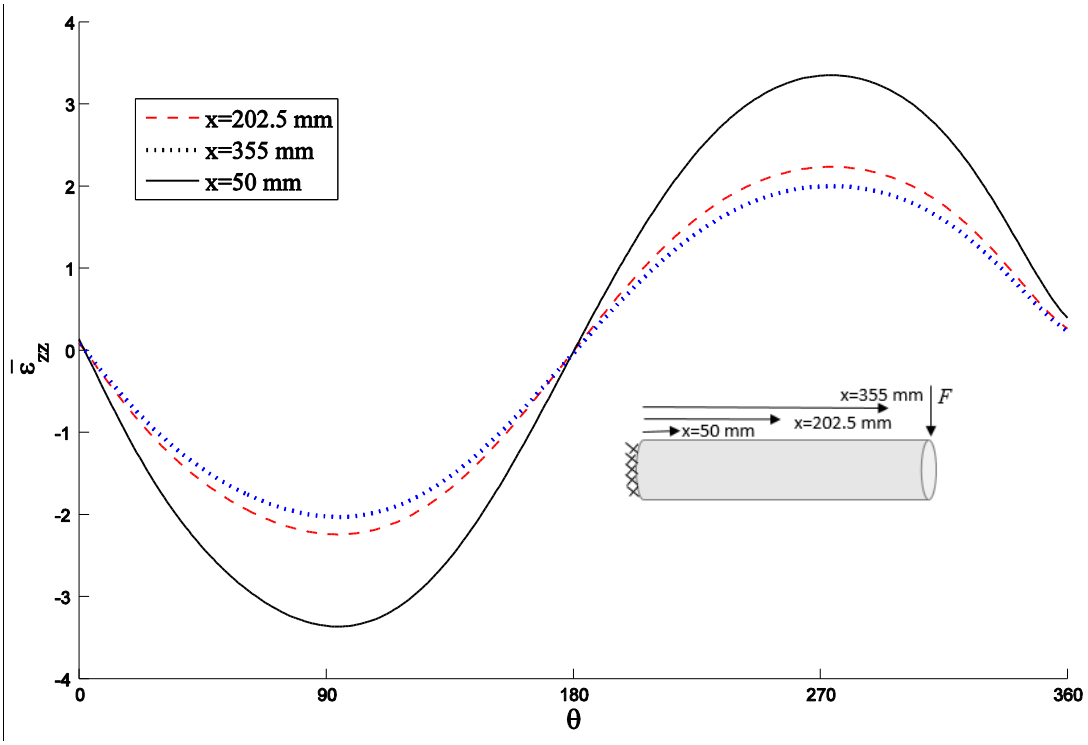

Figure 3.9b: Distribution of the radial strain, ε_{zz}, at the 0°/90° interface of the $[0°_{55}/90°_{55}]$ laminated straight tube at different cross sections.

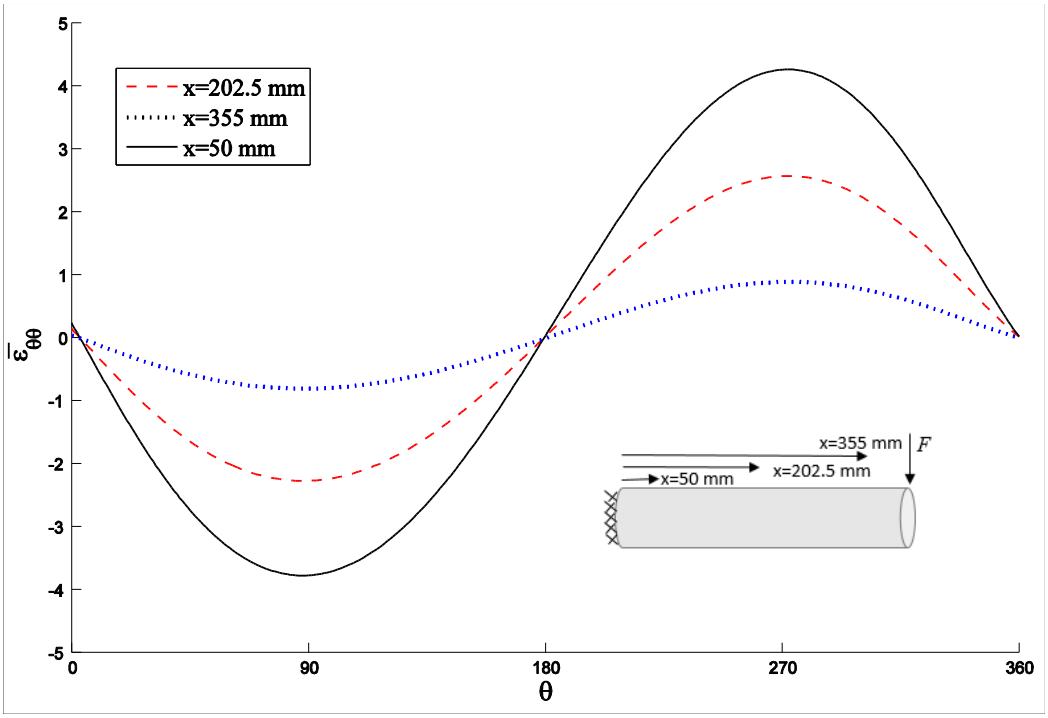

Figure 3.9c: Distribution of the hoop strain, $\varepsilon_{\theta\theta}$, at the 0°/90° interface of the $[0°_{55}/90°_{55}]$ laminated straight tube at different cross sections.

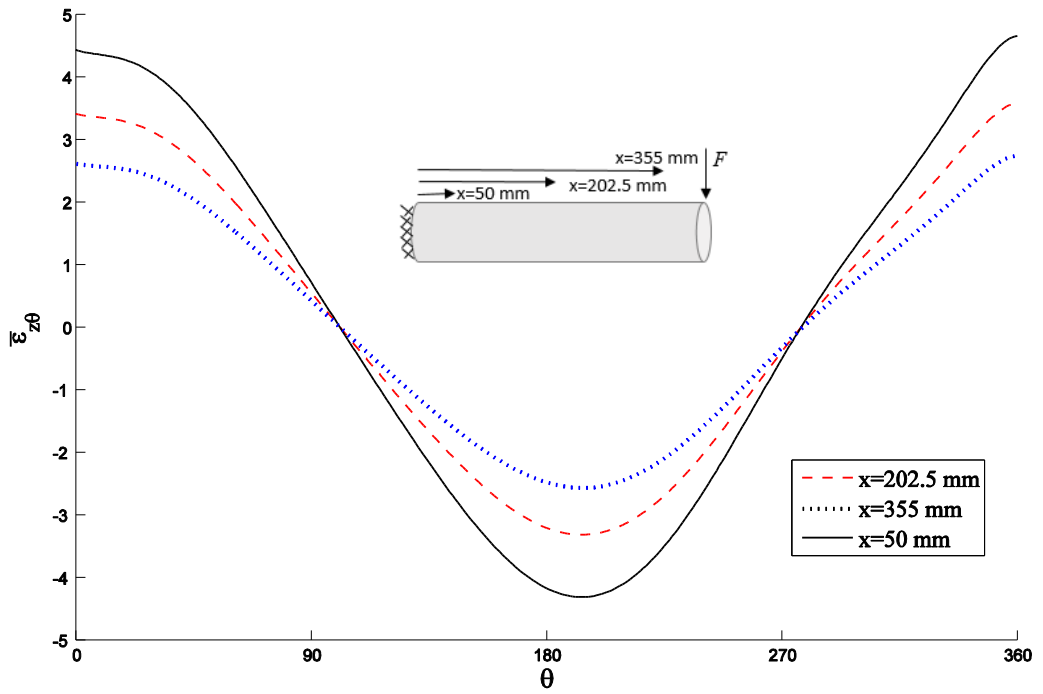

Figure 3.9d: Distribution of the shear strain, $\varepsilon_{z\theta}$, at the 0°/90° interface of the $[0°_{55}/90°_{55}]$ laminated straight tube at different cross sections.

Figure 3.10 presents the variation of strains, ε_{xx}, $\varepsilon_{x\theta}$ and ε_{xx}, at the 0°/90° interface of the $[0°_{55}/90°_{55}]$ cantilever laminated orthotropic tube. The strains depend on distance from neutral axis. It is also observed that the maximum positive value of ε_{xx} occurs at θ=90°, while the maximum positive value of $\varepsilon_{x\theta}$ occurs at θ=180° of the composite tube cross section.

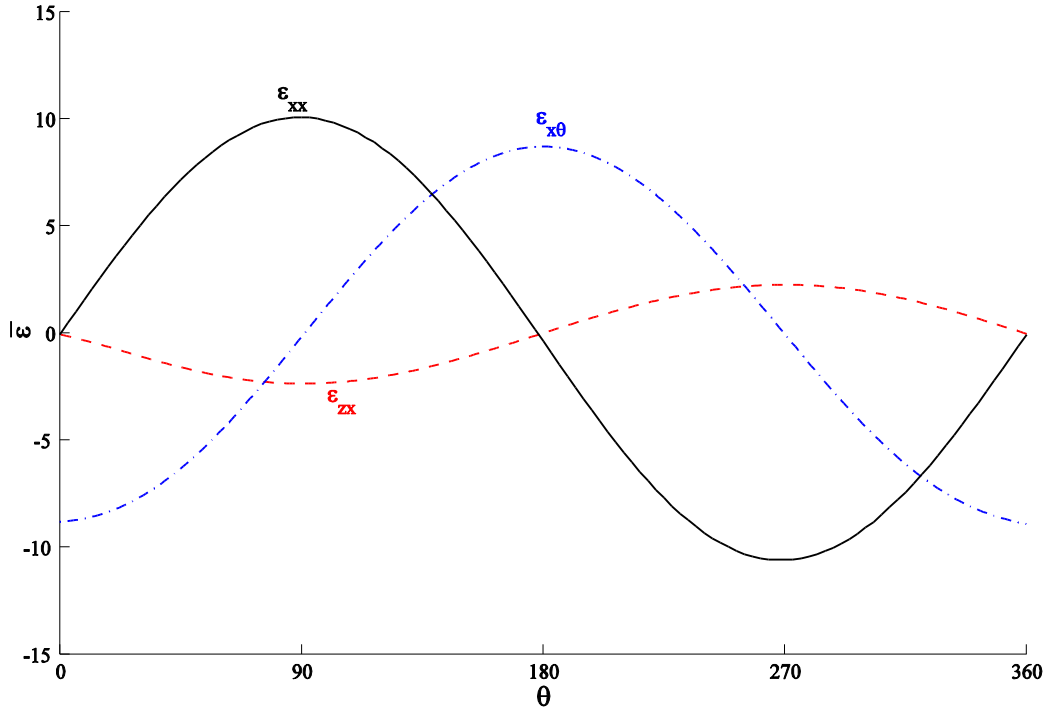

Figure 3.10: Distribution of the strains at the 0°/90° interface of the $[0°_{55}/90°_{55}]$ laminated straight tube at $x=a$.

3.7. Conclusions

The high-order simple-input displacement-based method was developed to investigate stresses and strains in thick laminated orthotropic cantilever straight tubes subjected to transverse loading. The most general form of the displacement field in laminated orthotropic cylindrical straight tubes was derived from the displacement-strain relations. LWT was then employed to analytically determine the displacement components. The equilibrium equations of LWT were subsequently solved through a state-space approach. Moreover, the accuracy of the stresses was examined by comparing the experimental results and those obtained by the proposed method. The numerical results showed good agreement between the present method with the experimental results, FEM and Lekhnitskii solution. Furthermore, the present method

was found to be more cost effective and accurate; therefore, it was employed to obtain the stresses and strains instead of using FEM. In the numerical study, various composite tubes were discussed to illustrate stress and strain distributions in the tube cross section. In addition, the stresses and strains were investigated at different cross sections and for different applied force values.

Chapter 4

In this chapter, by using the new simple-input displacement-based method developed in the previous chapter, the behavior of stress distributions in thick laminated composite straight tubes with different lay-up sequences considering effects of the shear load part of the cantilever loading condition is studied. Knowledge is extracted from the parametric study showing effects of the orientations of different layers on stresses.

Effects of Shear Loading on Stress Distributions at Sections in Thick Composite Tubes

Hamidreza Yazdani Sarvestani, Suong V. Hoa and Mehdi Hojjati

Department of Mechanical and Industrial Engineering, Concordia University, Montreal, Canada H3G 1M8

Abstract

In the previous study [92], the new simple-input displacement-based method (based on layer-wise formulation) was developed for the stress analysis of thick laminated composite straight tubes subjected to cantilever loading. This method provides a quick, convenient and accurate solution for the determination of 3D stresses in thick composite tubes subjected to both bending and shear loading. The technique in this method is now used to study the behavior of stress distributions in thick composite straight tubes with different lay-up sequences considering effects of the shear load part of cantilever loading. Knowledge is extracted from the parametric study showing effects of the orientations of different layers on the stresses.

Keywords: Shear load; Lay-up sequences; Thick composite cantilever straight tubes; Stress distribution; General displacement field.

4.1. Introduction

Composites have many applications due to the properties, which they provide with the essential advantages over other materials. In many examples, composite materials are the correct answer if designed, manufactured and used properly. Composites have specific advantages in many areas when their properties are designed into the ultimate product. The important thing is to use composite materials' uniqueness to get the best designs. However, over the years it has been learned that using composites for efficient structural parts requires

composites to be designed and manufactured with sound engineering judgment. One type of composite structures is a straight tube, which is frequently used in many engineering applications. In order to develop design guidelines, understanding effects of lay-up sequences on stresses, strains and deformations of composite straight tubes is essential.

Mackerle [31] reported a recent comprehensive review of finite element formulations for tubes. A nonlinear thick composite shell element was proposed to impose a cubic spline function on the thickness deformation [32]. Hamdallah and Engblom [33] developed a finite element formulation to analyze laminated circular cylindrical shells with both clamped and simply supported ends in order to observe effects of transverse interlaminar shear and normal stresses. An elasticity solution was obtained to investigate buckling of orthotropic cylindrical shells subjected to external pressure [5]. Lekhnitskii [2] has provided elasticity solutions for monolithic homogeneous orthotropic cylindrical shells. Miki and Sugiyama [6] proposed a method to optimum designs for required in-plane stiffness, maximum bending stiffness, buckling strength, and natural frequency of laminated plates by using the lamination parameters as fundamental design variables. Another investigation was performed for linear analysis of thick laminated anisotropic curved panels by using an improved finite element model [34]. Silvestre [18] proposed a beam theory to study the effect of non-classical consequences on the structural behavior of FRP composite circular hollow section members. By using the third-order shear deformation theory of Reddy with a meshless numerical method, the deformation of composite plates and shells was analyzed statically [36]. They also utilized an optimization technique to obtain the shape parameters. IJsselmuiden et al. [17] used Tsai-Wu failure criterion into the lamination parameter design space in the most general setting to derive a conservative failure envelope that guarantees a failure-free region of the lamination parameter space. A multi-step framework for design of composite panel was presented by using a guide-based genetic algorithm to avoid lay-up sequence mismatch [19]. Jolicoeur and Cardou [9] developed a general analytical solution for stresses and displacements of a composite cylinder subjected to bending, tensile and torsion loads. Shadmehri et al. [22] developed theoretical formulations by using a three-dimensional laminate theory to obtain the stiffness of composite tubes. They compared theoretical formulation and experimental results. The mechanical behavior of straight tubes subjected to bending was examined. Derisi et al. [21] found that the absorption of energy for composite

straight tubes upon fracture depended on the strategic placement of layers along the thickness direction. By using the Taylor series of expansion, a limit-based approach was presented to study stresses of composite tubes under bending moment [38]. The stress analysis of hollow composite cylindrical structures subjected to different loads was performed by Sun et al. [25]. Their method was efficient for thin hollow composite tubes. Bai et al. [39] investigated mechanical behavior of thermoplastic tubes under combined bending and tension based on the nonlinear ring theory. They verified formulations with FEM results obtained using ABAQUS. Menshykova and Guz [26] performed a stress analysis on thick laminated composite tubes subjected to bending loading. They found stresses as a function of the material properties, thickness, lay-up and the magnitude of bending load. Capela et al. [27] investigated the fatigue behavior of composite tubes under bending/torsion dynamic loadings. Recently, static analysis of carbon nanotube-reinforced composite cylinder under thermo-mechanical was studied using Mori-Tanaka theory [28]. A method was developed to analyze the pure bending of arbitrary laminated composite tubes. They used NASTRAN to compare with theoretical results [24].

Even though many works have been carried out for analyzing and designing composite tubes, no work has been found to provide a simple analytical method to develop design guidelines for lay-up sequences of thick composite tubes considering the effects of shear load part of cantilever loading at tube sections (*i.e.,* combined bending and shear loads). Although finite element methods are used, it is necessary to do the meshing for each structure every time some dimensions and/or lay-up sequences are changed. Therefore, it is desired to have a method where inputs to obtain the solution are simple. Recently, a method focused on the development of a simple-input analytical method to analyze stress distributions of the composite cantilever straight tube was developed [92]. This method is now used to examine effects of shear on the stress distributions at tube sections in thick composite cantilever tubes. The advantage of this method is simple-input as compared to elaborate-input as in FEM. Finally, effects of lay-up sequences of laminated composite straight tubes on stress distributions are discussed through a number of numerical results.

4.2. Motivation

In an effort to develop thermoplastic composite tubes for helicopter landing gears [1], Derisi designed and manufactured composite straight tubes and performed three-point bending tests to determine the strains to failure of different balanced laminates. These tubes are relatively thick (more than 100 layers giving thickness of more than 11 mm). Derisi used a procedure called strain-controlled design and based on that, lay-up sequences for composite tubes were developed. This procedure paid particular attention to the strain limit in each of the layer, in order to provide maximum flexibility for the tube, while maintaining good stiffness and strength. However, rigorous analytical techniques for the determination of stresses, strains and deformations are not available. Subsequently, different methods have been developed for the stress, strain and deformation for thick composite tubes subjected to pure bending [24, 38]. Recently, a simple method for the stress analysis of thick composite tubes subjected to cantilever loading (*i.e.,* combined bending and shear loads) was developed [92]. Due to the complexity of stress distributions in a thick composite tube, it is not easy to obtain some intuition as to the behavior of the tube under shearing load, for the purpose of design. In order to provide some insight into this behavior, the developed method is used for a parametric study. Systematic variation of lay-up sequences and effects of these lay-up sequences on the stress distributions have been examined. This chapter presents the knowledge obtained from this study.

4.3. Formulation

For completeness, a summary of the developed method is given below. More details are found in [92].

4.3.1. Elasticity Displacement Field

The general problem under study is a thick laminated orthotropic cantilever straight tube with mean radius R and thickness h subjected to the transverse loading F as shown in Figure 4.1a. The cylindrical coordinates (x, θ, r) are placed at the one of the tube's end so that x and r are the axial and radial coordinates, respectively. The appropriate integration of the linear

strain-displacement relations of elasticity, within cylindrical coordinate system will yield the following displacement field for the *k*th layer [92]:

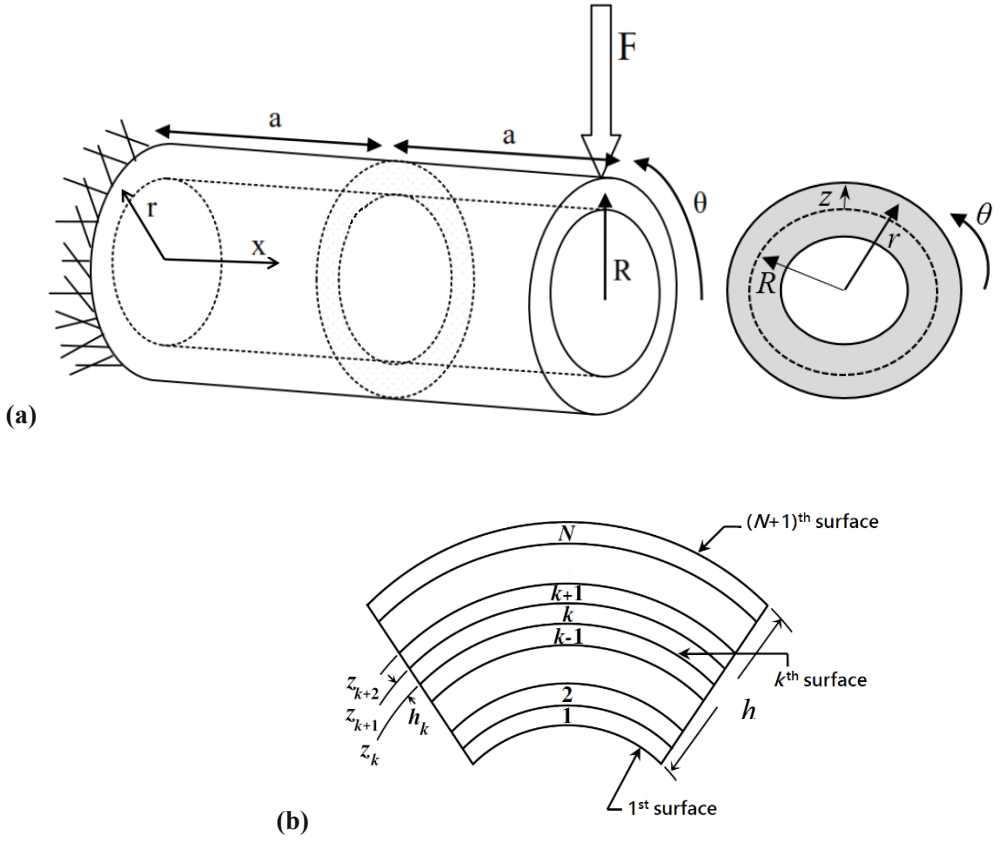

Figure 4.1: **(a)** The geometry of a straight tube and the coordinate system. **(b)** The ply sequencing in a laminated tube.

$$
\begin{aligned}
u_1^{(k)}(x,\theta,r) &= xr\left(C_5\cos\theta + C_4\sin\theta\right) + C_6 x + u^{(k)}(\theta,r) \\
u_2^{(k)}(x,\theta,r) &= x\left(C_1\cos\theta - C_2\sin\theta - C_3 r\right) - \frac{1}{2}x^2\left(C_4\cos\theta - C_5\sin\theta\right) + v^{(k)}(\theta,r) \\
u_3^{(k)}(x,\theta,r) &= x\left(C_1\sin\theta + C_2\cos\theta\right) - \frac{1}{2}x^2\left(C_5\cos\theta + C_4\sin\theta\right) + w^{(k)}(\theta,r)
\end{aligned}
\qquad (4.1)
$$

where $u_1^{(k)}(x,\theta,r)$, $u_2^{(k)}(x,\theta,r)$ and $u_3^{(k)}(x,\theta,r)$ represent the displacement components in the x, θ and r directions, respectively, of a material point located at (x, θ, r) in the *k*th ply of the laminated orthotropic tube as shown in Figure 4.1b.

4.3.2. Layer-wise Theory (LWT)

In the layer-wise theory (LWT), the displacement components of a generic point in the laminate are assumed as [53, 54]:

$$u_1(x,\theta,z) = u_k(x,\theta)\Phi_k(z)$$
$$u_2(x,\theta,z) = v_k(x,\theta)\Phi_k(z)$$
$$u_3(x,\theta,z) = w_k(x,\theta)\Phi_k(z) \qquad (k = 1,2,...,N+1) \qquad (4.2)$$

with k, here and in what follows, being a dummy index implying summation of terms from k=1 to k=N+1. In Eq. (4.2), u_1, u_2 and u_3 denote the total displacement components in the x, θ and z directions, respectively. Also, $u_k(x,\theta)$, $v_k(x,\theta)$ and $w_k(x,\theta)$ represent the displacements of the points initially located at the kth surface (defined by $z=z_k$, *see Figure 4.1b*) within the laminated composite straight tube in the x, θ and z directions, respectively. Furthermore, $\Phi_k(z)$ is the global Lagrangian interpolation function associated with the kth surface. Based on the elasticity displacement field in Eq. (4.1), the LWT displacement field in Eq. (4.2) is rewritten in a simpler form as:

$$u_1(x,\theta,z) = x(R+z)\left(C_5\cos\theta + C_4\sin\theta\right) + C_6 x + U_k(\theta)\Phi_k(z)$$
$$u_2(x,\theta,z) = x\left(C_1\cos\theta - C_2\sin\theta - C_3(R+z)\right) - \frac{1}{2}x^2\left(C_4\cos\theta - C_5\sin\theta\right) + V_k(\theta)\Phi_k(z)$$
$$u_3(x,\theta,z) = x\left(C_1\sin\theta + C_2\cos\theta\right) - \frac{1}{2}x^2\left(C_5\cos\theta + C_4\sin\theta\right) + W_k(\theta)\Phi_k(z) \qquad (4.3)$$

The equilibrium equations of a laminated composite straight tube with N numerical layers are obtained by employing strain-displacement relations in the principle of minimum total potential energy [89]. The results are, in general, *3(N+1)* local equilibrium equations corresponding to *3(N+1)* unknown functions U_k, V_k and W_k and six global equilibrium equations associated with the six parameters C_1, C_2, C_3, C_4, C_5 and C_6 derived as follow:

$$\delta U_k : Q_x^k - \frac{dM_{x\theta}^k}{d\theta} = 0$$
$$\delta V_k : Q_\theta^k - \frac{dM_\theta^k}{d\theta} - R_\theta^k = 0$$
$$\delta W_k : M_\theta^k - \frac{dR_\theta^k}{d\theta} + N_z^k = 0 \qquad (k = 1,2,...,N+1) \qquad (4.4)$$

$$\delta C_1 : \int_{-\pi}^{\pi}\int_{-h/2}^{+h/2} R\left(\sigma_{xz}\sin\theta+\sigma_{x\theta}\cos\theta\right)dzd\theta=0$$

$$\delta C_2 : \int_{-\pi}^{\pi}\int_{-h/2}^{+h/2} R\left(\sigma_{xz}\cos\theta-\sigma_{x\theta}\sin\theta\right)dzd\theta=0$$

$$\delta C_3 : \frac{1}{h}\int_{-\pi}^{\pi}\int_{-h/2}^{+h/2} R\sigma_{x\theta}\left(R+z\right)dzd\theta=-2F$$

$$\delta C_4 : \int_{-\pi}^{\pi}\int_{-h/2}^{+h/2} R\sigma_{x}\left(R+z\right)\sin\theta dzd\theta=0$$

$$\delta C_5 : \int_{-\pi}^{\pi}\int_{-h/2}^{+h/2} R\sigma_{x}\left(R+z\right)\cos\theta dzd\theta=0$$

$$\delta C_6 : \int_{-\pi}^{\pi}\int_{-h/2}^{+h/2} R\sigma_{x} dzd\theta=0 \qquad (4.5)$$

The following boundary conditions must be satisfied at the ends of the laminated straight tube:

$$R_\theta^k = Q_x^k = N_z^k = 0 \qquad \text{at}\left(\text{z}=\pm\text{h}/2\right) \qquad (4.6a)$$

$$u_1^{(k)} = u_2^{(k)} = u_3^{(k)} = 0 \qquad \text{at}\left(\text{x}=0\right) \qquad (4.6b)$$

Note that in Eq. (4.6), the superscript *k* refers to the *k*th surface in the laminated orthotropic tube. By substituting the strain-displacement relations into three-dimensional constitutive law, the stress resultants are obtained in terms of displacement functions. Then, the local displacement equilibrium equations within LWT are obtained merely by substituting displacement-based stress resultants into Eq. (4.4).

4.3.3. Analytical Solution

The system of displacement-based local equilibrium equations shows *3(N+1)* coupled ordinary differential equations with constant coefficients which may be displayed in a matrix form as:

$$[M]\{\eta''\}+[K]\{\eta\}=[F]\{C\} \tag{4.7}$$

where

$$\{\eta\}=\left\{\{U\}^T,\{V\}^T,\{\bar{W}\}^T\right\}^T, \qquad \{C\}=\{C_1 \quad C_2 \quad C_3 \quad C_4 \quad C_5 \quad C_6\}^T$$

$$\{U\}=\{U_1,U_2,...,U_{N+1}\}^T$$

$$\{V\}=\{V_1,V_2,...,V_{N+1}\}^T$$

$$\{\bar{W}\}=\{\bar{W}_1,\bar{W}_2,...,\bar{W}_{N+1}\}^T \tag{4.8a}$$

and

$$\bar{W}_j=\int^{\theta} W_j \mathrm{d}\theta \tag{4.8b}$$

It can readily be confirmed that the general solution of Eq. (4.7) may be presented as:

$$\{\eta\}=[\psi]\left[\sinh(\lambda\theta)\right]\{k\}+[K]^{-1}[F]\{C\} \tag{4.9}$$

and [sinh (λθ)] is a *3(N+1)*×*3(N+1)* diagonal matrix. That is:

$$\left[\sinh(\lambda\theta)\right]=diag\left(\sinh(\lambda_1\theta),\sinh(\lambda_2\theta),...,\sinh\left(\lambda_{3(N+1)}\theta\right)\right) \tag{4.10}$$

Also [ψ] and $\left(\lambda_1^2,\lambda_2^2,...,\lambda_{3(N+1)}^2\right)$ are the modal matrix and eigenvalues of (-[M]$^{-1}$[K]), respectively. Vector $\{k\}$ is an unknown vector representing *3(N+1)* integration constants. The constants *Cj* (*j*=1, 2, 3, 4, 5 and 6) must be calculated within LWT analysis. Therefore, the boundary conditions in Eq. (4.6) are first imposed to find the vector $\{k\}$ in terms of the unknown parameters *Cj*. These constants are next computed in terms of the specific shear force *F* by the satisfaction of the global equilibrium conditions in Eq. (4.5). The authors have developed the detailed procedures to obtain the solution in [92].

4.4. Obtaining Stresses for a Tube Subjected to Shear Loading

The thick composite straight tube as shown in Figure 4.1 is under cantilever loading. At any section of the tube, there is a shear load and a bending moment. In order to obtain the effect due to shear loading only, either one of the two following methods is used:

- Obtain the stress distribution at a section very close to the end of the tube (*i.e., x*≈*2a*). Since this section is close to the end of the tube, the bending moment is minimum.
- Obtain the stress distribution at a regular section (for example at *x*=*a*). The results are for the case where both bending moment and shear are involved. The results for the case of

pure bending moment are available using the method in reference [24]. The results from [24] with the same bending moment are subtracted from the results obtained using the developed method outlined in [92]. The difference should be the stresses due to the shear. In this following section, the results using both methods are obtained and compared.

Verifying the Proposed Method

Figure 4.2 presents the interlaminar stresses, $\bar{\sigma}_{zz}$ and $\bar{\sigma}_{z\theta}$ (*normalized refer to section 4.6*), of the $[\pm 30°]_{55}$ laminated orthotropic straight tube along the circumferential direction at *x=a, x≈2a* and *r=32.8 mm* for the case of cantilever loading and pure bending obtained by the present method and reference [24], respectively. Note that at *r=32.8 mm*, the magnitudes of the radial stresses are maximum. The solid lines show the stress distribution of the composite straight tube subjected to cantilever loading at *x=a*. Figure 4.2 also shows the stresses for the case of pure bending, using both methods of reference [92] (*dashed line*) and reference [24] (*points*). Good agreement is obtained. Results for the case of shear loading at tube sections are obtained using two methods. In method one, the results due to pure bending (*at x=a*) are subtracted from the results due to cantilever loading (*at x=a*). In method two, the results from cantilever loading (*at x≈2a*) are obtained. Good agreement is observed, as shown in Figure 4.2. Remark that the magnitudes of interlaminar stresses, $\bar{\sigma}_{zz}$ and $\bar{\sigma}_{z\theta}$, caused by the shear load are 0.12% to 0.15% of those obtained subjected to cantilever load for different lay-up sequences.

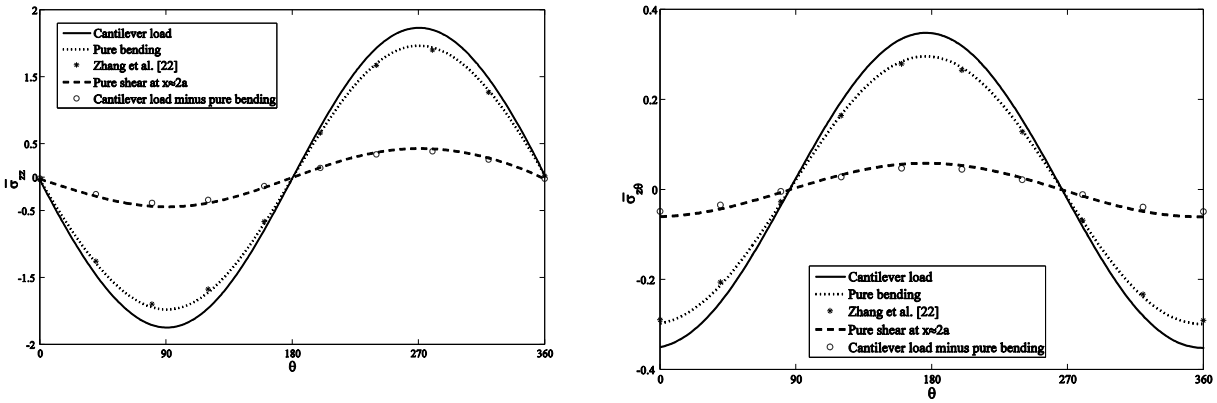

Figure 4.2: Comparison of interlaminar stresses obtained from the present method and another solution [24] of the $[\pm 30°]_{55}$ laminated straight tube at $x=a$, $x\approx 2a$ and $r=32.8$ *mm*. **(a)** Normal stress σ_{zz}, **(b)** Shear stress $\sigma_{z\theta}$.

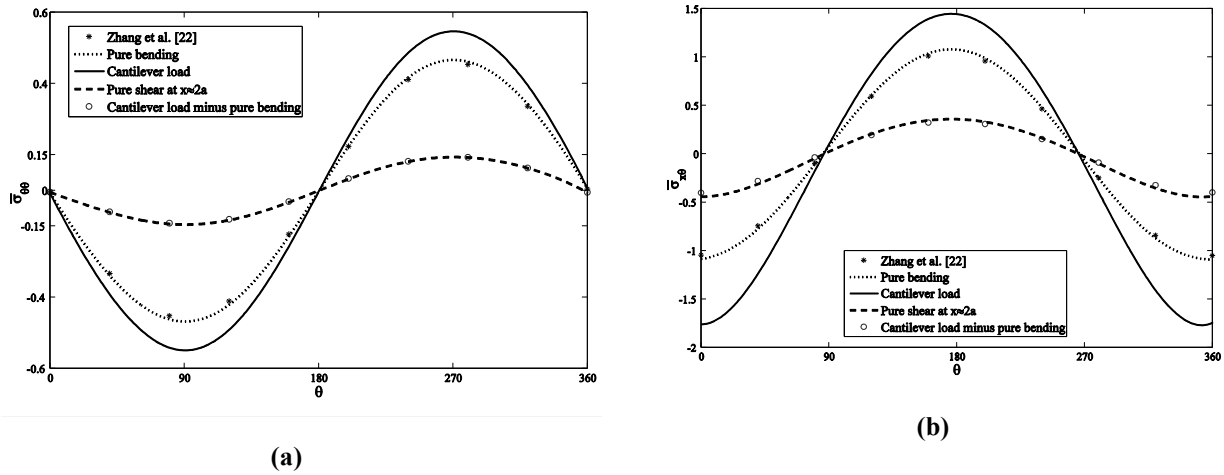

Figure 4.3: Comparison of stresses obtained from the present method and another solution [24] of the $[\pm 30°]_{55}$ laminated straight tube at $x=a$, $x\approx 2a$ and $r=28$ *mm*. **(a)** Hoop stress $\sigma_{\theta\theta}$, **(b)** Shear stress $\sigma_{x\theta}$.

Comparison of the hoop and shear stresses, $\bar{\sigma}_{\theta\theta}$ and $\bar{\sigma}_{x\theta}$, of the $[\pm 30°]_{55}$ laminated orthotropic straight tube along the circumferential direction at $x=a$, $x\approx 2a$ and $r=28$ *mm* obtained by the present method and another solution in [24] is shown in Figures 4.3a and 4.3b, respectively. Note that at $r=28$ *mm*, the magnitudes of the hoop and shear stresses are maximum. Similar agreement is obtained. The magnitudes of the hoop and shear stresses, $\bar{\sigma}_{\theta\theta}$ and $\bar{\sigma}_{x\theta}$, subjected to the shear load are 0.15% to 0.18% of those obtained subjected to cantilever load for different lay-up sequences. In addition, this range becomes 0.03% to 0.05% for the axial and shear stresses, σ_{xx} and σ_{zx}.

Another way to verify the proposed method is by checking Eq. (4.5). It is noted that the integration of the shear stress, $\sigma_{x\theta}$, on the whole cross section along the tube thickness is equal to total shear load, $-2F$. The tube cross section at $x\approx 2a$ is divided to 180 segments along the circumferential direction (*i.e.,* $rd\theta = 0.0349r$) and 110 segments along the thickness direction (*i.e.,* dr=0.1 mm) as shown schematically in Figure 4.4. The elements are assumed to be rectangle since they are small. The shear stresses, $\sigma_{x\theta}$, at all elements are known (calculated) and assumed to be constant. Integration their product with the element area (*i.e.,* $dr\times rd\theta$) on the whole elements in the tube cross section, the transverse loading is determined. This is

done numerically. For example, *F=5 N* is applied on the composite tube as shown in Figure 4.1. The shear stress is $\sigma_{x\theta}$=*6482 Pa* at *r=33.5 mm* and θ=180° obtained using the proposed method. By integrating elements over the whole section, the total shear load, 2*F= 9.84 N*, is calculated.

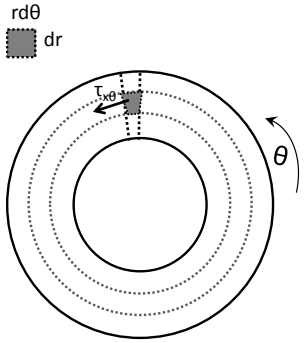

Figure 4.4: The tube cross section at *x≈2a* and one element.

4.5. Guidelines for the Parametric Study

As it is mentioned, Derisi [1] developed a lay-up sequence to be used for making composite landing gears for helicopters that may provide large deformation and gradual fracture. A composite straight tube with the $[(90°_{10}/0°_{10})_3/\pm45°_{25}]$ lay-up was manufactured and tested to study the behavior of orthotropic tubes subjected to bending load [1, 20]. In order to obtain generic knowledge from effects of the lay-up sequences, a systematic variation of the lay-up sequence is selected. Table 4.1 shows the different types of lay-up sequences considered. First, composite tubes with the lay-up sequences of the $[0°]_{110}$ and $[90°]_{110}$ tubes are examined. The number 110 is obtained based on the availability of experimental data for tubes with 110 layers [1, 20], for comparison purpose. Subsequently, composite tubes with lay-up sequences of the $[\theta°_{55}/-\theta°_{55}]$ and $[\pm\theta°]_{55}$ tubes with θ° having the values of 25°, 30°, 45° and 60° are studied. Finally, lay-up sequences of the $[90°_m/0°_m/(\pm\theta°)_k]$ tube are examined, where *m* and *k* take up different numbers and as shown in Table 4.1, and with θ° having the values of 25°, 30°, 45° and 60°.

Table 4.1: Lay-up sequence number.

Laminate number	Lay-up sequence	Laminate number	Lay-up sequence
1	$[0°]_{110}$	5	$[0°_n/(\pm\theta°)_k]$ $\theta = 25°, 30°, 45°$ and $60°$
2	$[90°]_{110}$	6	$[90°_m/(\pm\theta°)_k]$ $\theta = 25°, 30°, 45°$ and $60°$
3	$[\theta°_{55}/-\theta°_{55}]$ $\theta = 25°, 30°, 45°$ and $60°$	7	$[90°_m/0°_m/(\pm\theta°)_k]$ $\theta = 25°, 30°, 45°$ and $60°$
4	$[\pm\theta°]_{55}$ $\theta = 25°, 30°, 45°$ and $60°$	8	$[(90°_m/0°_m)_l/(\pm\theta°)_k]$ $\theta = 25°, 30°, 45°$ and $60°$

4.6. Results and Discussion

All physical laminates are assumed to have equal thickness (=0.1 mm [1]) and are modeled as being made up of *p* numerical layers. In all the subsequent calculations, *p* is set equal to 12 [92]. The on-axis mechanical properties of the composite tube are given in Table 4.2.

Table 4.2: Mechanical properties of the manufactured composite tube [1, 20].

Properties	E_1 (GPa)	$E_2=E_3$ (GPa)	$G_{12}=G_{13}=G_{23}$ (GPa)	$\upsilon_{12}=\upsilon_{13}$	υ_{23}
Carbon AS4/PEKK	140	10	5.56	0.31	0.33

It is noted that the axial stress, σ_{xx}, is estimated with a simple calculation; therefore, only the interlaminar radial and shear stresses (*i.e.*, σ_{zz}, σ_{xz} and $\sigma_{\theta z}$) are examined. In addition, the hoop stress, $\sigma_{\theta\theta}$, is selected to study. The hoop stress could show any significant variation along the circumferential direction and the radial stress could cause delamination between the layers. Although radial stresses show smaller values than the others do, they are important because they are out-of-plane and note that out-of-plane strengths are small for composite straight tubes. Furthermore, the stress components are normalized as $\bar{\sigma}_{ij}=\sigma_{ij}/\sigma_0$ where $\sigma_0=(F.x.r)/(\pi/64*(OD^4-ID^4))$ with the outer diameter *OD* and the inner diameter *ID* of the composite tube. In the present cases, the tube section has an internal diameter of 56 mm and an external diameter of 78 mm, i.e. a wall thickness of 11 mm. Also, the length of the composite tube is 405 mm [1]. Therefore, for this case $\sigma_0=(F.x.r)\times 7.5\times 10^5$. Assume $F=10\ N$, $x=405\ mm$ (mid length) and $r=33.5\ mm$ (mid thickness), $\sigma_0 = 0.1\ MPa$.

4.6.1. Simple Lay-ups (laminate numbers of 1, 2, 3 and 4)

In this part, effects of the shear load at tube sections with the consideration of different lay-up sequences on stress distributions of the orthotropic cantilever straight tube are studied. The $[0°]_{110}$, $[90°]_{110}$, $[\theta°_{55}/-\theta°_{55}]$ and $[\pm\theta°]_{55}$ tubes which have 110 layers in total are selected to study. The angle-plies of 25°, 30°, 45° and 60° are considered. The results are discussed based on the proposed method at $x \approx 2a$ (*i.e.,* shear load).

Figure 4.5 shows the comparison of the interlaminar radial stress, $\bar{\sigma}_{zz}$, of the $[0°]_{110}$, $[90°]_{110}$, $[\pm25°]_{55}$, $[\pm30°]_{55}$, $[\pm45°]_{55}$ and $[\pm60°]_{55}$ laminated orthotropic straight tubes at $x \approx 2a$ and $\theta=90°$ along the tube thickness. The followings are observed:

- The $[90°]_{110}$ tube shows minimum magnitude of the radial stress, while the $[0°]_{110}$ tube shows maximum magnitude of the radial stress.
- The magnitude of the radial stress of the $[\pm25°]_{55}$ tube is greater than those of the other $[\pm\theta°]_{55}$ tubes. In addition, the radial stress, $\bar{\sigma}_{zz}$, of all tubes are negative at $\theta=90°$ of cross section. The maximum positive value of $\bar{\sigma}_{zz}$ of the $[\pm\theta°]_{55}$ tube occurs at $\theta=270°$ (compression zone, *see Figure* 4.*2a*). Note that the positive radial stress, $\bar{\sigma}_{zz}$, could cause delamination failure in the composite tube.
- The maximum magnitude of the radial stress of the $[0°]_{110}$ tube occurs at $z_{max}=-0.7$ *mm* (*i.e., layer 48*, *see Figure* 4.*5*) which is *0.44* (*i.e., 48/110*) of the total thickness.
- Radial stresses have the same trend for all lay-up sequences.
- The location of the maximum magnitude of the radial stress (r_{max}) in the $[\pm\theta°]_k$ tubes is studied for all cases (*different values for θ*). It is observed that it occurs at 0.44 of the total thickness which is $r_{max}=0.44(2kt)+r_i$, where *t* is the thickness of a ply.
- The shape of the stress curves is parabolic.

Figure 4.6 illustrates the comparison of the interlaminar radial stress, $\bar{\sigma}_{zz}$, of the $[25°_{55}/-25°_{55}]$, $[30°_{55}/-30°_{55}]$, $[45°_{55}/-45°_{55}]$ and $[60°_{55}/-60°_{55}]$ laminated cantilever straight tubes at $x \approx 2a$ and $\theta=90°$ along the tube thickness. The followings are observed:

- The magnitude of the radial stress, $\bar{\sigma}_{zz}$, of the $[25°_{55}/-25°_{55}]$ tube is greater than those of the other lay-up sequences.

- Comparison of Figure 4.5 with Figure 4.6 shows that the magnitudes of the interlaminar radial stress, $\bar{\sigma}_{zz}$, of the $[\pm\theta°]_{55}$ tubes are greater than those of the $[\theta°_{55}/-\theta°_{55}]$ tubes.
- The maximum magnitude of the radial stress in the $[25°_{55}/-25°_{55}]$ tube occurs at z_{max}=*-2.4 mm* (*i.e., layer 31*, *see Figure 4.6*) which is *0.56* (*i.e., 31/55*) of thickness of the θ° part.
- Radial stresses have the same trend for all lay-up sequences.
- The location of the maximum magnitude of the radial stress (r_{max}) in the $[\theta°_k/-\theta°_k]$ tubes is investigated for all cases (*different values for θ*). It is seen that it occurs at 0.56 of the thickness of the θ° part which is $r_{max}=0.56(kt)+r_i$, where *t* is the thickness of a ply.

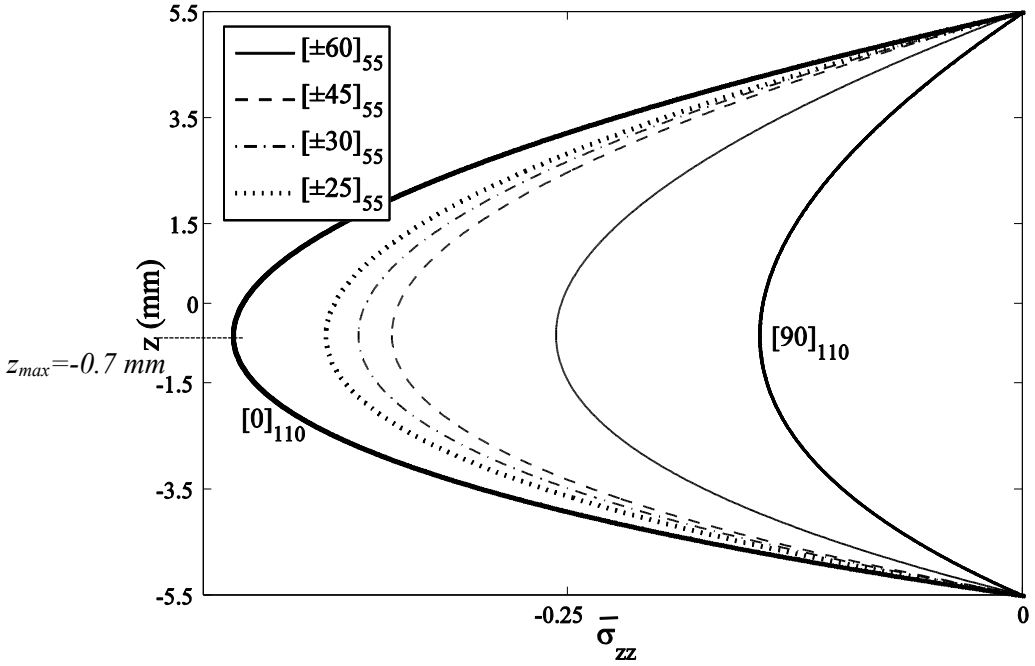

Figure 4.5: Comparison of the radial stress σ_{zz} of the $[0°]_{110}$, $[90°]_{110}$, $[\pm25°]_{55}$, $[\pm30°]_{55}$, $[\pm45°]_{55}$ and $[\pm60°]_{55}$ laminated cantilever straight tubes at $x\approx2a$ and θ=90° along the tube thickness (subjected to shear load *F*).

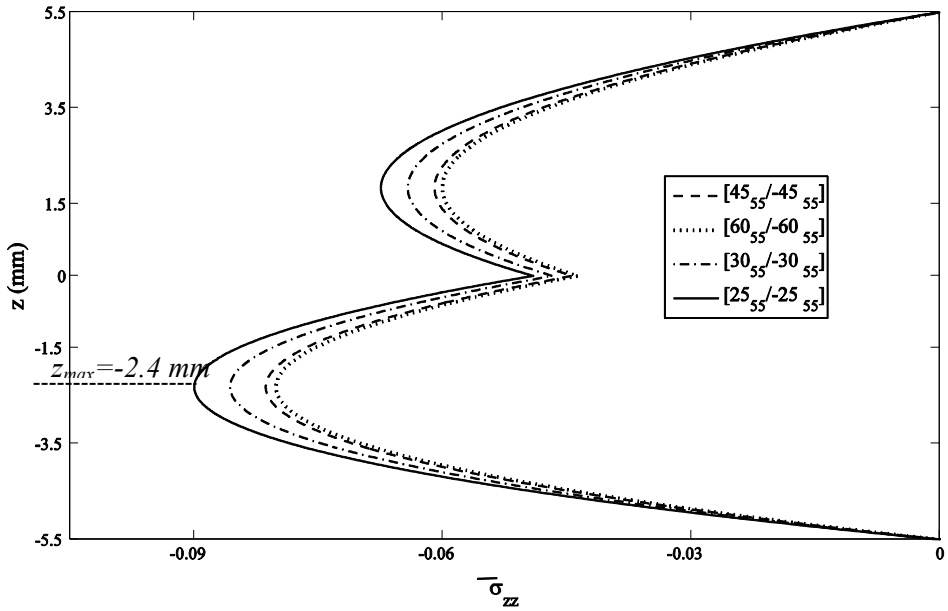

Figure 4.6: Comparison of the radial stress σ_{zz} of the [25°$_{55}$/-25°$_{55}$], [30°$_{55}$/-30°$_{55}$], [45°$_{55}$/-45°$_{55}$] and [60°$_{55}$/-60°$_{55}$] laminated cantilever straight tubes at $x \approx 2a$ and θ=90° along the tube thickness (subjected to shear load F).

To provide a reason why the magnitude of the interlaminar radial stress of the [0°]$_{110}$ tube is greater than those of the other tubes as observed in Figure 4.5, the formula for obtaining the radial stress of kth ply is reinvestigated as [92]:

$$\sigma_{zz}^{(k)} = \bar{C}_{13}^{(k)}\varepsilon_{xx}^{(k)} + \bar{C}_{23}^{(k)}\varepsilon_{\theta\theta}^{(k)} + \bar{C}_{33}^{(k)}\varepsilon_{zz}^{(k)} + \bar{C}_{36}^{(k)}\gamma_{x\theta}^{(k)} \tag{4.11}$$

The comparison of strains ε_{zz}, ε_{xx} and $\varepsilon_{\theta\theta}$ of the [±30°]$_{55}$ laminated orthotropic straight tube along the circumferential direction at $x \approx 2a$ and $r=32.8$ *mm* is displayed in Figure 4.7.

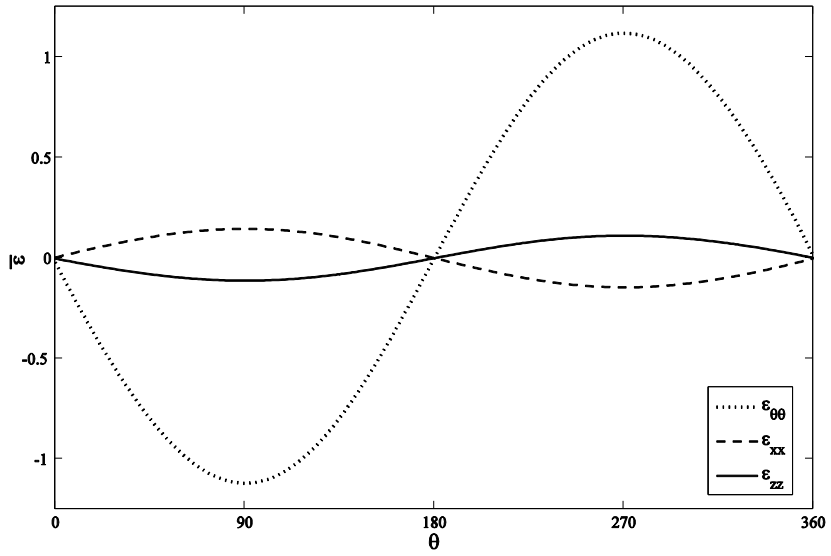

Figure 4.7: Comparison of strains ε_{zz}, ε_{xx} and $\varepsilon_{\theta\theta}$ of the $[\pm 30°]_{55}$ laminated orthotropic straight tube along the circumferential direction at $x \approx 2a$ and $r=32.8$ *mm* (subjected to shear load F).

As seen in Figure 4.7, the magnitudes of ε_{zz} and ε_{xx} are much less than that of $\varepsilon_{\theta\theta}$ for the case of shear load. Considering that $\bar{C}_{33}^{(k)}$ is same for all lay-up sequences, and at θ=90°, $\gamma_{x\theta}^{(k)}=0$; $\bar{C}_{13}^{(k)}\varepsilon_{xx}^{(k)}+\bar{C}_{33}^{(k)}\varepsilon_{zz}^{(k)}+\bar{C}_{36}^{(k)}\gamma_{x\theta}^{(k)}$ is neglected in calculating the radial stress, σ_{zz}. Consequently, the radial stress is compared for different lay-up sequences based on the following formula:

$$\sigma_{zz}^{(k)} \approx \bar{C}_{\quad}^{(k)}\varepsilon_{\quad}^{(k)} \qquad (4.12)$$

Based on Eq. (4.12), $\varepsilon_{\theta\theta}$ is dominant in the radial stress for the case of shear load. For example, the radial stress of the $[0°]_{55}$ tube is greater than that of the $[90°]_{55}$ tube (*see Figure 4.5*). That is because $\varepsilon_{\theta\theta}^{(k)}$ for the $[0°]_{55}$ tube is larger than $\varepsilon_{\theta\theta}^{(k)}$ for the $[90°]_{55}$ tube.

Comparison of the hoop stresses, $\bar{\sigma}_{\theta\theta}$, of the $[0°]_{110}$, $[90°]_{110}$, $[\pm 25°]_{55}$, $[\pm 30°]_{55}$, $[\pm 45°]_{55}$ and $[\pm 60°]_{55}$ laminated cantilever straight tubes at $x \approx 2a$ and θ=90° along the tube thickness is shown in Figure 4.8. The followings are observed:

- The hoop stress, $\bar{\sigma}_{\theta\theta}$, is 0 at $z=0.5$ *mm* which is *layer 60* (*5 layers upper mid-thickness*). The hoop stress varies linearly across the thickness of the laminate making up the wall of the tube.

- The $[0°]_{110}$ tube shows the minimum hoop stress while the $[90°]_{110}$ tube shows the maximum hoop stress.
- The magnitude of the hoop stress of the $[\pm 60°]_{55}$ tube is greater than those of the other lay-up sequences. This is explained by the fact that for composite tubes, 90° layers play the roles that enhance the hoop strength of the tube. Layers with fiber orientations closer to 90° would bear more loads, and as such would have higher hoop stress.
- At a certain radial location, the hoop stress sign of the $[90°]_{110}$ tube is opposite of those of the $[\pm\theta°]_{55}$ tubes.
- The maximum positive of the hoop stress in the $[\pm\theta°]_{55}$ tubes happens at θ=270° (*see Figure 4.3a*). The magnitude of the hoop stress increases with moving from the mid-thickness toward the outside surface of the composite tube for all lay-up sequences.
- The maximum positive of the hoop stress in the $[\pm\theta°]_k$ tubes occurs at the outside surface while the maximum negative of the hoop stress occurs at the inside surface.

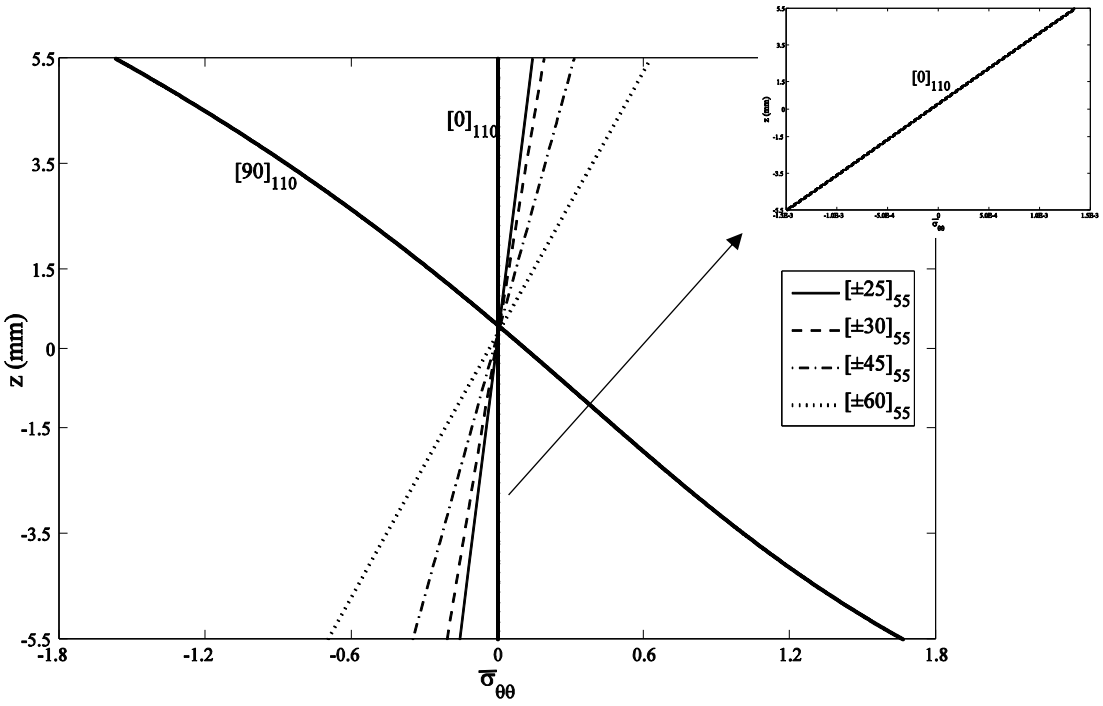

Figure 4.8: Comparison of the hoop stress $\sigma_{\theta\theta}$ of the $[0°]_{110}$, $[90°]_{110}$, $[\pm 25°]_{55}$, $[\pm 30°]_{55}$, $[\pm 45°]_{55}$ and $[\pm 60°]_{55}$ laminated cantilever straight tubes at $x \approx 2a$ and θ=90° along the tube thickness (subjected to shear load F).

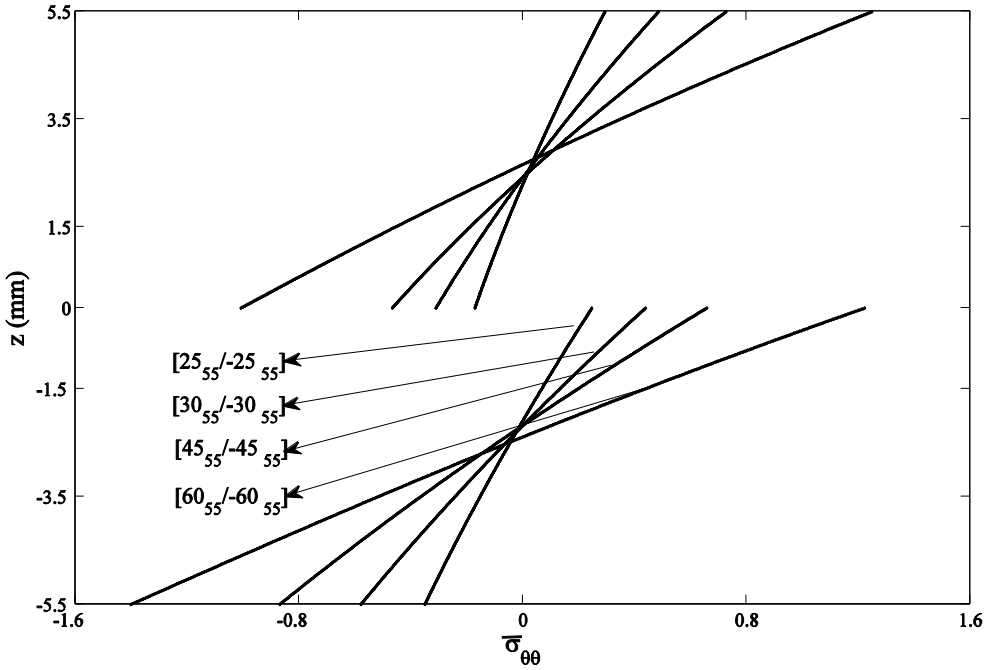

Figure 4.9: Comparison of the hoop stress $\sigma_{\theta\theta}$ of the [25°$_{55}$/-25°$_{55}$], [30°$_{55}$/-30°$_{55}$], [45°$_{55}$/-45°$_{55}$] and [60°$_{55}$/-60°$_{55}$] laminated cantilever straight tubes at $x \approx 2a$ and θ=90° along the tube thickness (subjected to shear load F).

Figure 4.9 presents the comparison of the hoop stress, $\bar{\sigma}_{\theta\theta}$, of the [25°$_{55}$/-25°$_{55}$], [30°$_{55}$/-30°$_{55}$], [45°$_{55}$/-45°$_{55}$] and [60°$_{55}$/-60°$_{55}$] laminated cantilever straight tubes at $x \approx 2a$ and θ=90° along the tube thickness. The followings are observed:

- The magnitude of the hoop stress, $\bar{\sigma}_{\theta\theta}$, of the [60°$_{55}$/-60°$_{55}$] tube is greater than those of the other lay-up sequences. It is seen that the θ° part of lay-up sequence has the same trend as -θ° part. The explanation is similar to that give for the behavior in Figure 4.7.
- The hoop stresses for the inner block of layers are 0 at the mid-thickness of this block. The hoop stress distribution is linear within the block.
- The hoop stresses for the outer block have the same value (not 0) at mid-thickness of the block. The hoop stress distribution is linear within the block.
- There is a discontinuity of the stress distribution at the interface between the two blocks of layers.
- The maximum positive of the hoop stress in the [θ°$_k$/-θ°$_k$] tubes occurs at the largest-diameter θ° part and the outside surface while the maximum negative of the hoop stress occurs at the inside surface of the tube.

Comparison of the shear stress, $\bar{\sigma}_{z\theta}$, of the $[\pm\theta°]_{55}$ and $[\theta°_{55}/-\theta°_{55}]$ (for θ = 25°, 30°, 45° and 60°) laminated orthotropic straight tubes at $x \approx 2a$ and θ=0° along the tube thickness is shown in Figures 4.10a and 4.10b, respectively. The shear stress, $\bar{\sigma}_{z\theta}$, could cause the movement of the layers on each other in the hoop direction of the laminated composite tube. The followings are observed:

- The magnitudes of the shear stress increase monotonically from the $[\pm60°]_{55}$ tube to the $[\pm25°]_{55}$ tube.
- The magnitudes of the shear stress increase monotonically from the $[60°_{55}/-60°_{55}]$ tube to the $[25°_{55}/-25°_{55}]$ tube.
- Note that the maximum shear stresses, $\bar{\sigma}_{z\theta}$, of the $[\pm\theta°]_{55}$ and $[\theta°_{55}/-\theta°_{55}]$ tubes occur at the same locations as the maximum normal stresses, σ_{zz} (*see Figure 4.5*).
- The maximum value for each curve moves toward the inside of the tube as the fiber angle increases from $[\pm25°]_{55}$ to $[\pm60°]_{55}$.

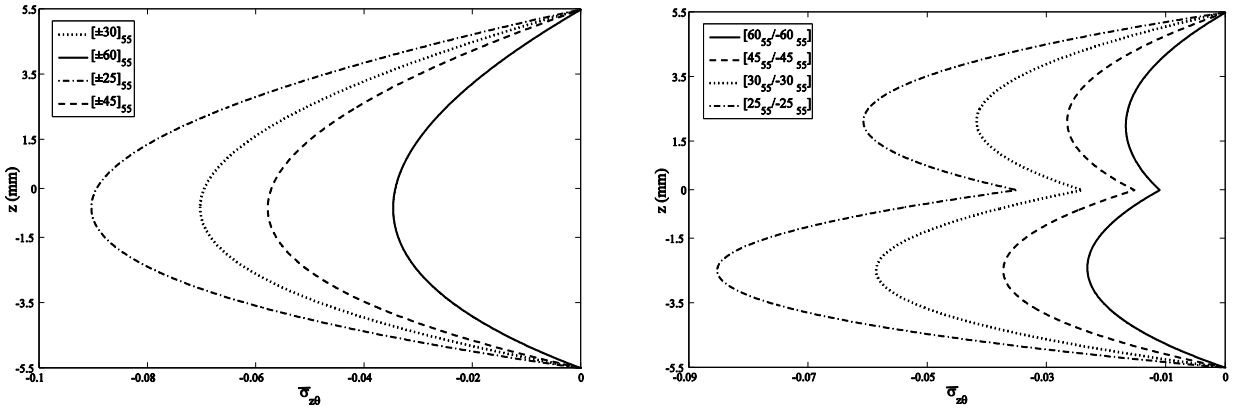

Figure 4.10: Comparison of the shear stress $\sigma_{z\theta}$ of the laminated cantilever straight tubes at $x \approx 2a$ and θ=0° along the tube thickness (subjected to shear load *F*) where the lay-up sequences of (**a**) are $[\pm25°]_{55}$, $[\pm30°]_{55}$, $[\pm45°]_{55}$ and $[\pm60°]_{55}$ and (**b**) are $[25°_{55}/-25°_{55}]$, $[30°_{55}/-30°_{55}]$, $[45°_{55}/-45°_{55}]$ and $[60°_{55}/-60°_{55}]$.

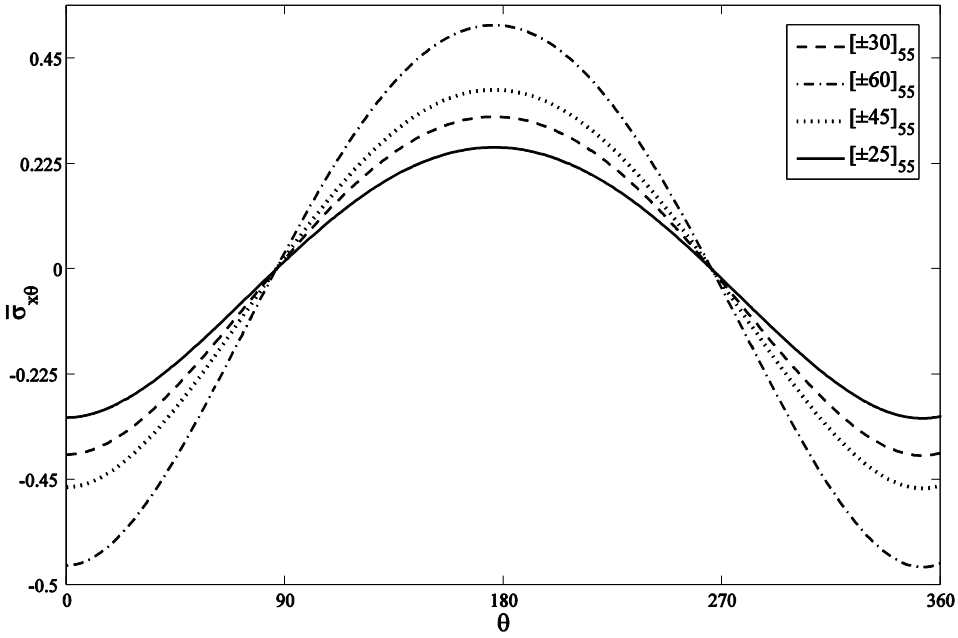

Figure 4.11: Comparison of shear stress $\sigma_{x\theta}$ of the $[\pm 25°]_{55}$, $[\pm 30°]_{55}$, $[\pm 45°]_{55}$ and $[\pm 60°]_{55}$ laminated cantilever straight tubes at *x≈2a* and *r=33.5 mm* (subjected to shear load *F*).

Figure 4.11 shows the comparison of the shear stress, $\bar{\sigma}_{x\theta}$, of the $[\pm 25°]_{55}$, $[\pm 30°]_{55}$, $[\pm 45°]_{55}$ and $[\pm 60°]_{55}$ laminated orthotropic straight tubes along the circumferential direction at *x≈2a* and *r=33.5 mm* (*i.e., layer 55*). It is observed that the shear stress, $\bar{\sigma}_{x\theta}$, of the $[\pm 60°]_{55}$ tube at *r=33.5 mm* is greater than those of the other lay-up sequences.

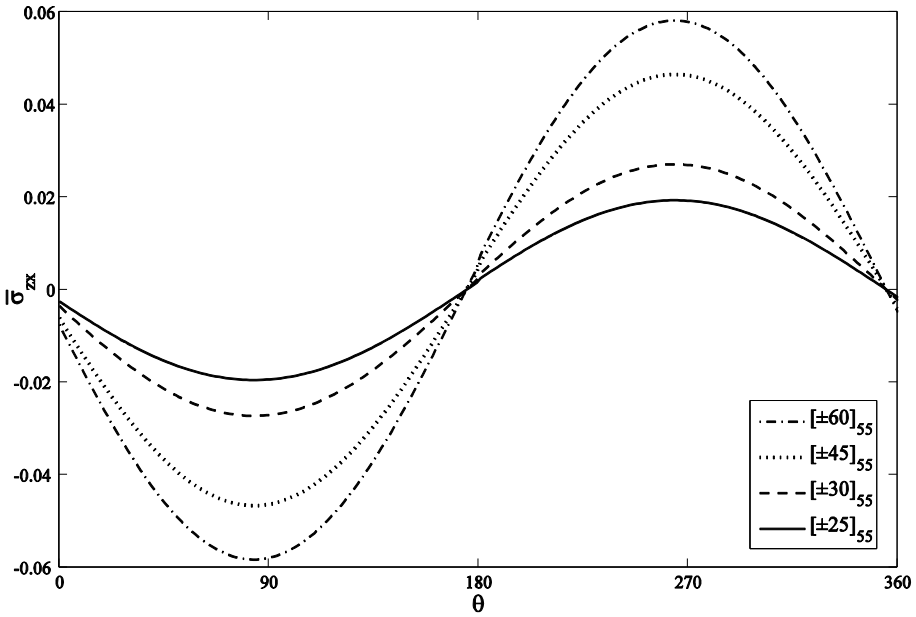

Figure 4.12: Comparison of shear stress σ_{zx} of the $[\pm25°]_{55}$, $[\pm30°]_{55}$, $[\pm45°]_{55}$ and $[\pm60°]_{55}$ laminated cantilever straight tubes at $x \approx 2a$ and $r=33.5$ *mm* (subjected to shear load *F*).

Figure 4.12 shows the comparison of the shear stress, $\bar{\sigma}_{zx}$, of the $[\pm25°]_{55}$, $[\pm30°]_{55}$, $[\pm45°]_{55}$ and $[\pm60°]_{55}$ laminated orthotropic straight tubes along the circumferential direction at $x \approx 2a$ and $r=33.5$ *mm* (*i.e., layer 55*). As compared to all lay-up sequences, the shear stress, $\bar{\sigma}_{zx}$, of the $[\pm25°]_{55}$ tube has the minimum magnitude. The shear stress, $\bar{\sigma}_{zx}$, could cause the movement of the layers on each other in the axial direction of the laminated composite straight tube. Therefore, considering Figure 4.12, the layers, placed between 0° to 180° of the tube cross section, may tend to move inward in the axial direction while the layers, placed between 180° to 360° of the tube cross section, may tend to move outward in the axial direction of the laminated composite tube.

4.6.2. Experimental Lay-ups (laminate numbers of 5, 6, 7 and 8)

4.6.2.1. Effects of 90° and 0°-plies on the $[\pm\theta°]_k$ Tube

In this section, effects of the addition of 90° and 0°-plies on distributions of interlaminar radial and hoop stresses of the $[\pm\theta°_k]$ laminated composite tube are examined considering the shear load part of subjected cantilever loading. The $[90°_m/\pm\theta°_k]$ and $[0°_m/\pm\theta°_k]$ tubes which

have 110 layers in total are selected to study. The 30°-plies are considered for ±θ°. The results are discussed based on the proposed method at $x \approx 2a$ (*i.e.,* shear load).

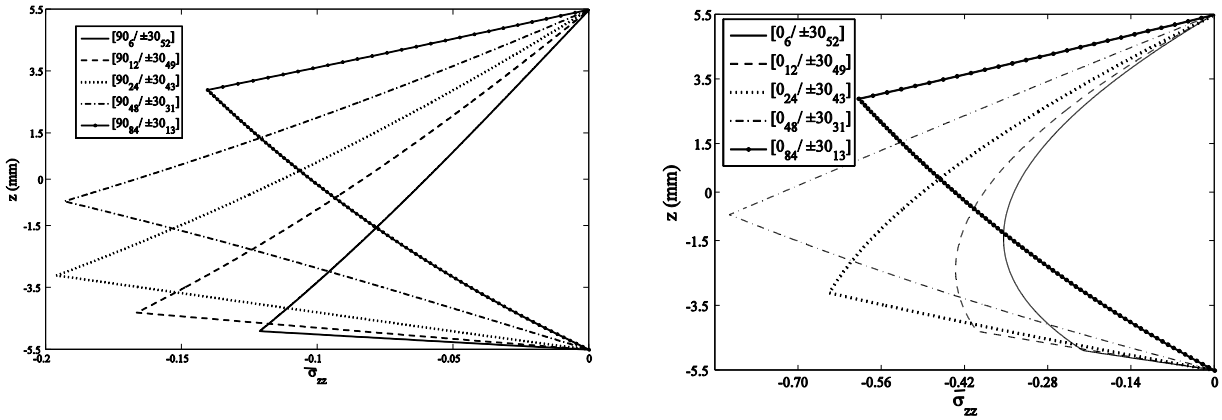

(a) **(b)**

Figure 4.13: Comparison of the radial stress σ_{zz} of the laminated cantilever straight tubes at $x \approx 2a$ and θ=90° along the tube thickness (subjected to shear load *F*) where the lay-up sequences of **(a)** is $[90°_m/\pm 30°_k]$ and **(b)** is $[0°_m/\pm 30°_k]$.

Figures 4.13a and 4.13b illustrate the comparison of the interlaminar radial stress, $\bar{\sigma}_{zz}$, of the $[90°_m/\pm 30°_k]$ and $[0°_m/\pm 30°_k]$ laminated cantilever straight tubes at $x \approx 2a$ and θ=90° along the tube thickness, respectively. It is seen from Figure 4.13a that the location of the maximum interlaminar radial stress, $\bar{\sigma}_{zz}$, of the $[90°_m/\pm 30°_k]$ tube always occurs at the end of the 90°-plies while the location of the maximum interlaminar radial stress, $\bar{\sigma}_{zz}$, of the $[0°_m/\pm 30°_k]$ tube depends on the number of 0°-plies of the lay-up sequence. In addition, the followings are observed:

- The behavior in Figure 4.13, does not seem to converge to the situation when there are the $[90°]_{110}$ or $[0°]_{110}$ tubes, as shown in Figure 4.5. Note that the existence of even one angle-ply in the lay-up sequence can make a significant change to the radial stress distribution. The radial stress has to adjust itself based on a lay-up sequence to distribute continuously since it is continuous along the tube thickness.
- When *m* and 2*k* are substantially close to each other, in the lay-up sequences of $[0°_m/\pm\theta°_k]$ and $[90°_m/\pm\theta°_k]$, the radial stress is at its maximum magnitude in comparison to all other possible *m* and *k* combinations.

- The location of the maximum magnitude of the radial stress (r_{max}) in the [90°$_m$/±θ°$_k$] tube is studied for all cases (*different values for θ*). It occurs at the largest-diameter 90°-ply of the lay-up sequence which is $r_{max}=mt+r_i$.
- The maximum magnitude of the radial stress of the [0°$_{24}$/±30°$_{43}$] tube occurs at *layer 24* which is the largest-diameter 0°-ply. In this case, 0°-plies make up 21% (*i.e.,* 24/110) of this lay-up sequence.
- The study is performed for the [0°$_m$/±θ°$_k$] tubes (*different values for θ*). r_{max} in the [0°$_m$/±θ°$_k$] tubes is dependent on *m*. When 0°-plies make up more than 20% of a lay-up sequence, the maximum magnitude of the radial stress will occur at the largest-diameter 0°-ply, which is $r_{max}=mt+r_i$; otherwise it varies along the tube thickness.

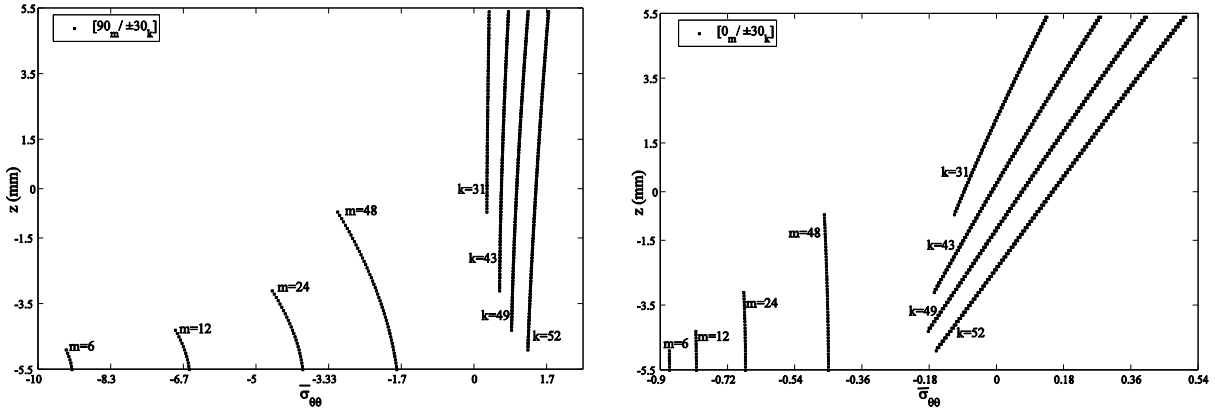

(a) **(b)**

Figure 4.14: Comparison of the hoop stress $\sigma_{\theta\theta}$ of the laminated cantilever straight tubes at $x\approx 2a$ and θ=90° along the tube thickness (subjected to shear load *F*) where the lay-up sequences of **(a)** is [90°$_m$/±30°$_k$] and **(b)** is [0°$_m$/±30°$_k$].

Figures 4.14a and 4.14b show the comparison of the hoop stress, $\bar{\sigma}_{\theta\theta}$, of the [90°$_m$/±30°$_k$] and [0°$_m$/±30°$_k$] laminated cantilever straight tubes at $x\approx 2a$ and θ=90° along the tube thickness, respectively. The followings are observed:

- Comparing Figure 4.14a with Figure 4.8, it is seen that with the addition of 90°-plies to the [±30°$_k$], the whole ±30°$_k$ part of the [90°$_m$/±30°$_k$] tube shifts to positive value while the trend is kept the same as before.

- With increasing the number of 90°-plies (*i.e.,* m) of the [$90°_m/\pm30°_k$] tube, the magnitude of the hoop stress, $\bar{\sigma}_{\theta\theta}$, of the $90°_m$ part decreases (*see Figure 4.14a*); because there are more 90°-plies to carry the hoop stress, $\bar{\sigma}_{\theta\theta}$. In addition, with increasing *m* (*i.e.,* decreasing *k*), the magnitude of the hoop stress of the 30°-plies decreases since there are more 90°-plies to carry hoop stress, $\bar{\sigma}_{\theta\theta}$.
- It is observed from Figure 4.14b that the trend of $\pm30°_k$ part of the [$0°_m/\pm30°_k$] tube is not changed much due to the addition of 0°-plies to the [$\pm30°_k$] tube (*see Figure 4.8*) while its magnitude is changed as seen in Figure 4.14b.
- The maximum positive of the hoop stress in the [$90°_m/\pm\theta°_k$] and [$0°_m/\pm\theta°_k$] tubes occurs at the outside surface while the maximum negative of the hoop stress occurs at the largest-diameter 90°-ply and 0°-ply, respectively.

4.6.2.2. Effects of Layer-group on the $[\pm\theta°]_k$ Tube

Finally, the [$(90°_{10}/0°_{10})_3/\pm25°_{25}$], [$(90°_{10}/0°_{10})_3/\pm30°_{25}$], [$(90°_{10}/0°_{10})_3/\pm45°_{25}$] and [$(90°_{10}/0°_{10})_3/\pm60°_{25}$] tubes which have 110 layers in total are selected to study effects of the shear load part of cantilever loading on stress distributions of the tube sections. The results are presented based on the proposed method at $x\approx2a$ (*i.e.,* shear load).

Figure 4.15a presents the comparison of the interlaminar radial stress, $\bar{\sigma}_{zz}$, of the [$(90°_{10}/0°_{10})_3/\pm25°_{25}$], [$(90°_{10}/0°_{10})_3/\pm30°_{25}$], [$(90°_{10}/0°_{10})_3/\pm45°_{25}$] and [$(90°_{10}/0°_{10})_3/\pm60°_{25}$] laminated cantilever straight tubes subjected to the shear load part at $x\approx2a$ and $\theta=90°$ along the tube thickness. The followings are observed:

- The magnitude of the radial stress, $\bar{\sigma}_{zz}$, of the [$(90°_{10}/0°_{10})_3/\pm25°_{25}$] tube is greater than those of the others. It is observed that the maximum magnitude of the interlaminar radial stress of different lay-up sequences occurs at *z=-0.5 mm* which is the last 90° layer-group from the inside (*i.e., layer 50*). Therefore, these layers tend to separate from 0° layer-group, with the largest possibility. Derisi [20] observed the same phenomena during his experimental tests.

- The maximum magnitude of the radial stress of the $[(90°_{10}/0°_{10})_3/\pm45°_{25}]$ tube occurs at *layer 50* which is the largest-diameter 90°-ply. In this case, 90° and 0°-plies make up 54% (*i.e.,* 60/110) of this lay-up sequence.
- The study is performed for the $[(90°_{10}/0°_{10})_3/\pm\theta°_{25}]$ tubes (*different values for θ*). The maximum magnitude of the radial stress (r_{max}) in the $[(90°_m/0°_m)_l/\pm\theta°_k]$ tubes is dependent on *m* and *l*. When 90° and 0°-plies make up more than 10% of a lay-up sequence, the maximum magnitude of the radial stress will occur at the largest-diameter 90°-ply, which is $r_{max} = (2ml-m)t + r_i$.

In addition, effects of lay-up sequences of layer-group on the stress distributions are investigated. Figure 4.15b shows the comparison of the radial stress, $\bar{\sigma}_{zz}$, of the $[90°_{30}/0°_{30}/\pm25°_{25}]$, $[90°_{30}/0°_{30}/\pm30°_{25}]$, $[90°_{30}/0°_{30}/\pm45°_{25}]$ and $[90°_{30}/0°_{30}/\pm60°_{25}]$ laminated cantilever straight tubes at $x\approx2a$ and θ=90° along the tube thickness. Comparison of Figures 4.15a and 4.15b, it is seen that by considering layer-group of the lay-up sequence, the first two 0° layer-groups are subjected to less radial stress. In addition, the maximum radial stress which occurs at *z=-0.5 mm* (*i.e., layer 50*) in Figure 4.15a shifts to the inside of the composite tube at *z=-2.5 mm* (*i.e., layer 30*) in Figure 4.15b while in both types of lay-up sequences, 90° layer-group tends to delaminate.

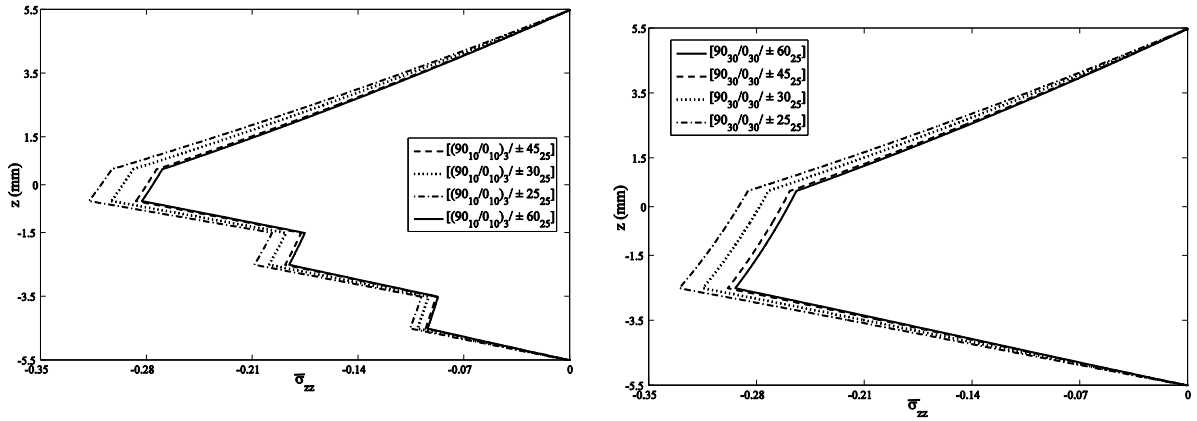

(a) **(b)**

Figure 4.15: Comparison of the radial stress σ_{zz} of the laminated cantilever straight tubes at $x\approx2a$ and θ=90° along the tube thickness (subjected to shear load *F*) where the lay-up sequences of **(a)** are $[(90°_{10}/0°_{10})_3/\pm25°_{25}]$, $[(90°_{10}/0°_{10})_3/\pm30°_{25}]$, $[(90°_{10}/0°_{10})_3/\pm45°_{25}]$ and $[(90°_{10}/0°_{10})_3/\pm60°_{25}]$ and **(b)** are $[90°_{30}/0°_{30}/\pm25°_{25}]$, $[90°_{30}/0°_{30}/\pm30°_{25}]$, $[90°_{30}/0°_{30}/\pm45°_{25}]$ and $[90°_{30}/0°_{30}/\pm60°_{25}]$.

In addition, observation of Figure 4.15 shows that the magnitude of the radial stress of the $[90°_{30}/0°_{30}/\pm25°_{25}]$ tube is greater than those of the other tubes are. This is explained by using Eq. (4.12).

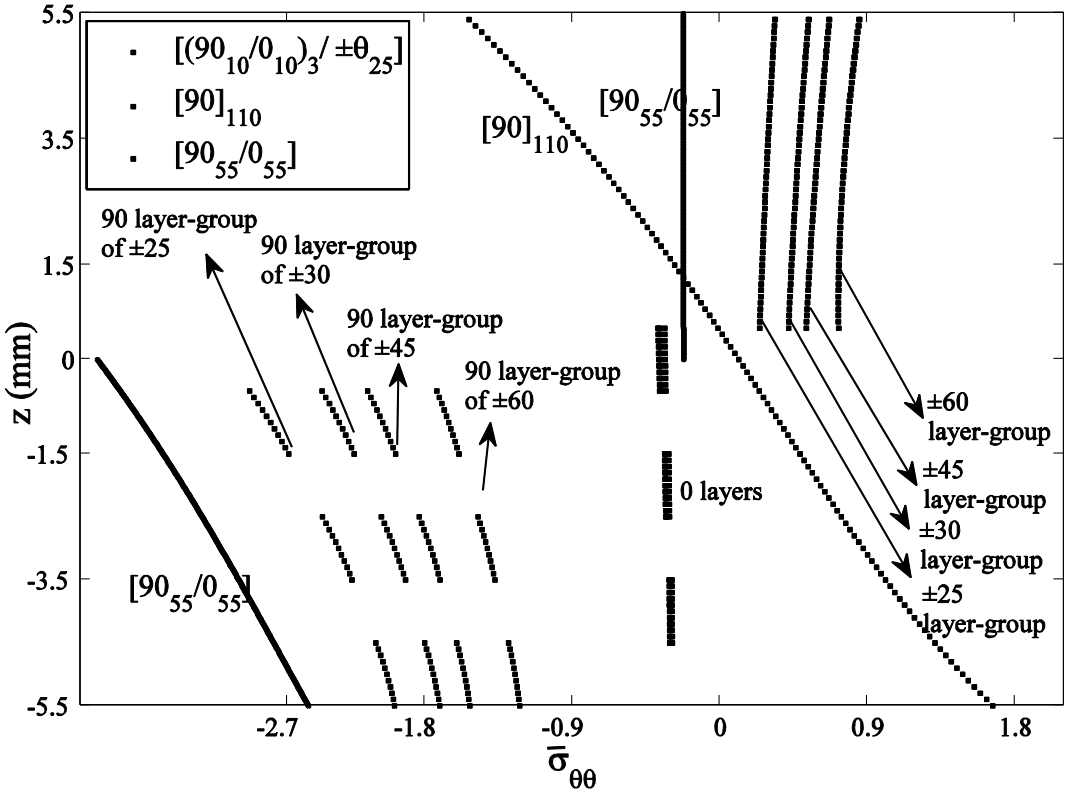

Figure 4.16: Comparison of the hoop stress $\sigma_{\theta\theta}$ of the $[(90°_{10}/0°_{10})_3/\pm25°_{25}]$, $[(90°_{10}/0°_{10})_3/\pm30°_{25}]$, $[(90°_{10}/0°_{10})_3/\pm45°_{25}]$, $[(90°_{10}/0°_{10})_3/\pm60°_{25}]$, $[90°]_{110}$ and $[90°_{55}/0°_{55}]$ laminated cantilever straight tubes at $x\approx2a$ and $\theta=90°$ along the tube thickness (subjected to shear load F).

Comparison of the hoop stress, $\bar{\sigma}_{\theta\theta}$, of the $[(90°_{10}/0°_{10})_3/\pm\theta°_{25}]$ (for θ = 25°, 30°, 45° and 60°), $[90°]_{110}$ and $[90°_{55}/0°_{55}]$ laminated cantilever straight tubes at $x\approx2a$ and $\theta=90°$ along the tube thickness is shown in Figure 4.16. The followings are observed:

- The $[90°]_{110}$ tube has positive hoop stress on the inner radius and negative hoop stress on the outer radius.
- For lay-ups containing the $\pm\theta°$ layer-group, the $\pm\theta°$ layer-group now assumes the tensile stress, while the 90° layer-group (in the inner side of the tube) now has compressive stress which is the opposite for the case of the $[90°]_{110}$ tube.
- Among the lay-up sequences containing the $\pm\theta°$ layer-group, tubes with $\pm60^o$ have higher magnitude of tensile stress than tubes with lower angle, with monotonic variation. This is

explained by the fact that the closer is the fiber orientation to 90°, the more load along the circumferential direction it will carry.

- The hoop stress, $\bar{\sigma}_{\theta\theta}$, of the 90° layer-group of the $[(90°_{10}/0°_{10})_3/\pm25°_{25}]$ tube is greater than those of the other lay-up sequences; because 25°-plies have less contributions in resisting hoop stress.
- The 0° layers contribute little to the support of the hoop stress, $\bar{\sigma}_{\theta\theta}$.
- The maximum positive of the hoop stress in the $[(90°_m/0°_m)_l/\pm\theta°_k]$ tubes occurs at the outside surface while the maximum negative of the hoop stress occurs at the largest-diameter 90°-ply.

Comparison of the shear stress, $\bar{\sigma}_{z\theta}$, of the $[(90°_{10}/0°_{10})_3/\pm25°_{25}]$, $[(90°_{10}/0°_{10})_3/\pm30°_{25}]$, $[(90°_{10}/0°_{10})_3/\pm45°_{25}]$ and $[(90°_{10}/0°_{10})_3/\pm60°_{25}]$ laminated orthotropic straight tubes at $x\approx2a$ and $\theta=0°$ along the tube thickness is presented in Figure 4.17. It is observed that the shear stress, $\bar{\sigma}_{z\theta}$, of the $[(90°_{10}/0°_{10})_3/\pm25°_{25}]$ tube is greater than those of the $[(90°_{10}/0°_{10})_3/\pm30°_{25}]$, $[(90°_{10}/0°_{10})_3/\pm45°_{25}]$ and $[(90°_{10}/0°_{10})_3/\pm60°_{25}]$ tubes.

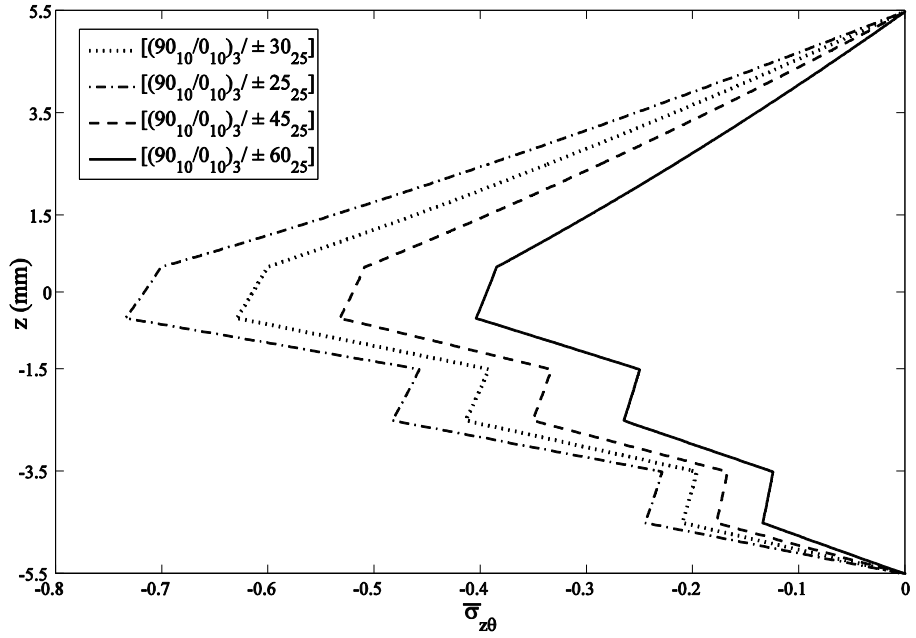

Figure 4.17: Comparison of the shear stress $\sigma_{z\theta}$ of the $[(90°_{10}/0°_{10})_3/\pm25°_{25}]$, $[(90°_{10}/0°_{10})_3/\pm30°_{25}]$, $[(90°_{10}/0°_{10})_3/\pm45°_{25}]$ and $[(90°_{10}/0°_{10})_3/\pm60°_{25}]$ laminated cantilever straight tubes at $x\approx2a$ and $\theta=0°$ along the tube thickness (subjected to shear load F).

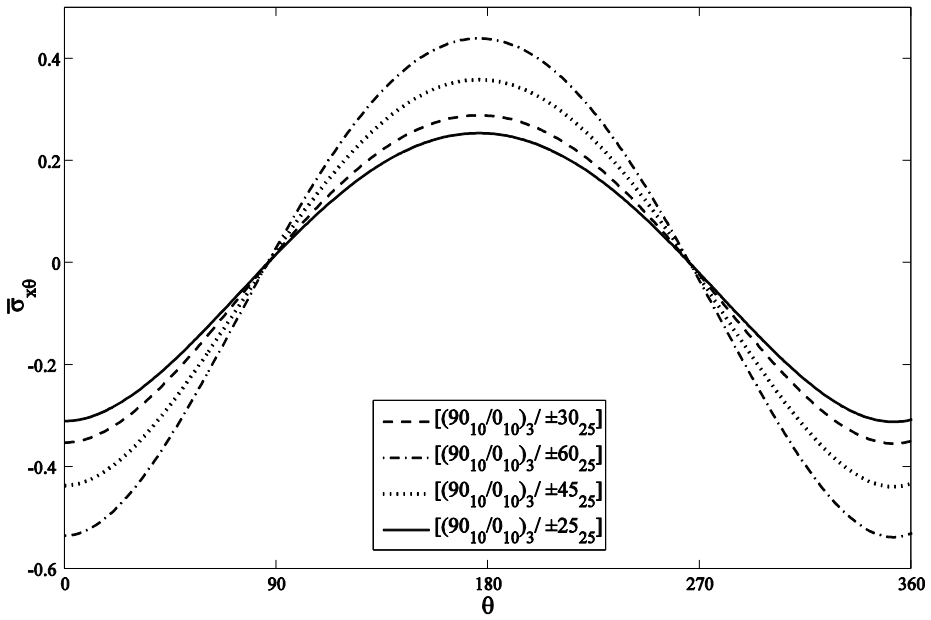

Figure 4.18: Comparison of the shear stress $\sigma_{x\theta}$ of the $[(90°_{10}/0°_{10})_3/\pm25°_{25}]$, $[(90°_{10}/0°_{10})_3/\pm30°_{25}]$, $[(90°_{10}/0°_{10})_3/\pm45°_{25}]$ and $[(90°_{10}/0°_{10})_3/\pm60°_{25}]$ laminated cantilever straight tubes at *r=35.3 mm* (subjected to shear load *F*).

Figure 4.18 displays the comparison of the shear stress, $\bar{\sigma}_{x\theta}$, of the $[(90°_{10}/0°_{10})_3/\pm25°_{25}]$, $[(90°_{10}/0°_{10})_3/\pm30°_{25}]$, $[(90°_{10}/0°_{10})_3/\pm45°_{25}]$ and $[(90°_{10}/0°_{10})_3/\pm60°_{25}]$ laminated straight tubes along the circumferential direction at $x\approx2a$ and *r=35.3 mm*. It is observed from Figure 4.18 that the shear stress, $\bar{\sigma}_{x\theta}$, of the $[(90°_{10}/0°_{10})_3/\pm60°_{25}]$ tube has the maximum values among these lay-ups. Since angle-plies are placed at *z=1.8 mm*, the 60°-plies of the $[(90°_{10}/0°_{10})_3/\pm60°_{25}]$ tube could carry more shear stress in comparison with the other angle-plies (*i.e.,* 25°, 30° and 45°) of the other lay-up sequences.

4.6.3. Advantages of the Proposed Method

The most important advantage of the proposed method is that the inputs for the modeling of composite structures with complex lay-ups are simple, easy to use and fast to run. Contrary, to model complex lay-up composite structures in FEM, it is necessary to create several parts individually, mesh every part separately, and assign every lay-up to the attributed part of structures. However, through using the proposed method, one just needs to simply define the dimensions and the lay-up at the beginning of the program. Therefore, it is

obvious that the modeling of complex lay-up orthotropic structures using FEM takes much longer than using the developed method. In addition, using FEM for parametric study is cumbersome. For example, to study the effect of thickness on stresses and strains distribution by using FEM, it is necessary to model the geometry for different thicknesses and obviously it takes longer than using the proposed method. By applying the proposed method, the parametric study for composite tubes is simple with low computational cost. To add to the advantages, high efficiency in terms of computational time is obtainable when the proposed method is used as compared with FEM.

4.6.4. Observations

A complete structural analysis for designing composite laminates is extensive and complicated. This usually requires different analysis steps such as laminate stress and strength analysis. Therefore, there is still a need to come up with some preliminary knowledge of the lay-up sequence of composite laminates. Generally, the lay-up sequences have influences on structural properties of composite laminates such as stiffness and strength. The obtained observations contain the followings:

1. The shear stress, $\sigma_{z\theta}$, shows the same behavior as the radial stress, $\bar{\sigma}_{zz}$, with a 90° phase shift.
2. Positive interlaminar radial stresses cause delamination at composite tubes. Radial stresses are positive at the compression zone of tube cross sections. Table 4.3 summarized the location (r_{max}) of the maximum magnitude of the interlaminar radial stress, $\bar{\sigma}_{zz}$, in different lay-up sequences along the tube thickness. Note that all plies are assumed to have equal thickness (= t). The composite tube thickness is h.
3. When there are enough 90°-plies in the lay-up sequence (*see Table 4.3*), always maximum magnitude of the interlaminar radial stress, $\bar{\sigma}_{zz}$, occurs at the last 90°-ply of the lay-up.
4. Locations of the maximum positive and negative of the hoop stress, $\bar{\sigma}_{\theta\theta}$, in different lay-up sequences are summarized in Table 4.4. Note that r_i and r_o indicate the inside and outside surfaces of the composite straight tube, respectively.

Table 4.3: Locations (r_{max}) of the maximum interlaminar radial stress σ_{zz} along the tube thickness.

Refer to	*Lay-up sequence*	*Position of maximum interlaminar radial stress*
Figure 4.5	$[\theta°_k]$	$r_{max} = 0.44h + r_i$ (*h=kt*)
Figure 4.5	$[\pm\theta°_k]$	$r_{max} = 0.44h + r_i$ (*h=2kt*)
Figure 4.6	$[\theta°_k/-\theta°_k]$	$r_{max} = 0.56(kt) + r_i$ (*h=2kt*)
Figure 4.13a	$[90°_m/\pm\theta°_k]$	$r_{max} = mt + r_i$ (*h=mt+2kt*)
Figure 4.13b	$[0°_n/\pm\theta°_k]$	If $(nt/h) >= 0.2 \rightarrow r_{max} = nt + r_i$ (*h=nt+2kt*)
Figure 4.15a	$[(90°_m/0°_m)_l/\pm\theta°_k]$	If $(2mlt/h) >= 0.1 \rightarrow r_{max} = (2ml-m)t + r_i$ (*h=2mlt+2kt*)
		If $(2mlt/h) < 0.1 \rightarrow r_{max} = 2mlt + 0.44(2kt) + r_i$ (*h=2mlt+2kt*)
Figure 4.15b	$[90°_m/0°_m/\pm\theta°_k]$	If $(2mt/h) >= 0.1 \rightarrow r_{max} = mt + r_i$ (*h=2mt+2kt*)
		If $(2mt/h) < 0.1 \rightarrow r_{max} = 2mt + 0.44(2kt) + r_i$ (*h=2mt+2kt*)

Table 4.4: Locations of the maximum hoop stress $\sigma_{\theta\theta}$ along the tube thickness.

Refer to	*Lay-up sequence*	*Maximum negative hoop stress*	*Zero hoop stress*	*Maximum positive hoop stress*
Figure 4.8	$[\theta°_k]$, $[\pm\theta°_k]$	r_i	$r_i+h/2$	r_o
Figure 4.8	$[90°_m]$	r_o	$r_i+h/2$	r_i
Figure 4.9	$[\theta°_k/-\theta°_k]$	r_i	$r_i+h/4$, $r_i+3/4h$	r_o, $r_i+h/2$
Figure 4.14	$[0°_m/\pm\theta°_k]$, $[90°_m/\pm\theta°_k]$	r_i+mt	----	r_o
Figure 4.16	$[90°_m/0°_m/\pm\theta°_k]$	r_i+mt	----	r_o
Figure 4.16	$[(90°_m/0°_m)_l/\pm\theta°_k]$	$r_i+(2ml-m)t$	----	r_o

4.7. Conclusions

A practical design of composite structures is a critical and time-consuming step to ensure that the composite stack would perform satisfactorily in service. In this chapter, effects of lay-up sequences and orientations on stress distributions at tube sections in thick orthotropic

straight tubes under shearing load are studied. The investigation was performed based on the new simple-input displacement-based method. The positive radial stress may cause delamination of some layers from the rest of the laminate. If such delamination occurs, the tube would fail prematurely by localized buckling. Since the radial stress affects delamination and the hoop stress affects buckling, the interlaminar radial and hoop stresses distributions were studied, in the majority of this chapter. Finally, locations for the maximum radial and hoop stresses in the composite straight tube with different lay-up sequences are given.

Chapter 5

In this chapter, the developed analytical method is used to study thick laminated composite straight tubes subjected to combined axial force, torque and bending moment. The accuracy of the proposed method is subsequently verified by comparing the numerical results obtained using the proposed method with finite element method (FEM) and experimental data. The proposed method provides advantages in terms of computational time compared to FEM.

A High-order Analytical Method for Thick Composite Tubes

Hamidreza Yazdani Sarvestani and Mehdi Hojjati

Department of Mechanical and Industrial Engineering, Concordia University, Montreal, Canada H3G 1M8

Abstract

In the present chapter, a new high-order simple-input analytical method is used to study thick laminated composite straight tubes subjected to combined axial force, torque and bending moment. The most general displacement field of elasticity for an arbitrary laminated composite straight tube is obtained to analytically calculate stresses under combined loadings based on a layer-wise method. The accuracy of the proposed method is subsequently verified by comparing the numerical results obtained using the proposed method with finite element method (FEM) and experimental data. The results show good correspondence. The proposed method provides advantages in terms of computational time compared to FEM.

Keywords: Stress analysis; Thick laminated composite straight tube; High-order displacement-based method; Combined loadings.

5.1. Introduction

Composite tube structures are increasingly used in many aerospace industries. The prediction of the state of stress in different layers of laminated composite tubes is of theoretical interest and subsequently practical applications. In aerospace applications, accurate design and analysis are important to ensure safety and proper performance of composite structures. Note that stress analysis of thick cylindrical composite structures is often a complex task. A few reasons exist for such a complexity. First, the governing equations of composite tubes are complicated. Second, a major source of intricacy is the layer-wise failure of composite materials. In fact, as soon as a layer fails, a delamination happens or a crack

propagates in between the plies, material properties degrade and sometimes the governing equations could be different. Moreover, the tube geometry is a lot more complicated than flat geometry.

Many researchers have performed investigations on composite straight tubes under different types of loadings. Lekhnitskii [2] developed the solution for composite tubes under bending load by using partial differential equations. Kollár and Springer [4] conducted a stress analysis on thin to thick composite tubes under hydrothermal and mechanical loads. Jolicoeur and Cardou [9] developed a general analytical solution in order to find stress and displacement fields of composite tubes subjected to bending, tensile and torsion loads. Tubes made of functionally graded materials (FGM) under tension and bending were analyzed [93]. An analysis on a cylindrically anisotropic elastic body was made when the body was subjected to extension, torsion, bending and thermo-mechanical loads [94]. Shadmehri et al. [22] developed theoretical formulations by using a three-dimensional laminate theory to obtain the stiffness of composite tubes. They compared theoretical formulation with experimental results. Zozulya and Zhang [95] developed a high order shell theory for FG axisymmetric cylindrical shells based on the expansion of the axisymmetric equations of elasticity. A method was presented to analyze arbitrary laminated composite tubes subjected to pure bending. They performed FEM using NASTRAN to compare with theoretical results [24]. The stress analysis of composite hollow cylindrical structures subjected to different loadings was performed [25]. Their method was efficient for thin composite hollow tubes. Based on the nonlinear ring theory, mechanical behavior of thermoplastic tubes under combined bending and tension was investigated [39]. They verified formulations with FEM results obtained using ABAQUS. Menshykova and Guz [26] performed a stress analysis on thick laminated composite tubes subjected to bending loading. They found stresses as a function of the material properties, thickness, lay-up sequences and the magnitude of bending load. Capela et al. [27] investigated the fatigue behavior of composite tubes under bending/torsion dynamic loadings. Recently, a static analysis of a carbon nanotube-reinforced composite tube under thermo-mechanical was studied using Mori-Tanaka theory [28]. A method to obtain and analyze stress distributions in composite cantilever straight tubes was developed [92, 95 and 97]. The effect of cumulative damage on the seismic behavior of steel tube-reinforced concrete columns through experimental testing was investigated [98]. Nowak

and Schmidt [29] compared some methods to study fiber metal laminated tubes under an axisymmetric load. The developed theoretical model was validated by FEM analyses. Jonnalagadda et al. [30] presented an analytical model for a special design of a thin composite tube subjected to combined bending and torsion. They verified the theoretical results with FEM analyses.

Although many works described above show promise to analyze composite tubes, it is desired to have a method where the inputs (*i.e.,* dimensions and lay-up sequences) for the solution are simple; i.e. one only needs to enter the actual dimensions without meshing work. The present chapter is devoted to develop a high-order analytical method that can provide stresses, strains and deformations with low computational cost for thick laminated composite straight tubes subjected to different mechanical loading conditions such as axial force, torque and bending moment.

5.2. Motivation

In an effort to develop thermoplastic composite tubes for helicopter landing gears, Derisi [1] designed and manufactured composite straight tubes and performed four-point and three-point bending tests to determine the strains to failure of different balanced laminates. Derisi used a procedure called strain-controlled design and based on that, lay-up sequences for composite tubes were developed. Even though they have done experimental works, the analytical method does not exist to analyze thick composite straight tubes. Due to the complexity of stress distributions in a thick composite tube, it is not easy to obtain some intuition as to the behavior of the tube under combined loadings, for the purpose of design. Now, in order to provide some insight into this behavior, a new high-order method is developed.

5.3. Theoretical Formulation

5.3.1. Displacement Field

A thick laminated composite straight tube with mean radius R and thickness h is subjected to an axial force F_0, torque T_0 and bending moment M_0 as shown in Figure 5.1. The cylindrical coordinates (x, θ, r) are placed at the middle surface of the composite straight tube where x

and *r* are the axial and radial coordinate, respectively. The appropriate integration of the linear strain-displacement relations of elasticity, within cylindrical coordinate system yields the following displacement field for the *k*th layer [92]:

$$u_1^{(k)}(x,\theta,r) = xr\left(C_5^{(k)}\cos\theta + C_4^{(k)}\sin\theta\right) + C_6^{(k)}x + u^{(k)}(\theta,r) \tag{5.1a}$$

$$u_2^{(k)}(x,\theta,r) = x\left(C_1^{(k)}\cos\theta - C_2^{(k)}\sin\theta - C_3^{(k)}r\right) - \frac{1}{2}x^2\left(C_4^{(k)}\cos\theta - C_5^{(k)}\sin\theta\right) + v^{(k)}(\theta,r) \tag{5.1b}$$

$$u_3^{(k)}(x,\theta,r) = x\left(C_1^{(k)}\sin\theta + C_2^{(k)}\cos\theta\right) - \frac{1}{2}x^2\left(C_5^{(k)}\cos\theta + C_4^{(k)}\sin\theta\right) + w^{(k)}(\theta,r) \tag{5.1c}$$

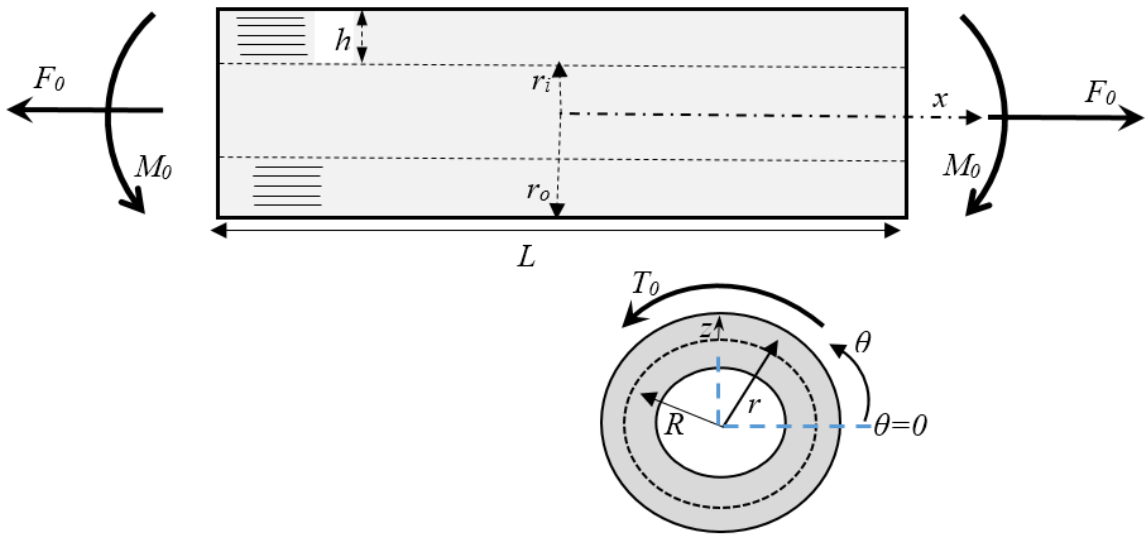

Figure 5.1: The geometry of a composite straight tube and the coordinate system.

where $u_1^{(k)}(x,\theta,r)$, $u_2^{(k)}(x,\theta,r)$ and $u_3^{(k)}(x,\theta,r)$ represent the displacement components in the *x*, θ and *r* directions, respectively, of a material point located at (*x*, θ, *r*) in the *k*th ply of the laminated composite straight tube in Figure 5.1. In order to satisfy the interfacial continuities of the displacement components, it is necessary that the integration constants appearing in Eqs. (5.1) to be the same for all layers. Thus, Eqs. (5.1) are represented as:

$$u_1^{(k)}(x,\theta,r) = xr\left(C_5\cos\theta + C_4\sin\theta\right) + C_6 x + u^{(k)}(\theta,r) \qquad (5.2a)$$

$$u_2^{(k)}(x,\theta,r) = x\left(C_1\cos\theta - C_2\sin\theta - C_3 r\right) - \frac{1}{2}x^2\left(C_4\cos\theta - C_5\sin\theta\right) + v^{(k)}(\theta,r) \qquad (5.2b)$$

$$u_3^{(k)}(x,\theta,r) = x\left(C_1\sin\theta + C_2\cos\theta\right) - \frac{1}{2}x^2\left(C_5\cos\theta + C_4\sin\theta\right) + w^{(k)}(\theta,r) \qquad (5.2c)$$

Moreover, in Eq. (5.2a), $u^{(k)}(\theta,r)$ is replaced by $-C_1 r\sin\theta + u^{(k)}(\theta,r)$. It is shown that the terms involving C_1 in Eq. (5.2) correspond to an infinitesimal rigid-body rotation. These terms will, therefore, be ignored in the following developments since they will not generate any strain. Similarly, it is readily shown that the terms involving C_2 must also be eliminated since they represent another rigid-body rotation of the tube. Furthermore, as long as the loading conditions at both ends of the tube are identical, the constant C_4 must vanish in order to satisfy the symmetry condition in deformation $u_3^{(k)}(x,\theta,r) = u_3^{(k)}(-x,-\theta,r)$. It is thus concluded that the most general form of the displacement field for the kth layer of a thick composite straight tube is given as:

$$u_1^{(k)}(x,\theta,r) = C_5 xr\cos\theta + C_6 x + u^{(k)}(\theta,r) \qquad (5.3a)$$

$$u_2^{(k)}(x,\theta,r) = -C_3 rx + \frac{1}{2}C_5 x^2\sin\theta + v^{(k)}(\theta,r) \qquad (5.3b)$$

$$u_3^{(k)}(x,\theta,r) = -\frac{1}{2}C_5 x^2\cos\theta + w^{(k)}(\theta,r) \qquad (5.3c)$$

5.3.2. Layer-wise Theory (LWT)

The equivalent single-layer theories are not capable of representing the local phenomena in laminated composites, like stress and strain distributions. However, LWTs, which consider real 3D behavior of each layer, are able to present accurate results considering the localized phenomena. In LWT, the displacement components of a generic point in the laminate are conveniently given as [52, 53]:

$$u_1(x,\theta,z) = u_k(x,\theta)\Phi_k(z) \qquad (5.4a)$$

$$u_2(x,\theta,z) = v_k(x,\theta)\Phi_k(z) \qquad (5.4b)$$

$$u_3(x,\theta,z) = w_k(x,\theta)\Phi_k(z) \qquad (k = 1,2,...,N+1) \qquad (5.4c)$$

where k, here and in what follows, being a dummy index implying summation of terms from k=1 to k=N+1. In Eqs. (5.4), u_1, u_2 and u_3 denote the displacement components in the x, θ and

z directions, respectively (*see Figure 5.1*). Also, $u_k(x,\theta)$, $v_k(x,\theta)$ and $w_k(x,\theta)$ represent the displacements of the points initially located on the kth surface of the laminated composite tube in the x, θ and z directions, respectively. Furthermore, $\Phi_k(z)$ is the global Lagrangian interpolation function that is used for the discretization of the displacement through-thickness and can have linear, quadratic or higher-order polynomial variations of the thickness coordinate z (*see Appendix D*). It is noted that the accuracy of LWT is enhanced by subdividing each physical layer into a finite number of numerical layers. Clearly, as the number of subdivision through-thickness (p) is increased, the number of governing equations and the accuracy of the results are increased. Based on the elasticity displacement field in Eqs. (5.3), LWT displacement field in Eqs. (5.4) is rewritten as:

$$u_1(x,\theta,z) = C_5 x (R+z)\cos\theta + C_6 x + U_k(\theta)\Phi_k(z) \qquad (5.5a)$$

$$u_2(x,\theta,z) = -C_3 (R+z)x + \frac{1}{2}C_5 x^2 \sin\theta + V_k(\theta)\Phi_k(z) \qquad (5.5b)$$

$$u_3(x,\theta,z) = -\frac{1}{2}C_5 x^2 \cos\theta + W_k(\theta)\Phi_k(z) \qquad (k=1,2,...,N+1) \qquad (5.5c)$$

It is pointed out here that, by employing through-thickness linear interpolation functions, the continuity of displacement components through the thickness of the laminate is identically satisfied. On the other hand, the transverse strain components remain discontinuous at the interfaces, which will subsequently amplify the possibility of having continuous interlaminar stresses at the interfaces of adjacent layers by increasing the number of numerical layers through the physical laminate. By introducing $r=R+z$ (see *Figure 5.1*), the strain-displacement relations are as given as:

$$\varepsilon_{xx} = \frac{\partial u_1}{\partial x}, \qquad \varepsilon_{\theta\theta} = \frac{1}{R+z}\frac{\partial u_2}{\partial \theta} + \frac{u_3}{R+z}, \qquad \gamma_{x\theta} = \frac{\partial u_2}{\partial x} + \frac{1}{R+z}\frac{\partial u_1}{\partial \theta}$$

$$\gamma_{\theta z} = \frac{1}{R+z}\frac{\partial u_3}{\partial \theta} + \frac{\partial u_2}{\partial z} - \frac{u_2}{R+z}, \qquad \gamma_{xz} = \frac{\partial u_3}{\partial x} + \frac{\partial u_1}{\partial z}, \qquad \varepsilon_{zz} = \frac{\partial u_3}{\partial z} \qquad (5.6)$$

Substitution of Eqs. (5.5) into the strain-displacement relations (5.6) yields the following results:

$$\varepsilon_{xx} = \left(R + z\right)\left(C_5 \cos\theta + C_4 \sin\theta\right) + C_6, \qquad \varepsilon_{\theta\theta} = \frac{V_k' + W_k}{R + z}\Phi_k, \qquad \varepsilon_{zz} = W_k \Phi_k'$$

$$\gamma_{\theta z} = \frac{W_k' - V_k}{R + z}\Phi_k + V_k \Phi_k', \qquad \gamma_{xz} = U_k \Phi_k' + \left(C_1 \sin\theta + C_2 \cos\theta\right),$$

$$\gamma_{x\theta} = \left(C_1 \cos\theta - C_2 \sin\theta - C_3 \left(R + z\right)\right) + \frac{U_k' \Phi_k}{R + z} \tag{5.7}$$

In Eq. (5.7) and what follows, a prime indicates an ordinary differentiation with respect to an appropriate variable (*i.e.,* either θ or z). The equilibrium equations of a thick composite straight tube with N numerical layers are obtained by employing Eqs. (5.7) in the principle of minimum total potential energy [89]. The results are, in general, *3(N+1)* local equilibrium equations corresponding to *3(N+1)* unknown functions U_k, V_k and W_k and three global equilibrium equations associated with three parameters C_3, C_5 and C_6. Employing the fundamental lemma of calculus of variations, the equilibrium equations of thick laminated composite straight tubes under axial force, torque and bending moment are obtained as:

$$\delta U_k : Q_x^k - \frac{dM_{x\theta}^k}{d\theta} = 0 \tag{5.8a}$$

$$\delta V_k : Q_\theta^k - \frac{dM_\theta^k}{d\theta} - R_\theta^k = 0 \tag{5.8b}$$

$$\delta W_k : M_\theta^k - \frac{dR_\theta^k}{d\theta} + N_z^k = 0 \tag{5.8c}$$

$$\delta C_3 : \int_{-\pi}^{\pi}\int_{-h/2}^{h/2} \sigma_{x\theta}\left(R + z\right)^2 dz d\theta = T_0 \tag{5.9a}$$

$$\delta C_5 : \int_{-\pi}^{\pi}\int_{-h/2}^{h/2} \sigma_{xx}\left(R + z\right)^2 \cos\theta dz d\theta = M_0 \tag{5.9b}$$

$$\delta C_6 : \int_{-\pi}^{\pi}\int_{-h/2}^{h/2} R\,\sigma_{xx} dz d\theta = F_0 \tag{5.9c}$$

where F_0, T_0 and M_0 represent the prescribed values of the axial force, torque and bending moment, respectively, applied at both ends of the composite straight tube. The generalized stress and moment resultants are defined as:

$$\left(N_z^k, Q_x^k, Q_\theta^k\right) = \int_{-h/2}^{h/2} \left(\sigma_{zz}, \sigma_{xz}, \sigma_{\theta z}\right)\Phi_k' \, dz \tag{5.10a}$$

$$\left(M_\theta^k, M_{x\theta}^k, R_\theta^k\right) = \int_{-h/2}^{h/2} \frac{1}{R + z}\left(\sigma_{\theta\theta}, \sigma_{x\theta}, \sigma_{\theta z}\right)\Phi_k \, dz \tag{5.10b}$$

Note that in Eqs. (5.8) and Eqs. (5.10), the superscript k refers to the kth surface in the laminated composite tube. Also, the following traction-free boundary conditions must be satisfied:

$$R_\theta^k = Q_x^k = N_z^k = 0 \qquad (\text{at } z=\pm h/2) \tag{5.11}$$

By substituting Eq. (5.7) into three-dimensional constitutive law and the subsequent results into Eqs. (5.10), the stress resultants are given the following relations:

$$\begin{aligned}\left(N_z^k, M_\theta^k, M_{x\theta}^k\right) &= \left(B_{36}^{jk}, H_{26}^{kj}, H_{66}^{kj}\right)U_j' + \left(B_{23}^{jk}, H_{22}^{kj}, H_{26}^{kj}\right)V_j' \\ &+ \left(B_{23}^{jk} + A_{33}^{kj}, H_{22}^{kj} + B_{23}^{kj}, H_{26}^{kj} + B_{36}^{kj}\right)W_j \\ &- \left(\bar{B}_{36}^k, B_{26}^k, B_{66}^k\right)C_3 + \left(\bar{B}_{13}^k, B_{12}^k, B_{16}^k\right)C_5\cos\theta \\ &+ \left(A_{13}^k, F_{12}^k, F_{16}^k\right)C_6\end{aligned}$$

$$\begin{aligned}\left(Q_x^k, Q_\theta^k, R_\theta^k\right) &= \left(A_{55}^{kj}, A_{45}^{kj}, B_{45}^{kj}\right)U_j + \left(B_{45}^{jk}, B_{44}^{jk}, H_{44}^{kj}\right)W_j' \\ &+ \left(A_{45}^{kj} - B_{45}^{jk}, A_{44}^{kj} - B_{44}^{jk}, B_{44}^{kj} - H_{44}^{kj}\right)V_j\end{aligned} \tag{5.12}$$

where the laminate rigidities in Eq. (5.12) are defined as:

$$\begin{aligned}\left(A_{pq}^{kj}, \bar{B}_{pq}^{kj}, D_{pq}^{kj}\right) &= \sum_{i=1}^{N}\int_{z_i}^{z_{i+1}} \bar{C}_{pq}^{(i)}\left(\phi_k'\phi_j', \phi_k\phi_j', \phi_k\phi_j\right)\mathrm{d}z \\ \left(B_{pq}^{kj}, H_{pq}^{kj}, G_{pq}^{kj}\right) &= \sum_{i=1}^{N}\int_{z_i}^{z_{i+1}} \bar{C}_{pq}^{(i)}\left(\frac{\phi_k\phi_j'}{R+z}, \frac{\phi_k\phi_j}{(R+z)^2}, \frac{\phi_k\phi_j}{R+z}\right)\mathrm{d}z \\ \left(A_{pq}^k, B_{pq}^k, \bar{B}_{pq}^k\right) &= \sum_{i=1}^{N}\int_{z_i}^{z_{i+1}} \bar{C}_{pq}^{(i)}\left(\phi_k', \phi_k, \phi_k'(R+z)\right)\mathrm{d}z \\ \left(D_{pq}^k, F_{pq}^k, E_{pq}^k\right) &= \sum_{i=1}^{N}\int_{z_i}^{z_{i+1}} \bar{C}_{pq}^{(i)}\left(\frac{\phi_k}{(R+z)^2}, \frac{\phi_k}{R+z}, \frac{\phi_k'}{R+z}\right)\mathrm{d}z \\ &\left(k, j = 1,2,...,N+1\right)\end{aligned} \tag{5.13}$$

The local displacement equilibrium equations within the proposed method are obtained by substituting Eq. (5.12) into Eq. (5.8):

$$\delta U_k : -H_{66}^{kj}U_j'' + A_{55}^{kj}U_j - H_{26}^{kj}V_j'' - B_{45}^{jk}V_j - \left(H_{26}^{kj} + B_{36}^{kj} - B_{45}^{jk}\right)W_j' = -B_{16}^{k}C_5 \sin\theta$$

$$\delta V_k : -H_{26}^{kj}U_j'' + \left(A_{45}^{kj} - B_{45}^{kj}\right)U_j - H_{22}^{kj}V_j'' + \left(A_{44}^{kj} - B_{44}^{kj} - B_{44}^{jk} + H_{44}^{kj}\right)V_j$$
$$-\left(H_{22}^{kj} + B_{23}^{kj} - B_{44}^{jk} + H_{44}^{kj}\right)W_j' = -B_{12}^{k}C_5 \sin\theta$$

$$\delta W_k : \left(-B_{45}^{kj} + H_{26}^{kj} + B_{36}^{jk}\right)U_j' + \left(H_{44}^{kj} - B_{44}^{kj} + H_{22}^{kj} + B_{23}^{jk}\right)V_j' - H_{44}^{kj}W_j''$$
$$+\left(H_{22}^{kj} + B_{23}^{jk} + B_{23}^{kj} + A_{33}^{kj}\right)W_j = \left(\bar{B}_{36}^{k} + B_{26}^{k}\right)C_3 - \left(\bar{B}_{13}^{k} + B_{12}^{k}\right)C_5 \cos\theta$$
$$-\left(A_{13}^{k} + F_{12}^{k}\right)C_6$$
$$k, j = 1, 2, ..., N+1 \qquad (5.14)$$

Also, the global equilibrium equations of the composite straight tube are expressed in terms of displacement functions by substituting Eq. (5.7) into three-dimensional constitutive law and the subsequent results into Eqs. (5.9). The results are given as:

$$\delta C_3 : \frac{1}{h}\int_{-\pi}^{\pi}\left(\bar{B}_{16}C_6 + \bar{D}_{16}C_5\cos\theta + B_{26}^{k}\left(V_j' + W_j\right) + \bar{B}_{36}^{k}W_j - \bar{D}_{66}C_3 + A_{66}^{k}U_j'\right)d\theta = T_0$$

$$\delta C_5 : \int_{-\pi}^{\pi}\begin{pmatrix}\bar{B}_{11}C_6\cos\theta + \bar{D}_{11}C_5\cos^2\theta + B_{12}^{k}\left(V_j' + W_j\right)\cos\theta \\ +F_{13}^{k}W_j\cos\theta - \bar{D}_{16}C_3\cos\theta + B_{16}^{k}U_j'\cos\theta\end{pmatrix}d\theta = M_0$$

$$\delta C_6 : \int_{-\pi}^{\pi}\left(\bar{A}_{11}C_6 + \bar{B}_{11}C_5\cos\theta + F_{12}^{k}\left(V_j' + W_j\right) + B_{13}^{k}W_j - \bar{B}_{16}C_3 + F_{16}^{k}U_j'\right)d\theta = F_0 \qquad (5.15)$$

where the extra laminate rigidities appearing in Eqs. (5.15) are written as:

$$\left(\bar{A}_{pq}, \bar{B}_{pq}, \bar{D}_{pq}\right) = \sum_{i=1}^{N}\int_{z_i}^{z_{i+1}}\bar{C}_{pq}^{(i)}\left(1, R+z, (R+z)^2\right)\mathrm{dz}$$

$$\left(\bar{F}_{pq}, \bar{E}_{pq}\right) = \sum_{i=1}^{N}\int_{z_i}^{z_{i+1}}\bar{C}_{pq}^{(i)}\left(\frac{1}{R+z}, \frac{1}{(R+z)^2}\right)\mathrm{dz} \qquad (5.16)$$

5.4. Analytical Solution

The system in Eqs. (5.14) shows *3(N+1)* coupled ordinary differential equations with constant coefficients which may be displayed in a matrix form as follows:

$$[M]\{\eta''\} + [K]\{\eta\} = \{F\}\{C\} \qquad (5.17)$$

where

$$\{\eta\}=\left\{\{U\}^T,\{V\}^T,\{\bar{W}\}^T\right\}^T$$

$$\{U\}=\{U_1,U_2,...,U_{N+1}\}^T \qquad \{C\}=\{C_3,C_5,C_6\}^T$$

$$\{V\}=\{V_1,V_2,...,V_{N+1}\}^T$$

$$\{\bar{W}\}=\{\bar{W}_1,\bar{W}_2,...,\bar{W}_{N+1}\}^T \qquad (5.18a)$$

and

$$\bar{W}_j=\int^{\theta} W_j \mathrm{d}\theta \qquad (5.18b)$$

The coefficient matrices [M], [K] and {F} in Eq. (5.17) are defined in *Appendix E*. It can readily be confirmed that the general solution of Eq. (5.17) may be presented as:

$$\{\eta\}=[\psi]\left[\sinh(\lambda\theta)\right]\{k\}+[K]^{-1}\{F\}\{C\} \qquad (5.19)$$

and [sinh (λθ)] is a *3(N+1)×3(N+1)* diagonal matrix. That is:

$$\left[\sinh(\lambda\theta)\right]=diag\left(\sinh(\lambda_1\theta),\sinh(\lambda_2\theta),...,\sinh\left(\lambda_{3(N+1)}\theta\right)\right) \qquad (5.20)$$

Also [ψ] and $\left(\lambda_1^2,\lambda_2^2,\ldots,\lambda_{3(N+1)}^2\right)$ are the model matrix and eigenvalues of (-[M]$^{-1}$[K]), respectively. Vector $\{k\}$ is an unknown vector representing *3(N+1)* integration constants. The constants *Cj* (j=3, 5 and 6) must be calculated within the analytical analysis. Therefore, the boundary conditions in Eq. (5.11) are first imposed to calculate the vector $\{k\}$ in terms of the unknown parameters *Cj* (j=3, 5 and 6). These constants are then obtained in terms of the specified axial force F_0 or/and bending moment M_0 or/and torque T_0 by the satisfaction of the global equilibrium conditions in Eqs. (5.15).

5.5. Lay-up Sequence Selection

Composite straight tubes with the [90°$_{20}$/0°$_{20}$] and [90°$_{30}$/±25°$_{45}$/90°$_5$/±30°$_{20}$/90°$_5$/±45°$_{20}$] lay-up sequences were manufactured and four-point and three-point bending tests were performed, respectively, to be used for making composite landing gears for helicopters [1]. Table 5.1 shows two types of lay-up sequences considered here. First, the [90°$_{20}$/0°$_{20}$] composite tube is selected to compare the numerical results obtained using the proposed method with finite element method (ANSYS) and experimental data for the thick laminated composite straight tube subjected to pure bending moment. Finally, the thick

$[90°_{30}/\pm25°_{45}/90°_{5}/\pm30°_{20}/90°_{5}/\pm45°_{20}]$ laminated composite tube is considered to study stress distributions in composite straight tubes under combined loading conditions.

Table 5.1: Lay-up sequence number.

Laminate number	Lay-up sequence
1	$[90°_{20}/0°_{20}]$ Available experimental data
2	$[90°_{30}/\pm25°_{45}/90°_{5}/\pm30°_{20}/90°_{5}/\pm45°_{20}]$ Study stress distributions

5.6. FEM Analysis

The stress analysis of the composite tube is conducted by finite element method using ANSYS. Stress distributions are also generated to compare with the numerical results obtained using the proposed method. The element used to perform the analysis was the layered solid element, SOLID 185. The properties of the composite tube are given in Table 5.2. The composite tubes are modeled according to the manufactured composite tube. The mesh-independency study is done for ANSYS. Mesh refining is performed two times while the element aspect ratio was kept constant. It is emphasized that for the initial mesh, 22680 elements (*9 (Axial) × 12 (circumferential) × 210 (thickness directions)*) are used to model the structure. For the 1st refined mesh, the thickness and circumferential directions are refined twice as much as the initial mesh (*90720 elements totally*). In addition, for the 2nd refined mesh, the axial and circumferential directions are refined twice as much as the initial mesh and the thickness direction is refined 4 times as much as the initial mesh to model the composite tube (*362880 elements totally*). Figure 5.2 presents the hoop stress distribution along the length in the thick laminated composite straight tube using ANSYS 14.5.

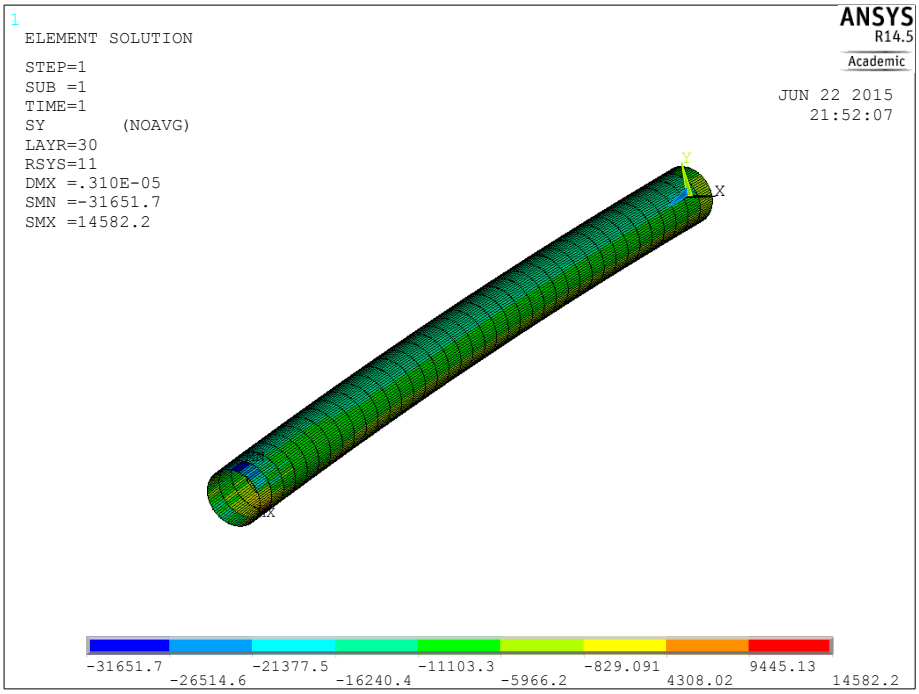

Figure 5.2: Distribution of the hoop stress in the composite tube subjected to combined loadings using ANSYS 14.5 (*unit: Pa*).

5.7. Results and Discussion

Numerical results are presented in four following sections. First, in Section 5.7.1, the comparison is made between the experimental data with those obtained using the present method. Second, in Section 5.7.2, the numerical results obtained by the proposed method are compared with FEM results. Third, in Section 5.7.3, the advantages of the proposed method over FEM and other methods are discussed. Finally, in Section 5.7.4, stress distributions in thick laminated composite straight tubes subjected to axial force, torque and bending moment are studied. In all the subsequent calculations, p is set equal to 12 [92]. The mechanical properties of the composite tube are given in Table 5.2 [1].

Table 5.2: Mechanical properties of the manufactured composite tube.

Properties	E_1 (GPa)	$E_2=E_3$ (GPa)	$G_{12}=G_{13}= G_{23}$ (GPa)	$\upsilon_{12}=\upsilon_{13}$	υ_{23}
Carbon AS4/PEEK	140	10	5.56	0.31	0.33

Furthermore, the stress components are normalized as $\bar{\sigma}_{ij}=\sigma_{ij}/\sigma_0$ where $\sigma_0=(M_0.r)/(\pi/64*(OD^4-ID^4)) + (T_0.r)/(\pi/32*(OD^4-ID^4)) + (F_0)/(\pi/4*(OD^2-ID^2))$ where the outer diameter and the inner diameter of the composite straight tube are represented as *OD* and *ID*, respectively. In the present cases, the tube section with the $[90°_{30}/\pm25°_{45}/90°_5/\pm30°_{20}/90°_5/\pm45°_{20}]$ lay-up sequence has an internal diameter of 56 mm and an external diameter of 98 mm, *i.e.* a wall thickness of 21 mm (totally 210 layers). Also, the length of the composite straight tube is 405 mm. Thickness is kept constant for all physical layers [1]. Note that in this chapter, mentioning combined loadings are meant by all loading conditions (*i.e.,* axial force, torque and bending moment) are applied together. In addition, remark that $M_0=10\ N.m$, $T_0=10\ N.m$ and $F_0=10\ N$ are assumed.

5.7.1. Comparison of the Proposed Method with Experimental Data

In this part, the proposed method results are compared with experimental data. The bending behavior of thick composite tubes was investigated experimentally [1]. The thick $[90°_{20}/0°_{20}]$ thermoplastic composite tubes were manufactured using automated fiber placement technique and tested using a four-point bending test setup. The properties of the manufactured composite tube are given in Table 5.2. In the experimental case, the tube section has an internal diameter of 56 mm and an external diameter of 64 mm. In addition, the whole length of the composite tube is 810 mm while the tube length under the pure bending condition is 405 mm. The composite tube was made with 40 layers. Since four-point bending test results are available, the composite tube is studied under pure bending moment just to compare with experimental data. In the experimental investigation [1], the strain gage was used on the surface of the composite tube at the top line of the tube ($\theta=90°$) to measure strains at the mid-span. The measured strain results are compared with the calculated strain results using the proposed method at $\theta=90°$. In Figure 5.3, the force variation versus experimental axial strains is shown. Good agreement is obtained between the analytical analysis and experimental results. In addition, FEM (ANSYS) (*see Figure 5.3*) is used to evaluate the accuracy of the proposed method. It is seen that the proposed method results are closer to the experimental data compared to those of FEM (ANSYS). In addition, the results obtained using the proposed method show good correspondence at the higher level of load compared to

those of FEM. It is noted that the 2nd refined mesh (*see Section 5.6*) is used to get FEM results here.

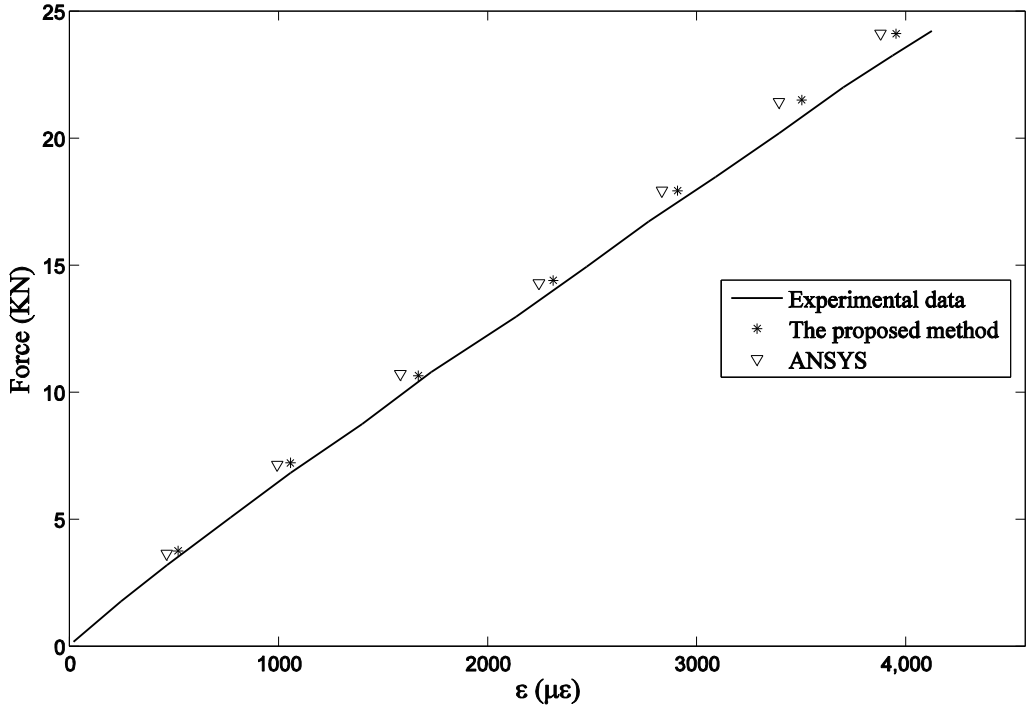

Figure 5.3: Force-axial strain at the top line of the tube (θ=90°).

5.7.2. Comparison of the Proposed Method and FEM

The interlaminar stresses, $\bar{\sigma}_{zz}$ and $\bar{\sigma}_{zx}$, of the $[90°_{30}/\pm25°_{45}/90°_{5}/\pm30°_{20}/90°_{5}/\pm45°_{20}]$ laminated composite straight tube under combined loadings at *r=31 mm* and *r=40 mm* obtained by the present method and FEM (ANSYS) are compared in Figure 5.4. Good agreement is observed between analytical analysis and FEM (ANSYS) results. Analyzing of the composite straight tube with the initial mesh takes around 1200 seconds while it takes around 2100 and 4200 seconds with the 1st refined and the 2nd refined meshes, respectively. However, the analyzing of the same structure (*same complex lay-up*) using the developed method takes 560 seconds.

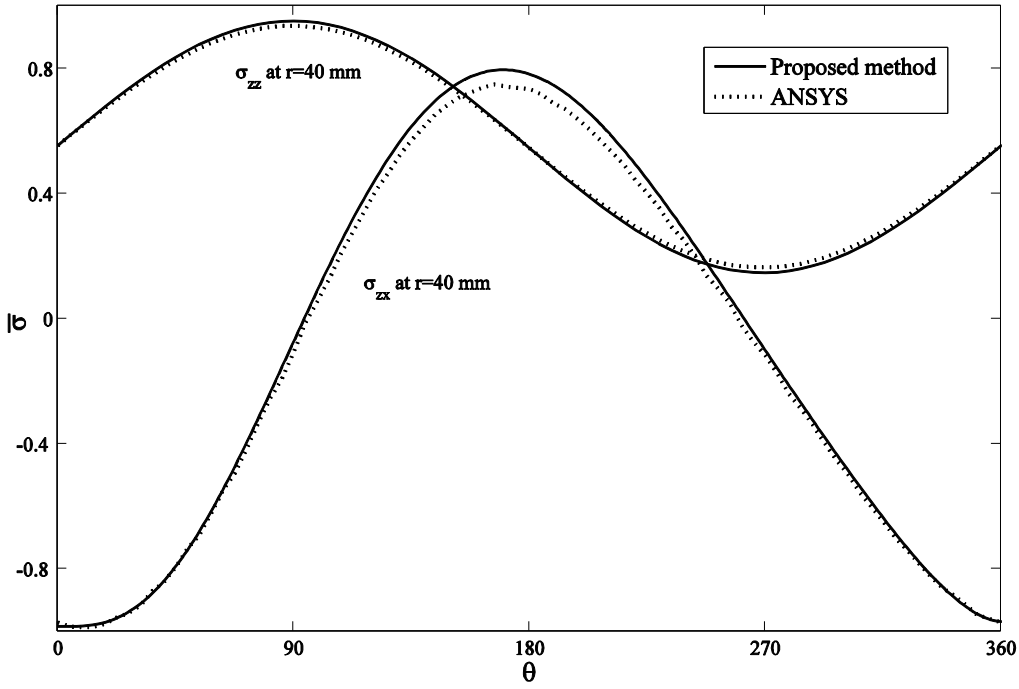

Figure 5.4: Comparison of the radial and shear stresses, $\bar{\sigma}_{zz}$ and $\bar{\sigma}_{zx}$, obtained from the proposed method and ANSYS of the $[90°_{30}/\pm25°_{45}/90°_{5}/\pm30°_{20}/90°_{5}/\pm45°_{20}]$ laminated composite straight tube.

5.7.3. Advantages of the Proposed Method

FEM has a unique limitation: every time the geometry, loading, lay-up sequences or materials change, simulations need to be carried out afresh, which might involve a new mesh generation and computation. The most important advantage of the proposed method is that inputs for the modeling of composite structures with complex lay-up sequences (*see Table 5.1*) are simple, easy to use, and fast to run. Contrary, to model complex lay-up composite structures in FEM, it is necessary to create individual sections and mesh them separately with different lay-up attributes. However, through using the proposed method, it is required to simply input dimensions and lay-up sequences at the beginning of the program. Therefore, it is obvious that the modeling of composite structures with complex lay-up sequences using FEM takes much longer compared to using the developed method. In addition, the proposed method takes less computational time as compared to the conventional 3D FEM and providing the better level of accuracy.

One of the other advantages of the developed method is the accuracy of the obtained results (*see Figure 5.3*). It was shown that the results obtained using the proposed method is more accurate than FEM results compared to experimental data. In addition, using FEM for parametric study is cumbersome while this method is applied easily for any parametric study with low computational cost. For example, to study the effects of thickness on stress and strain distributions by using FEM, it is necessary to model the geometry for different thicknesses and obviously it takes much longer than using the present method.

5.7.4. Stress Distributions

The thick $[90°_{30}/\pm25°_{45}/90°_{5}/\pm30°_{20}/90°_{5}/\pm45°_{20}]$ laminated composite tube which has 210 layers in total is selected to study stress distributions of the thick composite straight tube subjected to axial force, torque and bending moment. The results are presented based on the proposed method at *r=31 mm* (the last 90°-ply of the first 90° layer-group from inside, *i.e., layer 30*), *r=40 mm* (the last 25°-ply of the ±25° layer-group, *i.e., layer 120*), *r=44.5 mm* (the last 30°-ply of ±30° layer-group, *i.e., layer 165*) and *r=45 mm* (the last 90°-ply of the third 90° layer-group, *i.e., layer 170*) as shown in Figure 5.5.

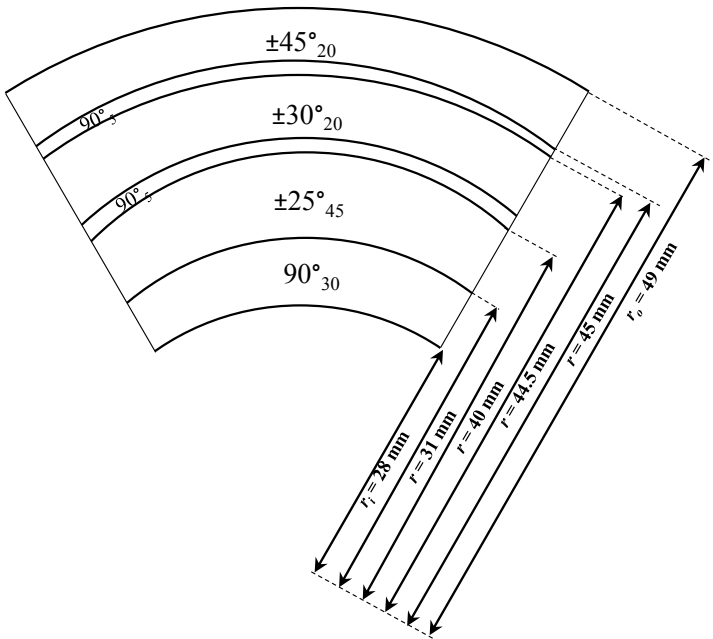

$[90°_{30}/\pm25°_{45}/90°_{5}/\pm30°_{20}/90°_{5}/\pm45°_{20}]$

Figure 5.5: The lay-up sequence of the thick laminated composite straight tube.

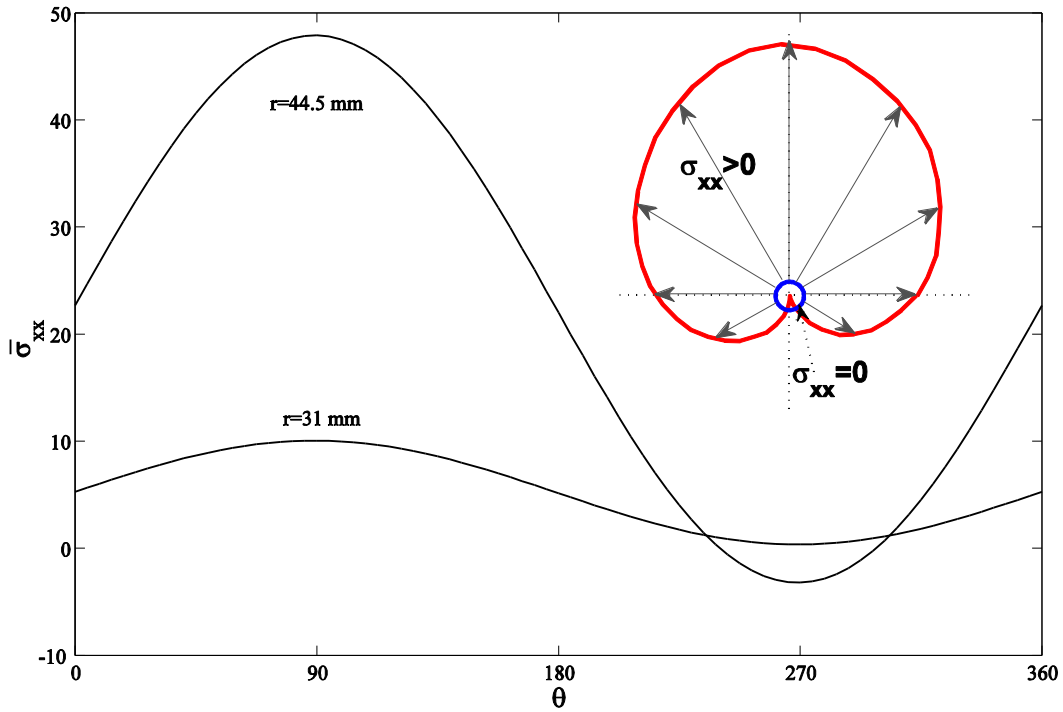

Figure 5.6a: Distributions of the axial stress $\bar{\sigma}_{xx}$ of the $[90°_{30}/\pm25°_{45}/90°_{5}/\pm30°_{20}/90°_{5}/\pm45°_{20}]$ laminated composite straight tube.

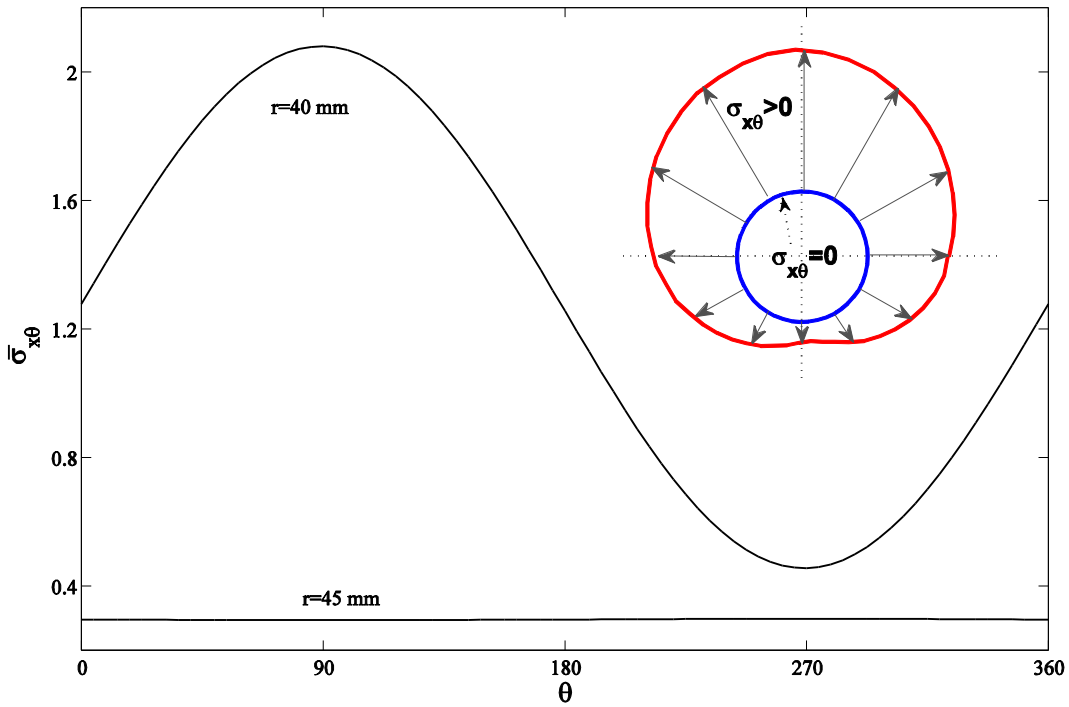

Figure 5.6b: Distributions of the shear stress $\bar{\sigma}_{x\theta}$ of the $[90°_{30}/\pm25°_{45}/90°_{5}/\pm30°_{20}/90°_{5}/\pm45°_{20}]$ laminated composite straight tube.

The distributions of the axial, $\bar{\sigma}_{xx}$, and shear stresses, $\bar{\sigma}_{x\theta}$, of the thick $[90°_{30}/\pm25°_{45}/90°_{5}/\pm30°_{20}/90°_{5}/\pm45°_{20}]$ laminated composite tube along the circumferential direction are shown in Figures 5.6a and 5.6b. It is seen that the axial, $\bar{\sigma}_{xx}$, and shear stresses, $\bar{\sigma}_{x\theta}$, have an asymmetric behavior. In addition, the shear stress, $\bar{\sigma}_{x\theta}$, is positive at the whole tube cross section while the axial stress, $\bar{\sigma}_{xx}$, is negative at a part of the lower region of the tube cross section (180°-360°). In addition, to understand the stress behavior better, the polar distribution of the axial stress, $\bar{\sigma}_{xx}$, and the shear stress, $\bar{\sigma}_{x\theta}$, at *r=44.5 mm* and *r=40 mm* of the thick laminated composite tube obtained by the present method is shown in Figures 5.6a and 5.6b, respectively. Note that in all polar distributions in the rest of the chapter, blue circle represents the zero stress condition while red lines represent the stress distributions. Also, the lengths of arrows represent the magnitudes of stresses. Therefore, those red lines where are placed inside the blue circle represent the compressive stress while the other red lines where are placed outside of the blue circle represent the tensile stress.

The distributions of the interlaminar radial stress, $\bar{\sigma}_{zz}$, and the shear stress, $\bar{\sigma}_{zx}$, of the $[90°_{30}/\pm25°_{45}/90°_{5}/\pm30°_{20}/90°_{5}/\pm45°_{20}]$ laminated composite tube along the circumferential direction are shown in Figure 5.7a. The positive maximum value of the interlaminar normal stress, $\bar{\sigma}_{zz}$, occurs at θ=270°. It is noted that the positive radial stress, $\bar{\sigma}_{zz}$, can cause delamination phenomena in the cross section of the composite tube. The magnitude of the interlaminar radial stress, $\bar{\sigma}_{zz}$, is greater than that of the shear stress $\bar{\sigma}_{zx}$. Figure 5.7b presents the polar distributions of the interlaminar radial stress, $\bar{\sigma}_{zz}$, and the shear stress, $\bar{\sigma}_{zx}$, of the $[90°_{30}/\pm25°_{45}/90°_{5}/\pm30°_{20}/90°_{5}/\pm45°_{20}]$ laminated composite tube over cross section at *r=45 mm* and *r=31 mm*, respectively, obtained based on the present method.

Figure 5.8a presents the distributions of the hoop stress, $\bar{\sigma}_{\theta\theta}$, and the shear stress, $\bar{\sigma}_{\theta z}$, of the $[90°_{30}/\pm25°_{45}/90°_{5}/\pm30°_{20}/90°_{5}/\pm45°_{20}]$ laminated composite tube along the circumferential direction. It is observed that the hoop stress, $\bar{\sigma}_{\theta\theta}$, is positive at the upper region of the tube cross section while the shear stress, $\bar{\sigma}_{\theta z}$, sign changes in this region (0°-180°). The maximum value of the hoop stress, $\bar{\sigma}_{\theta\theta}$, occurs at θ=90° while maximum value of the shear stress, $\bar{\sigma}_{\theta z}$, occurs at θ=0°. Figure 5.8b presents the polar distributions of the hoop stress, $\bar{\sigma}_{\theta\theta}$, and the shear stress, $\bar{\sigma}_{\theta z}$, of the $[90°_{30}/\pm25°_{45}/90°_{5}/\pm30°_{20}/90°_{5}/\pm45°_{20}]$ laminated composite tube over cross section at *r=44.5 mm* and *r=40 mm*, respectively, obtained based on the present method.

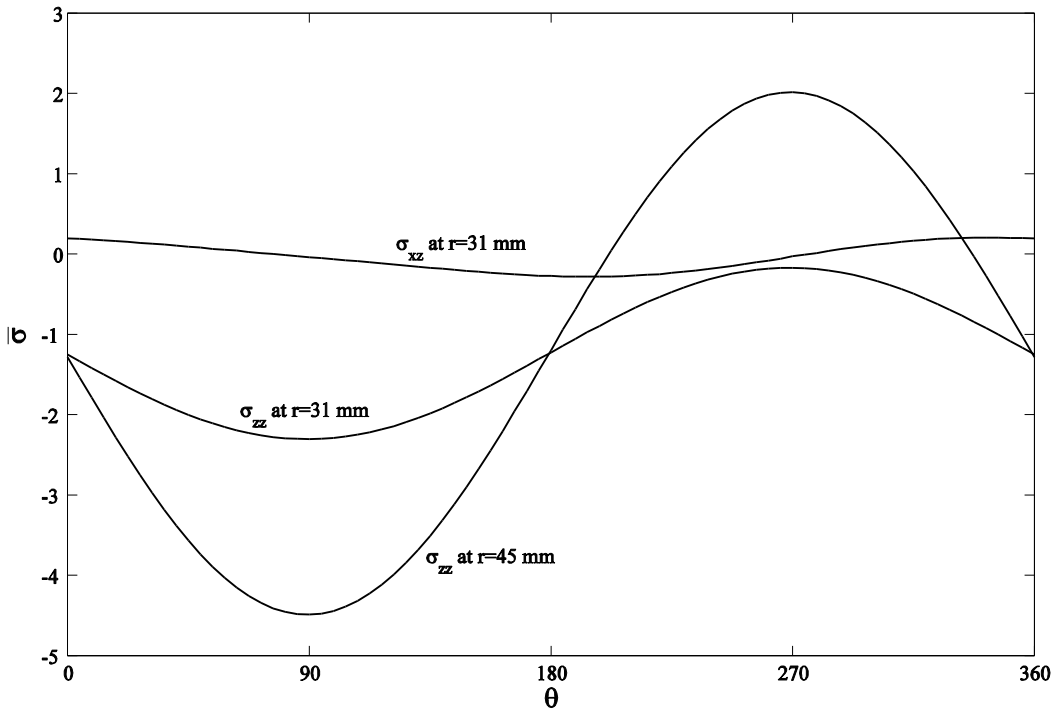

Figure 5.7a: Distributions of the interlaminar radial stress $\bar{\sigma}_{zz}$ and shear stress $\bar{\sigma}_{zx}$ of the $[90°_{30}/\pm25°_{45}/90°_{5}/\pm30°_{20}/90°_{5}/\pm45°_{20}]$ laminated composite straight tube.

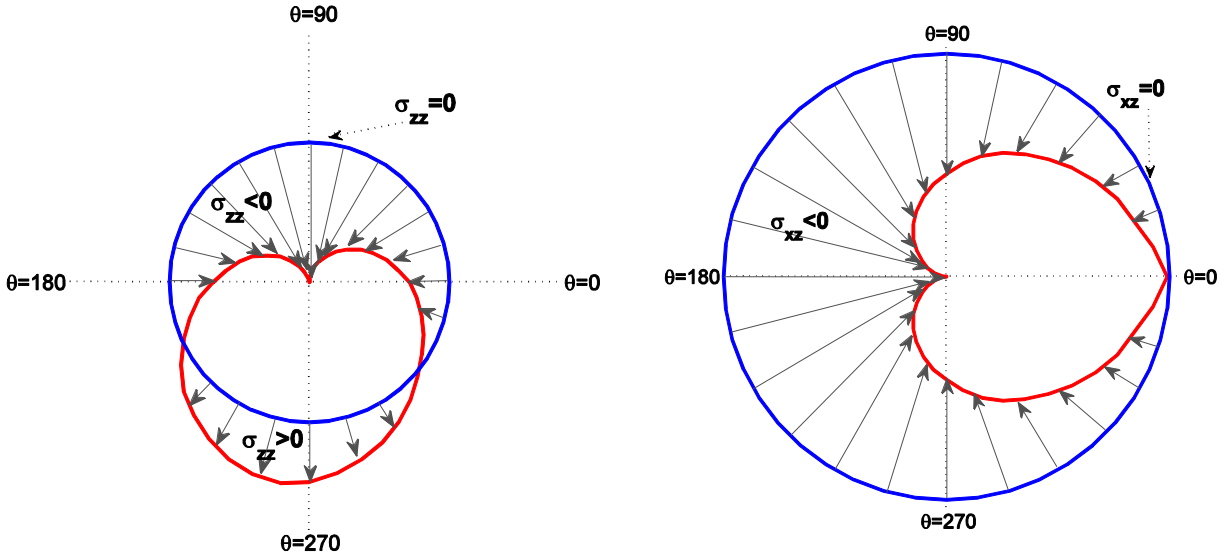

Figure 5.7b: Polar distributions of the interlaminar radial stress $\bar{\sigma}_{zz}$ and shear stress $\bar{\sigma}_{zx}$ of the $[90°_{30}/\pm25°_{45}/90°_{5}/\pm30°_{20}/90°_{5}/\pm45°_{20}]$ laminated composite straight tube.

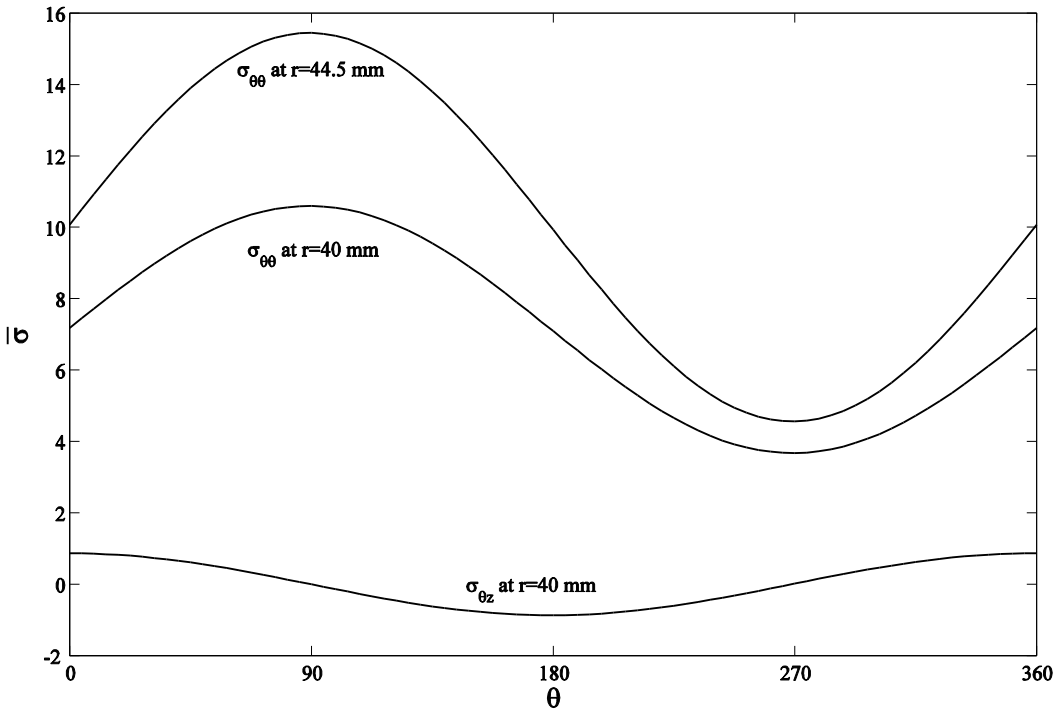

Figure 5.8a: Distributions of the hoop stress $\bar{\sigma}_{\theta\theta}$ and shear stress $\bar{\sigma}_{\theta z}$ of the $[90°_{30}/\pm25°_{45}/90°_{5}/\pm30°_{20}/90°_{5}/\pm45°_{20}]$ laminated composite straight tube.

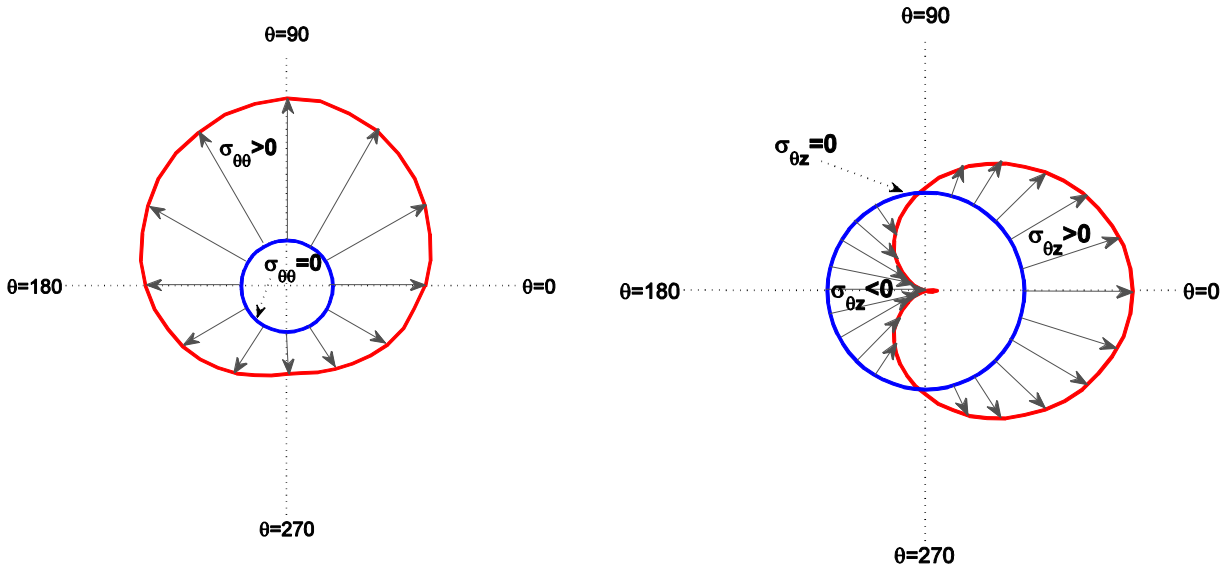

Figure 5.8b: Polar distributions of the hoop stress $\bar{\sigma}_{\theta\theta}$ and shear stress $\bar{\sigma}_{\theta z}$ of the $[90°_{30}/\pm25°_{45}/90°_{5}/\pm30°_{20}/90°_{5}/\pm45°_{20}]$ laminated composite straight tube.

Since the radial stress affects delamination and the hoop stress affects buckling, the interlaminar radial and hoop stresses distributions along the tube thickness are studied. The

distributions of the interlaminar radial stress, $\bar{\sigma}_{zz}$, and the hoop stress, $\bar{\sigma}_{\theta\theta}$, of the thick $[90°_{30}/\pm25°_{45}/90°_{5}/\pm30°_{20}/90°_{5}/\pm45°_{20}]$ laminated composite tube under pure bending moment along the thickness at θ=90° are shown in Figures 5.9a and 5.9b, respectively. It is seen that the radial stress, $\bar{\sigma}_{zz}$, is compressive totally along the tube thickness while the hoop stress, $\bar{\sigma}_{\theta\theta}$, is compressive at the inside surface and becoming positive by closing to the outside surface of the composite straight tube. As it is expected from Eqs. (5.11), Figure 5.9a shows that the interlaminar radial stress, $\bar{\sigma}_{zz}$, is zero at the inside and outside surfaces of the composite tube (N_z^k*=0 at z= ±h/2*). The maximum value of the radial stress, $\bar{\sigma}_{zz}$, occurs at *r=31 mm* along the tube thickness, where the last 90°-ply of the first 90° layer-group is placed. While the maximum magnitude of the hoop stress, $\bar{\sigma}_{\theta\theta}$, occurs at *r=45 mm*, where the last 90°-ply of the third 90° layer-group is placed.

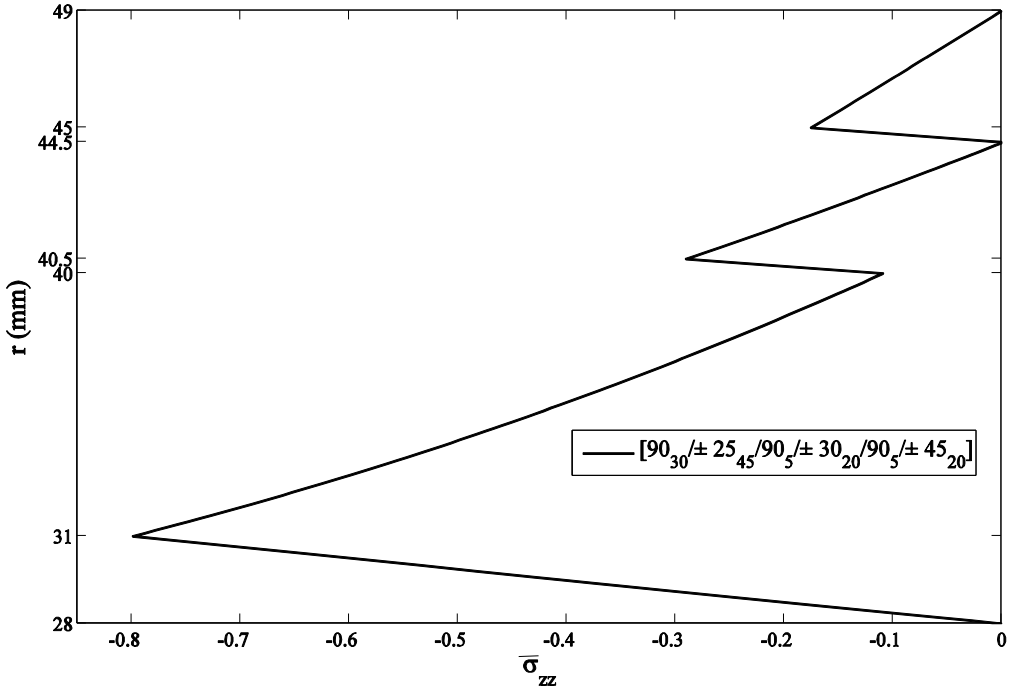

Figure 5.9a: Distributions of the interlaminar radial stress $\bar{\sigma}_{zz}$ of the $[90°_{30}/\pm25°_{45}/90°_{5}/\pm30°_{20}/90°_{5}/\pm45°_{20}]$ laminated composite straight tube along the thickness at θ=90°.

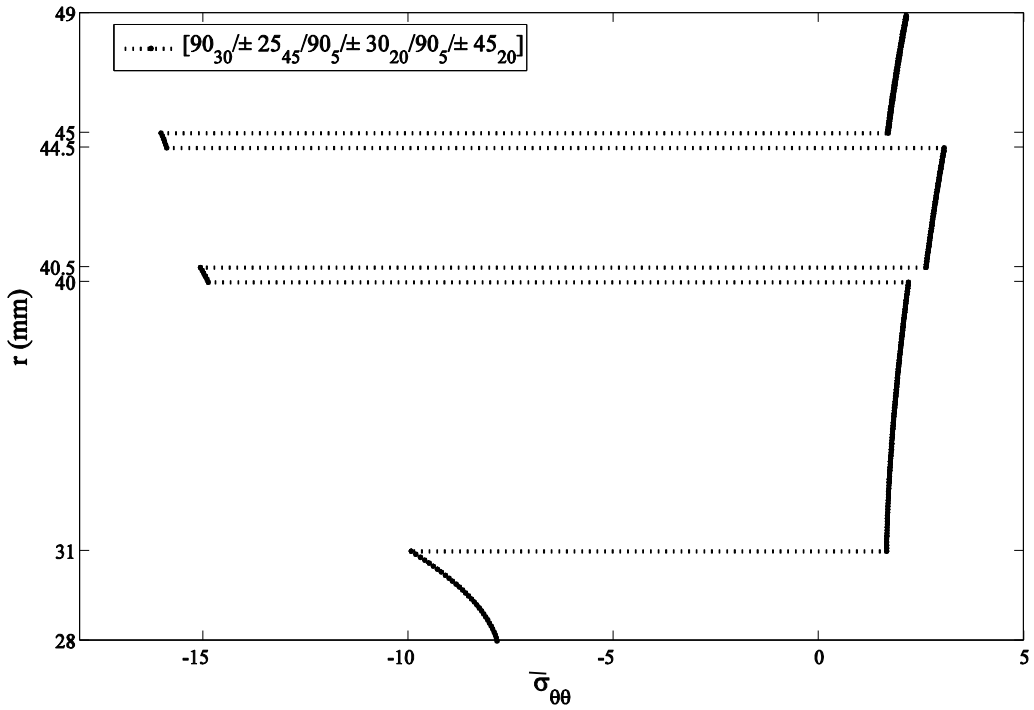

Figure 5.9b: Distributions of the hoop stress $\bar{\sigma}_{\theta\theta}$ of the $[90°_{30}/\pm25°_{45}/90°_{5}/\pm30°_{20}/90°_{5}/\pm45°_{20}]$ laminated composite straight tube along the thickness at $\theta=90°$.

5.8. Conclusions

A new high-order simple-input displacement-based method was developed to investigate stresses in thick laminated composite straight tubes subjected to axial force, torque and bending moment. LWT was used to analytically determine the displacement components considering the most general displacement field of elasticity. The equilibrium equations of LWT were subsequently derived through a state-space approach. Also, the accuracy of the results was studied by comparing the experimental data and FEM with numerical results obtained from the proposed method. Good agreement was seen. Furthermore, the stresses were obtained using the present method, which was shown to be more cost effective and accurate compared to FEM.

Chapter 6

This chapter proposes a new method to investigate single-layer composite curved tubes subjected to pure bending moment by employing a displacement approach of Toroidal Elasticity. The governing equations are developed in three toroidal coordinates system. The method of successive approximation is used to find the general solution. The accuracy of the proposed method is assessed by comparing the numerical results obtained using the present method with FEM, stress-based Toroidal Elasticity and Lekhnitskii solution.

Three-dimensional Stress Analysis of Orthotropic Curved Tubes-Part 1: Single-layer Solution

Hamidreza Yazdani Sarvestani, Suong V. Hoa and Mehdi Hojjati

Department of Mechanical and Industrial Engineering, Concordia University, Montreal, Quebec H3G 1M8, Canada

Abstract

In this chapter, a new displacement-based method is proposed to investigate orthotropic curved tubes subjected to pure bending moment. A displacement approach of Toroidal Elasticity is chosen to analyze orthotropic curved tubes with a single layer. The governing equations are developed in three toroidal coordinates system. The method of successive approximation is used to find the general solution. Then, the governing equations are decomposed into different orders, based on a small parameter. The formulas for calculating different order displacement components are derived. The accuracy of the proposed method is subsequently verified by comparing the numerical results obtained using the proposed method with finite element method (FEM), stress-based Toroidal Elasticity and Lekhnitskii solution. The results show good correspondence. The proposed method provides advantages in terms of computational time compared to FEM.

Keywords: Displacement approach of Toroidal Elasticity; Orthotropic curved tubes; Successive approximation; Stress analysis; Finite element method.

6.1. Introduction

Composite tubes are structures that are frequently used in the aerospace, offshore and infrastructure industries. Prediction of the state of stress and strain in different layers of composite tubes is of theoretical interest and practical importance. In all applications, accurate design and inclusive analysis are important to guarantee safety. It should be noted that stress

analysis of composite cylindrical structures is often a complex task. A few reasons are responsible for such a complexity such as governing equations of composite tubes and the layer-wise failure of composite materials. In addition, the curved tube geometry is a lot more complicated than a flat geometry. Many researchers have investigated composite shells and tubes. The following two sections are a literature review of composite shell and tube analyses, and are based on whether structures have free-edges (*i.e.,* shells) or closed cross sections (*i.e.,* tubes).

6.1.1. Shell Analysis

To obtain a prediction of structural response, a third-order shell theory was proposed by Huang [8] based on Reddy's parabolic shear strain distribution. The theoretical modelling of laminated composite shells of arbitrary shape was developed to estimate the shear stresses and avoid shear correction factors [56]. In a similar way, Di and Rothert [10] calculated stress field in orthotropic cylindrical shells. Elasticity solutions for other types of loading of homogeneous composite shells were summarized in [12]. Zhang et al. [57] presented an analytical method to obtain the interlaminar stresses at curved boundaries of symmetric composite shells under in-plane loading on the basis of a zero-order approximation of the boundary-layer theory. Khare et al. [15] analyzed thermo-mechanical behavior of simply supported cross-ply composite and sandwich laminated doubly curved cylindrical and spherical shell panels. Hossain [34] studied the stress of anisotropic thick composite doubly curved shells and shell panels using a finite element model. Kress et al. [35] proposed a finite element model, which diminished the number of free parameters for each layer, to determine interlaminar stress distributions in laminated singly curved structures. Oktem and Chaudhuri [60] used a higher order shear deformation theory to obtain analytical solution for the deformation of a finite-dimensional cross-ply doubly-curved panel. Interlaminar normal stress distributions in moderately thick single-curved laminates were obtained to predict the critical delamination loads observed in experiments [61, 62].

6.1.2. Tube Analysis

Lekhnitskii [2] developed elasticity solutions for monolithic homogeneous orthotropic cylindrical tubes. Kardomateas [5] developed the case of uniform external pressure. To find out the energy absorption characteristics of glass-fiber circular tubes, Pickett and Dayal [23] performed a study. A method was developed to analyze the pure bending of arbitrary laminated composite tubes [24]. They verified formulations with FEM results obtained using ABAQUS. Menshykova and Guz [26] performed a stress analysis on thick laminated composite tubes subjected to bending load. They found stresses as a function of the material properties, thickness, lay-up and the magnitude of loads. Capela et al. [27] investigated the fatigue behavior of composite tubes under bending/torsion dynamic loadings. Recently, Nowak and Schmidt [29] compared some methods to study fiber metal laminated cylinders under an axisymmetric load. A developed theoretical model was validated by FEM analysis. Jonnalagadda et al. [30] presented an analytical model for a special design of thin composite tubes subjected to combined bending and torsion. They verified the theoretical results with FEM analysis.

The above review shows that there has been no work done to predict stress distributions in composite curved tubes subjected to mechanical loadings. Although finite element methods are used for analyzing such structures, it is necessary to do the meshing for each structure every time some dimensions or lay-up sequences are changed. Therefore, it is desired to have a method where the inputs to obtain solutions are simple; i.e. one only needs to enter in the actual dimensions or lay-up sequences without re-meshing work. The present chapter is devoted to develop a method that can provide stresses for composite curved tubes subjected to pure bending moment based on simple inputs. Displacement approach of Toroidal Elasticity (TE) and successive approximation method are used. Comparison is made between results obtained for the proposed method with finite element method (FEM), stress-based Toroidal Elasticity (SBTE) and Lekhnitskii solution. Good agreement is seen.

6.2. Motivation

The conventional landing gears for helicopters consist of two parallel curved cross tubes, which are connected by two longitudinal skid tubes as seen in Figure 6.1. The cross tube of

the helicopter landing gear consists of straight and curved tubes. Derisi [1] designed and manufactured composite straight tubes and performed four-point bending test to determine the strains to failure of different laminates. Recently, a method for the stress analysis of thick composite straight tubes subjected to cantilever loading was developed [92, 97]. Now, in order to provide some insight into the mechanical behavior of the curved part of helicopter landing gear, a simple-input displacement-based method is developed to examine stresses in a composite curved tube.

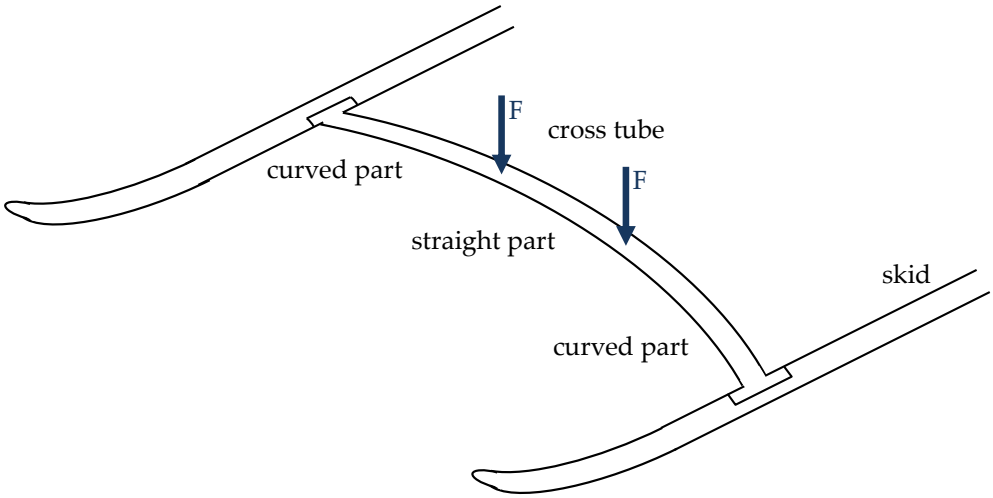

Figure 6.1: Helicopter landing gear.

6.3. Displacement Field of a Single-layer Composite Curved Tube

Toroidal Elasticity (TE) is a three-dimensional theory used for the elastostatic analysis of thick curved tubes. Although a few researchers performed earlier studies on TE, Lang [78] made a major improvement on the development of TE. This researcher employed specifically a stress approach, obtaining solutions and satisfying the equilibrium equations. Redekop [87] developed a displacement approach of TE for isotropic materials. Solutions satisfied Navier equations. Such an approach has the advantage of yielding immediately the displacements, as well as stresses. In this study, the displacement field of a single-layer composite curved tube is derived using a displacement approach of Toroidal Elasticity and the method of successive approximation.

6.3.1. Governing Equations in Toroidal Coordinates

An orthotropic curved tube with a bend radius R and thickness h is subjected to a pure bending moment, M, acted in the plane of ϕ=90° as shown in Figure 6.2. Annular cross section is bounded by radii a and b. Toroidal coordinate system (r, ϕ, θ) is placed at the mid-span of the composite curved tube where r and ϕ are polar coordinates in the plane of the tube cross section and θ defines the position of the tube cross section.

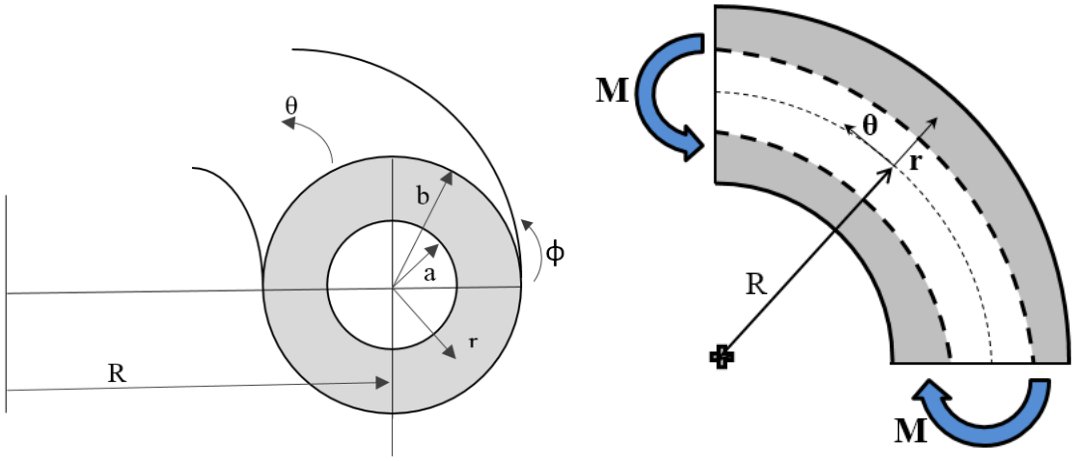

Figure 6.2: Geometry and coordinate system of the composite curved tube.

Zhu and Redekop [87] have given a derivation of the governing equations for linear three-dimensional theory of elasticity in the toroidal coordinates for isotropic material. The theory is extended here to cover the case for orthotropic materials. The toroidal governing equations are presented as [87]:

$$\frac{\partial \sigma_{rr}}{\partial r}+\frac{1}{r}\frac{\partial \sigma_{r\phi}}{\partial \phi}+\frac{1}{r}\left(\sigma_{rr}-\sigma_{\phi\phi}\right)+\frac{1}{\rho}\left(\frac{\partial \sigma_{r\theta}}{\partial \theta}+\left(\sigma_{rr}-\sigma_{\phi\phi}\right)\cos\phi-\sigma_{r\phi}\sin\phi\right)=0$$

$$\frac{\partial \sigma_{r\phi}}{\partial r}+\frac{1}{r}\frac{\partial \sigma_{\phi\phi}}{\partial \phi}+\frac{2}{r}\sigma_{r\phi}+\frac{1}{\rho}\left(\frac{\partial \sigma_{\phi\theta}}{\partial \theta}+\sigma_{r\phi}\cos\phi-\left(\sigma_{\phi\phi}-\sigma_{\theta\theta}\right)\sin\phi\right)=0$$

$$\frac{\partial \sigma_{r\theta}}{\partial r}+\frac{1}{r}\frac{\partial \sigma_{\phi\theta}}{\partial \phi}+\frac{1}{r}\sigma_{r\theta}+\frac{1}{\rho}\left(\frac{\partial \sigma_{\theta\theta}}{\partial \theta}+2\sigma_{r\theta}\cos\phi-2\sigma_{\phi\theta}\sin\phi\right)=0 \qquad (6.1)$$

where $\rho=R+r\cos\phi$. The kinematics relations are:

$$\varepsilon_{rr}=\frac{\partial u}{\partial r},\qquad \varepsilon_{r\phi}=\frac{1}{2}\left(\frac{1}{r}\frac{\partial u}{\partial \phi}+\frac{\partial v}{\partial r}-\frac{v}{r}\right),$$

$$\varepsilon_{\phi\phi}=\frac{u}{r}+\frac{1}{r}\frac{\partial v}{\partial \phi},\qquad \varepsilon_{r\theta}=\frac{1}{2}\left(\frac{\partial w}{\partial r}+\frac{1}{\rho}\frac{\partial u}{\partial \theta}-\frac{w}{\rho}\cos\phi\right),$$

$$\varepsilon_{\theta\theta}=\frac{1}{\rho}\left(u\cos\phi-v\sin\phi+\frac{\partial w}{\partial \theta}\right),\qquad \varepsilon_{\phi\theta}=\frac{1}{2}\left(\frac{1}{r}\frac{\partial w}{\partial \phi}+\frac{1}{\rho}\frac{\partial v}{\partial \theta}+\frac{w}{\rho}\sin\phi\right) \tag{6.2}$$

where u, v and w represent the displacement components in the r, ϕ and θ directions, respectively. For the orthotropic materials, the constitutive equations are [91]:

$$\{\sigma\}=[C]\{\varepsilon\} \tag{6.3}$$

where $C_{ij}^{(k)}$ represent the off-axis stiffnesses. Upon substitution of Eqs. (6.2) into Eq. (6.3), the stress-displacement relations are obtained:

$$\sigma_{rr}=C_{11}\frac{\partial u}{\partial r}+C_{12}\frac{u}{r}+\frac{C_{12}}{r}\frac{\partial v}{\partial \phi}+\frac{C_{13}}{\rho}\left(u\cos\phi-v\sin\phi+\frac{\partial w}{\partial \theta}\right)$$

$$\sigma_{\phi\phi}=C_{12}\frac{\partial u}{\partial r}+C_{22}\frac{u}{r}+\frac{C_{22}}{r}\frac{\partial v}{\partial \phi}+\frac{C_{23}}{\rho}\left(u\cos\phi-v\sin\phi+\frac{\partial w}{\partial \theta}\right)$$

$$\sigma_{\theta\theta}=C_{13}\frac{\partial u}{\partial r}+C_{23}\frac{u}{r}+\frac{C_{23}}{r}\frac{\partial v}{\partial \phi}+\frac{C_{33}}{\rho}\left(u\cos\phi-v\sin\phi+\frac{\partial w}{\partial \theta}\right)$$

$$\sigma_{r\phi}=\frac{C_{44}}{2}\left(\frac{1}{r}\frac{\partial u}{\partial \phi}+\frac{\partial v}{\partial r}-\frac{v}{r}\right)$$

$$\sigma_{r\theta}=\frac{C_{55}}{2}\left(\frac{\partial w}{\partial r}+\frac{1}{\rho}\frac{\partial u}{\partial \theta}-\frac{w}{\rho}\cos\phi\right)$$

$$\sigma_{\phi\theta}=\frac{C_{66}}{2}\left(\frac{1}{r}\frac{\partial w}{\partial \phi}+\frac{1}{\rho}\frac{\partial v}{\partial \theta}+\frac{w}{\rho}\sin\phi\right) \tag{6.4}$$

Substituting Eq. (6.4) into Eq. (6.1), the governing Navier equations in toroidal coordinate are obtained as:

$$\left(\frac{1}{\rho}\right)^0 U+\left(\frac{1}{\rho}\right)^1 \bar{U}+\left(\frac{1}{\rho}\right)^2 \hat{U}=0$$

$$\left(\frac{1}{\rho}\right)^0 V+\left(\frac{1}{\rho}\right)^1 \bar{V}+\left(\frac{1}{\rho}\right)^2 \hat{V}=0$$

$$\left(\frac{1}{\rho}\right)^0 W+\left(\frac{1}{\rho}\right)^1 \bar{W}+\left(\frac{1}{\rho}\right)^2 \hat{W}=0 \tag{6.5}$$

where the coefficients in Eqs. (6.5) are defined in *Appendix F*. The three Navier equations

serve as the fundamental equations for the displacement-based Toroidal Elasticity. Eqs. (6.5) are composed of three parts. The first part is independent of *1/ρ*. The second part and the third part are linear and non-linear parts of *1/ρ*. The Navier equations (Eqs. (6.5)) in the toroidal coordinate system are much more complicated than those in the Cartesian system. As it is impossible to find an exact solution for the Navier equations, the method of successive approximation is used to obtain an approximate solution.

6.3.2. Method of Successive Approximation

The method of successive approximation is a useful and powerful method to obtain solutions to equations. The solution for each component of the displacement is assumed a series in terms of a small parameter. The parameter ε is chosen as $\varepsilon=a/R$. Therefore, the displacement components take the following form:

$$\begin{aligned} u &= u_0 + \varepsilon u_1 + \varepsilon^2 u_2 + \varepsilon^3 u_3 + \ldots \\ v &= v_0 + \varepsilon v_1 + \varepsilon^2 v_2 + \varepsilon^3 v_3 + \ldots \\ w &= w_0 + \varepsilon w_1 + \varepsilon^2 w_2 + \varepsilon^3 w_3 + \ldots \end{aligned} \qquad (6.6)$$

where the subscripts of the right hand side terms indicate the order of the displacement components in the series. The functions of Navier equations are expanded as:

$$\begin{aligned} U &= U_0 + \varepsilon U_1 + \varepsilon^2 U_2 + \varepsilon^3 U_3 + \ldots \\ \bar{U} &= \bar{U}_0 + \varepsilon \bar{U}_1 + \varepsilon^2 \bar{U}_2 + \varepsilon^3 \bar{U}_3 + \ldots \\ \hat{U} &= \hat{U}_0 + \varepsilon \hat{U}_1 + \varepsilon^2 \hat{U}_2 + \varepsilon^3 \hat{U}_3 + \ldots \end{aligned} \qquad (6.7a)$$

$$\begin{aligned} V &= V_0 + \varepsilon V_1 + \varepsilon^2 V_2 + \varepsilon^3 V_3 + \ldots \\ \bar{V} &= \bar{V}_0 + \varepsilon \bar{V}_1 + \varepsilon^2 \bar{V}_2 + \varepsilon^3 \bar{V}_3 + \ldots \\ \hat{V} &= \hat{V}_0 + \varepsilon \hat{V}_1 + \varepsilon^2 \hat{V}_2 + \varepsilon^3 \hat{V}_3 + \ldots \end{aligned} \qquad (6.7b)$$

$$\begin{aligned} W &= W_0 + \varepsilon W_1 + \varepsilon^2 W_2 + \varepsilon^3 W_3 + \ldots \\ \bar{W} &= \bar{W}_0 + \varepsilon \bar{W}_1 + \varepsilon^2 \bar{W}_2 + \varepsilon^3 \bar{W}_3 + \ldots \\ \hat{W} &= \hat{W}_0 + \varepsilon \hat{W}_1 + \varepsilon^2 \hat{W}_2 + \varepsilon^3 \hat{W}_3 + \ldots \end{aligned} \qquad (6.7c)$$

where the coefficients in Eqs. (6.7) are defined in *Appendix F*. The quantities *1/ρ* and $(1/\rho)^2$ which appear in the Navier equations are functions of *r*. These quantities are expanded in a series of the parameter ε using the Taylor Theorem as:

$$\frac{1}{\rho} = \varepsilon - \varepsilon^2 r\cos\phi + \varepsilon^3 r^2\cos^2\phi - \ldots$$

$$\left(\frac{1}{\rho}\right)^2 = \varepsilon^2 - 2\varepsilon^3 r\cos\phi + 3\varepsilon^4 r^2\cos^2\phi - \ldots \qquad (6.8)$$

Substituting the expanded Navier functions (Eqs. (6.7)) and Eq. (6.8) into Eqs. (6.5), matching terms in ε, and setting the coefficients for each order of ε to zero, one obtains the governing equations for the different orders. The equations are expressed for the zeroth order as:

$$\begin{aligned} U_0 &= 0 \\ V_0 &= 0 \\ W_0 &= 0 \end{aligned} \qquad (6.9)$$

For the first order as:

$$\begin{aligned} U_1 &= -\bar{U}_0 \\ V_1 &= -\bar{V}_0 \\ W_1 &= -\bar{W}_0 \end{aligned} \qquad (6.10)$$

For the second order as:

$$\begin{aligned} U_2 &= -\bar{U}_1 + \bar{U}_0 r\cos\phi - \hat{U}_0 \\ V_2 &= -\bar{V}_1 + \bar{V}_0 r\cos\phi - \hat{V}_0 \\ W_2 &= -\bar{W}_1 + \bar{W}_0 r\cos\phi - \hat{W}_0 \end{aligned} \qquad (6.11)$$

And for the third order as:

$$\begin{aligned} U_3 &= -\bar{U}_2 + \bar{U}_1 r\cos\phi - \bar{U}_0 r^2\cos^2\phi - \hat{U}_1 + 2\hat{U}_0 r\cos\phi \\ V_3 &= -\bar{V}_2 + \bar{V}_1 r\cos\phi - \bar{V}_0 r^2\cos^2\phi - \hat{V}_1 + 2\hat{V}_0 r\cos\phi \\ W_3 &= -\bar{W}_2 + \bar{W}_1 r\cos\phi - \bar{W}_0 r^2\cos^2\phi - \hat{W}_1 + 2\hat{W}_0 r\cos\phi \end{aligned} \qquad (6.12)$$

The solution series through successive approximation method are local in ε and global in r. When ε is small, a good approximation to the solution by summing the first few terms of the series is obtained. When ε is not small, it may still be possible to generate a good approximation to the solution from converging series. In general, it is possible to select a ε so that the zeroth-order solution is found as a closed-form analytical expression.

The zeroth order governing equations (Eqs. (6.9)) are homogeneous equations. The right hand side terms for orders greater than zero carry contributions from the lower orders, and the complexity of the right hand side terms increases with order (*see Eqs. (6.9)-(6.12)*). There is

only a complementary solution for the zeroth order governing equations. For orders greater than zeroth, the solutions are made of a complementary and a particular part. The complementary part is obtained from the homogeneous part of that order's governing equations, which has the same form as that of the zeroth order. The particular part is found to satisfy the right hand side terms of the governing equations. The particular part is determined by using trial displacement functions with free constants, to match the right hand side terms of the governing equations of that order.

Solutions are developed consecutively for the various orders, starting from the zeroth order. The zeroth order solution is selected from the trial displacement functions. For orders greater than zero, the right hand side members of the Navier equations are obtained. The particular part is set up using trial functions. The total solution is the sum of the particular and complementary solutions of all orders factored by the appropriate power of ε (*see Eq. (6.6)*).

6.3.3. General Solution for In-plane Pure Bending

The solution is requested for a single-layer composite curved tube subjected to pure bending moment. The equations for the complementary part have the same form for all orders and it is useful to derive a general solution. A direct solution is formulated to avoid the complications, which arise from the use of stress function. The solution for the displacement components is thus sought in the following form for orders n=0, 1, 2 and 3:

$$\begin{aligned} u_n &= p_n r^m \cos(n\phi)\cos(\theta) \\ v_n &= x_n r^m \sin(n\phi)\cos(\theta) \\ w_n &= s_n r^{\bar{m}} \cos(n\phi)\sin(\theta) \end{aligned} \qquad (6.13)$$

The quantities p_n, x_n, s_n, m and $\bar{m}$ are constants and parameters. By substituting Eq. (6.13) into the homogeneous parts of Eqs. (6.9)-(6.12) for each order separately, the quantities p_n, x_n, s_n, m and $\bar{m}$ are determined for each order (*see Table 6.1*). The solution in the successive approximation method is given up to the 3rd order. The detailed solution is presented for a 90° composite curved tube with a single layer subjected to bending moment, M, as shown in Figure 6.2. Some points are fixed to avoid rigid body motion. It is seen from Eq. (6.13) that $w=0$ at θ=0°, and u and v are zero at ϕ=90° and 270°, respectively. In addition, the boundary conditions satisfied for the problem are as follows:

On the free curved surfaces, on $r=a$ and $r=b$

$$\sigma_{rr} = \sigma_{r\theta} = \sigma_{r\phi} = 0 \qquad (6.14)$$

On the end surfaces, at $\theta = \pm\pi/4$

$$M_n = \int_a^b \int_0^{2\pi} (\sigma_{\theta\theta n} r \sin\phi) r d\phi dr \qquad \text{for n=0,1,2 and 3} \qquad (6.15a)$$

$$M = M_0 + \varepsilon M_1 + \varepsilon^2 M_2 + \varepsilon^3 M_3 + \ldots \qquad (6.15b)$$

where M and M_n are the total applied bending moment and the moment component of the *nth* order, respectively. Note that the boundary conditions, Eq. (6.14), are satisfied by each order separately. Since total stresses are the sum of stresses of all orders factored by the appropriate power of ε, it is concluded that imposing the boundary conditions on each order physically represent correctly the problem. Therefore, these boundary conditions, Eq. (6.14), are applicable not only for each order but also on the whole solution. In addition, the moment components, M_n, are obtained for each order based on Eq. (6.15a) and then, Eq. (6.15b) is used to link all moment components to the total applied bending moment. The contributions from the various orders to the total solution are now developed, starting from the zeroth order.

6.3.3.1. The Zeroth Order Solution

The zeroth order governing equations are homogeneous, and thus only the complementary solution is required. By substituting Eq. (6.13) into Eqs. (6.9), considering Eqs. (D.1), (D.4) and (D.7) simultaneously, the zeroth order governing equations are obtained as:

Complementary solution (the zeroth order):

$$u_{0c} = a_0 B_{1,m_0} \cos(\theta)$$

$$v_{0c} = -a_0 A_{2,m_0} \cos(\theta)$$

$$w_{0c} = 0 \qquad (6.16a)$$

Particular solution (the zeroth order):

$$u_{0p} = 0$$

$$v_{0p} = 0$$

$$w_{0p} = 0 \qquad (6.16b)$$

Therefore, the zeroth order displacement components are obtained as:

$$u_0 = u_{0c} + u_{0p} = a_0 B_{1,m_0} \cos(\theta)$$
$$v_0 = v_{0c} + v_{0p} = -a_0 A_{2,m_0} \cos(\theta)$$
$$w_0 = w_{0c} + w_{0p} = 0 \qquad (6.17)$$

where the parameters B_{1,m_0} and A_{2,m_0} are defined in Eq. (6.28b). Constant a_0 of this order is to be determined later from the boundary conditions at the ends of the composite curved tube, Eq. (6.15).

6.3.3.2. The First Order Solution

In preparation for the solution of the first order, the right hand side terms of the governing equations are first evaluated (*see Eq. (6.10)*). Those are found from Eqs. (D.2), (D.5), (D.8), Eq. (6.10) and the zeroth order displacement components (Eq. (6.17)). The first order solutions comprise of a complementary and a particular part. The complementary part is obtained from Eq. (6.13) as follow:

$$u_1 = p_1 r^m \cos(\phi)\cos(\theta)$$
$$v_1 = x_1 r^m \sin(\phi)\cos(\theta) \qquad (6.18)$$
$$w_1 = s_1 r^{\bar{m}} \cos(\phi)\sin(\theta)$$

By substituting Eq. (6.13) into the homogeneous parts of Eqs. (D.1), (D.4) and (D.7), the quantities p_1, x_1, s_1, m and $\bar{m}$ are determined for the first order as below:

$$U_1 = 0 \quad \rightarrow \quad \cos(\phi)\cos(\theta) r^{m_1-2}\left(p_1(A_1) + x_1(B_1)\right) = 0$$
$$A_1 = m_1^2 C_{11} - \frac{1}{2}C_{44} - C_{22}$$
$$B_1 = -\left(C_{22} + \frac{1}{2}C_{44}\right) + m_1\left(\frac{1}{2}C_{44} + C_{12}\right) \qquad (6.19a)$$

$$V_1 = 0 \quad \rightarrow \quad \cos(\phi)\cos(\theta) r^{m_1-2}\left(p_1(A_2) + x_1(B_2)\right) = 0$$
$$A_2 = -\left(C_{22} + \frac{1}{2}C_{44}\right) - m_1\left(\frac{1}{2}C_{44} + C_{12}\right)$$
$$B_2 = \frac{1}{2}m_1^2 C_{44} - C_{22} - \frac{1}{2}C_{44} \qquad (6.19b)$$

$$W_1 = 0 \qquad \rightarrow \qquad \sin(\theta) r^{\bar{m}_1 - 2} (s_1 A_3) = 0$$

$$A_3 = \frac{1}{2} \bar{m}_1^{\,2} C_{55} - \frac{1}{2} C_{66} \tag{6.19c}$$

Since p_1 and x_1 are connected to each other with observing Eq. (6.19a) and (6.19b), the solution is found from the following equations:

$$U_1 = 0 \qquad \rightarrow \qquad p_1 (A_1) + x_1 (B_1) = 0$$
$$V_1 = 0 \qquad \rightarrow \qquad p_1 (A_2) + x_1 (B_2) = 0 \tag{6.20}$$

In order to find a solution set for Eq. (6.20):

$$(A_1)(B_2) - (B_1)(A_2) = 0 \qquad \rightarrow$$
$$\left(\frac{1}{2} C_{44} C_{11}\right) m_1^{\,4} + \left(-C_{11} C_{22} - \frac{1}{2} C_{11} C_{44} - \frac{1}{2} C_{44} C_{22} + C_{12} C_{44} + C_{12}^{\,2}\right) m_1^{\,2} = 0 \tag{6.21}$$

By solving Eq. (6.21), the roots are obtained as:

$$m_1 = 0$$

$$m_1 = \pm \left(\frac{2C_{22} + C_{44}}{C_{44}} + \frac{C_{22} - 2C_{12}}{C_{11}} - \frac{2C_{12}^{\,2}}{C_{11} C_{44}} \right)^{\frac{1}{2}} \tag{6.22}$$

Also, from Eq. (6.19c), it is concluded that:

$$A_3 = \frac{1}{2} \bar{m}_1^{\,2} C_{55} - \frac{1}{2} C_{66} = 0 \qquad \rightarrow \qquad \bar{m}_1 = \pm \left(\frac{C_{66}}{C_{55}} \right)^{\frac{1}{2}} \tag{6.23}$$

Therefore, the complementary part of the first order is derived as:

Complementary solution (the first order):

$$u_{1c} = \left(\frac{1}{2} a_1 B_{1,m_1'} + \frac{1}{2} b_1 B_{1,m_1} r^{m_1} + \frac{1}{2} c_1 B_{1,-m_1} r^{-m_1} \right) \cos\phi \cos(\theta)$$

$$v_{1c} = \left(-\frac{1}{2} a_1 A_{2,m_1'} - \frac{1}{2} b_1 A_{2,m_1} r^{m_1} - \frac{1}{2} c_1 A_{2,-m_1} r^{-m_1} \right) \sin\phi \cos(\theta)$$

$$w_{1c} = \left(e_1 r^{\bar{m}_1} + f_1 r^{-\bar{m}_1} \right) \sin(\theta) \tag{6.24a}$$

The particular part is derived to match the right hand side of the governing equations.

Particular solution (the first order):

$$u_{1p} = \frac{\left(C_{13} - C_{23}\right)}{C_{22}} r a_0 B_{1,m_0} \cos\phi \cos\left(\theta\right)$$

$$v_{1p} = 0$$

$$w_{1p} = \frac{\left(C_{66} - C_{55}\right)}{C_{66}} r e_1 \sin\left(\theta\right) \qquad (6.24b)$$

where the parameters B_{1,m_1}, $B_{1,m_1'}$, A_{2,m_1} and $A_{2,m_1'}$ are defined in Eq. (6.28b). Adding together the complementary and particular parts (Eqs. (6.24a) and (6.24b)), the first order displacement components are determined. The free constants a_1, b_1, c_1, e_1 and f_1 are determined by forcing the stress components $\sigma_{rr} = \sigma_{r\theta} = \sigma_{r\phi} = 0$ (on r=a and b) to satisfy the boundary conditions, Eq. (6.14). Constant a_0 is still later determined by applying Eq. (6.15).

The displacement components for the second and third orders are derived with the similar procedure that is used to obtain the first order displacement components.

Integrating the longitudinal stress, $\sigma_{\theta\theta}$, up to the 3rd order over both end surfaces, is expressed as:

$$M = M_0 + \varepsilon M_1 + \varepsilon^2 M_2 + \varepsilon^3 M_3 + \ldots \qquad (6.25)$$

$$M_n = \int_a^b \int_0^{2\pi} \left(\sigma_{\theta\theta n} r \sin\phi\right) r d\phi dr \qquad \text{at } \theta = \pm\frac{\pi}{4}, \text{ for n=0, 1, 2 and 3} \qquad (6.26)$$

Note that M is the specific applied bending moment while M_n of all orders is unknown only based on constant a_0. Thus, Eq. (6.25) is enough to determine constant a_0. Therefore, the total solution for a single-layer composite curved tube subjected to pure bending moment is developed by considering the solutions for all orders and substituting them into Eqs. (6.6). Eventually, the general form displacement field of single-layer composite curved tubes up to the nth order is presented as:

$$u\left(r,\phi,\theta\right) = \varepsilon^n B_n\left(r\right)\cos\left(n\phi\right)\cos\left(\theta\right)$$

$$v\left(r,\phi,\theta\right) = \varepsilon^n A_n\left(r\right)\sin\left(n\phi\right)\cos\left(\theta\right)$$

$$w\left(r,\phi,\theta\right) = \varepsilon^n C_n\left(r\right)\cos\left(\left(n-1\right)\phi\right)\sin\left(\theta\right) \qquad (6.27)$$

with n being a dummy index implying summation of orders from n=0 to the nth order (n=1, 2, 3,…). Moreover,

$$B_n(r)=\left(\frac{1}{n+1}a_nB_{1,m_n}r^{m_n}+\frac{1}{n+1}b_nB_{1,m_n'}r^{m_n'}+\frac{1}{n+1}c_nB_{1,-m_n}r^{-m_n}+\frac{1}{n+1}d_nB_{1,-m_n'}r^{-m_n'}\right)$$

$$A_n(r)=\left(-\frac{1}{n+1}a_nA_{2,m_n}r^{m_n}-\frac{1}{n+1}b_nA_{2,m_n'}r^{m_n'}-\frac{1}{n+1}c_nA_{2,-m_n}r^{-m_n}-\frac{1}{n+1}d_nA_{2,-m_n'}r^{-m_n'}\right)$$

$$C_n(r)=\left(e_nr^{\bar{m}_n}+f_nr^{-\bar{m}_n}\right) \qquad (6.28a)$$

$$\bar{m}_n=\pm n\left(\frac{\bar{C}_{66}}{\bar{C}_{55}}\right)^{\frac{1}{2}}$$

$$B_{1,m_n}=-(n+1)\left(\bar{C}_{22}+\frac{1}{2}\bar{C}_{44}\right)+nm_n\left(\frac{1}{2}\bar{C}_{44}+\bar{C}_{12}\right)$$

$$A_{2,m_n}=-(n+1)\left(\bar{C}_{22}+\frac{1}{2}\bar{C}_{44}\right)-nm_n\left(\frac{1}{2}\bar{C}_{44}+\bar{C}_{12}\right) \qquad (6.28b)$$

and $m_n, -m_n, m_n'$ and $-m_n'$ are, in general, the 4 roots of the following equation:

$$\left(\frac{1}{2}\bar{C}_{44}\bar{C}_{11}\right)m_n{}^4+\left(-n^2\bar{C}_{11}\bar{C}_{22}-\frac{1}{2}\bar{C}_{11}\bar{C}_{44}-\frac{1}{2}\bar{C}_{44}\bar{C}_{22}+n^2\bar{C}_{12}\bar{C}_{44}+n^2\bar{C}_{12}{}^2\right)m_n{}^2$$
$$+\frac{n^4-2n^2+1}{2}\bar{C}_{22}\bar{C}_{44}=0 \qquad (6.29)$$

where $\bar{C}_{ij}$ represent the off-axis stiffnesses and n presents the order number (*i.e.,* n = 0, 1, 2, 3, …). The unknowns in stresses and displacements cannot be solved for simultaneously but independently through a set of equations of the boundary conditions. For example, the unknowns in the bending moment stress (i.e., a_0) and displacements (i.e., a_n, b_n, c_n, d_n, e_n and f_n) are solved through Eq. (6.25) and Eq. (6.14) respectively (*see Table 6.1*).

Table 6.1: Unknowns and equations.

Type	Unknown constants or parameters	Equation number
1	p_n, x_n, s_n, m and $\bar{m}$ at Eq. (6.13)	Eqs. (6.9)-(6.12)
2	a_n, b_n, c_n, d_n, e_n and f_n of orders n=1, 2, and 3 at Eq. (6.28a)	Eq. (6.14)
3	a_0 of order n=0 at Eq. (6.17)	Eq. (6.25)

6.4. Results and Discussion

The single-layer composite curved tube with 0.1 mm thickness is examined. The mechanical properties of the materials making up the composite curved tube are given in Table 6.2. In the present cases, the composite curved tube section has an internal radius of *28*

mm. In addition, a composite curved tube spanning a curved segment of 90° with *R/a=10* is considered (unless otherwise mentioned). Furthermore, the stress components are normalized as $\bar{\sigma}_{ij} = \sigma_{ij}/\sigma_0$ where $\sigma_0 = (M_0.r)/(\pi/4*(b^4-a^4))$ with the outer radius *b* and the inner radius *a* of the composite curved tube. The results are presented based on the proposed method at θ=0°. Note that there is a possibility of compression buckling of the composite curved tube in bending, which is not taken into account in the proposed formulation.

Table 6.2: Mechanical properties of the materials making up the composite curved tube [1].

Properties	E_1 (GPa)	$E_2=E_3$ (GPa)	$G_{12}=G_{13}= G_{23}$ (GPa)	$\upsilon_{12}=\upsilon_{13}$	υ_{23}
Carbon AS4/PEKK	140	10	5.56	0.31	0.33

6.4.1. FEM Analysis

The stress analysis of a single-layer composite curved tube is conducted by finite element method using ANSYS. Stress distributions are also generated to compare with the results obtained using the proposed method. The element used to perform the analysis is the layered solid element, SOLID 185. A rigid surface is modeled and glued to both end surfaces of the composite curved tube. Then, a bending moment is applied to the center node of the surface meshed using shell elements, SHELL 181. This is how the bending moment applied for the composite curved tube in FEM. The mesh-independency study is done for ANSYS based on Table 6.3. Mesh refining is performed two times while the element aspect ratio is kept constant. For the initial mesh, Mesh Number 1, 36000 elements are used to model the structure. For Mesh Number 2, the thickness and circumferential directions are refined twice as much as the initial mesh. For Mesh Number 3, the axial and circumferential directions are refined twice as much as the initial mesh and the thickness direction is refined 4 times as much as the initial mesh to model the curved tube (*see Table 6.3*). Figure 6.3a shows the meshed composite curved tube used to perform the stress analysis using ANSYS 14.5. Figure 6.3b presents the radial and hoop stresses obtained using ANSYS for different Mesh Numbers mentioned in Table 6.3. As Figure 6.3b shows, the differences of the stresses for Mesh Numbers 2 and 3 are 1%, therefore, Mesh Number 2 is selected to obtain the results using FEM to compare with the theoretical results. Mesh Number 2 is called the final mesh in the following sections.

Table 6.3: Mesh characteristics.

Mesh Number	Mesh size (Axial)×(Circumferential)×(Thickness)	Number of elements	Analyzing time (sec)
1	9×10×4	360	180
2	9×20×8	1440	400
3	18×20×16	5760	600

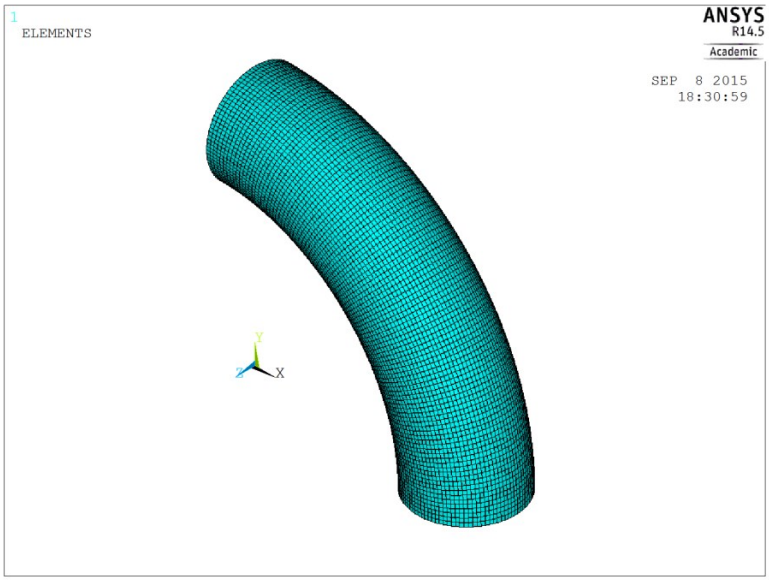

Figure 6.3a: Modeling of the composite curved tube using ANSYS.

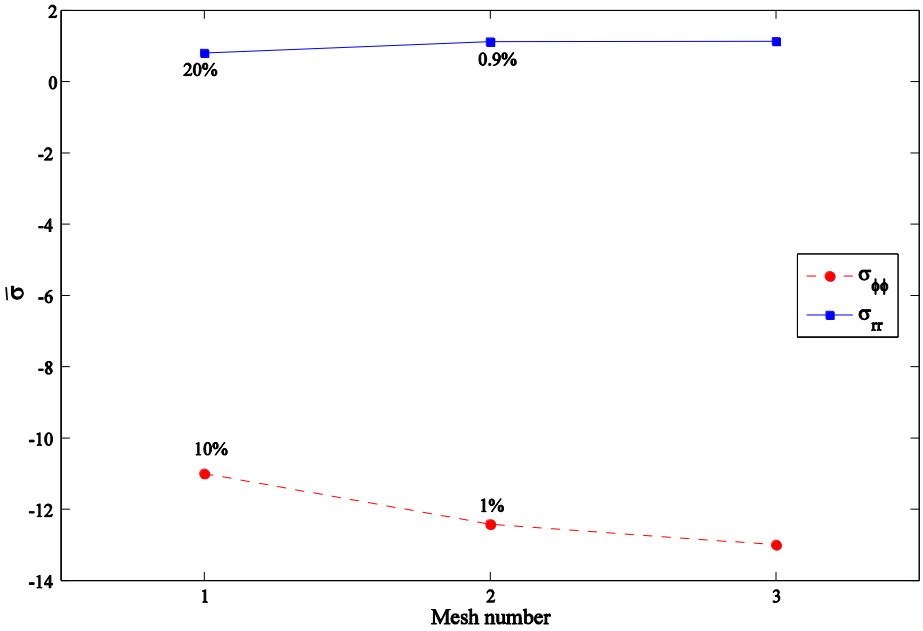

Figure 6.3b: The mesh-independency study of the composite curved tube.

6.4.2. Verifying the Proposed method

The developed method is compared and verified with the 3 other methods or data. First, in Section 6.4.2.1, the developed method is applied for an isotropic material case so that results could be compared with the results available in the literature. Then, in Section 6.4.2.2, the results obtained for a composite curved tube with a single layer using the developed method are compared with the results obtained using FEM. Finally, in Section 6.4.2.3, the results are compared for a composite curved tube based on the developed method with Lekhnitskii solution [2]. In addition, the convergence study for developed method regarding using different numbers of orders is performed.

6.4.2.1. Comparison of the Proposed Method for the Isotropic Case

Lang [78] used stress-based Toroidal Elasticity (SBTE) to present a solution for an isotropic curved tube subjected to in-plane bending moment. The following geometric and material parameters are considered for the isotropic case:

b/a=2, *R/a=10*, ν=0.3, E=206 GPa

The convergence study is performed to find out how many orders are enough to get accurate results. Table 6.4 presents the radial and hoop stresses obtained based on the present method considering different orders and SBTE. Note that the stresses in Table 6.4 are obtained at ϕ=270°, θ=0° and the middle surface of the isotropic curved tube. It is seen that with increasing the number of orders used in the developed method, the difference between the obtained results using the developed method in comparison with SBTE decreases. Since the differences for considering up to the 2nd and 3rd orders in comparison with SBTE are close to each other, the solution up to the 2nd order is selected to compare the results for the isotropic case.

Table 6.4: The convergence study for the isotropic curved tube.

Order number / Normalized Stress	The 0th order (Difference %)	Up to 1st order (Difference %)	**Up to 2nd order (Difference %)**	Up to 3rd order (Difference %)	SBTE [78]
Radial stress	0.366 (22%)	0.336 (12%)	**0.312 (4%)**	0.309 (3%)	0.30
Hoop stress	-0.384 (24%)	-0.350 (13%)	**-0.326 (5%)**	-0.319 (3%)	-0.31

Figure 6.4a presents the comparison for the radial and hoop stresses, $\bar{\sigma}_{rr}$ and $\bar{\sigma}_{\phi\phi}$, at the middle surface of the isotropic curved tube obtained based on the present method and SBTE. Good agreement between the developed method up to the 3rd order and SBTE results is obtained as seen in Figures 6.4a and 6.4b. The shear stresses, $\bar{\sigma}_{\theta r}$ and $\bar{\sigma}_{\phi\theta}$, at the middle surface of the isotropic curved tube obtained based on the present method and SBTE are compared in Figure 6.4b.

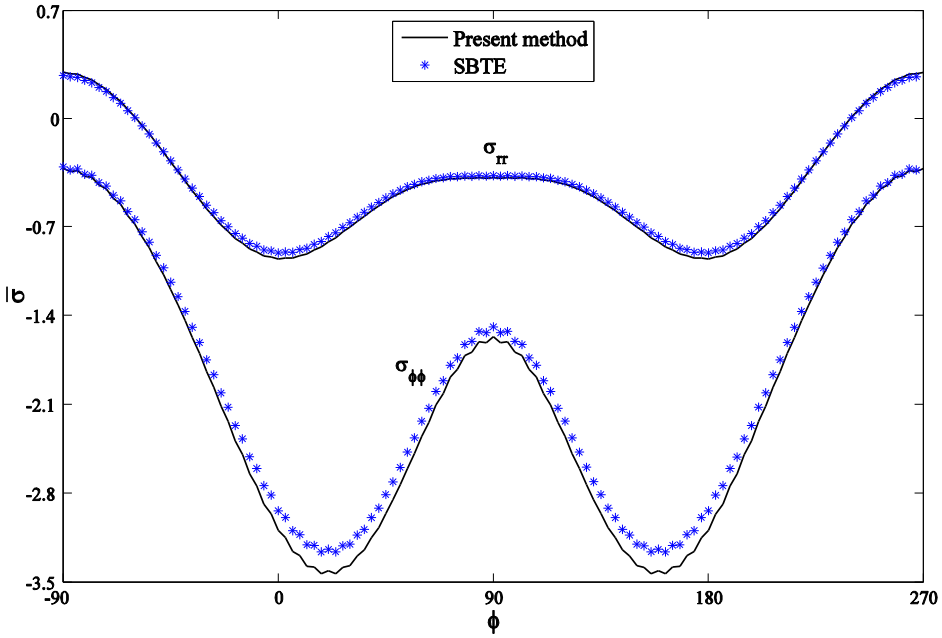

Figure 6.4a: Comparison of the stresses, $\bar{\sigma}_{rr}$ and $\bar{\sigma}_{\phi\phi}$, at the middle surface of the isotropic curved tube obtained using the present method up to the 3rd order and SBTE.

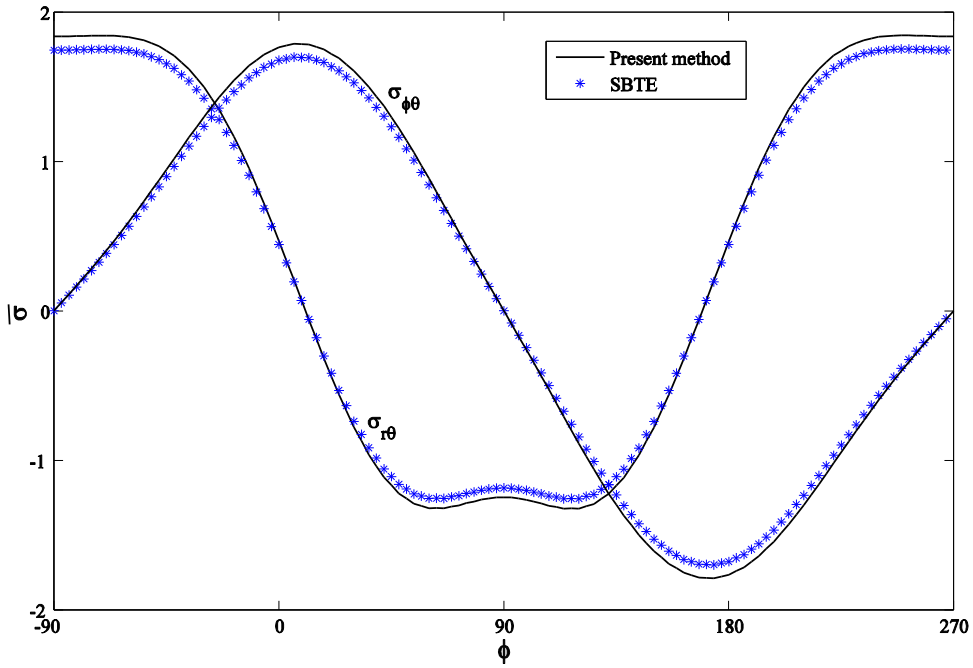

Figure 6.4b: Comparison of the shear stresses, $\bar{\sigma}_{\theta r}$ and $\bar{\sigma}_{\phi\theta}$, at the middle surface of the isotropic curved tube obtained using the present method up to the 3rd order and SBTE.

The deformations of the isotropic curved tube cross sections subjected to bending moments at θ= 0°, 22.5° and 45° are plotted in Figure 6.5. All cross sections at the top and bottom regions (at ϕ=90° and 270°) deform inward while they deform outward at both sides (at ϕ=0° and 180°). As the cross section is getting closer to the end surfaces of the curved tube (θ=45°, *see Figure 6.2*), the deformation of the tube cross section increases. Note that the magnitudes of the deformations of the same tube cross-section at ϕ=0° and 90° are identical. Note that in the developed method, the end sections of the curved tube are free to deform in their planes, whereas in the FEM model they are not.

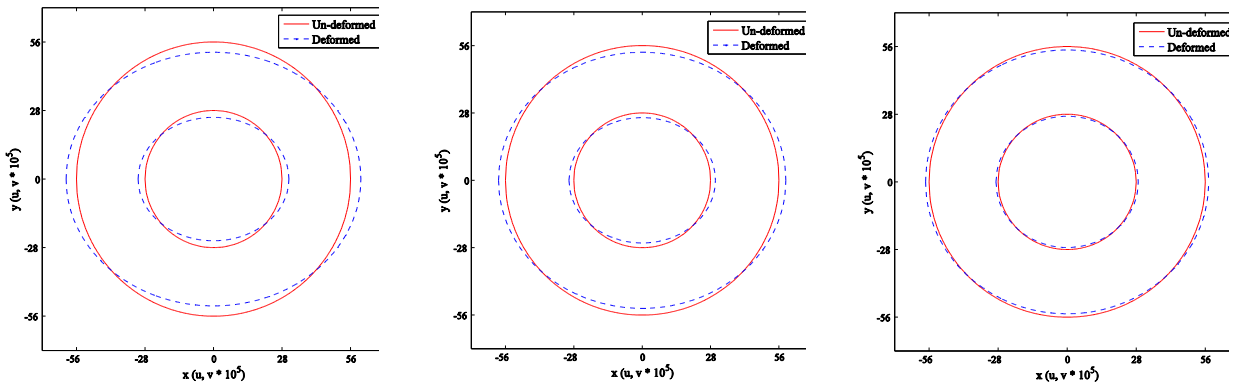

At θ=45° At θ=22.5° At θ=0°

Figure 6.5: Plots of displacements for different cross-sections.

6.4.2.2. Comparison of the Proposed Method with FEM

In this section, the convergence study for a composite curved tube with a single layer using the developed method is performed. The study is done to see how many orders are enough to obtain accurate results (*see Eq. (6.6)*). Table 6.5 presents the convergence study done for the [0°] composite curved tube in comparison with FEM (ANSYS) using the final mesh (*see part 6.4.1*). Remark that the [0°] composite curved tube means that the fibers are along the θ direction (*see Figure 6.2*). The stresses are obtained at ϕ=270°, θ=0° and the middle surface of the composite curved tube. It is seen that with considering more orders to obtain the total solution, the difference between the results obtained using the developed method and FEM decreases. Observing Table 6.5, the solution up to the 2nd order is selected in the developed method to obtain results for the single-layer composite curved tube.

Table 6.5: The convergence study for the single-layer composite curved tube.

Order number / Normalized Stress	The 0th order (Difference %)	Up to 1st order (Difference %)	**Up to 2nd order (Difference %)**	Up to 3rd order (Difference %)	FEM (ANSYS)
Radial stress	1.34 (20%)	1.23 (10%)	**1.18 (5%)**	1.16 (4%)	1.12
Hoop stress	-15.15 (22%)	-13.79 (11%)	**-13.16 (6%)**	-13.04 (5%)	-12.42
Longitudinal stress	-32.71 (21%)	-29.73 (10%)	**-28.65 (6%)**	-28.38 (5%)	-27.03

The radial stress, $\bar{\sigma}_{rr}$, at the middle surface of the [0°] composite curved tube obtained on the basis of the present method and FEM (ANSYS) is compared in Figure 6.6. Good agreement between the developed analysis and FEM (ANSYS) results using the final mesh is obtained. The analyzing of the orthotropic curved tube using ANSYS with Mesh Number 1 takes around 180 seconds while it takes around 400 and 600 seconds for Mesh Numbers 2 and 3, respectively, while the analyzing of the same structure using the developed method considering up to the 2nd order takes 60 seconds (*see Table 6.3*). It is seen that the radial stress, $\bar{\sigma}_{rr}$, is tensile from 225° to 315° (90° of the upper region of the tube cross section). It is observed that the maximum positive value of $\bar{\sigma}_{rr}$ occurs at ϕ=270°.

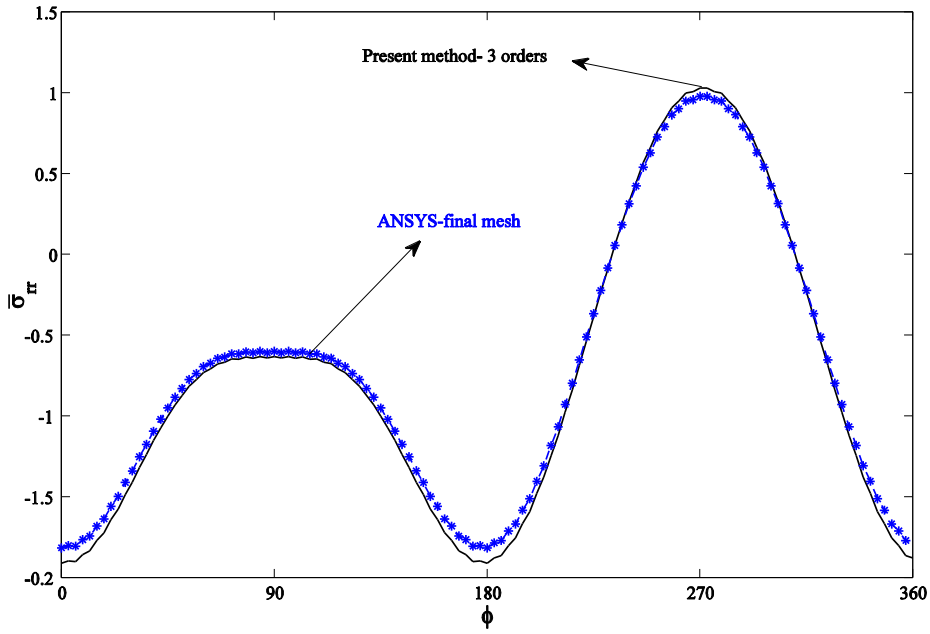

Figure 6.6: Comparison of the radial stress, $\bar{\sigma}_{rr}$, obtained from the present method and ANSYS at the middle surface of the [0°] curved tube.

The comparison of the hoop stress, $\bar{\sigma}_{\phi\phi}$, with FEM (ANSYS) over cross section at the middle surface of the [0°] composite curved tube is presented in Figure 6.7. Good agreement between the proposed analysis and FEM (ANSYS) results using the final mesh is obtained. It is seen that the hoop stress, $\bar{\sigma}_{\phi\phi}$, is tensile from 225° to 315°. In addition, the maximum value of the hoop stress is positive and it occurs at ϕ=270°.

The comparison of the shear stresses, $\bar{\sigma}_{\theta r}$ and $\bar{\sigma}_{\phi\theta}$, over cross section at the middle surface of the [0°] composite curved tube obtained based on the present method and FEM (ANSYS) is presented in Figure 6.8. Good agreement is seen for the results obtained using the developed method with the results obtained using FEM based on the final mesh. Note that the shear stress, $\bar{\sigma}_{\theta r}$, is positive at the whole upper region of the cross section (180° to 360°) while the shear stress, $\bar{\sigma}_{\phi\theta}$, is positive from 0° to 90° and 270° to 360°. In addition, the maximum positive value of $\bar{\sigma}_{\theta r}$ occurs at ϕ=225° and ϕ=315° of the tube cross section while maximum positive and negative values of the shear stress, $\bar{\sigma}_{\phi\theta}$, are at ϕ=0° and ϕ=180°, respectively.

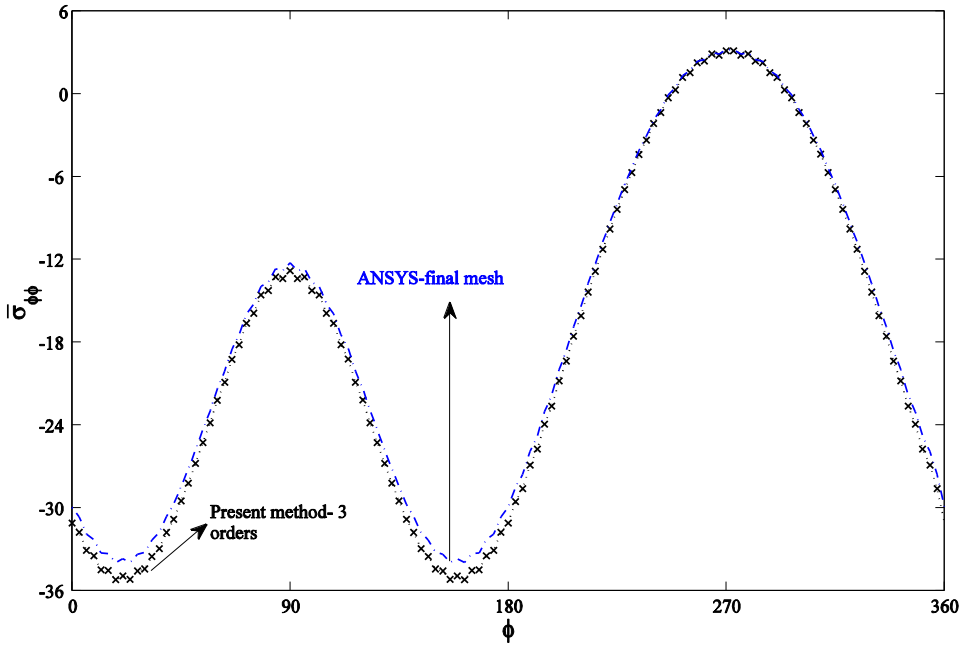

Figure 6.7: Comparison of the hoop stress, $\bar{\sigma}_{\phi\phi}$, obtained using the present method and ANSYS at the middle surface of the [0°] curved tube.

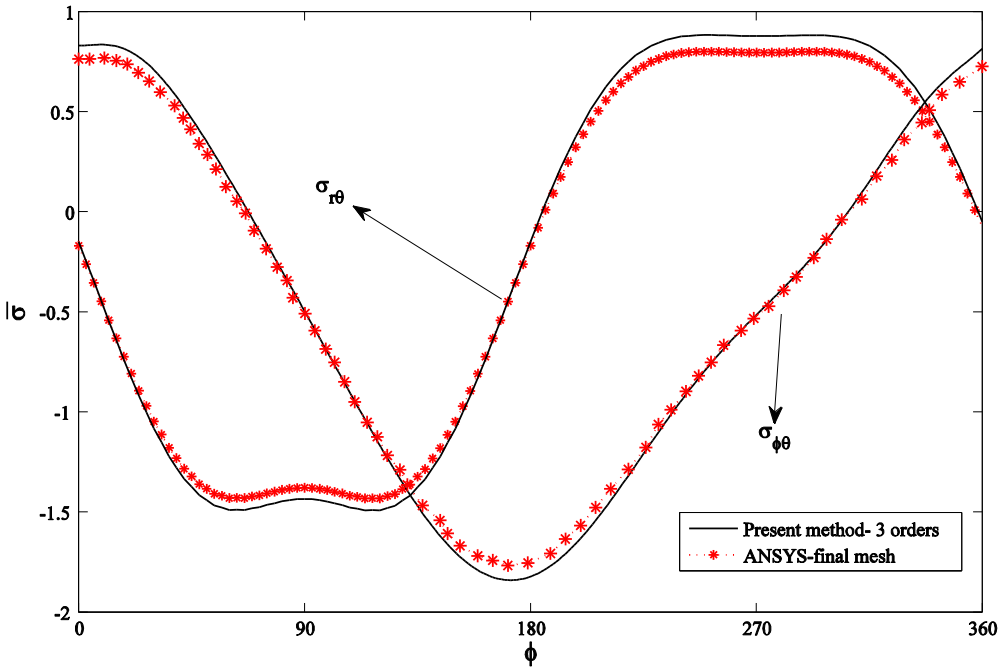

Figure 6.8: Comparison of the shear stresses, $\bar{\sigma}_{\theta r}$, and $\bar{\sigma}_{\phi\theta}$, obtained using the present method and ANSYS at the middle surface of the [0°] curved tube.

The comparisons of the longitudinal stress, $\bar{\sigma}_{\theta\theta}$, and the shear stress, $\bar{\sigma}_{r\phi}$, obtained using the developed method and FEM (ANSYS) over cross section at the middle surface of the [0°] composite curved tube are presented in Figures 6.9a and 6.9b, respectively. The theoretical results show good correspondence with FEM using the final mesh. Observing from Figure 6.9a, the maximum magnitude of the longitudinal stress, $\bar{\sigma}_{\theta\theta}$, is compressive and it occurs at ϕ=-90°. It is seen that the longitudinal stress is tensile at the upper region of the curved tube cross section. Figure 6.8b shows that the shear stress, $\bar{\sigma}_{r\phi}$, is positive from 0° to 90° and 180° to 270°. The positive maximum value of $\bar{\sigma}_{r\phi}$ occurs at ϕ=45° and then at ϕ=225°.

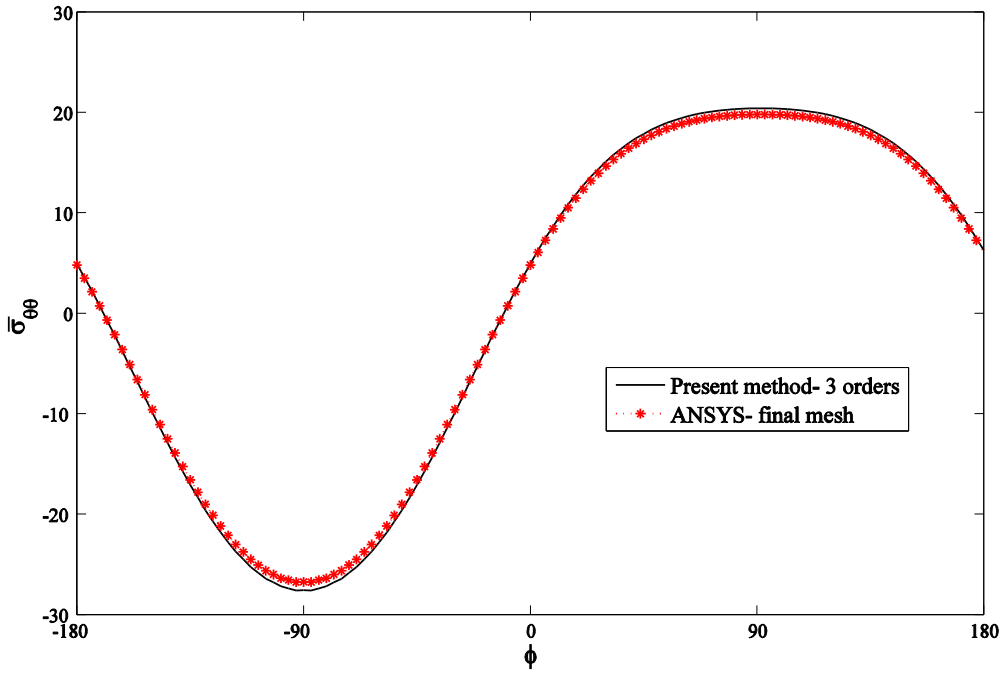

Figure 6.9a: Comparison of the longitudinal stress, $\bar{\sigma}_{\theta\theta}$, obtained using the present method and ANSYS at the middle surface of the [0°] curved tube.

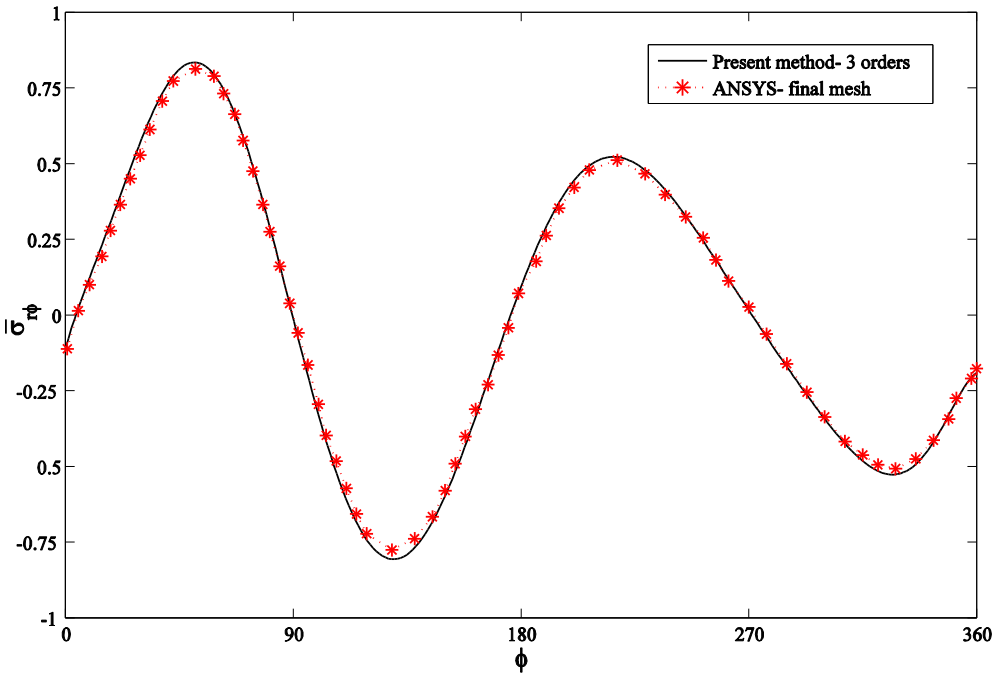

Figure 6.9b: Comparison of the shear stress, $\bar{\sigma}_{r\phi}$, obtained using the present method and ANSYS at the middle surface of the [0°] curved tube.

6.4.2.3. Comparison of the Proposed Method with Lekhnitskii Solution

Lekhnitskii [2] proposed the elasticity method for monolithic homogeneous orthotropic cylindrical straight shells subjected to pure bending moment with $\sigma_{\theta\phi}=\sigma_{r\theta}=0$ assumptions. Therefore, the [0°] composite curved tube is considered to compare the results between the proposed method and Lekhnitskii solution. Note that a composite straight tube is modeled based on the present method by assuming the bend radius *R* to be very large compared to *r*, so that a curved tube will be closer to a straight tube. In order to obtain the results using the proposed method, the solution up to the 2^{nd} order is obtained.

The convergence and verification studies are performed for the developed method against Lekhnitskii solution [2] with considering different *R/a* ratios. Figure 6.10a presents the convergence of the radial stress, $\bar{\sigma}_{rr}$, obtained based on the present method against Lekhnitskii solution at the middle surface of the [0°] composite curved tube considering *R/a*=10, 15, 25, 35, 50 and 75 ratios. It is seen from Figure 6.10a that the results obtained using *R/a*=75 in the developed method are close enough to the results obtained based on Lekhnitskii solution [2]. Therefore, considering *R/a*=75 causes that the composite curved tube with a single layer is modeled as the composite straight tube with a single layer. In addition, as *R/a* ratio increases, the distribution of the radial stress appears to be more asymmetric. Note that the magnitudes of the radial stress, $\bar{\sigma}_{rr}$, decrease as *R/a* ratio increases.

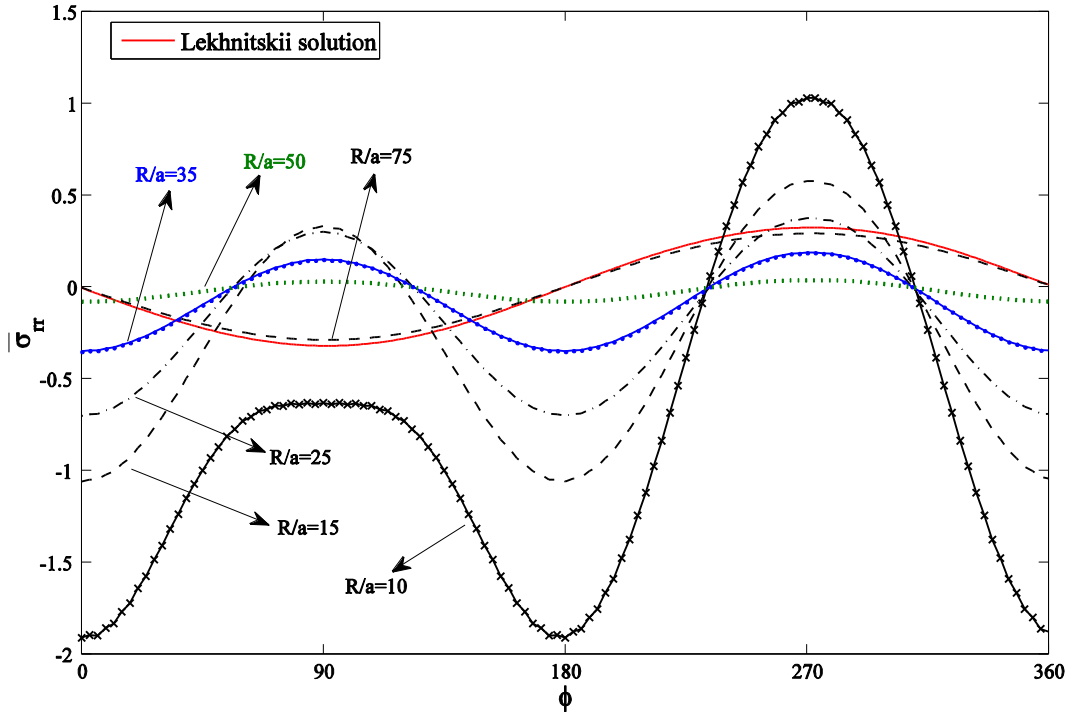

Figure 6.10a: Convergence of the radial stress, $\bar{\sigma}_{rr}$, obtained using the present method against Lekhnitskii solution at the middle surface of the [0°] curved tube considering different *R/a* ratios.

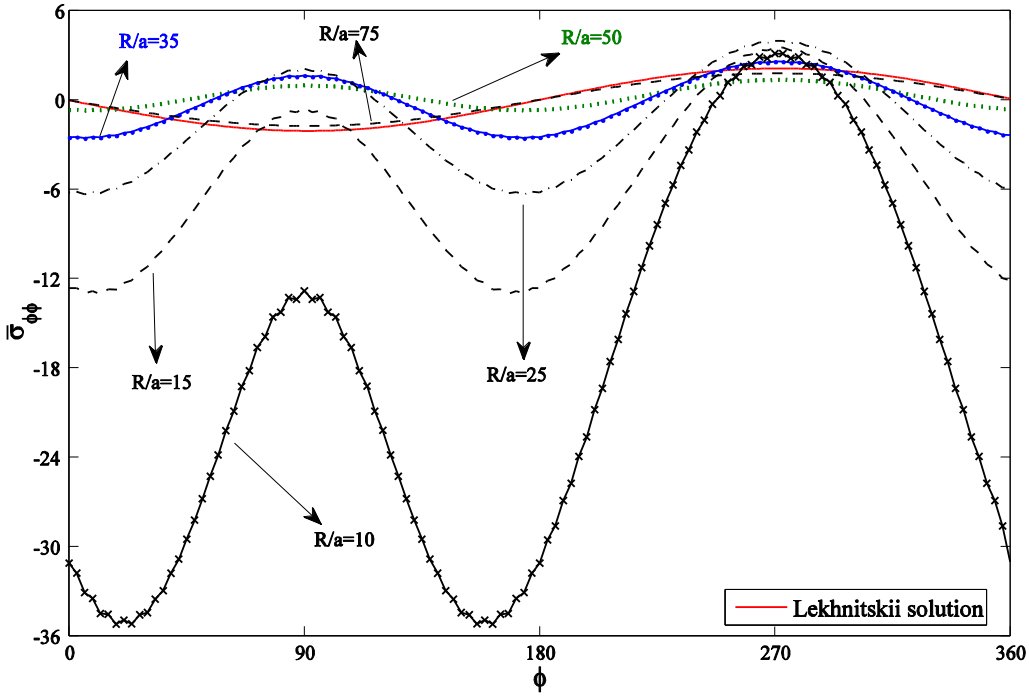

Figure 6.10b: Convergence of the hoop stress, $\bar{\sigma}_{\phi\phi}$, obtained using the present method against Lekhnitskii solution at the middle surface of the [0°] curved tube considering different *R/a* ratios.

Figure 6.10b presents the convergence of the hoop stress, $\bar{\sigma}_{\phi\phi}$, obtained on the basis of the present method against Lekhnitskii solution at the middle surface of the [0°] composite curved tube considering *R/a*=10, 15, 25, 35, 50 and 75 ratios. Good agreement between Lekhnitskii solution and the developed method using *R/a*=75 is obtained. Observing Figure 6.10b, with increasing *R/a* ratio, as the shape of the composite curved tube is getting closer to the composite straight tube, the magnitude of the hoop stress decreases and its distribution is getting more anti-symmetric. The convergence of the longitudinal stress, $\bar{\sigma}_{\theta\theta}$, obtained based on the present method against Lekhnitskii solution [2] at the middle surface of the [0°] composite curved tube considering *R/a*=10, 15 and 25 ratios is shown in Figure 6.11. The developed method using *R/a*=25 and Lekhnitskii solution results show good correspondence. For the convergence study of the longitudinal stress, *R/a* =25 seems accurate enough so that the composite curved tube is modeled as the composite straight tube and consequently, good agreement is seen between two method's results at *R/a* =25.

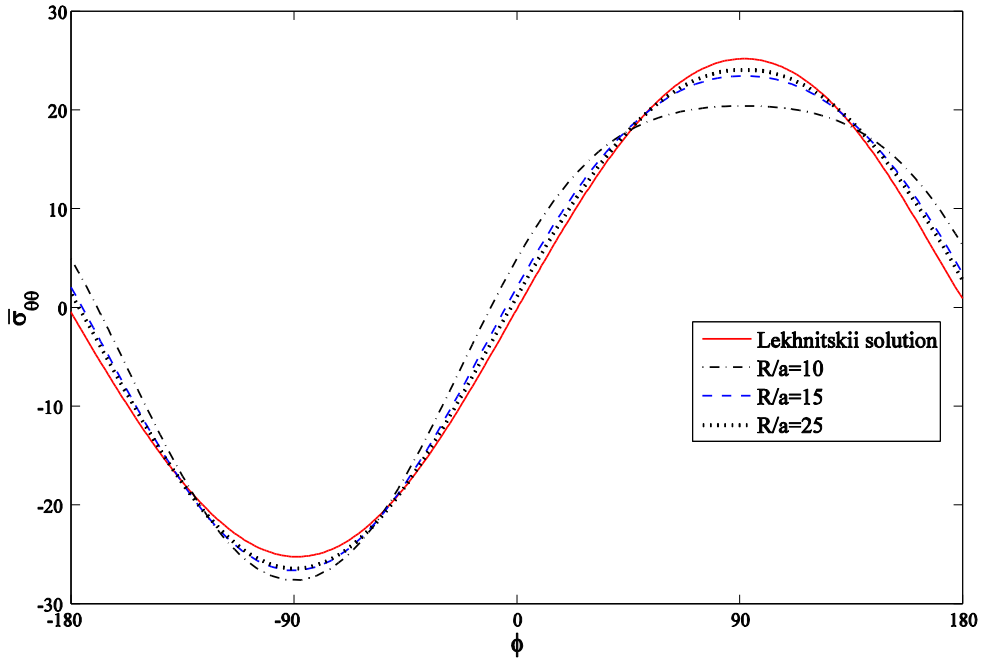

Figure 6.11: Convergence of the longitudinal stress, $\bar{\sigma}_{\theta\theta}$, obtained using the present method against Lekhnitskii solution at the middle surface of the [0°] curved tube considering different *R/a* ratios.

6.5. Concluding Remarks

The displacement-based Toroidal Elasticity for orthotropic materials was proposed to address challenges within the study of stress fields of single-layer orthotropic curved tubes subjected to pure bending moment. The most general form of the displacement field in an orthotropic curved tube with a single layer was derived using Toroidal Elasticity (TE) and successive approximation method. The accuracy of the results was examined by comparing the proposed method with FEM and Lekhnitskii solution. The present method has the advantage of yielding the displacements as well as the stresses as compared with SBTE. Moreover, the zeroth order displacement functions required for starting the approach of successive approximation are easily set up based on the general mechanical knowledge. Note that displacement components are important information for considering special restriction and for fracture analysis. Furthermore, the present method promises to be more cost effective and accurate; therefore, it is employed to obtain the stresses instead of using FEM.

Chapter 7

In this chapter, the displacement field of single-layer composite curved tubes obtained in the previous chapter is used to develop the most general displacement field of elasticity for thick arbitrary laminated composite curved tubes. The principle of minimum total potential energy is applied to calculate stresses in thick composite curved tubes under pure bending moment. The accuracy of the proposed method is evaluated by comparing the numerical results obtained from the developed method against FEM, experimental data and a solution available in the literature.

Three-dimensional Stress Analysis of Orthotropic Curved Tubes-Part 2: Laminate Solution

Hamidreza Yazdani Sarvestani and Mehdi Hojjati

Department of Mechanical and Industrial Engineering, Concordia University, Montreal, Quebec H3G 1M8, Canada

Abstract

The study described in this chapter presents a new simple-input method to study thick laminated composite curved tubes subjected to pure bending moment. First, a displacement approach of Toroidal Elasticity was chosen to obtain the displacement field of single-layer orthotropic curved tubes. Then, a layer-wise method is employed to develop the most general displacement field of elasticity for arbitrary laminated orthotropic curved tubes. The principle of minimum total potential energy is applied to develop governing equations in thick composite curved tubes under pure bending moment. The accuracy of the proposed method is subsequently verified by comparing the numerical results obtained using the proposed method with finite element method (FEM), experimental data and a solution available in the literature. The results show good correspondence. In addition, the proposed method provides advantages in terms of computational time compared to FEM.

Keywords: Thick laminated composite curved tubes; Displacement field; Layer-wise method; Stress analysis; Lay-up sequences; Helicopter landing gear.

7.1. Introduction

Composite tubes are structures that are frequently used in the aerospace, offshore and infrastructure industries. These structures usually have thin or moderately thick walls and are subjected to certain loads such as tension, torsion, shear and bending. Prediction of the state of stress and strain in different layers of composite tubes is of theoretical interest and practical

importance. In all applications, accurate design and inclusive analysis are important to guarantee safety. It should be noted that stress analysis of cylindrical composite structures is often a complex task. A few reasons are responsible for such a complexity such as: governing equations of composite tubes and the layer-wise failure of composite materials. In addition, the curved tube geometry is a lot more complicated than flat geometries. Many researchers have investigated composite straight and curved tubes.

7.1.1. Straight Beams and Tubes

Lekhnitskii [2] developed elasticity solutions for monolithic homogeneous orthotropic cylindrical shells. Kollár and Springer [4] studied stress analysis of composite cylinders and cylindrical segments subjected to hygrothermal and mechanical loads. Kardomateas [5] developed the case of uniform external pressure and orthotropic homogeneous material. Three-dimensional stress and displacement analyses of transversely loaded for laminated hollow cylinders with cross-ply lay-up were investigated [7]. To find out the energy absorption characteristics of glass-fiber circular tubes, Pickett and Dayal [23] performed a study. Sun et al. [25] performed a general stress analysis for anisotropic hollow composite cylindrical structures subjected to different loads. A method was developed to analyze the pure bending of arbitrary laminated composite tubes [24]. They verified formulations with FEM results obtained using ABAQUS. Menshykova and Guz [26] performed a stress analysis on thick laminated composite pipes subjected to bending loads. They found stresses as a function of the material properties, thickness, lay-up and the magnitude of load. Recently, static analysis of carbon nanotube-reinforced composite cylinder under thermo-mechanical was studied using Mori-Tanaka theory [28]. Nowak and Schmidt [29] compared some methods to study fiber metal laminate cylinders under an axisymmetric load. A developed theoretical model was validated by FEM analysis. Jonnalagadda et al. [30] presented an analytical model for a special design of thin composites tube subjected to combined bending and torsion. They verified the theoretical results with FEM analysis.

7.1.2. Curved Beams and Tubes

Qatu [55] analyzed thin and moderately thick laminated composite curved beams to find natural frequencies. Shearing and radial stresses in curved beams were derived based on satisfying both equilibrium equations and static boundary conditions on the surfaces of beams [58]. Dryden [59] obtained stress distributions across a functionally graded circular beam subjected to pure bending by using stress functions. The free vibration analysis was performed on functionally graded beams with curved axis by using the finite element method to discretize the motion equations [63]. A first-order shear deformation theory was used to study static and free vibration behavior of generally laminated curved beams [64]. Wang and Liu [66] presented elasticity solutions for curved beams with orthotropic functionally graded layers subjected to a uniform load on the outer surface by means of Airy stress function method. A mathematical model was developed to analyze behavior of laminated curved glass beams [67].

The above review shows that there is a need of developing a simple-input method to analyze thick laminated composite curved tubes. Although finite element methods are used for analyzing such structures, it is necessary to do meshing for each structure every time some dimensions or lay-up sequences are changed. Therefore, it is desired to have a method where inputs to obtain solutions are simple; i.e. one only needs to enter in the actual dimensions or lay-up sequences without re-meshing work. The present chapter is devoted to develop a method that can predict stresses in thick composite curved tubes subjected to pure bending moment with simple inputs. Displacement approach of Toroidal Elasticity (TE) and a layer-wise method are used. Comparison is made between results obtained for the proposed procedure with experimental data, FEM (ANSYS) and a solution available in the literature. Good agreement is obtained.

7.2. Formulation

The displacement field of single-layer composite curved tubes was derived using Toroidal Elasticity and method of successive approximation [99]. In this chapter, by developing the displacement field of laminated composite curved tubes based on the displacement field of single-layer composite curved tubes using a layer-wise method, a new displacement-based

method is proposed to analyze stresses in thick laminated orthotropic curved tubes subjected to pure bending moment.

7.2.1. Displacement Field of Laminated Composite Curved Tubes

A thick laminated orthotropic curved tube with a bend radius R, mean radius R_1 and thickness h is subjected to pure bending moment, M, as shown in Figure 7.1a. Annular cross section is bounded by radii a and b. Toroidal coordinate system (r, ϕ, θ) is placed at the mid-span of the composite curved tube where r and ϕ are polar coordinates in the plane of the curved tube cross section and θ defines the position of the tube cross section.

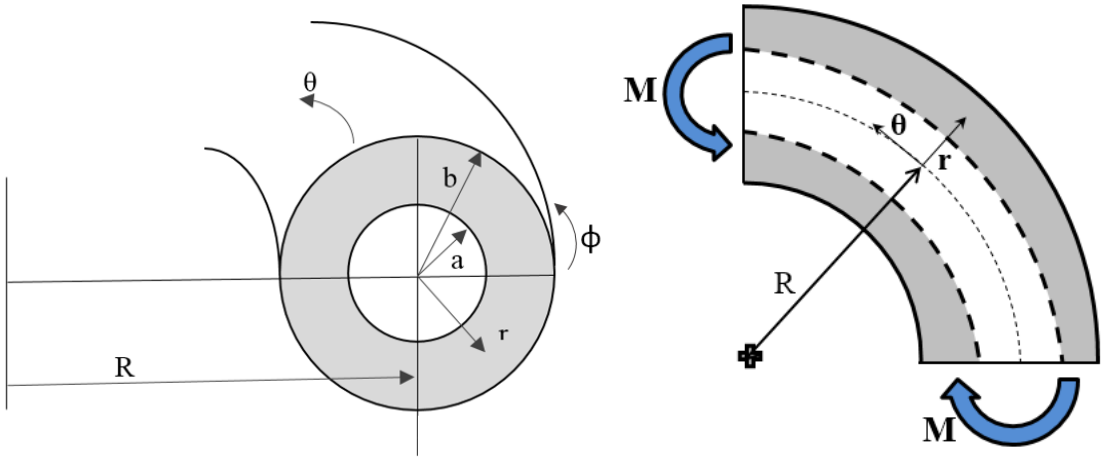

(a)

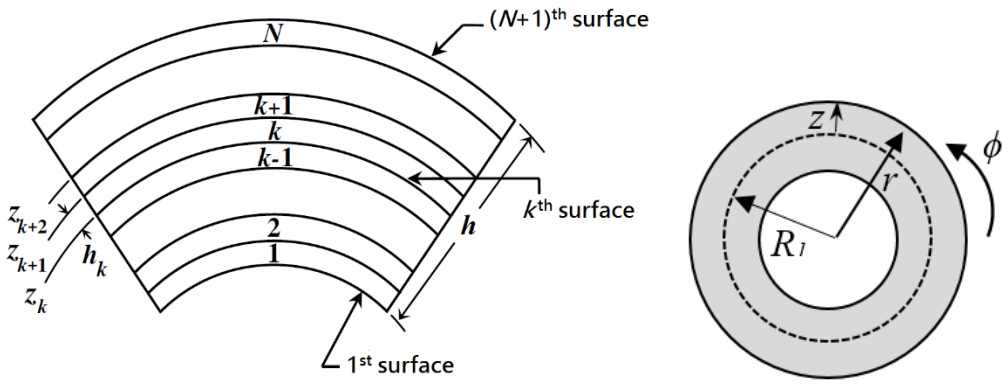

(b

Figure 7.1: **(a)** Geometry and coordinate system of the composite curved tube. **(b)** The ply sequencing in a thick laminated composite curved tube.

Based on the developed displacement components in [99], the general form displacement field of single-layer composite curved tubes of the *k*th plane and up to the *n*th order is presented as (the detailed derivation is found in [99]):

$$U^{(k)}(r,\phi,\theta)=\varepsilon^n B_n^{(k)}(r)\cos(n\phi)\cos(\theta)$$
$$V^{(k)}(r,\phi,\theta)=\varepsilon^n A_n^{(k)}(r)\sin(n\phi)\cos(\theta)$$
$$W^{(k)}(r,\phi,\theta)=\varepsilon^n C_n^{(k)}(r)\cos((n-1)\phi)\sin(\theta) \qquad (7.1)$$

where

$$B_n^{(k)}(r)=\left(a_n^{(k)}B_{1,m_n^{(k)}}r^{m_n^{(k)}}+b_n^{(k)}B_{1,m_n'^{(k)}}r^{m_n'^{(k)}}+c_n^{(k)}B_{1,-m_n^{(k)}}r^{-m_n^{(k)}}+d_n^{(k)}B_{1,-m_n'^{(k)}}r^{-m_n'^{(k)}}\right)$$
$$A_n^{(k)}(r)=-\left(a_n^{(k)}A_{2,m_n^{(k)}}r^{m_n^{(k)}}+b_n^{(k)}A_{2,m_n'^{(k)}}r^{m_n'^{(k)}}+c_n^{(k)}A_{2,-m_n^{(k)}}r^{-m_n^{(k)}}+d_n^{(k)}A_{2,-m_n'^{(k)}}r^{-m_n'^{(k)}}\right)$$
$$C_n^{(k)}(r)=\left(e_n^{(k)}r^{\bar{m}_n^{(k)}}+f_n^{(k)}r^{-\bar{m}_n^{(k)}}\right) \qquad (7.2a)$$
$$\bar{m}_n^{(k)}=\pm n\left(\frac{\bar{C}_{66}^{(k)}}{\bar{C}_{55}^{(k)}}\right)^{\frac{1}{2}}$$
$$B_{1,m_n^{(k)}}=-\left(\bar{C}_{22}^{(k)}+\frac{1}{2}\bar{C}_{44}^{(k)}\right)+\frac{n}{(n+1)}m_n^{(k)}\left(\frac{1}{2}\bar{C}_{44}^{(k)}+\bar{C}_{12}^{(k)}\right)$$
$$A_{2,m_n^{(k)}}=-\left(\bar{C}_{22}^{(k)}+\frac{1}{2}\bar{C}_{44}^{(k)}\right)-\frac{n}{(n+1)}m_n^{(k)}\left(\frac{1}{2}\bar{C}_{44}^{(k)}+\bar{C}_{12}^{(k)}\right) \qquad (7.2b)$$

and $m_n^{(k)}, -m_n^{(k)}, m_n'^{(k)}$ and $-m_n'^{(k)}$ are the 4 roots of the following equation:

$$\left(\frac{1}{2}\bar{C}_{44}^{(k)}\bar{C}_{11}^{(k)}\right)m_n^{(k)4}+\left(-n^2\bar{C}_{11}^{(k)}\bar{C}_{22}^{(k)}-\frac{1}{2}\bar{C}_{11}^{(k)}\bar{C}_{44}^{(k)}-\frac{1}{2}\bar{C}_{44}^{(k)}\bar{C}_{22}^{(k)}+n^2\bar{C}_{12}^{(k)}\bar{C}_{44}^{(k)}+n^2\bar{C}_{12}^{(k)2}\right)m_n^{(k)2}$$
$$+\frac{n^4-2n^2+1}{2}\bar{C}_{22}^{(k)}\bar{C}_{44}^{(k)}=0 \qquad (7.2c)$$

with *n*, here and in what follows, being a dummy index implying summation of orders from *n*=0 to the *n*th order. $\bar{C}_{ij}^{(k)}$ represent the off-axis stiffnesses. Also, *n* and *k* present the order number (i.e., *n=0, 1, 2, 3, 4,...*) and plane number (i.e., *k=1, 2,..., N+1*), respectively.

7.2.2. Layer-wise Theory (LWT)

The equivalent single-layer theories are not able to precisely find stresses and strains in laminated composites. However, LWT allows each layer of the laminate to act like a real

three-dimensional layer while being able to present good results for the local quantities. In LWT, the displacement components of a generic point in the laminate are assumed as:

$$U\left(\mathrm{z},\phi,\theta\right)=u_k\left(\phi,\theta\right)\Omega_k\left(z\right)$$
$$V\left(\mathrm{z},\phi,\theta\right)=v_k\left(\phi,\theta\right)\Omega_k\left(z\right)$$
$$W\left(\mathrm{z},\phi,\theta\right)=w_k\left(\phi,\theta\right)\Omega_k\left(z\right)\qquad\left(k=1,2,...,N+1\right)\qquad(7.3)$$

with k, here and in what follows, being a dummy index implying summation of terms from k=1 to k=N+1. Note that z is the local direction starting from the mid-thickness of the curved tube cross section. The variable N corresponds to the total number of numerical layers within the laminated orthotropic curved tube. In Eq. (7.3), U, V and W denote the total displacement components in the z, ϕ and θ directions, respectively (*see Figure 7.1b*). Moreover, $u_k\left(\phi,\theta\right)$, $v_k\left(\phi,\theta\right)$ and $w_k\left(\phi,\theta\right)$ represent the displacements of the points initially located at the kth plane within the laminated composite curved tube in the z, ϕ and θ directions, respectively. $\Omega_k\left(z\right)$ is the global Lagrangian interpolation function associated with the kth plane. Depending upon the polynomial order of the interpolation function, Eq. (7.3) exhibits piecewise polynomial variation. It is noted that the accuracy of LWT is enhanced by subdividing each physical layer into a finite number of numerical layers. Clearly, as the number of subdivisions (p) through-thickness is increased, the number of governing equations and the accuracy of the results are increased.

The procedure for solving a specific problem can now be outlined. The displacement components of a single-layer composite curved tube are taken based on Eq. (7.1). By applying layer-wise method, Eq. (7.3), the displacement components of a laminated composite curved tube are obtained. Then, by employing the displacement components and their corresponding strains in the principle of minimum total potential energy and using the fundamental lemma of calculus of variations, the equilibrium equations and associated boundary conditions of laminated composite curved tubes under pure bending moment are obtained.

Consequently, by applying the LWT displacement field (Eq. (7.3)) on general displacement field of single-layer composite curved tubes in Eq. (7.1), the elasticity displacement field of thick laminated composite curved tubes is rewritten up to the nth order in following form as:

$$U(z,\phi,\theta)=\varepsilon^n B_n^{(k)}(R_1+z)\cos(n\phi)\cos(\theta)+U_k(\phi)\Phi_k(z)$$
$$V(z,\phi,\theta)=\varepsilon^n A_n^{(k)}(R_1+z)\sin(n\phi)\cos(\theta)+V_k(\phi)\Phi_k(z)\qquad(k=1,2,...,N+1)$$
$$W(z,\phi,\theta)=\varepsilon^n C_n^{(k)}(R_1+z)\cos((n-1)\phi)\sin(\theta)+W_k(\phi)\Phi_k(z)\qquad(7.4)$$

In order to satisfy the interfacial continuities of the displacement components, it is necessary that the constants appearing in Eqs. (7.4) (i.e., a_n, b_n, c_n, d_n, e_n and f_n) to be the same for all layers. Also, by employing linear interpolation functions, the continuity of displacement components through-thickness of the laminated curved tube is identically satisfied. Thus, Eqs. (7.4) are represented as:

$$U(z,\phi,\theta)=\varepsilon^n\begin{pmatrix}a_n B_{1,m_n^{(k)}}(R_1+z)^{m_n^{(k)}}+b_n B_{1,m_n'^{(k)}}(R_1+z)^{m_n'^{(k)}}\\+c_n B_{1,-m_n^{(k)}}(R_1+z)^{-m_n^{(k)}}+d_n B_{1,-m_n'^{(k)}}(R_1+z)^{-m_n'^{(k)}}\end{pmatrix}\cos(n\phi)\cos(\theta)+U_k(\phi)\Phi_k(z)$$
$$V(z,\phi,\theta)=-\varepsilon^n\begin{pmatrix}a_n A_{2,m_n^{(k)}}(R_1+z)^{m_n^{(k)}}+b_n A_{2,m_n'^{(k)}}(R_1+z)^{m_n'^{(k)}}\\+c_n A_{2,-m_n^{(k)}}(R_1+z)^{-m_n^{(k)}}+d_n A_{2,-m_n'^{(k)}}(R_1+z)^{-m_n'^{(k)}}\end{pmatrix}\sin(n\phi)\cos(\theta)+V_k(\phi)\Phi_k(z)$$
$$W(z,\phi,\theta)=\varepsilon^n\left(e_n(R_1+z)^{\bar{m}_n^{(k)}}+f_n(R_1+z)^{-\bar{m}_n^{(k)}}\right)\cos((n-1)\phi)\sin(\theta)+W_k(\phi)\Phi_k(z)\qquad(7.5)$$

The linear global interpolation function is defined as:

$$\Phi_k(z)=\begin{cases}0 & z\le z_{k-1}\\ \psi_{k-1}^2(z)=\dfrac{1}{h_{j-1}}(z-z_{k-1}) & z_{k-1}\le z\le z_k\\ \psi_k^1(z)=\dfrac{1}{h_j}(z_{k+1}-z) & z_k\le z\le z_{k+1}\\ 0 & z\ge z_{k+1}\end{cases}\qquad(7.6)$$

where $\psi_k^i\ (i=1\text{and}2)$ are the local Lagrangian linear interpolation functions, with h_j is the thickness of the jth layer. By introducing $r=R_1+z$ and $\rho=R+r\cos\phi$ (*see Figure 7.1b*), the strain-displacement relations are as given as:

$$\varepsilon_{zz}=\frac{\partial U}{\partial z},\qquad \gamma_{z\phi}=\frac{1}{R_1+z}\frac{\partial U}{\partial \phi}+\frac{\partial V}{\partial z}-\frac{V}{R_1+z},$$

$$\varepsilon_{\phi\phi}=\frac{U}{R_1+z}+\frac{1}{R_1+z}\frac{\partial V}{\partial \phi},\qquad \gamma_{z\theta}=\frac{\partial W}{\partial z}+\frac{1}{\rho}\frac{\partial U}{\partial \theta}-\frac{W}{\rho}\cos\phi,$$

$$\varepsilon_{\theta\theta}=\frac{1}{\rho}\left(U\cos\phi-V\sin\phi+\frac{\partial W}{\partial \theta}\right),\qquad \gamma_{\phi\theta}=\frac{1}{R_1+z}\frac{\partial W}{\partial \phi}+\frac{1}{\rho}\frac{\partial V}{\partial \theta}+\frac{W}{\rho}\sin\phi \qquad (7.7)$$

Substitution of Eq. (7.5) into the strain-displacement relations (7.7) yields the following results:

$$\begin{aligned}
\varepsilon_{zz} &= \varepsilon^n B_n'\cos(n\phi)\cos(\theta)+U_k\Phi_k'\\
\varepsilon_{\phi\phi} &= \frac{\varepsilon^n}{R_1+z}\left(B_n+nA_n\right)\cos(n\phi)\cos(\theta)+\frac{1}{R_1+z}\left(V_k'\Phi_k+U_k\Phi_k\right)\\
\varepsilon_{\theta\theta} &= \frac{\varepsilon^n}{\rho}\left(B_n\cos(n\phi)\cos\phi-A_n\sin(n\phi)\sin\phi+C_n\cos\left((n-1)\phi\right)\right)\cos(\theta)-\frac{1}{\rho}\left(U_k\Phi_k\cos\phi-V_k\Phi_k\sin\phi\right)\\
\gamma_{\theta z} &= \varepsilon^n\left(C_n'\cos\left((n-1)\phi\right)-\frac{\cos\phi}{\rho}C_n\cos\left((n-1)\phi\right)-\frac{1}{\rho}B_n\cos(n\phi)\right)\sin(\theta)+W_k\left(\Phi_k'-\frac{\cos\phi}{\rho}\Phi_k\right)\\
\gamma_{z\phi} &= -\frac{\varepsilon^n}{R_1+z}\left(nB_n\sin(n\phi)+A_n\sin(n\phi)\right)\cos(\theta)+\varepsilon^n A_n'\sin(n\phi)\cos(\theta)+V_k\Phi_k'\\
&\quad+\frac{1}{R_1+z}\left(U_k'\Phi_k-V_k\Phi_k\right)\\
\gamma_{\phi\theta} &= \frac{1}{R_1+z}\left(-\varepsilon^n C_n(n-1)\sin\left((n-1)\phi\right)\sin(\theta)+W_k'\Phi_k\right)+\frac{\sin\phi}{\rho}\left(W_k\Phi_k\right)\\
&\quad-\frac{\varepsilon^n}{\rho}\left(A_n\sin(n\phi)+C_n\cos\left((n-1)\phi\right)\sin\phi\right)\sin(\theta)
\end{aligned}\qquad (7.8)$$

In Eq. (7.8) and what follows, a prime indicates an ordinary differentiation with respect to an appropriate variable (*i.e.,* either ϕ or z). The equilibrium equations of a laminated orthotropic curved tube with N numerical layers are obtained by employing Eq. (7.8) in the principle of minimum total potential energy [90]. The results are, in general, *3(N+1)* local equilibrium equations corresponding to *3(N+1)* unknown functions U_k, V_k and W_k and, in general, six global equilibrium equations for every order (n=0, 1, 2, 3,…) up to the nth order associated with six parameters a_n, b_n, c_n, d_n, e_n and f_n of the same order.

According to the principle of minimum total potential energy at the equilibrium configuration of a body, the variation of the total potential energy Π of the body must vanish. That is:

$$\delta\Pi \equiv \delta U + \delta V = 0 \tag{7.9}$$

where δU is the variation of total strain energy of the structure, i.e.,

$$\delta U = \int_{-\pi/4}^{\pi/4}\int_{-h/2}^{+h/2}\int_{-\pi}^{\pi}\left(\sigma_{zz}\delta\varepsilon_{zz} + \sigma_{\theta\theta}\delta\varepsilon_{\theta\theta} + \sigma_{\phi\phi}\delta\varepsilon_{\phi\phi} + \sigma_{\theta z}\delta\gamma_{\theta z} + \sigma_{\phi\theta}\delta\gamma_{\phi\theta} + \sigma_{\phi z}\delta\gamma_{\phi z}\right)\mathrm{d}\phi\mathrm{d}z\mathrm{d}\theta \tag{7.10}$$

and V is negative of the work done on the structure by the specified external forces. Here,

$$V = -2M\frac{W\left(\theta=\pi/4,\phi,z\right)}{r} = -\frac{2M}{R_1+z}\left(\frac{\sqrt{2}}{2}C_n\varepsilon^n\cos\left(\left(n-1\right)\phi\right)+W_k\,\Phi_k\right) \tag{7.11a}$$

and therefore,

$$\delta V = \frac{-2M}{R_1+z}\left(\frac{\sqrt{2}}{2}\left(\delta e_n\left(R_1+z\right)^{\bar{m}_n^{(k)}} + \delta f_n\left(R_1+z\right)^{-\bar{m}_n^{(k)}}\right)\varepsilon^n\cos\left(\left(n-1\right)\phi\right)+\Phi_k\,\delta W_k\right) \tag{7.11b}$$

It is noted that M represents the bending moment applied at both ends of the composite curved tube as shown in Figure 7.1a.

Upon substituting δV into variations of strains (Eq. (7.8)), carrying out necessary integrations and employing the fundamental lemma of calculus of variations, the equilibrium equations of laminated composite curved tubes under bending moments up to the nth order are obtained as:

$$\delta U_k : N_z^k + M_\phi^k + M_\theta^k\cos\phi - \frac{dR_{z\phi}^k}{d\phi} = 0$$

$$\delta V_k : Q_\phi^k - R_{z\phi}^k + M_\theta^k\sin\phi - \frac{dM_\phi^k}{d\phi} = 0$$

$$\delta W_k : Q_\theta^k - R_\theta^k\cos\phi + R_{\phi\theta}^k\sin\phi - \frac{dM_{\phi\theta}^k}{d\phi} = \frac{4}{\pi}\frac{M}{R_1+z}\Phi_k \qquad \left(k=1,2,...,N+1\right) \tag{7.12}$$

$$\delta a_n : \int_{-\pi/4}^{\pi/4}\int_{-h/2}^{+h/2}\int_{-\pi}^{\pi}\left(\Theta 1\right)\mathrm{d}\phi\mathrm{d}z\mathrm{d}\theta = 0 \qquad \text{for } n=0,1,2,3,... \tag{7.13a}$$

$$\delta b_n : \int_{-\pi/4}^{\pi/4}\int_{-h/2}^{+h/2}\int_{-\pi}^{\pi}\left(\Theta 2\right)\mathrm{d}\phi\mathrm{d}z\mathrm{d}\theta = 0 \qquad \text{for } n=1,2,3,... \tag{7.13b}$$

$$\delta c_n : \int_{-\pi/4}^{\pi/4}\int_{-h/2}^{+h/2}\int_{-\pi}^{\pi}\left(\Theta 3\right)\mathrm{d}\phi\mathrm{d}z\mathrm{d}\theta = 0 \qquad \text{for } n=1,2,3,... \tag{7.13c}$$

$$\delta d_n : \int_{-\pi/4}^{\pi/4}\int_{-h/2}^{+h/2}\int_{-\pi}^{\pi}\left(\Theta 4\right)\mathrm{d}\phi\mathrm{d}z\mathrm{d}\theta = 0 \qquad \text{for } n=2,3,... \tag{7.13d}$$

$$\delta e_n : \int_{-\pi/4}^{\pi/4}\int_{-h/2}^{+h/2}\int_{-\pi}^{\pi}(\Theta 5)\,\mathrm{d}\phi\mathrm{d}z\mathrm{d}\theta = -\sqrt{2}\varepsilon^n M\left(R_1+z\right)^{\bar{m}_n^{(k)}-1}\cos\left((n-1)\phi\right)$$

$$\text{for } n=1,2,3,... \qquad (7.13e)$$

$$\delta f_n : \int_{-\pi/4}^{\pi/4}\int_{-h/2}^{+h/2}\int_{-\pi}^{\pi}(\Theta 6)\,\mathrm{d}\phi\mathrm{d}z\mathrm{d}\theta = -\sqrt{2}\varepsilon^n M\left(R_1+z\right)^{-\bar{m}_n^{(k)}-1}\cos\left((n-1)\phi\right)$$

$$\text{for } n=1,2,3,... \qquad (7.13f)$$

where the functions Θ1, Θ2, Θ3, Θ4, Θ5 and Θ6 in Eqs. (7.13) are defined in *Appendix G*. The generalized stress and moment resultants are defined as:

$$\left(N_z^k, Q_\theta^k, Q_\phi^k\right) = \int_{-h/2}^{+h/2}\left(\sigma_{zz}, \sigma_{\theta z}, \sigma_{z\phi}\right)\Phi_k' \, dz$$

$$\left(M_\theta^k, R_\theta^k, M_{z\phi}^k, R_{\phi\theta}^k\right) = \int_{-h/2}^{+h/2}\frac{1}{\rho}\left(\sigma_{\theta\theta}, \sigma_{\theta z}, \sigma_{z\phi}, \sigma_{\phi\theta}\right)\Phi_k \, dz$$

$$\left(M_\phi^k, M_{\phi\theta}^k, R_{z\phi}^k\right) = \int_{-h/2}^{+h/2}\frac{1}{R_1+z}\left(\sigma_{\phi\phi}, \sigma_{\phi\theta}, \sigma_{z\phi}\right)\Phi_k \, dz \qquad (7.14)$$

Note that the numbers of the global equilibrium equations, Eqs. (7.13), depend on the numbers of unknown constants are employed in Eq. (7.5) to develop the displacement field for laminated composite curved tubes. Based on the detailed derivation in [99], there are one unknown constant for the zeroth order (i.e., a_0), 5 unknown constants for the 1st order (i.e., a_1, b_1, c_1, e_1 and f_1) and 6 unknown constants for the nth order (n=2, 3,…) (i.e., a_n, b_n, c_n, d_n, e_n and f_n). Table 7.1 presents unknown constants and corresponding global equilibrium equations, which are used to calculate them.

Table 7.1: Unknowns and equations.

Type	Unknown constants	Equation number
The zeroth order	a_0 of the zeroth order	Eq. (7.13a) for *n=0*
Up to the 1st order	a_0 of the zeroth order	Eq. (7.13a) for *n=0*
	a_1, b_1, c_1, e_1 and f_1 of the first order	Eqs. (7.13a), (7.13b), (7.13c), (7.13e) and (7.13f) for *n=1*
Up to the 2nd order	a_0 of the zeroth order	Eq. (7.13a) for *n=0*
	a_1, b_1, c_1, e_1 and f_1 of the first order	Eqs. (7.13a), (7.13b), (7.13c), (7.13e) and (7.13f) for *n=1*
	a_2, b_2, c_2, d_2, e_2 and f_2 of the 2nd order	Eqs. (7.13a), (7.13b), (7.13c), (7.13d), (7.13e) and (7.13f) for *n=2*

Up to the *n*th order	a_0 of the zeroth order	Eq. (7.13a) for $n=0$
	a_1, b_1, c_1, e_1 and f_1 of the first order	Eqs. (7.13a), (7.13b), (7.13c), (7.13e) and (7.13f) for $n=1$
	a_n, b_n, c_n, d_n, e_n and f_n of the *n*th orders n=2, 3, …	Eqs. (7.13a), (7.13b), (7.13c), (7.13d), (7.13e) and (7.13f) for $n=2, 3, ...$

The following boundary conditions must be satisfied on the free inner and outer curved surfaces:

$$R_\theta^k = Q_x^k = N_z^k = 0 \qquad \text{at}\left(\text{z}=\pm\text{h}/2\right) \qquad \left(k=1,2,...,N+1\right) \tag{7.15}$$

Note that in Eq. (7.15) the superscript k refers to the kth interface in the laminated orthotropic curved tube. By substituting Eq. (7.8) into three-dimensional constitutive law [33] and the subsequent results into Eq. (7.14), the stress resultants based on displacement components are obtained which are presented in *Appendix H*. The local displacement-based equilibrium equations are obtained by substituting Eqs. (F.1)-(F.5) into Eqs. (7.12). Also, the global equilibrium equations of the laminated composite curved tube are expressed in terms of displacement functions by substituting Eq. (7.8) into three-dimensional constitutive law and the subsequent results into Eqs. (7.13).

7.3. Analytical Solution

The system of local displacement equilibrium equations (Eq. (7.12)) shows $3(N+1)$ coupled ordinary differential equations with constant coefficients which may be displayed in a matrix form as:

$$\left[M\right]\left\{\eta''\right\}+\left[K_1\right]\left\{\eta'\right\}+\left[K_2\right]\left\{\eta\right\}=\left\{F\right\} \tag{7.16}$$

where

$$\left\{\eta\right\}=\left\{\left\{U\right\}^T,\left\{V\right\}^T,\left\{W\right\}^T\right\}^T$$

$$\left\{U\right\}=\left\{U_1,U_2,...,U_{N+1}\right\}^T$$

$$\left\{V\right\}=\left\{V_1,V_2,...,V_{N+1}\right\}^T$$

$$\left\{W\right\}=\left\{W_1,W_2,...,W_{N+1}\right\}^T \tag{7.17}$$

The coefficient matrices [M], [K_1], [K_2] and {F} in Eq. (7.16) are defined in *Appendix I*. It is confirmed that the general solution of Eq. (7.16) is presented as [100]:

$$\{\eta\} = [X_0]\left[\exp(\phi T_0)\right]\{k\} +$$
$$[X_0]\int_0^{\phi}\left(\begin{array}{l}\left[\exp\left(T_0(\phi - s)\right)\right][X_0]^{-1}\left[\exp\left(s\left([M]^{-1}[K_1] + [X_0][T_0][X_0]^{-1}\right)\right)\right] \\ \left(\{k\} + \int_0^{s}\left(\left[\exp\left(u\left([M]^{-1}[K_1] + [X_0][T_0][X_0]^{-1}\right)\right)\right][M]^{-1}\{F(u)\}\right)du\right)\end{array}\right)ds \tag{7.18}$$

where

$$[T_0]_{(N+1)\times(N+1)} = diag\left(T_1, T_2, ..., T_{N+1}\right) \tag{7.19}$$

And T_i *(i=1, 2,..., N+1)* are Jordan blocks associated to the eigenvalues of matrix [Q] where

$$[Q]_{6(N+1)\times 6(N+1)} = \begin{bmatrix}[0]_{3(N+1)\times 3(N+1)} & [I]_{3(N+1)\times 3(N+1)} \\ -[M]^{-1}[K_2] & -[M]^{-1}[K_1]\end{bmatrix} \tag{7.20}$$

In addition,

$$[X_0]_{3(N+1)\times 3(N+1)} = [X_1, X_2, ..., X_{N+1}] \tag{7.21}$$

where X_i *(i=1, 2,..., N+1)* are co-solutions of $[X_i][T_i]^2+[M]^{-1}[K_1][X_i][T_i]+[M]^{-1}[K_2][X_i]=[0]$.

Vector {k} is unknown vector representing *3(N+1)* integration constants. The constants a_n, b_n, c_n, d_n, e_n and f_n must be calculated within LWT analysis through the following steps:

1. The boundary conditions in Eq. (7.15) are first imposed to calculate vector {k} in terms of the unknown constants a_n, b_n, c_n, d_n, e_n and f_n.
2. These constants are then obtained by the satisfaction of the global equilibrium conditions in Eqs. (7.13) as presented in Table 7.1.

7.4. Lay-up Sequence Selection

Derisi [1] developed a lay-up sequence to be used for making composite landing gears for helicopters that may provide large deformation and gradual fracture. A composite straight tube with the $[90°_{20}/0°_{20}]$ lay-up was manufactured and a four-point test was performed. Table 7.2 shows the lay-up sequences considered here. The lay-up sequence of the $[90°_{20}/0°_{20}]$ composite curved tube is selected to verify the numerical results obtained using the proposed

method with finite element method (ANSYS) and experimental data for the thick laminated composite curved tube subjected to pure bending moment. Moreover, the $[25°_{20}/-25°_{20}]$ lay-up is considered to compare the developed method with a solution available in the literature [9].

Table 7.2: Lay-up sequence number.

Laminate number	Lay-up sequence	Purpose
1	$[90°_{20}/0°_{20}]$	Compare with experimental data and FEM
2	$[25°_{20}/-25°_{20}]$	Compare with a solution available in the literature

7.5. Results and Discussion

All physical layers are assumed to have equal thickness (=0.1 mm [1]) and are modeled as being made up of *p* numerical layers. In all the subsequent calculations, *p* is set equal to 12 [92]. The mechanical properties of the materials making up the composite curved tube are given in Table 7.3. In the present cases, the curved tube section has an internal radius of *28 mm* and an external radius of *32 mm*, i.e. a wall thickness of *4 mm*. In addition, a composite curved tube spanning a curved segment of 90° with *R/a=10* is considered (unless otherwise mentioned). Furthermore, the stress components are normalized as $\bar{\sigma}_{ij} = \sigma_{ij}/\sigma_0$ where $\sigma_0 = (M.r)/(\pi/4*(b^4-a^4))$ with the outer radius *b* and the inner radius *a* of the composite curved tube. The results are presented based on the proposed method at θ=0°.

Table 7.3: Mechanical properties of the materials making up the composite curved tube [1].

Properties	E_1 (GPa)	$E_2=E_3$ (GPa)	$G_{12}=G_{13}= G_{23}$ (GPa)	$\upsilon_{12}=\upsilon_{13}$	υ_{23}
Carbon AS4/PEKK	140	10	5.56	0.31	0.33

7.5.1. FEM Analysis

The stress analysis of the thick composite curved tube is conducted by finite element method using ANSYS. Stress distributions are also generated to compare with the results obtained using the proposed method. The element used to perform the analysis is the layered solid element, SOLID 185. The number of integration points (1, 3, 5, 7 or 9), located through the thickness of each layer used for element calculations, is designated. Two points are

located on the top and bottom surfaces and the remaining points are distributed with an equal distance between two points. Here, three integration points are used through the thickness of each layer. In addition, one element or more, depend on Mesh Number (*see Table 7.4*) for each layer in the lay-up sequence, is defined to recover the interlaminar stresses in FEM. A rigid surface is modeled and glued to both end surfaces of the composite curved tube. Then, a bending moment is applied to the center node of the surface meshed using shell elements, SHELL 181. This is how the bending moment applied for the composite curved tube in FEM. The mesh-independency study is done for ANSYS (*see Table 7.4*). Mesh refining is performed two times while the element aspect ratio is kept constant. It is emphasized that for the initial mesh, Mesh Number 1, 360000 elements are used to model the structure. For Mesh Number 2, the thickness and circumferential directions are refined twice as much as the initial mesh. For Mesh Number 3, the axial and circumferential directions are refined twice as much as the initial mesh and the thickness direction is refined 4 times as much as the initial mesh to model the curved tube (*see Table 6.4*). Figure 7.2a shows the meshed composite curved tube used to perform the stress analysis using ANSYS 14.5. Figure 7.2b presents the radial and hoop stresses obtained using ANSYS for different mesh numbers mentioned in Table 7.4. As Figure 7.2b shows, the differences of the stresses for Mesh Numbers 2 and 3 are less than 2%, therefore, Mesh Number 2 is selected to obtain the results using FEM to compare with the theoretical results. Mesh Number 2 is called the final mesh in the following sections. Note that in the developed method, the end sections of the composite curved tube are free to deform in their planes, whereas in the FEM model they are not.

Table 7.4: Mesh characteristics.

Mesh Number	Mesh size (Axial)×(Circumferential)×(Thickness)	Number of elements	Analyzing time (sec)
1	9×10×40	3600	1800
2	9×20×80	14400	4000
3	18×20×160	57600	6000

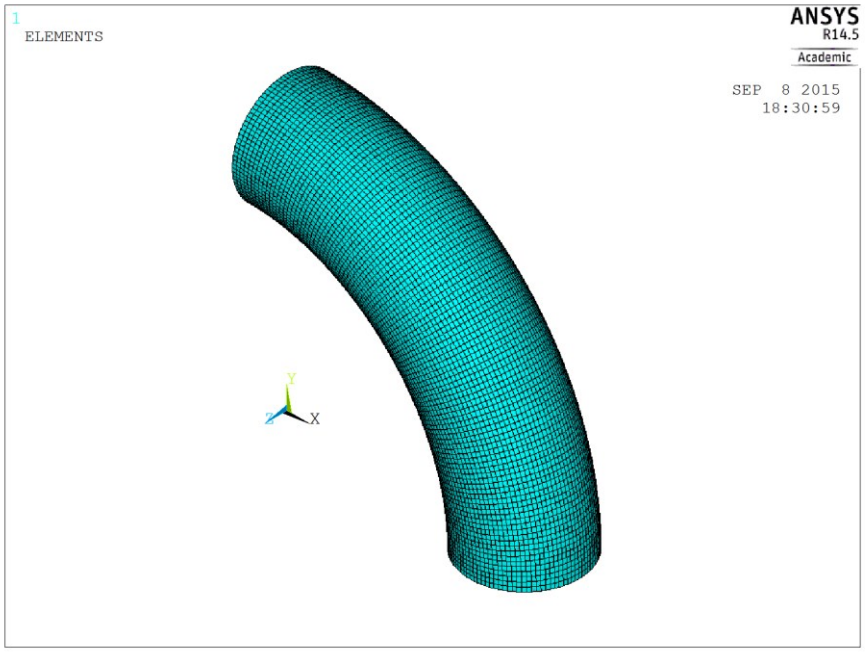

Figure 7.2a: Modeling of the composite curved tube using ANSYS.

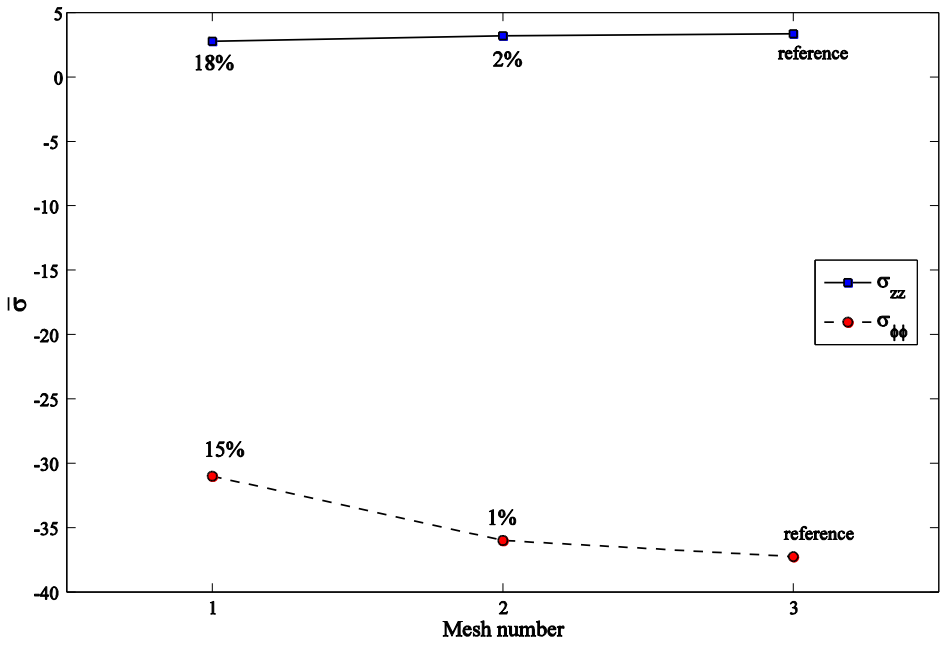

Figure 7.2b: The mesh independency study of the laminated composite curved tube.

7.5.2. Verifying the Proposed method

The proposed method is compared and verified with other 3 methods or data. First, in Section 7.5.2.1, the results are compared for a laminated curved tube using the developed

method with FEM. In addition, the convergence study for the developed method is performed. Then, in Section 7.5.2.2, the verification is done with the experimental data. Finally, in Section 7.5.2.3, the proposed method is verified with a solution available in the literature [9].

7.5.2.1. Comparison of the Proposed Method for Laminated Curved tubes with FEM

Here, the results obtained for a laminated composite curved tube using the developed method are compared with results obtained using FEM (ANSYS) based on the final mesh. First, the convergence study is performed for the $[90°_{20}/0°_{20}]$ laminated orthotropic curved tube. Table 7.5 presents the radial, hoop and longitudinal stresses obtained at ϕ=270°, θ=0° and the middle surface of the $[90°_{20}/0°_{20}]$ laminated orthotropic curved tube with considering different order numbers in the developed method to obtain the total solution. It is seen that with increasing the order number, the difference between the present method and FEM decreases. Eventually, the solution up to the 3rd order is considered to obtain stresses based on the developed method.

Table 7.5: The convergence study for the laminated composite curved tube.

Order number / Normalized Stress	The 0th order (Difference)	Up to the 1st order (Difference)	Up to the 2nd order (Difference)	**Up to the 3rd order (Difference)**	Up to the 4th order (Difference)	FEM
Radial stress	4.54 (35%)	4.10 (22%)	3.76 (12%)	**3.59 (7%)**	3.53 (5%)	3.36
Hoop stress	-51.05 (37%)	-46.58 (25%)	-41.36 (11%)	**-39.50 (6%)**	-39.12 (5%)	-37.26
Longitudinal stress	-107.85 (33%)	-97.31 (20%)	-89.20 (10%)	**-85.14 (5%)**	-84.33 (4%)	-81.09

The interlaminar radial stress, $\bar{\sigma}_{zz}$, at the middle surface (*r=30 mm, 90°/0° interface*) of the $[90°_{20}/0°_{20}]$ laminated orthotropic curved tube obtained based on the present method and FEM (ANSYS) is compared in Figure 7.3a. Good agreement between theoretical analysis and FEM (ANSYS) results based on the final mesh is obtained. The analyzing of the laminated orthotropic curved tube using ANSYS based on the initial mesh, Mesh Number 1, takes around 1800 seconds while it takes around 4000 and 6000 seconds for Mesh Numbers 2 and 3, respectively; while the analyzing of the same structure (*same lay-up*) based on the

developed method considering up to the 3rd order takes 310 seconds. In addition, to understand better the stress behavior, the polar distribution of the radial stress, $\bar{\sigma}_{zz}$, at the middle surface of the composite curved tube obtained by the present method is shown in Figure 7.3a. Note that in all polar distributions in the rest of this chapter, blue circle represents the zero stress condition while red lines represent the stress distributions. In addition, the lengths of arrows represent the magnitudes of stresses. Therefore, those red lines where are placed inside the blue circle represent the compressive stress while the other red lines where are placed outside of the blue circle represent the tensile stress.

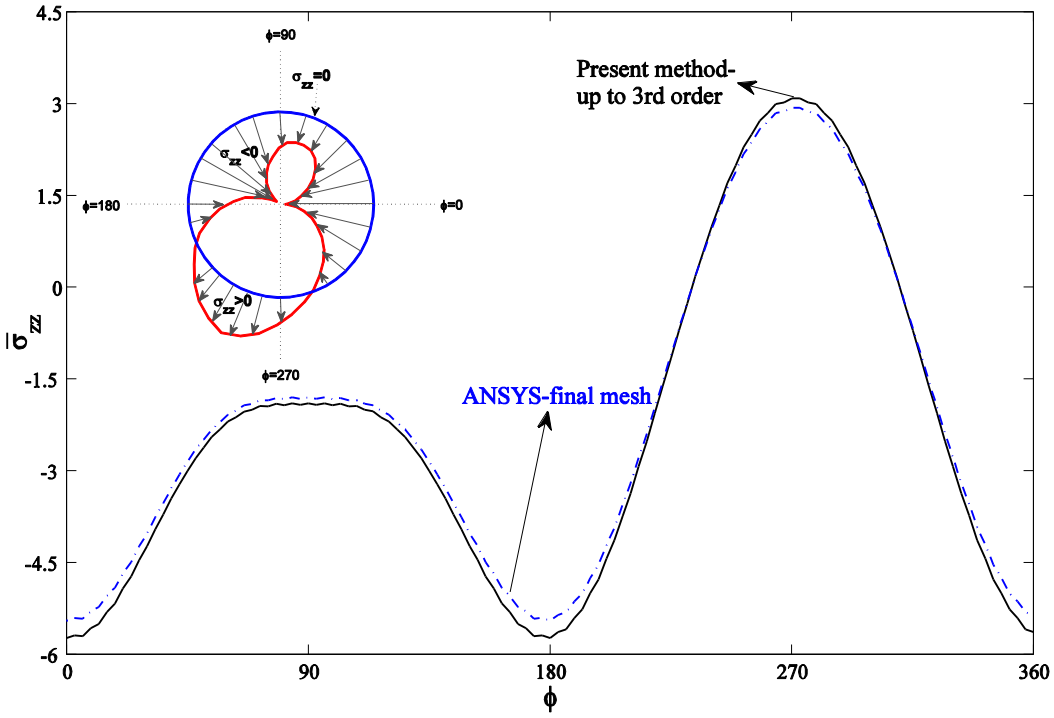

Figure 7.3a: Comparison of the radial stress, $\bar{\sigma}_{zz}$, obtained using the present method and ANSYS at the 90°/0° interface of the $[90°_{20}/0°_{20}]$ laminated curved tube.

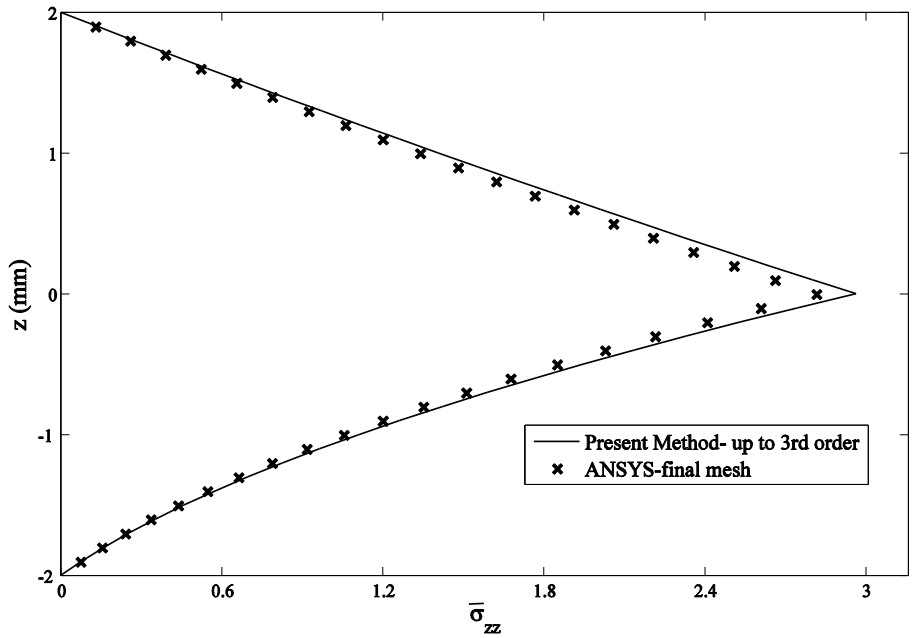

Figure 7.3b: Comparison of the interlaminar radial stress, $\bar{\sigma}_{zz}$, obtained using the present method and ANSYS of the $[90°_{20}/0°_{20}]$ laminated curved tubes at ϕ=270° along tube thickness.

To ensure the verifications are done in all layers of the laminated composite curved tube, the comparison must be performed by using the developed method and FEM (ANSYS) based on the final mesh along tube thickness. Figure 7.3b presents the comparison of the interlaminar radial stress, $\bar{\sigma}_{zz}$, of the $[90°_{20}/0°_{20}]$ laminated orthotropic curved tube at ϕ=270° along the tube thickness based on the present method and ANSYS based on the final mesh. There is a good agreement seen along tube thickness. Note that the maximum magnitude of the interlaminar radial stress occurs at *z=0 mm* where is the last 90°-ply placed (*i.e., layer 20*). Therefore, these layers tend to separate from 0°-plies, with the largest possibility. The interlaminar radial stress, $\bar{\sigma}_{zz}$, is zero at the inside and outside surfaces of the composite curved tube as expected from Eqs. (7.13) (N_z^k*=0 at z= ±h/2*).

Figure 7.4a compares the hoop stress, $\bar{\sigma}_{\phi\phi}$, obtained based on the proposed method and FEM (ANSYS) over cross section at the outside surface of the $[90°_{20}/0°_{20}]$ laminated orthotropic curved tube. Good agreement between theoretical analysis and FEM (ANSYS) results using the final mesh is obtained. Note that the hoop stress, $\bar{\sigma}_{\phi\phi}$, is compressive from 45° to 135° and 225° to 315°. In addition, the maximum values of the hoop stress are negative and they occur at ϕ=90° and then, at ϕ=270°.

Comparison of the hoop stress, $\bar{\sigma}_{\phi\phi}$, of the $[90°_{20}/0°_{20}]$ laminated orthotropic curved tube at ϕ=90° along tube thickness using the developed method and ANSYS based on the final mesh is shown in Figure 7.4b. The final mesh used in FEM to obtain results makes a good agreement along the tube thickness. Note that the 0° layer-group experiences a compressive stress while the hoop stress of the 90° layer-group (in the inner surface of the curved tube) is tensile. The maximum positive of the hoop stress in the $[90°_{20}/0°_{20}]$ laminated orthotropic curved tube occurs at the largest-diameter 90°-ply while the maximum negative of the hoop stress occurs at the outside surface.

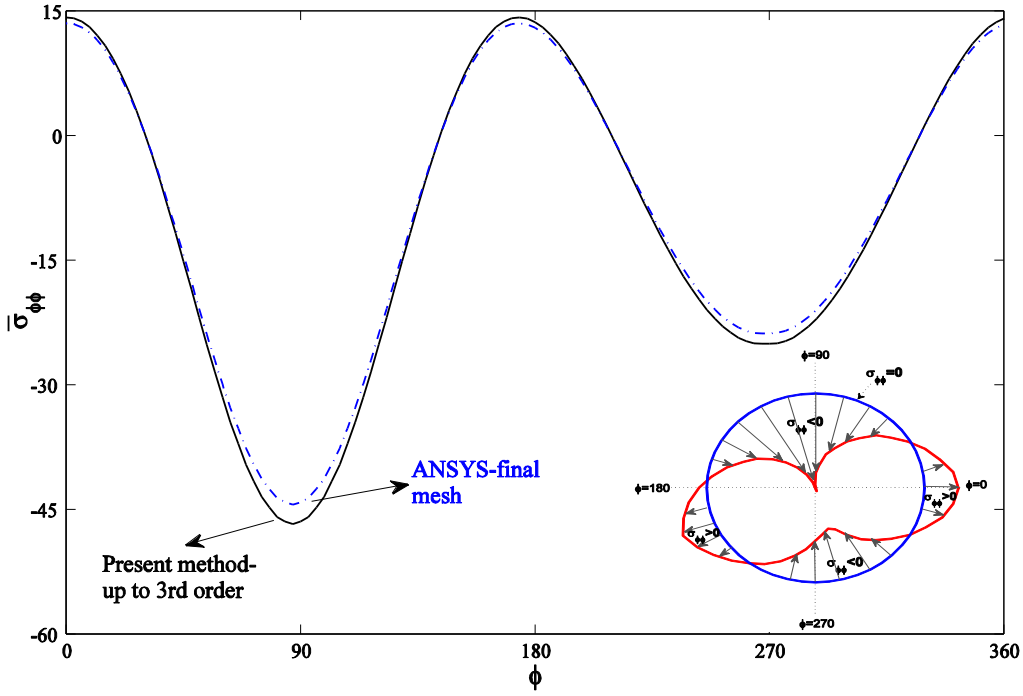

Figure 7.4a: Comparison of the hoop stress, $\bar{\sigma}_{\phi\phi}$, obtained using the present method and ANSYS at the outside surface of the $[90°_{20}/0°_{20}]$ laminated curved tube.

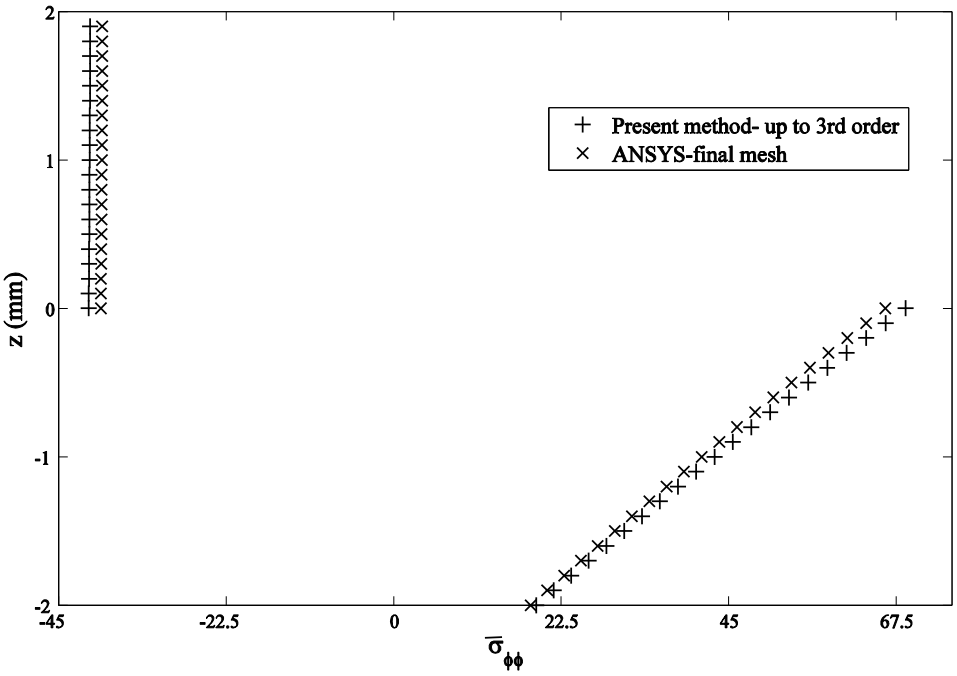

Figure 7.4b: Comparison of the hoop stresses, $\bar{\sigma}_{\phi\phi}$, obtained using the present method and ANSYS of the $[90°_{20}/0°_{20}]$ laminated curved tube at ϕ=90° along tube thickness.

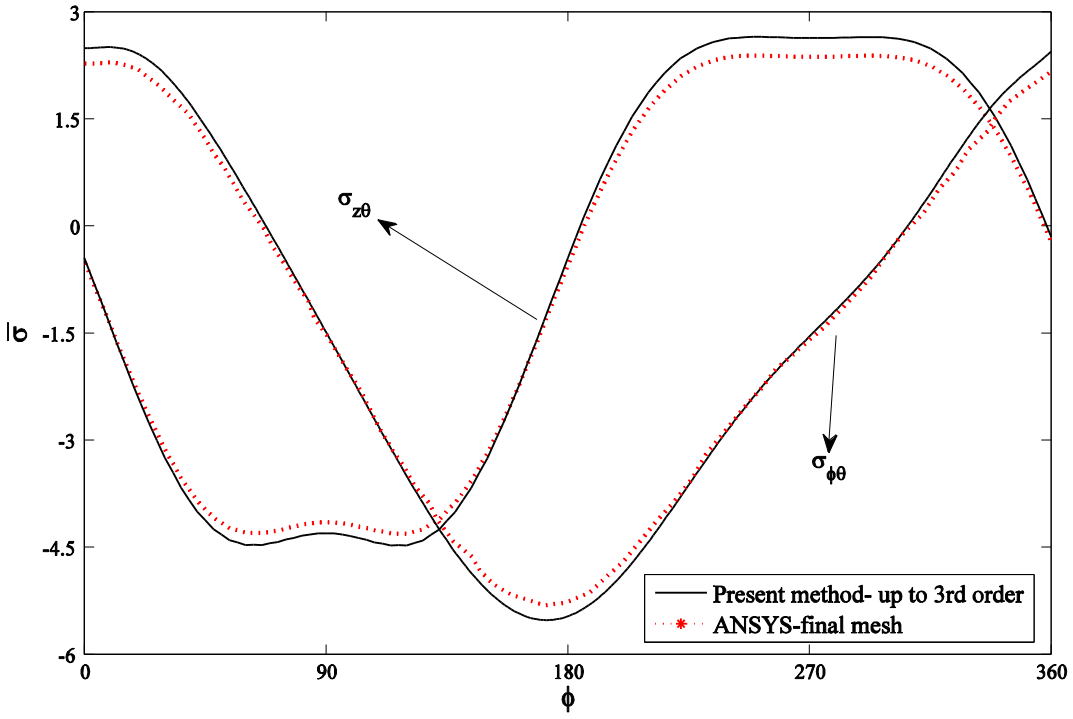

Figure 7.5a: Comparison of the shear stresses, $\bar{\sigma}_{\theta z}$, and $\bar{\sigma}_{\phi\theta}$, obtained using the present method and ANSYS at the 90°/0° interface of the $[90°_{20}/0°_{20}]$ laminated curved tube.

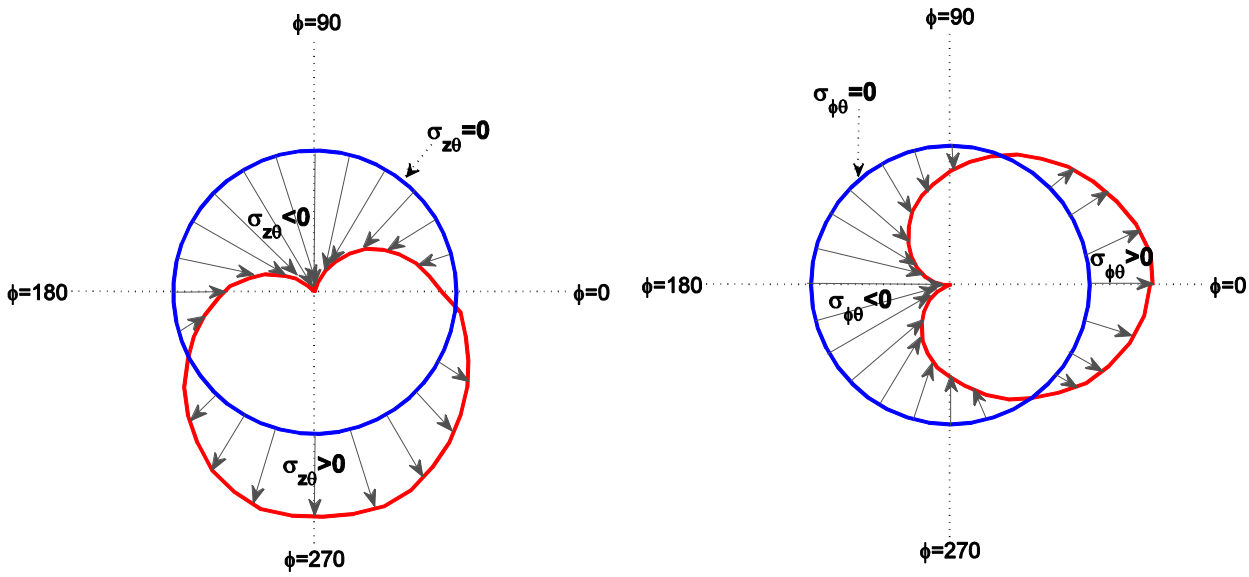

Figure 7.5b: Polar distributions of the shear stresses, $\bar{\sigma}_{\theta z}$, and $\bar{\sigma}_{\phi\theta}$, obtained using the present method at the 90°/0° interface of the $[90°_{20}/0°_{20}]$ laminated composite curved tube.

The comparison of the shear stresses, $\bar{\sigma}_{\theta z}$ and $\bar{\sigma}_{\phi\theta}$, over cross section at the middle surface of the $[90°_{20}/0°_{20}]$ laminated orthotropic curved tube obtained based on the present method and FEM (ANSYS) is presented in Figure 7.5. Good agreement is seen for the results obtained using the developed method with the results obtained using FEM based on the final mesh. Note that the shear stress, $\bar{\sigma}_{\theta z}$, is positive at the whole upper region of the cross section (180° to 360°) while the other shear stress, $\bar{\sigma}_{\phi\theta}$, is tensile from 0° to 60° and 300° to 360°. In addition, the maximum positive values of $\bar{\sigma}_{\theta z}$ occur at ϕ=225° and ϕ=315° of the tube cross section while maximum negative values of the shear stress, $\bar{\sigma}_{\phi\theta}$, occur at ϕ=45° and ϕ=135°. Figure 7.5b presents the polar distributions of the shear stresses, $\bar{\sigma}_{\theta z}$ and $\bar{\sigma}_{\phi\theta}$, over cross section at the middle surface of the $[90°_{20}/0°_{20}]$ laminated composite curved tube obtained based on the present method.

The comparisons of the longitudinal stress, $\bar{\sigma}_{\theta\theta}$, and the shear stress, $\bar{\sigma}_{z\phi}$, obtained based on the developed method and FEM (ANSYS) using the final mesh over cross section at the inside, middle and outside surfaces of the $[90°_{20}/0°_{20}]$ laminated orthotropic curved tube are plotted in Figures 7.6a and 7.6b, respectively. The results show good correspondence in all plotted layers. Observing from Figure 7.6a that the maximum longitudinal stress, $\bar{\sigma}_{\theta\theta}$, at the middle and outside surfaces is compressive and it occurs at ϕ=-90°, while at the inside surface

it occurs at ϕ=90° and it is tensile. It is seen that the longitudinal stress is compressive at the upper region of the composite curved tube cross section.

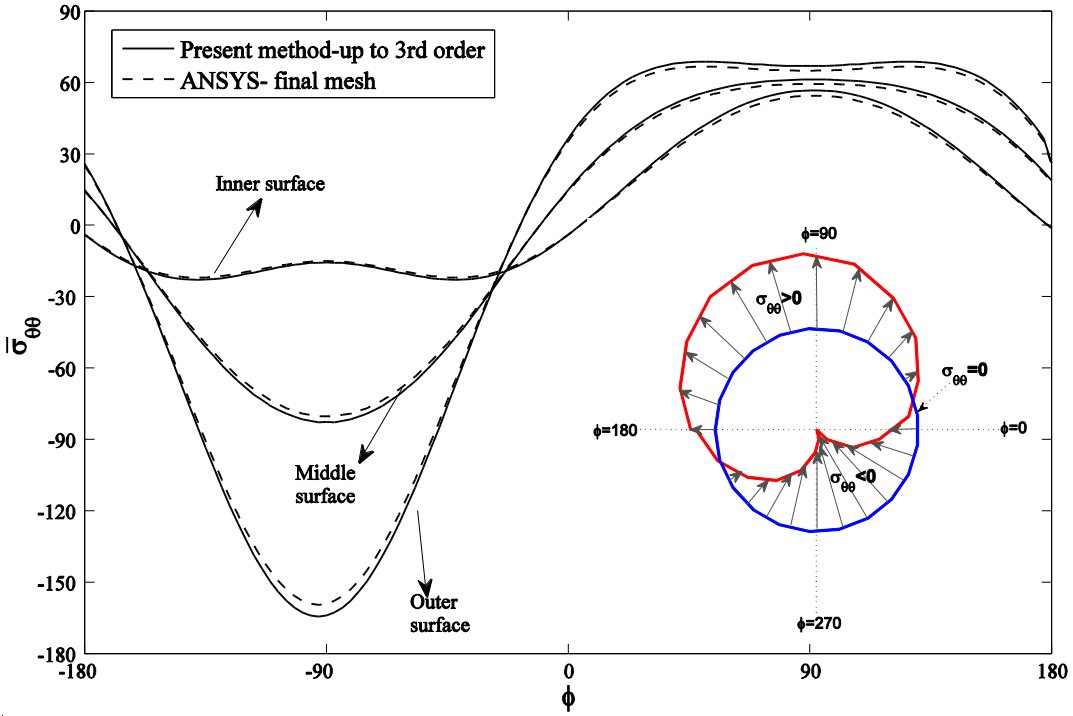

Figure 7.6a: Comparison of the longitudinal stress, $\bar{\sigma}_{\theta\theta}$, obtained using the present method and ANSYS over cross section at the inside, middle and outside surfaces of the $[90°_{20}/0°_{20}]$ laminated curved tube.

Figure 7.6b shows that the shear stress, $\bar{\sigma}_{z\phi}$, is positive from 0° to 90° and 180° to 270°. The positive maximum values for $\bar{\sigma}_{z\phi}$ occur at ϕ=45° and then, at ϕ=225°. Note that the trends of the shear stress, $\bar{\sigma}_{z\phi}$, for the inside, middle and outside surfaces are the same. The magnitude of the shear stress, $\bar{\sigma}_{z\phi}$, for the middle surface is maximum while the magnitude of the shear stress, $\bar{\sigma}_{z\phi}$, for the outside surface is minimum, in comparison with the other surfaces.

To examine the accuracy of the developed method for complex lay-up sequences, the thick $[(90°_{10}/0°_{10})_3/\pm45°_{25}]$ laminated composite curved tube is selected for the comparison purpose. Note that this lay-up sequence was used to manufacture a thick straight tube used for composite helicopter landing gear applications [1]. Figure 7.7 presents the comparison of the interlaminar radial stress, $\bar{\sigma}_{zz}$, of the thick $[(90°_{10}/0°_{10})_3/\pm45°_{25}]$ laminated composite curved tube at ϕ=270° along the tube thickness based on the present method and ANSYS based on the final mesh. There is a good agreement seen along tube thickness.

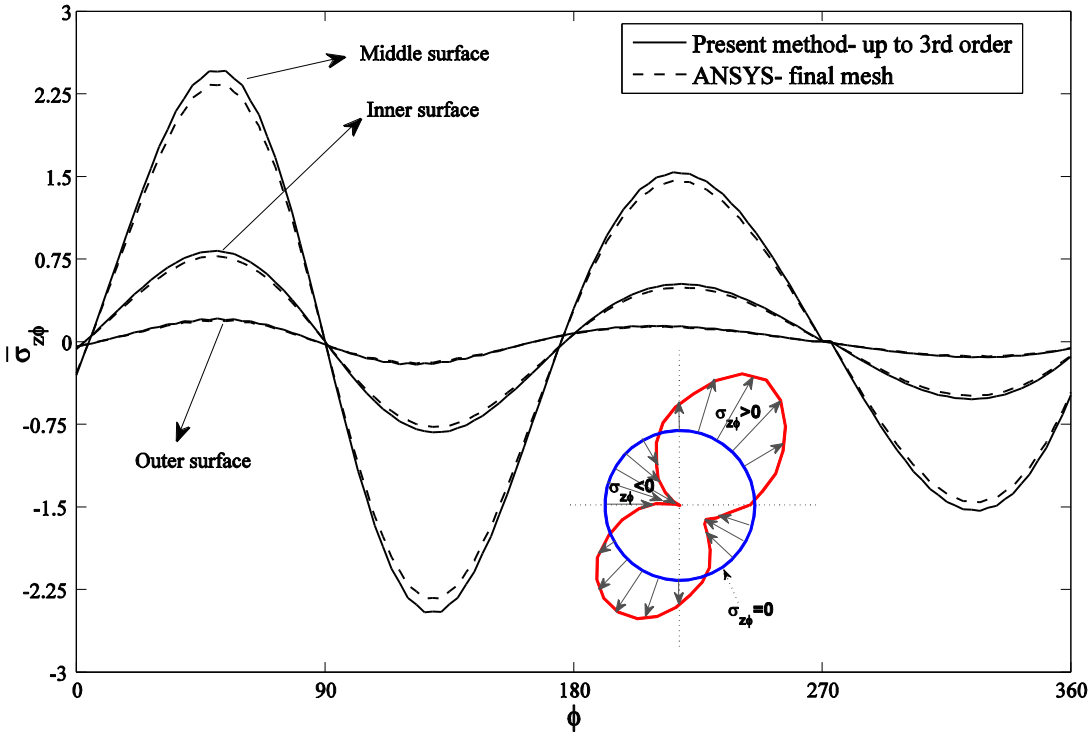

Figure 7.6b: Comparison of the shear stress, $\bar{\sigma}_{z\phi}$, obtained using the present method and ANSYS over cross section at the inside, middle and outside surfaces of the $[90°_{20}/0°_{20}]$ laminated curved tube.

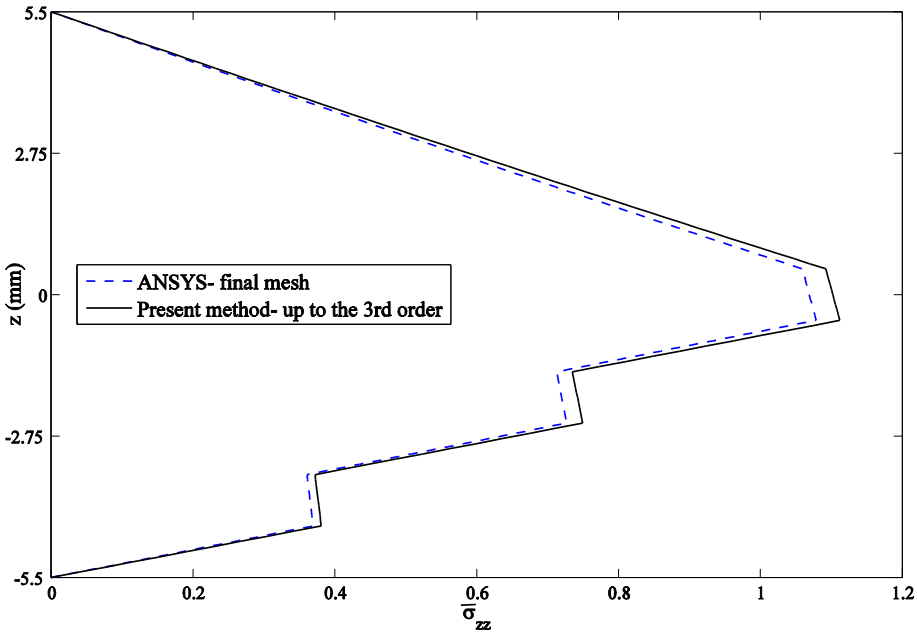

Figure 7.7: Comparison of the interlaminar radial stress, $\bar{\sigma}_{zz}$, obtained using the present method and ANSYS of the $[(90°_{10}/0°_{10})_3/\pm45°_{25}]$ laminated composite curved tubes at ϕ=270° along tube thickness.

7.5.2.2. Comparison of the Proposed Method with Experimental Data

In this section, the proposed method results are validated against the experimental data. The bending behavior of thick composite straight tubes was investigated experimentally [1]. The thick [$90°_{20}/0°_{20}$] thermoplastic composite straight tubes were manufactured using automated fiber placement technique and tested using a four-point bending test setup. The properties of the manufactured composite tube are given in Table 7.3. In the experimental investigation [1], the strain gage was used at the top line of the composite straight tube (ϕ=90°) to measure strains at the mid-span as seen in Figure 7.8a. A composite straight tube is modeled using the present method by assuming the bend radius *R* to be very large compared to *r*, so that a curved tube will be close to a straight tube (*see Figure 7.8a*). Since the experimental strains are measured at mid-span of the straight tube, the theoretical strains are obtained based on the proposed method at θ=0° of the curved tube, for the comparison purpose. The measured strain results are compared with the calculated strain results using the proposed method at ϕ=270°. In Figure 7.8b, the force variation versus experimental axial strains is shown. The theoretical analysis results in good agreement with the observations from the experiment done in [1]. As Figure 7.8b shows, the theoretical results are getting closer to experimental results with increasing *R/a*, while the shape of the curved tube is getting closer to the straight tube.

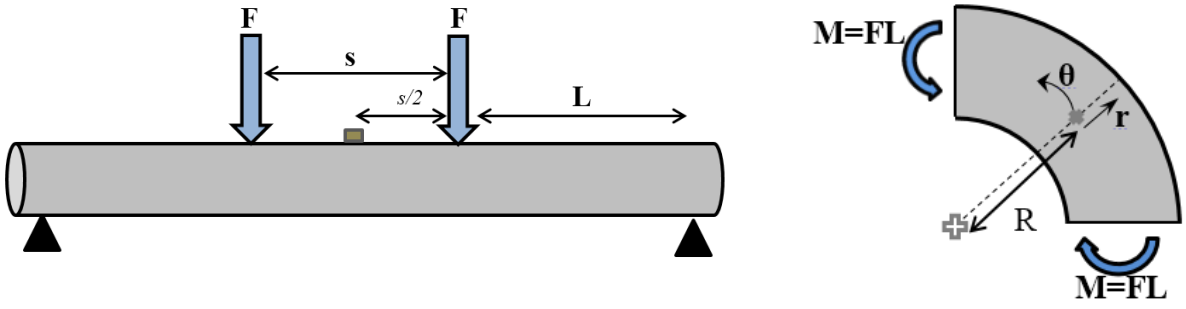

Figure 7.8a: Four-point bending test and a composite curved tube.

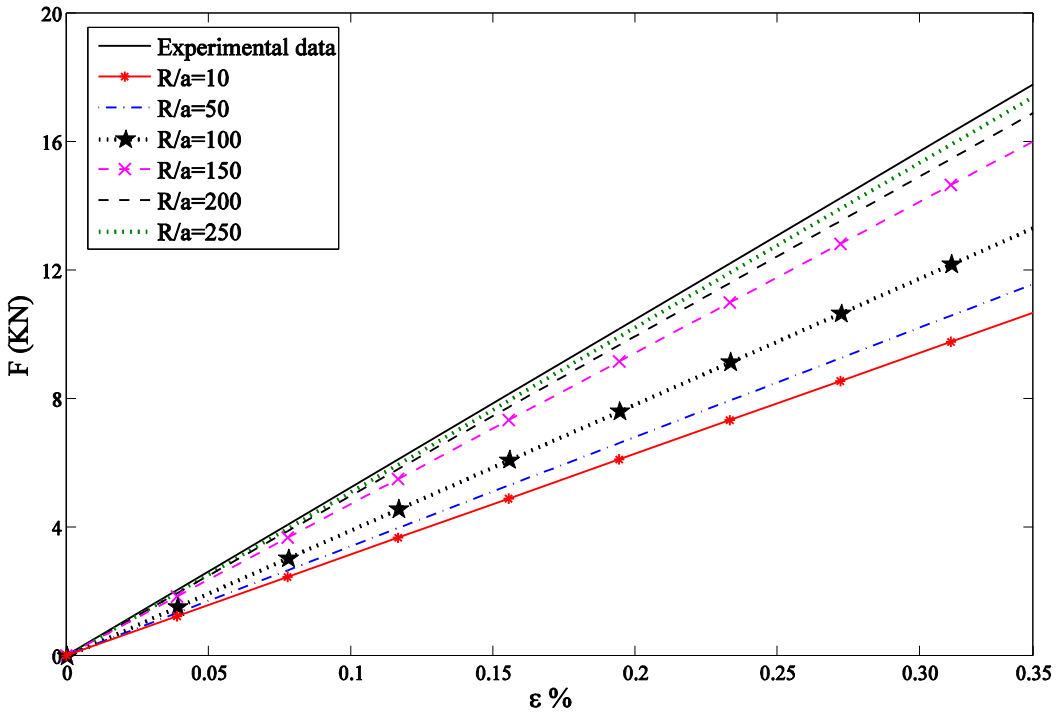

Figure 7.8b: Load-axial strain at the mid-span.

7.5.2.3. Comparison of the Proposed Method with a Solution in Literature

Jolicoeur and Cardou [9] presented a solution to obtain stresses in an orthotropic straight hollow circular cylinder subjected to bending, tensile and torsion loads. The solution was developed just for angle-ply lay-up sequences. Here, that solution under bending moment [9] was programed so that it is compared with the present method. The $[25°_{20}/-25°_{20}]$ lay-up sequence for a composite straight tube with the same geometrical and mechanical properties used in the previous sections is considered based on Jolicoeur and Cardou [9] to make comparison with the results obtained based on the present method. A composite straight tube is modeled based on the present method by assuming the bend radius R to be large compared to r. In order to obtain stresses using the proposed method, the solution up to the 3rd order is taken in the theoretical procedure.

Figure 7.9 shows the convergence of the interlaminar radial stress, $\bar{\sigma}_{zz}$, obtained based on the present method against Jolicoeur and Cardou solution [9] at ϕ=90° along the tube thickness of the $[25°_{20}/-25°_{20}]$ laminated orthotropic curved tube considering different R/a=10, 50, 100, 300 and 500 ratios. It is observed that the magnitude of the interlaminar

radial stress decreases with increasing *R/a* ratios. With considering *R/a=500* in the proposed method, the radial stress is in good agreement with the results obtained based on reference [9]. Note that with increasing *R/a* ratio, the shape of the composite curved tube is getting closer to the composite straight tube.

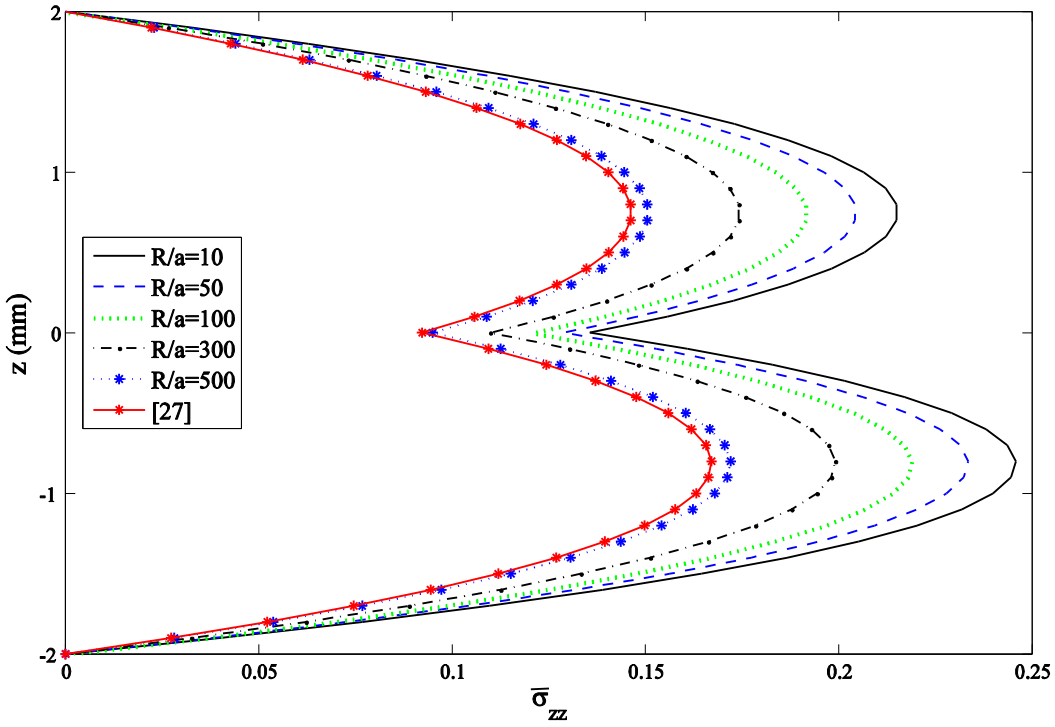

Figure 7.9: Convergence of the radial stress, $\bar{\sigma}_{zz}$, obtained using the present method against another solution at ϕ=90° along tube thickness of the [25°$_{20}$/-25°$_{20}$] laminated curved tube considering different *R/a* ratios.

The convergence of the hoop stress obtained using the present method against Jolicoeur and Cardou solution [9] at ϕ=90° along tube thickness of the [25°$_{20}$/-25°$_{20}$] laminated orthotropic curved tube considering different *R/a*=10, 50, 100, 300 and 500 ratios is plotted in Figure 7.10. By using *R/a=500* in the proposed method, good correlation between the results obtained based on two methods is seen in Figure 7.9. In addition, the magnitude of the hoop stress decreases as the shape of the composite curved tube is getting closer to the composite straight tube with increasing the *R/a* ratio.

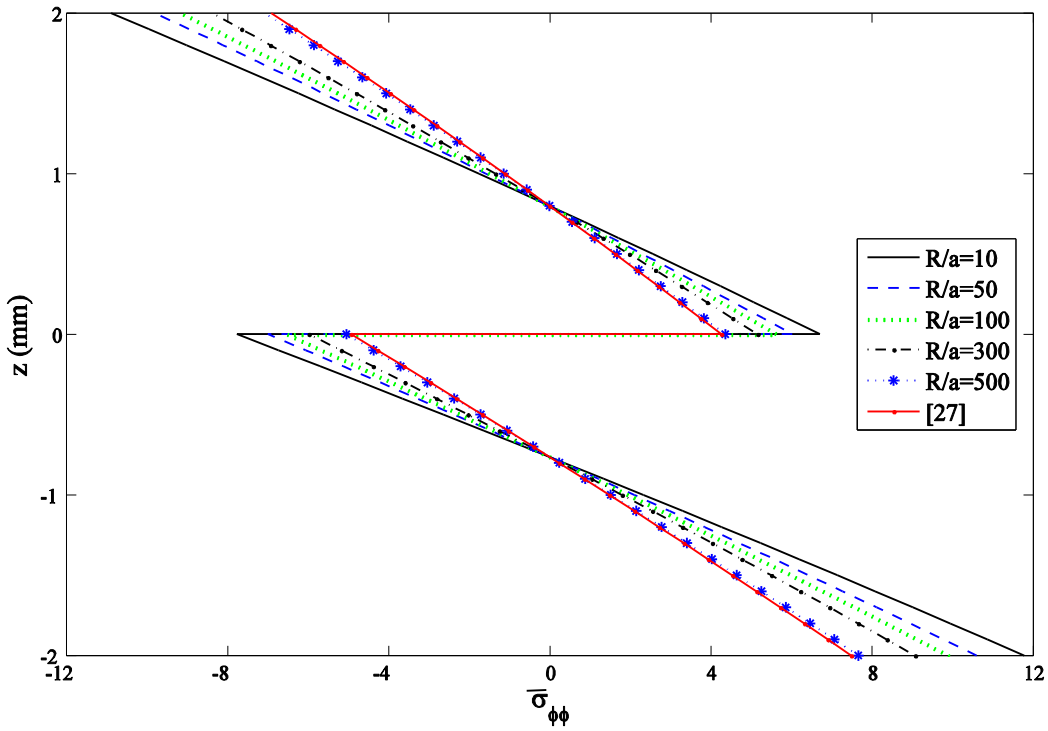

Figure 7.10: Convergence of the hoop stress, $\bar{\sigma}_{\phi\phi}$, obtained using the present method against another solution at ϕ=90° along tube thickness of the [25°$_{20}$/-25°$_{20}$] laminated curved tube considering different *R/a* ratios.

7.5.3. Advantages of the Proposed Method

Indeed, one can use FEM to analyze thick composite curved tubes. However, for structures such as thick laminated composite curved tubes where the geometry is not that complex (the only complexity is the layers in the thickness), the use of FEM is unnecessarily cumbersome. The discretization has to be done along three directions (axial, circumferential and radial). In addition, to keep the aspect ratio between different directions of the element to be reasonable, one has to use a large number of elements. Each time one changes some parameters such as number of layers, orientation of layers, length, radius of curved tube, etc. The structure has to be re-meshed which is time-consuming. The method we propose does not require meshing. It simplifies greatly inputs that the user has to do, once the program for solution is available. This presents a clear advantage over FEM. Therefore, the most important advantage of the proposed method is that inputs for the modeling of composite curved tubes with complex lay-up sequences are simple, easy to use and fast to run.

Note that it is almost impossible for real composite structures to use a large number of elements since there are many layers of small thickness. Therefore, the laminated approximation in thickness direction has to be employed not only for laminated shell elements but also for composite solid elements. For this reason, researchers are always interested in theoretical methods for composite structures. LWT is a popular candidate to obtain the solution with more accuracy for composite structures. However, for general composite structures subjected to different mechanical loadings, LWT can only be used in the thickness direction together with the company of FEM in other directions. For this sense, LWT can only be considered as a better laminated approximation in the thickness direction than CLT (the classical lamination theory). In this chapter, the accurate solution for thick laminated composite curved tubes is obtained not only by using LWT in the thickness direction (i.e., the radial direction) as a general case but also by using displacement approach of Toroidal Elasticity in other directions, including the longitudinal direction. To add to the advantages, high efficiency in terms of computational time is obtainable when the proposed method is used as compared with FEM.

7.6. Conclusion

The displacement-based approaches were used to investigate stresses in thick orthotropic curved tubes subjected to pure bending moment. The most general form of the displacement field of laminated orthotropic curved tubes was derived using Toroidal Elasticity (TE) and layer-wise method. The accuracy of the results was examined by comparing the experimental results and those obtained from the proposed method. The numerical results showed good agreement between the present method with the experimental results, FEM (ANSYS) and a solution available in the literature. Furthermore, the present method was found to be more cost effective and accurate in order to gain an in-depth and comprehensive understanding of stress analysis of composite curved tubes; therefore, it is employed to obtain stresses instead of using FEM.

Chapter 8

This chapter presents failure analysis of thick laminated composite curved tubes subjected to pure bending moment. By employing results of the proposed method, the progressive failure analysis is performed using Tsai-Wu criterion. Effects of lay-up sequences of thick composite curved tubes on stress distributions and failure sequences are investigated.

Failure Analysis of Thick Composite Curved Tubes

Hamidreza Yazdani Sarvestani and Mehdi Hojjati

Department of Mechanical and Industrial Engineering, Concordia University, Montreal, Quebec H3G 1M8, Canada

Abstract

In the present chapter, the failure analysis on thick laminated composite curved tubes subjected to pure bending moment is conducted by proposing a novel high-order displacement-based method. The most general displacement field of elasticity of thick laminated composite curved tubes is developed by employing a displacement approach of Toroidal Elasticity and a layer-wise method. Subsequently, the accuracy of the proposed method is verified by comparing the numerical results obtained using the proposed method with finite element method (FEM) and experimental data. By employing the results of the proposed method, the progressive failure analysis is performed using Tsai-Wu criterion. Finally, effects of lay-up sequences of thick composite curved tubes on stress distributions and failure sequences are investigated.

Keywords: Thick laminated composite curved tubes; Toroidal Elasticity; Layer-wise method; Stress analysis; Progressive failure analysis; Lay-up sequences.

8.1. Introduction

Composite straight and curved tubes are used as primary load-bearing structures in many engineering fields such as aerospace, offshore and infrastructure industries. One such application is that of the cross-piece for helicopter landing gears. These structures usually are moderately thick and they are subjected to certain loads such as tension, torsion, shear and bending. The study on failure behavior of composite tubes subjected to mechanical loadings is required to figure out their design capability. Due to the anisotropic behavior, composite

curved tubes are much more difficult in analysis especially in an ultimate failure analysis than an isotropic tube. Moreover, prediction of the state of stress and strain in different layers of laminated composite tubes is of theoretical interest and practical importance. The accurate evolution of stresses is essential for failure analysis and better design of these structures. A large number of studies have been conducted to obtain stresses and perform failure analysis on composite straight and curved tubes.

8.1.1. Stress Analysis

8.1.1.1. Isotropic Curved Tubes

Von Karman [71] found a theoretical explanation for the phenomenon of a curved tube having more flexibility in bending than a straight one. The particular case of the Karman problem, the so-called Brazier effect, which included the buckling analysis of straight or curved tubes, was more complex [101]. Their works provided the fundamentals for much of the subsequent tube analyses. Boyle [102] used a nonlinear theory of shells to formulate the tube bending problem. Emmerling [103] determined the nonlinear deformation of elastic curved tubes subjected to bending loads. He also studied the pre-critical deformation of tubes based on the semi-membrane theory. Levyakov and Pavshok [104] investigated a thin elastic curved tube subjected to pure bending by using finite element method. In addition, the buckling behavior of curved tubes was analyzed and effects of geometrical parameters of tubes on the critical bending moment were studied. The stress analysis of curved tubes subjected to in-plane bending was performed based on finite curved elements [105]. A fifth-order polynomial and Fourier series were used to define displacement components. Kolesnikov [106] analyzed large pure bending deformations of homogenous, incompressible, isotropic and hyperelastic curved tubes with a closed cross-section. The equilibrium equations were reduced to ordinary differential equations in his chapter based on the membrane assumptions. Yudo and Yoshikawa [107] used nonlinear FEA to study the buckling phenomenon for straight and curved tubes under a pure bending moment. Effects of a cross-sectional deformation on elastic buckling moment were investigated by considering the length-to-diameter ratio and the diameter-to-thickness ratio.

8.1.1.2. Orthotropic Curved Beams and Tubes

Ting [108] and Chen et al. [109] investigated a cylindrical anisotropic circular tube subjected to pressure, shear, torsion and extensive loads for axisymmetric deformation of a homogeneous tube assuming the stresses as a function of radial distance. Shearing and radial stresses in curved beams were developed based on satisfying both equilibrium equations and static boundary conditions on the surfaces of beams [58]. Dryden [59] obtained stress distributions across a functionally graded circular beam subjected to pure bending by using stress functions. The free vibration analysis was performed on functionally graded beams with curved axis by using the finite element method to discretize the motion equations [63]. A first order shear deformation theory was used to study static and free vibration behavior of generally laminated curved beams [64]. Wang and Liu [66] presented elasticity solutions for curved beams with orthotropic functionally graded layers subjected to a uniform load on the outer surface by means of Airy stress function method. A mathematical model was developed to analyze the mechanical behavior of laminated glass curved beams [67].

8.1.2. Failure Analysis

Thuis and Metz [110] investigated effects of the lay-up sequence on the energy absorption of composite cylinders loaded in compression. Different failure modes for the different laminates were observed. An energy based failure model was used to analyze the impact resistance of laminated composite shells [111]. Effects of pressure and curvature on the impact response were investigated. In another work [112], ABAQUS finite element code was used to study composite laminates and shell structures subjected to low-velocity impact. Element type, impactor modeling method, meshing pattern and contact modeling were investigated to obtain an accurate solution. Ismail et al. [113] studied buckling failures of thin composite cylindrical shells under axial compressive loading. Initial geometric and loading imperfections were investigated to find out their effects on buckling failure. Romano et al. [114] performed a progressive failure analysis to study both post buckling and final failure of damaged composite stiffened panels subjected to compressive load. Damage locations and the reduction of the panel stiffness were studied. Mahdavi et al. [115] investigated different failure mechanisms of filament-wound tubes subjected to tensile forces. They obtained the

hoop and tensile strength of tubes with the specific geometry and layer numbers. Chaudhuri [116] studied long thick composite cylindrical shells subjected to applied hydrostatic pressure. Effects of modal imperfections, transverse shear/normal deformation on propagation of fracture mode were analyzed. Tan et al. [117] performed experimental tests to investigate failure mechanisms of a quasi-isotropic CFRP laminate, containing a circular hole, under combined tension and shear or compression.

The above review shows that there is a need to work on stress and failure analyses for thick composite curved tubes subjected to mechanical loadings. Although finite element methods are used for analyzing such structures, it is necessary to do meshing for each structure every time some dimensions or lay-up sequences are changed. In response to this need for an alternative, rapid and low computational cost method, the focus of this chapter is to propose a method where inputs to obtain solutions are simple; i.e. one only needs to enter in the actual dimensions or lay-up sequences without re-meshing work. The present chapter is devoted to develop a method that can provide stresses, strains and displacements for thick composite curved tubes subjected to pure bending moment with simple inputs. Displacement approach of Toroidal Elasticity (TE) and layer-wise method are used. Comparison is made between results obtained for the proposed analytical method with experimental data and FEM. There is a good agreement of the developed method with experimental data and FEM. Practical lay-up sequences are considered to study their effects on stress distributions of thick laminated composite curved tubes. Finally, the progressive failure analysis using Tsai-Wu criterion is conducted to determine maximum bending moments and failure sequences of thick composite curved tubes.

8.2. Motivation

Conventional helicopter landing gears consist of two skids running along the main direction of the helicopter, and two parallel cross tubes connecting the skids together. The cross tubes of the helicopter landing gear consist of both straight and curved tubes which support the weight of the helicopter. Despite the numerous advantages of composite materials, they generally suffer from poor impact resistance, poor fracture toughness and poor delamination strength when used in the aforementioned applications. These problems are

addressed by using thermoplastic-matrix composites. Derisi [1] designed and manufactured thermoplastic composite straight tubes for helicopter landing gears. Another technique to solve the drawbacks of thermoset-matrix composites, such as poor delamination strength, is the lay-up sequence design. Recently, a method for stress analysis of thick composite straight tubes subjected to cantilever loading was developed [92, 97]. Now, in order to provide some insight into the mechanical behavior of the curved part of composite helicopter landing gears, a simple-input displacement-based method is developed. Specifically, the method is used to evaluate stresses and perform failure analysis in thick laminated composite curved tubes.

8.3. Formulation

First, in Section 8.3.1, the displacement field for a composite curved tube with a single layer is derived using Toroidal Elasticity and the method of successive approximation. Then, in Section 8.3.2, by using the developed displacement field of single-layer composite curved tubes and layer-wise method, a new displacement-based method is proposed to analyze thick laminated composite curved tubes. Note that the detailed derivations are found in [99, 118]. Here, the necessary formulations are explained briefly allowing readers to understand the procedure.

8.3.1. Displacement Field of Single-layer Composite Curved Tubes

Toroidal elasticity is a three dimensional theory used for the elastostatic analysis of thick curved tubes. Here, a displacement approach of Toroidal Elasticity is chosen to analyze composite curved tubes. The governing equations are developed in three toroidal coordinate system. The method of successive approximation is used to obtain the displacement field of single-layer composite curved tubes.

8.3.2. Governing Equations in Toroidal Coordinates

A thick laminated composite curved tube with a bend radius R, mean radius R_1 and thickness h is subjected to a pure bending moment, M, as shown in Figure 8.1a. Annular cross section is bounded by radii a and b. Toroidal coordinate system (r, ϕ, θ) is placed at the mid-

span of the composite curved tube where r and ϕ are polar coordinates in the plane of the curved tube cross section and θ defines the position of the curved tube cross section.

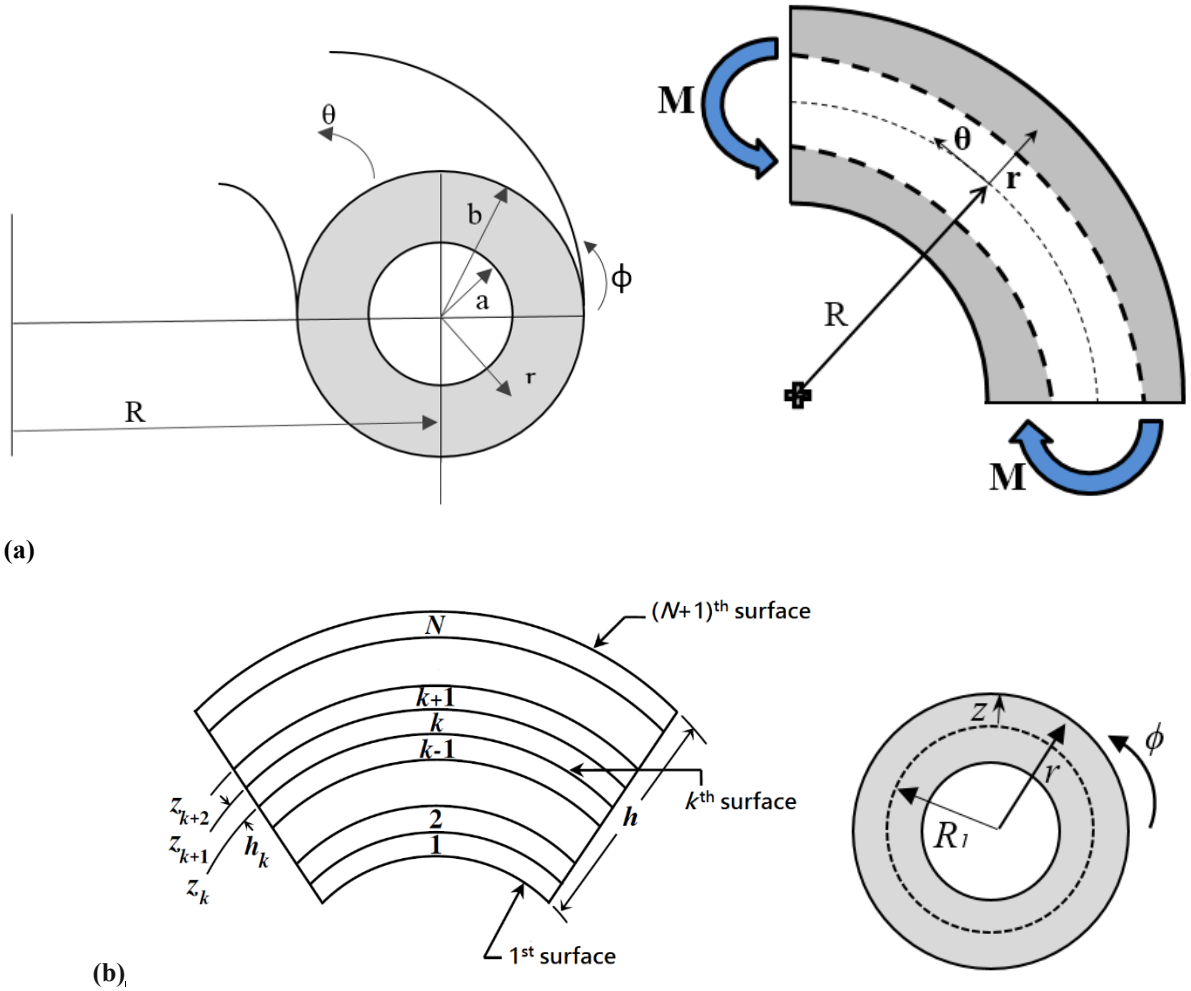

Figure 8.1: **(a)** Geometry and the coordinate system of a composite curved tube. **(b)** The lay-up sequence in a thick laminated composite curved tube.

Zhu and Redekop [87] have given a derivation of the governing equations for linear three-dimensional theory of elasticity in the toroidal coordinates for isotropic materials. The theory is extended here to cover the case for orthotropic materials. The toroidal governing equations are presented as [87]:

$$\frac{\partial \sigma_{rr}}{\partial r}+\frac{1}{r}\frac{\partial \sigma_{r\phi}}{\partial \phi}+\frac{1}{r}\left(\sigma_{rr}-\sigma_{\phi\phi}\right)+\frac{1}{\rho}\left(\frac{\partial \sigma_{r\theta}}{\partial \theta}+\left(\sigma_{rr}-\sigma_{\phi\phi}\right)\cos\phi-\sigma_{r\phi}\sin\phi\right)=0$$

$$\frac{\partial \sigma_{r\phi}}{\partial r}+\frac{1}{r}\frac{\partial \sigma_{\phi\phi}}{\partial \phi}+\frac{2}{r}\sigma_{r\phi}+\frac{1}{\rho}\left(\frac{\partial \sigma_{\phi\theta}}{\partial \theta}+\sigma_{r\phi}\cos\phi-\left(\sigma_{\phi\phi}-\sigma_{\theta\theta}\right)\sin\phi\right)=0$$

$$\frac{\partial \sigma_{r\theta}}{\partial r}+\frac{1}{r}\frac{\partial \sigma_{\phi\theta}}{\partial \phi}+\frac{1}{r}\sigma_{r\theta}+\frac{1}{\rho}\left(\frac{\partial \sigma_{\theta\theta}}{\partial \theta}+2\sigma_{r\theta}\cos\phi-2\sigma_{\phi\theta}\sin\phi\right)=0 \qquad (8.1)$$

where $\rho = R + r\cos\phi$. The kinematics relations are:

$$\varepsilon_{rr}=\frac{\partial u}{\partial r}, \qquad \varepsilon_{r\phi}=\frac{1}{2}\left(\frac{1}{r}\frac{\partial u}{\partial \phi}+\frac{\partial v}{\partial r}-\frac{v}{r}\right),$$

$$\varepsilon_{\phi\phi}=\frac{u}{r}+\frac{1}{r}\frac{\partial v}{\partial \phi}, \qquad \varepsilon_{r\theta}=\frac{1}{2}\left(\frac{\partial w}{\partial r}+\frac{1}{\rho}\frac{\partial u}{\partial \theta}-\frac{w}{\rho}\cos\phi\right),$$

$$\varepsilon_{\theta\theta}=\frac{1}{\rho}\left(u\cos\phi-v\sin\phi+\frac{\partial w}{\partial \theta}\right), \qquad \varepsilon_{\phi\theta}=\frac{1}{2}\left(\frac{1}{r}\frac{\partial w}{\partial \phi}+\frac{1}{\rho}\frac{\partial v}{\partial \theta}+\frac{w}{\rho}\sin\phi\right) \qquad (8.2)$$

where u, v and w represent the displacement components in the r, ϕ and θ directions, respectively. For orthotropic materials, the constitutive equations are [91]:

$$\{\sigma\}=[C]\{\varepsilon\} \qquad (8.3)$$

where $C_{ij}^{(k)}$ represent the off-axis stiffnesses. Upon substitution of Eqs. (8.2) into Eq. (8.3), the stress-displacement relations are obtained:

$$\sigma_{rr}=C_{11}\frac{\partial u}{\partial r}+C_{12}\frac{u}{r}+\frac{C_{12}}{r}\frac{\partial v}{\partial \phi}+\frac{C_{13}}{\rho}\left(u\cos\phi-v\sin\phi+\frac{\partial w}{\partial \theta}\right)$$

$$\sigma_{\phi\phi}=C_{12}\frac{\partial u}{\partial r}+C_{22}\frac{u}{r}+\frac{C_{22}}{r}\frac{\partial v}{\partial \phi}+\frac{C_{23}}{\rho}\left(u\cos\phi-v\sin\phi+\frac{\partial w}{\partial \theta}\right)$$

$$\sigma_{\theta\theta}=C_{13}\frac{\partial u}{\partial r}+C_{23}\frac{u}{r}+\frac{C_{23}}{r}\frac{\partial v}{\partial \phi}+\frac{C_{33}}{\rho}\left(u\cos\phi-v\sin\phi+\frac{\partial w}{\partial \theta}\right)$$

$$\sigma_{r\phi}=\frac{C_{44}}{2}\left(\frac{1}{r}\frac{\partial u}{\partial \phi}+\frac{\partial v}{\partial r}-\frac{v}{r}\right)$$

$$\sigma_{r\theta}=\frac{C_{55}}{2}\left(\frac{\partial w}{\partial r}+\frac{1}{\rho}\frac{\partial u}{\partial \theta}-\frac{w}{\rho}\cos\phi\right)$$

$$\sigma_{\phi\theta}=\frac{C_{66}}{2}\left(\frac{1}{r}\frac{\partial w}{\partial \phi}+\frac{1}{\rho}\frac{\partial v}{\partial \theta}+\frac{w}{\rho}\sin\phi\right) \qquad (8.4)$$

Substituting Eq. (8.4) into Eq. (8.1), the governing Navier equations in toroidal coordinates are obtained as:

$$\left(\frac{1}{\rho}\right)^0 U + \left(\frac{1}{\rho}\right)^1 \bar{U} + \left(\frac{1}{\rho}\right)^2 \hat{U} = 0$$
$$\left(\frac{1}{\rho}\right)^0 V + \left(\frac{1}{\rho}\right)^1 \bar{V} + \left(\frac{1}{\rho}\right)^2 \hat{V} = 0$$
$$\left(\frac{1}{\rho}\right)^0 W + \left(\frac{1}{\rho}\right)^1 \bar{W} + \left(\frac{1}{\rho}\right)^2 \hat{W} = 0 \qquad (8.5)$$

where the coefficients in Eq. (8.5) are defined in [99]. The three Navier equations serve as the fundamental equations for the displacement-based Toroidal Elasticity. Eqs. (8.5) are composed of three parts. The first part is independent of *1/ρ*. The second part and the third part are linear and non-linear parts of *1/ρ*. The Navier equations (Eq. (8.5)) in the toroidal coordinate system are much more complicated than those in Cartesian system are. As it is impossible to find an exact solution for the Navier equations, the method of successive approximation is used to obtain an approximate solution.

8.3.3. General Solution for In-plane Pure Bending

A direct solution is formulated to avoid the complications, which arise from the use of stress function. The solution for the displacement is thus sought in the following form:

$$u = ar^m \cos(n\phi)\cos(\theta)$$
$$v = br^m \sin(n\phi)\cos(\theta) \qquad (8.6)$$
$$w = cr^{\bar{m}} \cos(n\phi)\sin(\theta)$$

The quantities *a*, *b*, *c*, *m*, $\bar{m}$ and *n* are constants and parameters, which are determined in the reference [99]. Eventually, the general form displacement field of single-layer composite curved tubes of the *k*th plane and up to the *n*th order is presented as (the detailed derivation is found in [99]):

$$u^{(k)}(r,\phi,\theta) = \varepsilon^n B_n^{(k)}(r)\cos(n\phi)\cos(\theta)$$
$$v^{(k)}(r,\phi,\theta) = \varepsilon^n A_n^{(k)}(r)\sin(n\phi)\cos(\theta)$$
$$w^{(k)}(r,\phi,\theta) = \varepsilon^n C_n^{(k)}(r)\cos((n-1)\phi)\sin(\theta) \qquad (8.7)$$

where

$$B_n^{(k)}(r)=a_n^{(k)}B_{1,m_n^{(k)}}r^{m_n^{(k)}}+b_n^{(k)}B_{1,m_n'^{(k)}}r^{m_n'^{(k)}}+c_n^{(k)}B_{1,-m_n^{(k)}}r^{-m_n^{(k)}}+d_n^{(k)}B_{1,-m_n'^{(k)}}r^{-m_n'^{(k)}}$$

$$A_n^{(k)}(r)=-a_n^{(k)}A_{2,m_n^{(k)}}r^{m_n^{(k)}}-b_n^{(k)}A_{2,m_n'^{(k)}}r^{m_n'^{(k)}}-c_n^{(k)}A_{2,-m_n^{(k)}}r^{-m_n^{(k)}}-d_n^{(k)}A_{2,-m_n'^{(k)}}r^{-m_n'^{(k)}}$$

$$C_n^{(k)}(r)=e_n^{(k)}r^{\bar{m}_n^{(k)}}+f_n^{(k)}r^{-\bar{m}_n^{(k)}} \qquad (8.8a)$$

$$\bar{m}_n^{(k)}=\pm n\left(\frac{\bar{C}_{66}^{(k)}}{\bar{C}_{55}^{(k)}}\right)^{\frac{1}{2}}$$

$$B_{1,m_n^{(k)}}=-\left(\bar{C}_{22}^{(k)}+\frac{1}{2}\bar{C}_{44}^{(k)}\right)+\frac{n}{(n+1)}m_n^{(k)}\left(\frac{1}{2}\bar{C}_{44}^{(k)}+\bar{C}_{12}^{(k)}\right)$$

$$A_{2,m_n^{(k)}}=-\left(\bar{C}_{22}^{(k)}+\frac{1}{2}\bar{C}_{44}^{(k)}\right)-\frac{n}{(n+1)}m_n^{(k)}\left(\frac{1}{2}\bar{C}_{44}^{(k)}+\bar{C}_{12}^{(k)}\right) \qquad (8.8b)$$

and $m_n^{(k)},-m_n^{(k)},m_n'^{(k)}$ and $-m_n'^{(k)}$ are the 4 roots of the following equation:

$$\left(\frac{1}{2}\bar{C}_{44}^{(k)}\bar{C}_{11}^{(k)}\right)m_n^{(k)4}+\left(-n^2\bar{C}_{11}^{(k)}\bar{C}_{22}^{(k)}-\frac{1}{2}\bar{C}_{11}^{(k)}\bar{C}_{44}^{(k)}-\frac{1}{2}\bar{C}_{44}^{(k)}\bar{C}_{22}^{(k)}+n^2\bar{C}_{12}^{(k)}\bar{C}_{44}^{(k)}+n^2\bar{C}_{12}^{(k)2}\right)m_n^{(k)2}$$
$$+\frac{n^4-2n^2+1}{2}\bar{C}_{22}^{(k)}\bar{C}_{44}^{(k)}=0 \qquad (8.8c)$$

with *n*, here and in what follows, being a dummy index implying summation of orders from *n*=0 to the *n*th order. $\bar{C}_{ij}^{(k)}$ represents the off-axis stiffnesses. Also, *n* and *k* present the order number (i.e., *n=0, 1, 2, 3, 4,...*) and plane number (i.e., *k=1, 2,..., N+1*), respectively.

8.3.4. Displacement Field of Thick Laminated Composite Curved Tubes

8.3.4.1. Layer-wise Theory (LWT)

The equivalent single-layer theories are not able to precisely find stresses and strains in laminated composite structures. However, LWT allows each layer of the laminate to act like a real three-dimensional layer while being able to present good results for the local quantities. In LWT, the displacement components of a generic point in the laminate are assumed as:

$$U(z,\phi,\theta)=u_k(\phi,\theta)\Phi_k(z)$$
$$V(z,\phi,\theta)=v_k(\phi,\theta)\Phi_k(z)$$
$$W(z,\phi,\theta)=w_k(\phi,\theta)\Phi_k(z) \qquad (k=1,2,...,N+1) \qquad (8.9)$$

with k, here and in what follows, being a dummy index implying summation of terms from k=1 to k=N+*1*. Note that z is the local direction starting from the mid-thickness of the curved tube cross section (*see Figure 8.1b*). The variable N corresponds to the total number of numerical layers within the laminated composite curved tube. In Eq. (8.9), U, V and W represent the total displacement components in the z, ϕ and θ directions, respectively. Moreover, $u_k(\phi,\theta)$, $v_k(\phi,\theta)$ and $w_k(\phi,\theta)$ represent the displacements of the points initially located at the kth plane within the laminated composite curved tube in the z, ϕ and θ directions, respectively. $\Phi_k(z)$ is the global Lagrangian interpolation function associated with the kth plane. Depending upon the polynomial order of the interpolation function, Eq. (8.9) exhibits piecewise polynomial variation. Note that the accuracy of LWT is enhanced by subdividing each physical layer into a finite number of numerical layers. Clearly, as the number of subdivisions (p) through-thickness is increased, the number of governing equations and the accuracy of the results are increased.

The procedure for solving a specific problem can now be outlined. The displacement components of single-layer composite curved tubes are taken based on Eq. (8.7). By applying layer-wise method, Eq. (8.9), the displacement components of thick laminated composite curved tubes are obtained. Then, by employing the displacement components and their corresponding strains in the principle of minimum total potential energy and using the fundamental lemma of calculus of variations, the equilibrium equations of composite curved tubes under pure bending moment are derived.

According to the previous discussion, by applying the LWT displacement field (Eq. (8.9)) on general displacement field of single-layer composite curved tubes in Eq. (8.7), the elasticity displacement field of thick laminated composite curved tubes is rewritten up to the nth order in following form as:

$$
\begin{aligned}
&U\left(z,\phi,\theta\right)=\varepsilon^{n}B_{n}^{(k)}\left(R_{1}+z\right)\cos\left(n\phi\right)\cos\left(\theta\right)+U_{k}\left(\phi\right)\Phi_{k}\left(z\right)\\
&V\left(z,\phi,\theta\right)=\varepsilon^{n}A_{n}^{(k)}\left(R_{1}+z\right)\sin\left(n\phi\right)\cos\left(\theta\right)+V_{k}\left(\phi\right)\Phi_{k}\left(z\right)\qquad\left(k=1,2,...,N+1\right)\\
&W\left(z,\phi,\theta\right)=\varepsilon^{n}C_{n}^{(k)}\left(R_{1}+z\right)\cos\left(\left(n-1\right)\phi\right)\sin\left(\theta\right)+W_{k}\left(\phi\right)\Phi_{k}\left(z\right)\qquad\left(8.10\right)
\end{aligned}
$$

By employing linear interpolation functions, the continuity of displacement components through-thickness of laminate is identically satisfied. Thus, Eqs. (8.10) are represented as:

$$U\left(\mathrm{z},\phi,\theta\right)=\varepsilon^{n}\left(\begin{array}{l}a_{n}B_{1,m_{n}^{(k)}}\left(R_{1}+z\right)^{m_{n}^{(k)}}+b_{n}B_{1,m_{n}^{\prime(k)}}\left(R_{1}+z\right)^{m_{n}^{\prime(k)}}\\+c_{n}B_{1,-m_{n}^{(k)}}\left(R_{1}+z\right)^{-m_{n}^{(k)}}+d_{n}B_{1,-m_{n}^{\prime(k)}}\left(R_{1}+z\right)^{-m_{n}^{\prime(k)}}\end{array}\right)\cos\left(n\phi\right)\cos\left(\theta\right)+U_{k}\left(\phi\right)\Phi_{k}\left(z\right)$$

$$V\left(\mathrm{z},\phi,\theta\right)=-\varepsilon^{n}\left(\begin{array}{l}a_{n}A_{2,m_{n}^{(k)}}\left(R_{1}+z\right)^{m_{n}^{(k)}}+b_{n}A_{2,m_{n}^{\prime(k)}}\left(R_{1}+z\right)^{m_{n}^{\prime(k)}}\\+c_{n}A_{2,-m_{n}^{(k)}}\left(R_{1}+z\right)^{-m_{n}^{(k)}}+d_{n}A_{2,-m_{n}^{\prime(k)}}\left(R_{1}+z\right)^{-m_{n}^{\prime(k)}}\end{array}\right)\sin\left(n\phi\right)\cos\left(\theta\right)+V_{k}\left(\phi\right)\Phi_{k}\left(z\right)$$

$$W\left(\mathrm{z},\phi,\theta\right)=\varepsilon^{n}\left(e_{n}\left(R_{1}+z\right)^{\bar{m}_{n}^{(k)}}+f_{n}\left(R_{1}+z\right)^{-\bar{m}_{n}^{(k)}}\right)\cos\left(\left(n-1\right)\phi\right)\sin\left(\theta\right)+W_{k}\left(\phi\right)\Phi_{k}\left(z\right)\qquad(8.11)$$

In order to satisfy the interfacial continuities of the displacement components, it is necessary that the constants appearing in Eqs. (8.11) (i.e., a_n, b_n, c_n, d_n, e_n and f_n) to be the same for all layers. The linear global interpolation function is defined as:

$$\Phi_{k}\left(z\right)=\begin{cases}0 & z\le z_{k-1}\\ \psi_{k-1}^{2}\left(z\right)=\dfrac{1}{h_{j-1}}\left(z-z_{k-1}\right) & z_{k-1}\le z\le z_{k}\\ \psi_{k}^{1}\left(z\right)=\dfrac{1}{h_{j}}\left(z_{k+1}-z\right) & z_{k}\le z\le z_{k+1}\\ 0 & z\ge z_{k+1}\end{cases}\qquad(8.12)$$

where ψ_k^i (i=1 and 2) are the local Lagrangian linear interpolation functions, with h_j is the thickness of the jth layer. By introducing $r=R_1+z$ and $\rho=R+r\cos\phi$ (*see Figure 8.1b*), the strain-displacement relations are as given as:

$$\begin{aligned}\varepsilon_{zz}&=\frac{\partial U}{\partial z}, & \gamma_{z\phi}&=\frac{1}{R_{1}+z}\frac{\partial U}{\partial\phi}+\frac{\partial V}{\partial z}-\frac{V}{R_{1}+z},\\ \varepsilon_{\phi\phi}&=\frac{U}{R_{1}+z}+\frac{1}{R_{1}+z}\frac{\partial V}{\partial\phi}, & \gamma_{z\theta}&=\frac{\partial W}{\partial z}+\frac{1}{\rho}\frac{\partial U}{\partial\theta}-\frac{W}{\rho}\cos\phi,\\ \varepsilon_{\theta\theta}&=\frac{1}{\rho}\left(U\cos\phi-V\sin\phi+\frac{\partial W}{\partial\theta}\right), & \gamma_{\phi\theta}&=\frac{1}{R_{1}+z}\frac{\partial W}{\partial\phi}+\frac{1}{\rho}\frac{\partial V}{\partial\theta}+\frac{W}{\rho}\sin\phi\end{aligned}\qquad(8.13)$$

The equilibrium equations of a thick composite curved tube with N numerical layers are obtained by employing Eq. (8.13) in the principle of minimum total potential energy [90], carrying out necessary integrations and employing the fundamental lemma of calculus of variations. The results are, in general, *3(N+1)* local equilibrium equations corresponding to *3(N+1)* unknown functions U_k, V_k and W_k and, in general, six global equilibrium equations for every order (n=0, 1, 2, 3,…) up to the nth order associated with the six parameters a_n, b_n, c_n,

d_n, e_n and f_n of the same order. The equilibrium equations of thick laminated composite curved tubes under bending moments up to the nth order are obtained as:

$$\delta U_k : N_z^k + M_\phi^k + M_\theta^k \cos\phi - \frac{dR_{z\phi}^k}{d\phi} = 0$$

$$\delta V_k : Q_\phi^k - R_{z\phi}^k + M_\theta^k \sin\phi - \frac{dM_\phi^k}{d\phi} = 0$$

$$\delta W_k : Q_\theta^k - R_\theta^k \cos\phi + R_{\phi\theta}^k \sin\phi - \frac{dM_{\phi\theta}^k}{d\phi} = \frac{4}{\pi}\frac{M}{R_1 + z}\Phi_k \qquad (k = 1,2,...,N+1) \tag{8.14}$$

$$\delta a_n : \int_{-\pi/4}^{\pi/4}\int_{-h/2}^{+h/2}\int_{-\pi}^{\pi} (\Theta 1)\,\mathrm{d}\phi\mathrm{d}z\mathrm{d}\theta = 0 \qquad \text{for } n = 0,1,2,3,... \tag{8.15a}$$

$$\delta b_n : \int_{-\pi/4}^{\pi/4}\int_{-h/2}^{+h/2}\int_{-\pi}^{\pi} (\Theta 2)\,\mathrm{d}\phi\mathrm{d}z\mathrm{d}\theta = 0 \qquad \text{for } n = 1,2,3,... \tag{8.15b}$$

$$\delta c_n : \int_{-\pi/4}^{\pi/4}\int_{-h/2}^{+h/2}\int_{-\pi}^{\pi} (\Theta 3)\,\mathrm{d}\phi\mathrm{d}z\mathrm{d}\theta = 0 \qquad \text{for } n = 1,2,3,... \tag{8.15c}$$

$$\delta d_n : \int_{-\pi/4}^{\pi/4}\int_{-h/2}^{+h/2}\int_{-\pi}^{\pi} (\Theta 4)\,\mathrm{d}\phi\mathrm{d}z\mathrm{d}\theta = 0 \qquad \text{for } n = 2,3,... \tag{8.15d}$$

$$\delta e_n : \int_{-\pi/4}^{\pi/4}\int_{-h/2}^{+h/2}\int_{-\pi}^{\pi} (\Theta 5)\,\mathrm{d}\phi\mathrm{d}z\mathrm{d}\theta = -\sqrt{2}\varepsilon^n M \left(R_1 + z\right)^{\bar{m}_n^{(k)}-1}\cos\left((n-1)\phi\right)$$

$$\text{for } n = 1,2,3,... \tag{8.15e}$$

$$\delta f_n : \int_{-\pi/4}^{\pi/4}\int_{-h/2}^{+h/2}\int_{-\pi}^{\pi} (\Theta 6)\,\mathrm{d}\phi\mathrm{d}z\mathrm{d}\theta = -\sqrt{2}\varepsilon^n M \left(R_1 + z\right)^{-\bar{m}_n^{(k)}-1}\cos\left((n-1)\phi\right)$$

$$\text{for } n = 1,2,3,... \tag{8.15f}$$

where the functions Θ1, Θ2, Θ3, Θ4, Θ5 and Θ6 in Eqs. (8.15) are defined in [118]. Note that M represents the bending moment applied at both ends of the composite curved tube as shown in Figure 8.1a. The generalized stress and moment resultants are defined as:

$$\left(N_z^k, Q_\theta^k, Q_\phi^k\right) = \int_{-h/2}^{+h/2}\left(\sigma_{zz}, \sigma_{\theta z}, \sigma_{z\phi}\right)\Phi_k'\, dz$$

$$\left(M_\theta^k, R_\theta^k, M_{z\phi}^k, R_{\phi\theta}^k\right) = \int_{-h/2}^{+h/2}\frac{1}{\rho}\left(\sigma_{\theta\theta}, \sigma_{\theta z}, \sigma_{z\phi}, \sigma_{\phi\theta}\right)\Phi_k\, dz$$

$$\left(M_\phi^k, M_{\phi\theta}^k, R_{z\phi}^k\right) = \int_{-h/2}^{+h/2}\frac{1}{R_1 + z}\left(\sigma_{\phi\phi}, \sigma_{\phi\theta}, \sigma_{z\phi}\right)\Phi_k\, dz \tag{8.16}$$

Note that the numbers of the global equilibrium equations, Eqs. (8.15), depend on the numbers of unknown constants are employed in Eq. (8.11) to develop the displacement field for laminated composite curved tubes. Based on the detailed derivation in [99], there are one unknown constant for the zeroth order (i.e., a_0), five unknown constants for the 1st order (i.e., a_1, b_1, c_1, e_1 and f_1) and six unknown constants for the nth order (n=2, 3,…) (i.e., a_n, b_n, c_n, d_n, e_n and f_n). Table 8.1 presents unknown constants and corresponding global equilibrium equations, which are used to calculate them.

Table 8.1: Unknowns and equations.

Type	Unknown constants	Equation number
The zeroth order	a_0 of the zeroth order	Eq. (8.15a) for $n=0$
Up to the 1st order	a_0 of the zeroth order	Eq. (8.15a) for $n=0$
	a_1, b_1, c_1, e_1 and f_1 of the first order	Eqs. (8.15a), (8.15b), (8.15c), (8.15e) and (8.15f) for $n=1$
Up to the 2nd order	a_0 of the zeroth order	Eq. (8.15a) for $n=0$
	a_1, b_1, c_1, e_1 and f_1 of the first order	Eqs. (8.15a), (8.15b), (8.15c), (8.15e) and (8.15f) for $n=1$
	a_2, b_2, c_2, d_2, e_2 and f_2 of the 2nd order	Eqs. (8.15a), (8.15b), (8.15c), (8.15d), (8.15e) and (15f) for $n=2$
Up to the nth order	a_0 of the zeroth order	Eq. (8.15a) for $n=0$
	a_1, b_1, c_1, e_1 and f_1 of the first order	Eqs. (8.15a), (8.15b), (8.15c), (8.15e) and (8.15f) for $n=1$
	a_n, b_n, c_n, d_n, e_n and f_n of the nth orders n=2, 3, …	Eqs. (8.15a), (8.15b), (15c), (8.15d), (8.15e) and (8.15f) for $n=2, 3,$ ...

The following boundary conditions must be satisfied on the free inner and outer curved surfaces:

$$R_\theta^k = Q_x^k = N_z^k = 0 \qquad \text{at}\left(z=\pm h/2\right) \qquad \left(k=1,2,...,N+1\right) \qquad (8.17)$$

Note that in Eq. (8.17) the superscript k refers to the kth interface in the laminated composite curved tube. By substituting the strain-displacement relations into three-dimensional constitutive law [90] and the subsequent results into Eq. (8.16), the stress resultants based on displacement components are obtained which are presented in [118]. The local displacement-based equilibrium equations are obtained by substituting Eqs. (8.16), the stress resultants based on displacement components, into Eqs. (8.14). In addition, the global equilibrium

equations of laminated composite curved tubes are expressed in terms of displacement functions by substituting the strain-displacement relations into three-dimensional constitutive law and the subsequent results into Eqs. (8.15).

8.4. Analytical Solution

The system of local displacement equilibrium equations (Eq. (8.14)) shows *3(N+1)* coupled ordinary differential equations with constant coefficients which may be displayed in a matrix form as:

$$[M]\{\eta''\}+[K_1]\{\eta'\}+[K_2]\{\eta\}=\{F\} \tag{8.18}$$

where

$$\{\eta\}=\left\{\{U\}^T,\{V\}^T,\{W\}^T\right\}^T$$
$$\{U\}=\{U_1,U_2,...,U_{N+1}\}^T,\qquad \{V\}=\{V_1,V_2,...,V_{N+1}\}^T,\qquad \{W\}=\{W_1,W_2,...,W_{N+1}\}^T \tag{8.19}$$

The coefficient matrices [M], [K_1], [K_2] and {F} in Eq. (8.18) are defined in [118]. It is confirmed that the general solution of Eq. (8.18) is presented as [100]:

$$\{\eta\}=[X_0]\left[\exp(\phi T_0)\right]\{k\}+$$
$$[X_0]\int_0^{\phi}\left(\begin{array}{l}\left[\exp\left(T_0(\phi-s)\right)\right][X_0]^{-1}\left[\exp\left(s\left([M]^{-1}[K_1]+[X_0][T_0][X_0]^{-1}\right)\right)\right]\\ \left(\{k\}+\int_0^{s}\left(\left[\exp\left(u\left([M]^{-1}[K_1]+[X_0][T_0][X_0]^{-1}\right)\right)\right][M]^{-1}\{F(u)\}\right)du\right)\end{array}\right)ds \tag{8.20}$$

where

$$[T_0]_{(N+1)\times(N+1)}=diag\left(T_1,T_2,...,T_{N+1}\right) \tag{8.21}$$

And T_i *(i=1, 2,..., N+1)* are Jordan blocks associated to the eigenvalues of matrix [Q] where

$$[Q]_{6(N+1)\times6(N+1)}=\begin{bmatrix}[0]_{3(N+1)\times3(N+1)} & [I]_{3(N+1)\times3(N+1)}\\ -[M]^{-1}[K_2] & -[M]^{-1}[K_1]\end{bmatrix} \tag{8.22}$$

In addition,

$$\left[X_0\right]_{3(N+1)\times 3(N+1)} = \left[X_1, X_2, ..., X_{N+1}\right] \qquad (8.23)$$

where X_i *(i=1, 2,..., N+1)* are co-solutions of $[X_i][T_i]^2+[M]^{-1}[K_1][X_i][T_i]+[M]^{-1}[K_2][X_i]=[0]$.

Vector {k} in Eq. (8.20) is unknown vector representing *3(N+1)* integration constants. The constants a_n, b_n, c_n, d_n, e_n and f_n must be calculated within the analysis through the following steps:

3. The boundary conditions in Eq. (8.17) are first imposed to calculate vector {k} in terms of the unknown constants a_n, b_n, c_n, d_n, e_n and f_n.
4. These constants are then obtained by the satisfaction of the global equilibrium conditions in Eqs. (8.15) as presented in Table 8.1.

8.5. FEM Analysis

The stress analysis of the thick composite curved tube is conducted by finite element method using ANSYS. Stress distributions are also generated to compare with the results obtained using the proposed method. The element used to perform the analysis is the layered solid element, SOLID 185. A rigid surface is modeled and glued to both end surfaces of the composite curved tube. Then, a bending moment is applied to the center node of the surface meshed using shell elements, SHELL 181. This is how the bending moment applied for the composite curved tube in FEM. The mesh-independency study is done for ANSYS (*see Table 8.2*). Mesh refining is performed two times while the element aspect ratio is kept constant. It is emphasized that for the initial mesh, Mesh Number 1, 3600 elements are used to model the structure. For Mesh Number 2, the thickness and circumferential directions are refined twice as much as the initial mesh. For Mesh Number 3, the axial and circumferential directions are refined twice as much as the initial mesh; and the thickness direction is refined 4 times as much as the initial mesh to model the curved tube (*see Table 8.2*).

Table 8.2: Mesh characteristics.

Mesh Number	Mesh size (Axial)×(Circumferential)×(Thickness)	Number of elements	Analyzing time (sec)
1	9×10×40	3600	1800
2	9×20×80	14400	4000
3	18×20×160	57600	6000

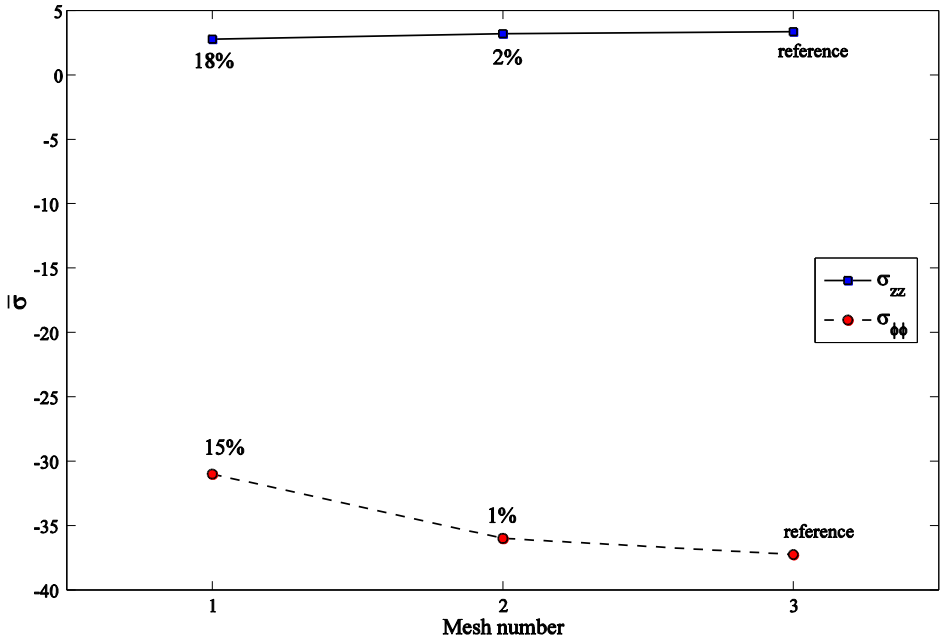

Figure 8.2: The mesh independency study of the laminated composite curved tube.

The stress components are normalized as $\bar{\sigma}_{ij}=\sigma_{ij}/\sigma_0$ where $\sigma_0=(M.r)/(\pi/64*(OD^4-ID^4))$ where the outer diameter and the inner diameter of the composite curved tube are presented as *OD* and *ID*, respectively. Figure 8.2 presents the radial and hoop stresses obtained using ANSYS for different mesh numbers mentioned in Table 8.2. As Figure 8.2b shows, the differences of stresses for Mesh Numbers 2 and 3 are less than 2%, therefore, Mesh Number 2 is selected to obtain the results using FEM to compare with the theoretical results. Mesh Number 2 is named as the final mesh in the following sections.

8.6. Lay-up Sequences for the Parametric Study

Derisi [1] developed a lay-up sequence used for making straight tubes in helicopter composite landing gears that may provide large deformation and gradual fracture. Composite

straight tubes with the $[90°_{20}/0°_{20}]$ and $[90°_{30}/\pm25°_{45}/90°_{5}/\pm30°_{20}/90°_{5}/\pm45°_{20}]$ lay-up sequences were manufactured and four-point bending tests were performed. Table 8.3 shows two types of lay-up sequences considered here. The lay-up sequence of the $[90°_{20}/0°_{20}]$ composite curved tube is selected to compare the numerical results obtained using the proposed method with finite element method (ANSYS) and experimental data for the composite straight tube subjected to pure bending moment. The $[90°_{30}/\pm\alpha°_{45}/90°_{5}/\pm\alpha°_{20}/90°_{5}/\pm45°_{20}]$ lay-up, a systematic variation of the lay-up sequence, is selected in order to obtain generic knowledge from effects of lay-up sequences as presented in Table 8.3. The 90°-plies are placed at the innermost layer to resist the hoop stress. The ±45°-plies, placed as a jacket at the outermost layer to provide large deformation, are necessary in lay-up sequences for composite helicopter landing gears. In addition, thin 90°-plies are placed between the layers to help connecting layers in the lay-up sequence to provide large deformation in the composite tube [1]. The latter is one of techniques, which addresses the composite toughness. Subsequently, thick $[90°_{30}/\pm\alpha°_{45}/90°_{5}/\pm\alpha°_{20}/90°_{5}/\pm45°_{20}]$ laminated composite curved tubes are examined where α having the values of 0°, 25°, 30°, 45° and 60°. Note that the ±α° layer-groups are the main layers responsible for flexural and extensional stiffness of this specific thick composite curved tube.

Table 8.3: Lay-up sequence number.

Laminate number	Application	Lay-up sequence
1	Comparison with FEM and experimental data	$[90°_{20}/0°_{20}]$
2	Parametric study	$[90°_{30}/\pm\alpha°_{45}/90°_{5}/\pm\alpha°_{20}/90°_{5}/\pm45°_{20}]$ α=0°, 25°, 30°, 45° and 60°

8.7. Results and Discussion

All physical plies are assumed to have equal thickness (=0.1 mm [1]) and are modeled as being made up of *p* numerical layers. In all the subsequent calculations, *p* is set equal to 12 [118]. The mechanical properties of the composite curved tube are given in Table 8.4 [1]. In addition, a thick laminated composite curved tube spanning a curved segment of 90° with *R/a=10* is considered (unless otherwise mentioned). In the present cases, the thick laminated composite curved tube sections with the $[90°_{30}/\pm\alpha°_{45}/90°_{5}/\pm\alpha°_{20}/90°_{5}/\pm45°_{20}]$ lay-up sequence

have an internal diameter of 56 mm and an external diameter of 98 mm, i.e. a wall thickness of 21 mm (totally 210 layers). The results are presented based on the proposed method at $\theta=0°$ (*see Figure 8.1*). Since the radial stress affects delamination and the hoop stress affects buckling, interlaminar radial and hoop stress distributions are investigated.

Table 8.4: Mechanical properties of the composite curved tube.

Mechanical properties	Value
E_{11}	140 (GPa)
$E_{22}=E_{33}$	10 (GPa)
$G_{12}= G_{13}= G_{23}$	5.56 (GPa)
$\upsilon_{12}=\upsilon_{13}$	0.31
υ_{23}	0.33

8.7.1. Verifying the Proposed method

The proposed method is compared and verified with FEM and experimental data. First, in Section 8.7.1.1, the results are compared for the composite curved tube using the developed method with FEM. In addition, the convergence study for the developed method is performed. Then, in Section 8.7.1.2, the verification is done with the experimental data for the case of the composite straight tube.

8.7.1.1. Comparison of the Proposed Method for Laminated Curved tubes with FEM

Here, the results obtained for a laminated composite curved tube using the developed method are compared with results obtained using FEM (ANSYS) based on the final mesh. To ensure the verifications are done in all layers of the laminated composite curved tube, the comparison must be performed by using the developed method and FEM (ANSYS) based on the final mesh along tube thickness. Figure 8.3 presents the comparison of the interlaminar radial stress, $\bar{\sigma}_{zz}$, of the $[90°_{20}/0°_{20}]$ laminated composite curved tube at $\phi=270°$ along the tube thickness based on the present method and ANSYS based on the final mesh. There is a good agreement seen along tube thickness between the theoretical analysis and FEM (ANSYS) results based on the final mesh. The analyzing of the thick composite curved tube using ANSYS based on the initial mesh, Mesh Number 1, takes around 1800 seconds while it takes around 4000 and 6000 seconds for Mesh Numbers 2 and 3, respectively, while the analyzing

of the same structure (*same lay-up*) based on the developed method considering up to the 3rd order takes 310 seconds.

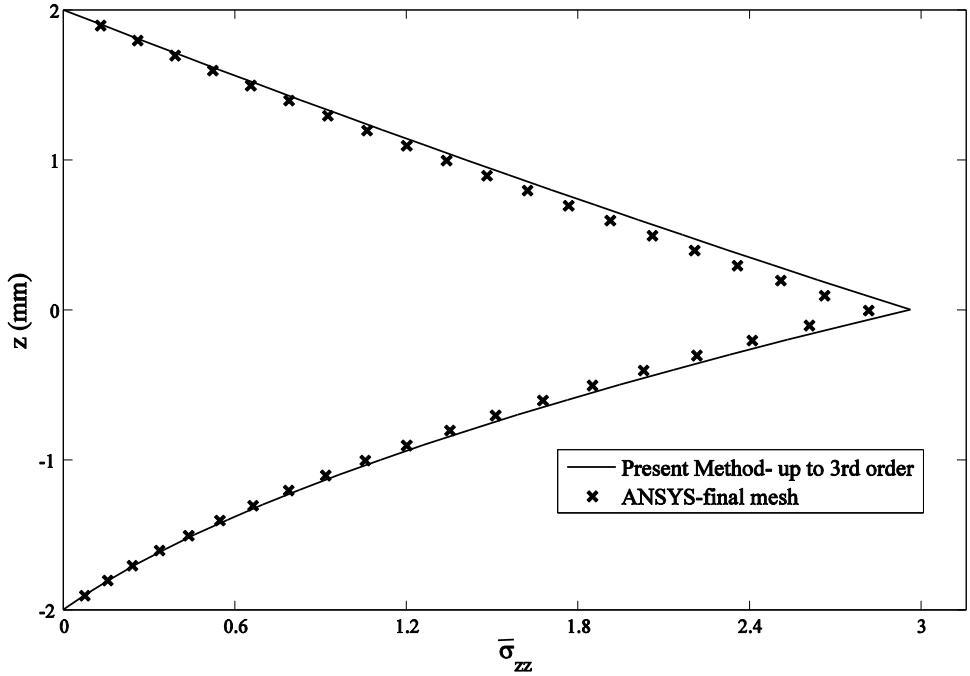

Figure 8.3: Comparison of the interlaminar radial stress, $\bar{\sigma}_{zz}$, obtained using the present method and ANSYS of the $[90°_{20}/0°_{20}]$ laminated curved tubes at ϕ=270° along tube thickness.

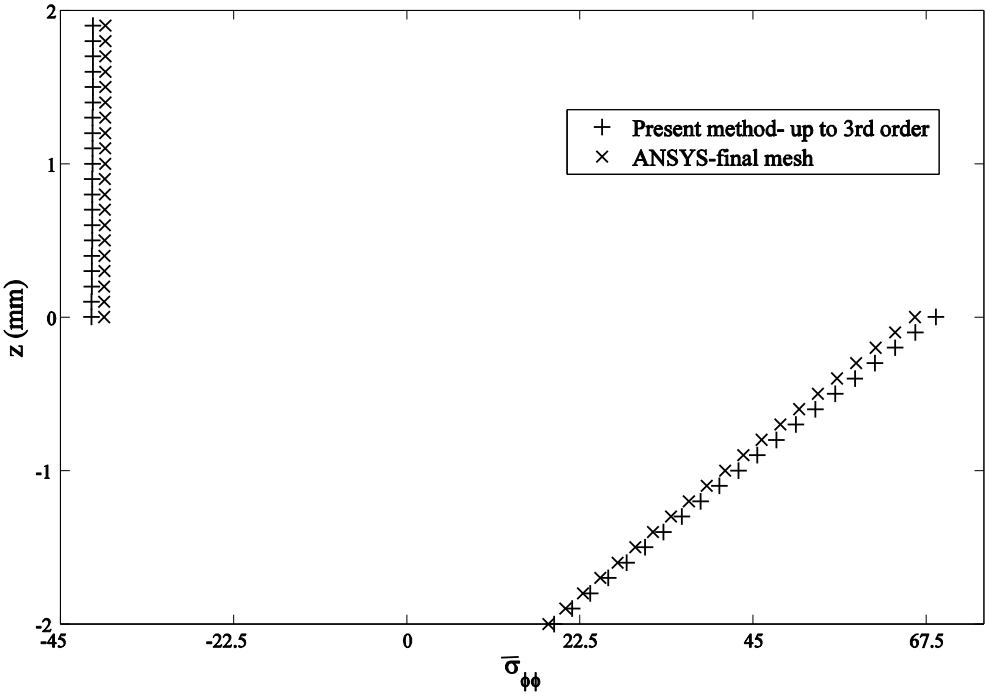

Figure 8.4: Comparison of the hoop stresses, $\bar{\sigma}_{\phi\phi}$, obtained using the present method and ANSYS of the $[90°_{20}/0°_{20}]$ laminated curved tube at ϕ=90° along tube thickness.

Comparison of the hoop stress, $\bar{\sigma}_{\phi\phi}$, of the $[90°_{20}/0°_{20}]$ laminated composite curved tube at ϕ=90° along tube thickness using the developed method and FEM based on the final mesh is shown in Figure 8.4. The final mesh used in FEM to obtain results makes a good agreement along the tube thickness. Note that the 0° layer-group experiences a compressive stress while the hoop stress of the 90° layer-group (in the inner surface of the curved tube) is tensile.

8.7.1.2. Comparison of the Proposed Method with Experimental Data

In this section, the proposed method results are validated against the experimental data. The bending behavior of thick composite straight tubes was investigated experimentally [1]. The thick $[90°_{20}/0°_{20}]$ thermoplastic composite straight tubes were manufactured using automated fiber placement technique and tested using a four-point bending test setup. The properties of the manufactured composite tube are given in Table 8.4. In the experimental investigation [1], the strain gage was used at the top line of the composite straight tube (ϕ=90°) to measure strains at the mid-span. A composite straight tube is modeled using the present method by assuming the bend radius R to be very large compared to r, so that a curved tube will be close to a straight tube. Since the experimental strains are measured at mid-span of the straight tube, the theoretical strains are obtained based on the proposed method at θ=0° of the curved tube, for the comparison purpose. The measured strain results are compared with the calculated strain results using the proposed method at ϕ=270°. In Figure 8.5, the force variation versus experimental axial strains is shown. The theoretical analysis results in good agreement with the observations from the experiment done in the reference [1]. As Figure 8.5 shows, the theoretical results are getting closer to experimental results with increasing R/a, while the shape of the curved tube is getting closer to the straight tube.

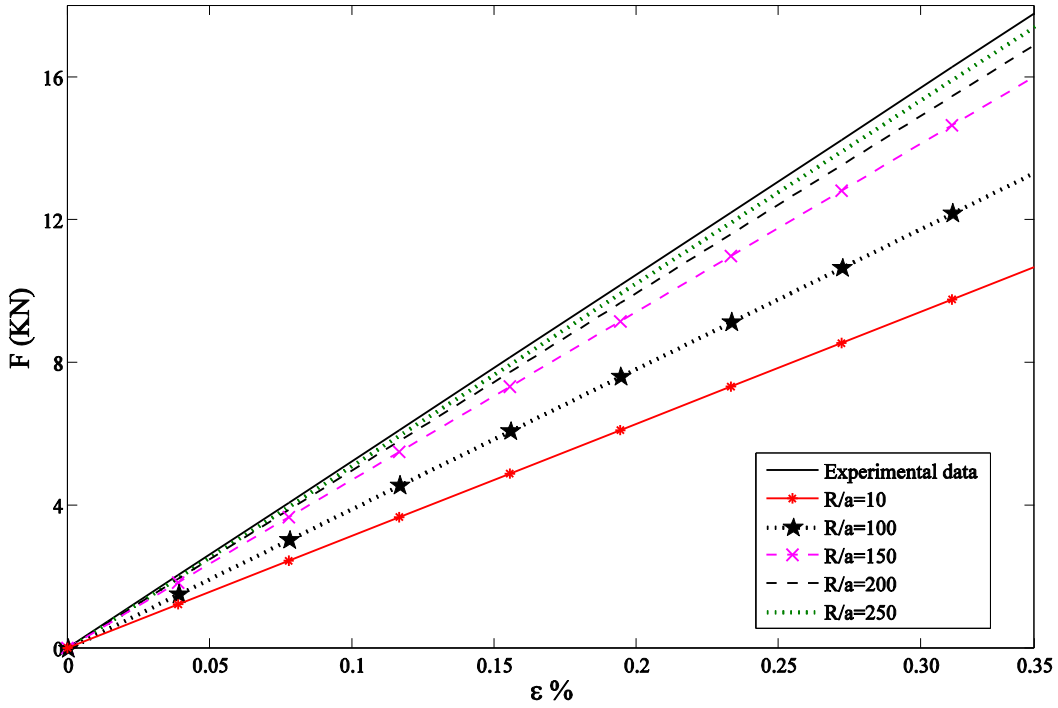

Figure 8.5: Load-axial strain at the mid-span.

8.7.2. Effects of Lay-up Sequences on Stress Distributions

The thick $[90°_{30}/\pm\alpha°_{45}/90°_{5}/\pm\alpha°_{20}/90°_{5}/\pm45°_{20}]$ laminated composite curved tubes with considering α=0°, 25°, 30°, 45° and 60° which have 210 layers in total are selected to study stress distributions of the composite curved tube subjected to pure bending moment. The results are presented based on the proposed method.

Figure 8.6 presents the comparison of the interlaminar radial stress, $\bar{\sigma}_{zz}$, of the $[90°_{30}/\pm\alpha°_{45}/90°_{5}/\pm\alpha°_{20}/90°_{5}/\pm45°_{20}]$ (for α=0°, 25°, 30°, 45° and 60°) laminated composite curved tubes subjected to pure bending moment at ϕ=90° along the tube thickness. The followings are observed:

- The magnitude of the radial stress, $\bar{\sigma}_{zz}$, of the $[90°_{30}/\pm45°_{45}/90°_{5}/\pm45°_{20}/90°_{5}/\pm45°_{20}]$ composite curved tube is greater than those of the others are. It is observed that the maximum magnitude of the radial stress of different lay-up sequences occurs at *z=-0.3 mm* which is the last ply from the first 90° layer-group from the inside surface (*i.e., layer 30*). Therefore, these layers tend to separate from the ±α° layer-group, with the largest

possibility. Derisi [21] observed the same phenomena during the experimental tests for a composite straight tube with the same lay-up sequence.

- The radial stress, $\bar{\sigma}_{zz}$, of all composite curved tubes are compressive at ϕ=90° of the cross section. The maximum positive value of $\bar{\sigma}_{zz}$ of the $[90°_{30}/\pm\alpha°_{45}/90°_{5}/\pm\alpha°_{20}/90°_{5}/\pm45°_{20}]$ composite curved tube occurs at ϕ=270° (compression zone). Note that the positive radial stress could cause delamination failure in composite tubes.
- Radial stresses have the same trend for all lay-up sequences.
- The location of the maximum magnitude of the interlaminar radial stress of the thick $[90°_{30}/\pm\alpha°_{45}/90°_{5}/\pm\alpha°_{20}/90°_{5}/\pm45°_{20}]$ laminated composite curved tubes is investigated. Locally, it occurs at the end of 90° layer-group while globally, it occurs at the last ply of the innermost 90° layer-group.
- The interlaminar radial stress is zero at the inside and outside surfaces of the composite curved tube.

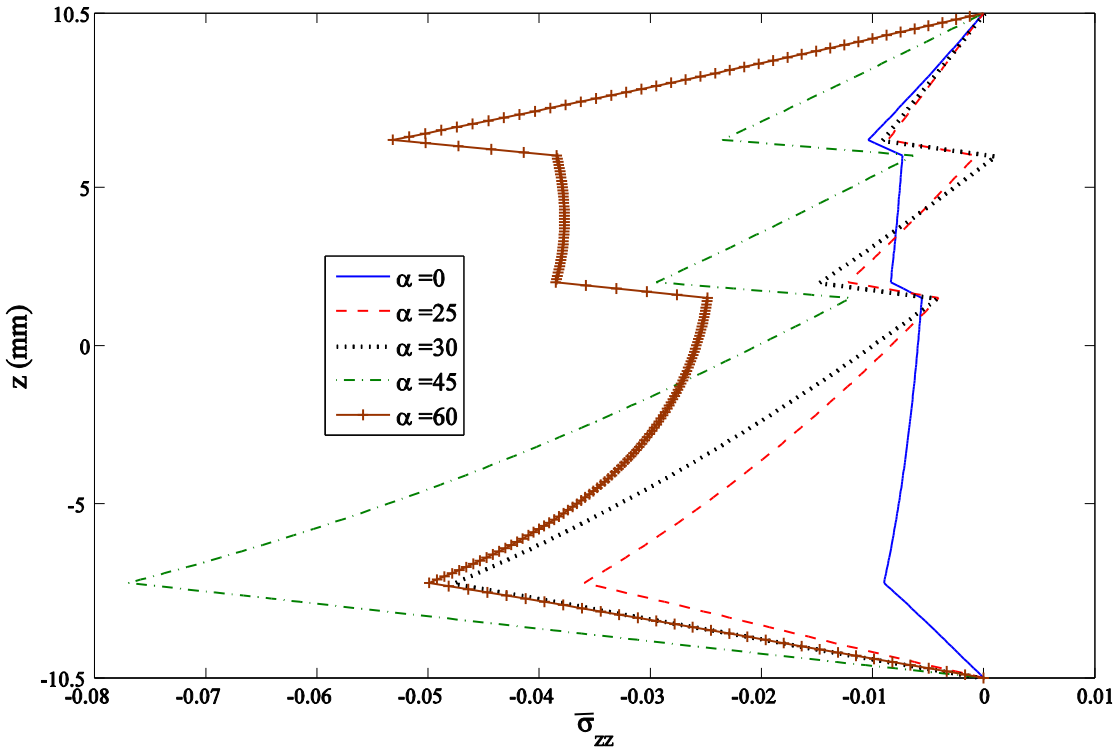

Figure 8.6: Comparison of the radial stress, σ_{zz}, of the $[90°_{30}/\pm\alpha°_{45}/90°_{5}/\pm\alpha°_{20}/90°_{5}/\pm45°_{20}]$ laminated composite curved tubes for α=0°, 25°, 30°, 45° and 60° at ϕ=90° along the curved tube thickness.

Comparison of the hoop stress, $\bar{\sigma}_{\phi\phi}$, of the $[90°_{30}/\pm\alpha°_{45}/90°_5/\pm\alpha°_{20}/90°_5/\pm45°_{20}]$ (for α=0°, 25°, 30° and 45°) laminated composite curved tubes subjected to pure bending moment at ϕ=90° along the tube thickness is shown in Figure 8.7. The followings are observed:

- Fibers with orientation angles closer to 90° carry more the circumferential direction load.
- The hoop stress, $\bar{\sigma}_{\phi\phi}$, of the 90° layer-group of the $[90°_{30}/\pm0°_{45}/90°_5/\pm0°_{20}/90°_5/\pm45°_{20}]$ composite curved tube is greater than those of the other lay-up sequences; because the 0°-plies have less contributions in resisting the hoop stress.
- The 0°-plies contribute little to the support of the hoop stress, $\bar{\sigma}_{\phi\phi}$.

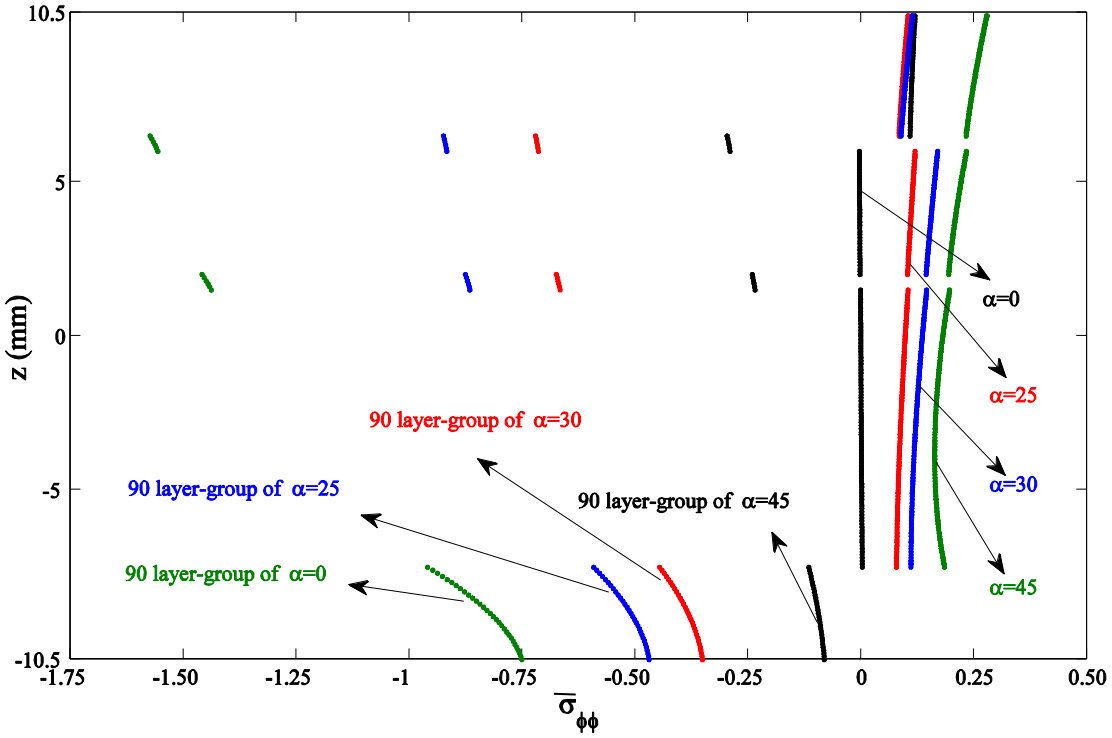

Figure 8.7: Comparison of the hoop stress, $\bar{\sigma}_{\phi\phi}$, of the $[90°_{30}/\pm\alpha°_{45}/90°_5/\pm\alpha°_{20}/90°_5/\pm45°_{20}]$ laminated composite curved tubes for α=0°, 25°, 30° and 45° at ϕ=90° along the curved tube thickness.

- The maximum positive of the hoop stress in the $[90°_{30}/\pm\alpha°_{45}/90°_5/\pm\alpha°_{20}/90°_5/\pm45°_{20}]$ laminated composite curved tubes occurs at the outside surface while the maximum negative of the hoop stress occurs at the largest-diameter 90°-ply from the innermost 90° layer-group.

- The magnitude of the hoop stress, $\bar{\sigma}_{\phi\phi}$, of the 45° layer-group of the $[90°_{30}/\pm\alpha°_{45}/90°_{5}/\pm\alpha°_{20}/90°_{5}/\pm45°_{20}]$ laminated composite curved tube (for α=0°, 25°, 30° and 45°) is greater than those of the other ±α° layer-groups. This is explained by the fact that for composite curved tubes, 90° layers play the roles that enhance the hoop strength of a tube. Layers with the fiber orientation closer to 90° would bear more loads, and as such would have the higher hoop stress.

8.7.3. Effects of Lay-up Sequences on Failure

In this section, failure analysis of the aforementioned tube is performed with investigating failure locations, failure sequences and failure modes. Following obtaining stress distributions in the composite tube by employing the proposed method, progressive failure analysis using Tsai-Wu criterion is done subsequently to find out the maximum bending moment and failure sequence of the thick laminated composite curved tube up to the final failure. This analysis shows the ability of the developed method to represent a low computational-cost method for failure analyzing thick composite curved structures.

8.7.3.1. Procedure for the Failure Analysis

The procedure used to determine the ultimate bending moment and failure sequence is as follows:

1. Use the developed method to find the local stresses in each ply under the assumed bending moment.
2. Compare the stresses of each ply of the lay-up sequence with the failure criterion.
3. Once failure is predicted, the elastic properties of that ply are degraded before the analysis is resumed as follows:

$$[E_{11}, E_{22}, G_{ij}, \nu_{12}, \nu_{23}] \rightarrow [0.01E_{11}, 0.01E_{22}, 0.01G_{ij}, 0.01\nu_{12}, 0.01\nu_{23}]$$

where E_{11}, E_{22}, G_{ij} and ν_{ij} are the longitudinal modulus, transverse modulus, shear modulus and Poisson's ratio, respectively.

4. Use again the developed method to find the local stresses under the same assumed bending moment to re-check the failure for each ply.
5. Apply the incremental bending moment and go to step 1.

6. Continue the above steps with the reduced properties until all plies in the laminated composite curved tube have failed. The maximum bending moment where all plies of the lay-up sequence have failed is called the ultimate bending moment for the composite tube.

Note that the properties of the materials are defined in Table 8.5 [1]. A parametric study is performed to examine effects of lay-up sequences on the maximum bending moment of the thick laminated composite curved tubes.

Table 8.5: Mechanical properties of Carbon AS4/PEKK.

Material properties	Value
0° Tension strength	2.42 (GPa)
90° Tension strength	0.044 (GPa)
0° Compression strength	1.561 (GPa)
90° Compression strength	0.24 (GPa)
Interlaminar shear strength	0.1 (GPa)
In-plane shear strength	0.175 (GPa)

8.7.3.2. Prediction of the Failure Sequence

Figure 8.8 presents the cross section of the thick laminated composite curved tube. The failure sequence in different layers of the $[90°_{30}/\pm\alpha°_{45}/90°_{5}/\pm\alpha°_{20}/90°_{5}/\pm45°_{20}]$ composite curved tube based on the developed method using the mentioned failure procedure is shown by locations 1 to 6 in Figure 8.8. The failure starts in the lower part (*i.e.,* ϕ=270°) of the composite curved tube where is under the tensile interlaminar radial stress and then jumps to the upper part (*i.e.,* ϕ=90°) of the composite curved tube where is subjected to the compressive interlaminar radial stress. The detailed failure sequences are explained as follow:

1. 90º-plies are expected to fail first since these layers have minimum bending stiffness in the bending loading condition. There are three 90º layer-groups in the lay-up sequence. As the bending moment increases, the stress at the lower part of $90°_5$ layers, indicated with location 1, exceeds the failure criterion of 90º layers, and this layer fails.
2. Further increase in the bending moment will cause the stress in other two 90º layer-groups (*i.e.,* $90°_5$ and $90°_{30}$ layers) to overpass from the failure criterion of 90º layers. Therefore, the subsequent failed layers are shown in Figure 8.8 by locations 2 and 3.

3. At higher bending moment levels, the ±α° layer-groups in the upper part (*i.e.,* ϕ=90°) of the composite curved tube would fail due to their lower strength in compression than in tension since they are subjected to the compressive interlaminar radial stress. The failure starts from the $\pm\alpha^{\circ}_{20}$ layers where are at further distance from the centroid and carry higher load. The failure sequence in ±α° layer-groups is shown in Figure 8.8 by locations 4 and 5.
4. At this point, the $\pm45^{\circ}_{20}$ layers still are able to keep the integrity of the composite curved tube. As the bending moment increases, the $\pm45^{\circ}_{20}$ layers would also fail due to shear and normal stresses indicated with location 6 in Figure 8.8. At this point, it is expected that the composite curved tube would totally fail. The final failure is in compression.

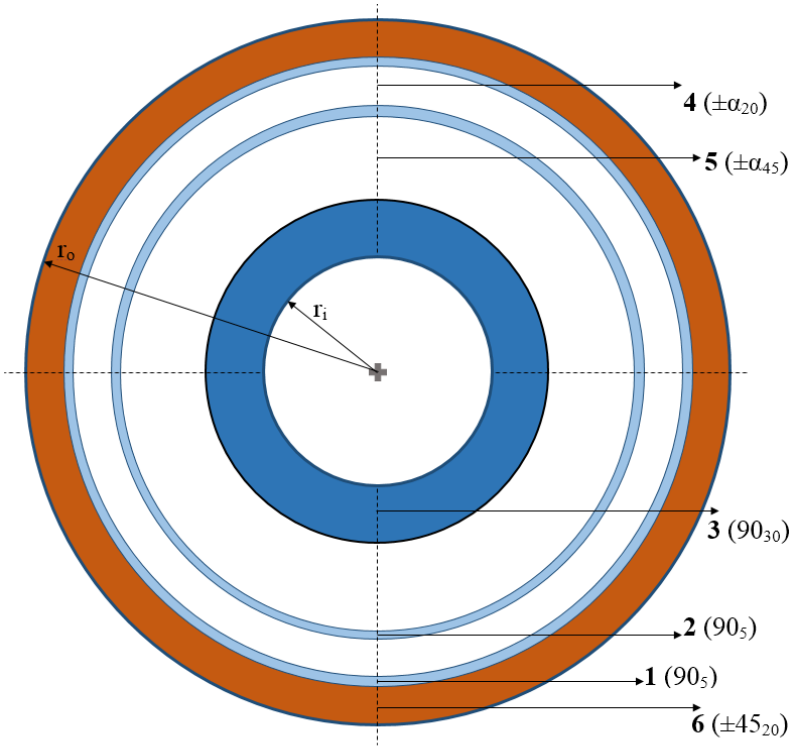

$[90^{\circ}_{30}/\pm\alpha^{\circ}_{45}/90^{\circ}_{5}/\pm\alpha^{\circ}_{20}/90^{\circ}_{5}/\pm45^{\circ}_{20}]$

Figure 8.8: Cross section of the composite curved tube and its failure sequence from 1 to 6.

The proposed method and the progressive failure analysis are employed to predict the maximum bending moments presented in Table 8.6 for the different assumed lay-up sequences for thick laminated composite curved tubes. The thick $[90^{\circ}_{30}/\pm0^{\circ}_{45}/90^{\circ}_{5}/\pm0^{\circ}_{20}/90^{\circ}_{5}/\pm45^{\circ}_{20}]$ composite curved tube could carry the maximum bending moment of *50.2 kN.m* theoretically before the final failure. However, this composite curved

tube (*i.e.,* the composite curved tube with α=0° in the lay-up sequence) does not show the highest fracture strain in comparison with the other composite curved tubes.

Table 8.6: Effects of lay-up sequences on maximum bending moments.

Lay-up sequences of thick composite curved tubes	Maximum bending moment ($kN.m$)
$[90°_{30}/\pm0°_{45}/90°_{5}/\pm0°_{20}/90°_{5}/\pm45°_{20}]$	50.2
$[90°_{30}/\pm25°_{45}/90°_{5}/\pm25°_{20}/90°_{5}/\pm45°_{20}]$	38.6
$[90°_{30}/\pm30°_{45}/90°_{5}/\pm30°_{20}/90°_{5}/\pm45°_{20}]$	35.2
$[90°_{30}/\pm45°_{45}/90°_{5}/\pm45°_{20}/90°_{5}/\pm45°_{20}]$	30.8
$[90°_{30}/\pm60°_{45}/90°_{5}/\pm60°_{20}/90°_{5}/\pm45°_{20}]$	32.9

It is observed from Table 8.6 that with increasing α from 0° to 45° in the lay-up sequence, the maximum bending moment, which the composite curved tube can carry, decreases while with increasing α from 45° to 60°, the maximum bending moment increases. Note that fiber orientations in the lay-up sequences of thick composite tubes have different effects on the tube's strength and bending stiffness than in thin composite tubes. Consequently, thick composite tubes show different failure behavior compared to thin composite tubes. Thick composite tubes fail because of partial delamination of the outer layers while thin composite tubes fail due to buckling [119]. Although the inner layers of thick laminated composite curved tubes have lower bending stiffnesses, they play a significant role in tube strength. They are employed as stiffeners in the axial and hoop directions for the outer layers. This prevents buckling of the thick composite tubes subjected to bending moment. For thick composite curved tubes subjected to bending moment, the most important parameter is the longitudinal flexural stiffness and the ±α° layer-groups are the main layers responsible for this as mentioned. Therefore, the thick $[90°_{30}/\pm0°_{45}/90°_{5}/\pm0°_{20}/90°_{5}/\pm45°_{20}]$ composite curved tube, where α=0° in the lay-up sequence, can carry the higher bending moment up to failure compared to the other composite curved tubes (*i.e.,* α=25°, 30°, 45° or 60° in the lay-up sequence). Figure 8.9 presents the maximum bending moments versus the axial strains for the thick $[90°_{30}/\pm\alpha°_{45}/90°_{5}/\pm\alpha°_{20}/90°_{5}/\pm45°_{20}]$ laminated composite curved tubes (for α=0°, 25°, 30°, 45° and 60° in the lay-up sequence) at the mid-span of the curved tubes (*i.e.,* θ=0°, ϕ=90° and r=b). Note that the maximum bending moments of all composite curved tubes occur right

after failing the first ply in the lay-up sequences. It is seen from Figure 8.9 that with increasing α from 0° to 45°, the bending stiffness and strength of thick composite curved tubes decrease while with increasing α from 45° to 60°, the bending stiffness and strength increase. It is noted that with increasing the bending stiffness and strength, the deflections of the tubes decrease. Moreover, it is observed back from Figure 8.6 that the $[90°_{30}/\pm0°_{45}/90°_{5}/\pm0°_{20}/90°_{5}/\pm45°_{20}]$ composite curved tube has the minimum interlaminar radial stress in comparison with the other tubes. α=0° in the lay-up sequence makes the interlaminar strength of the composite curved tube increases. This can improve the resistance of thick composite curved tubes for delamination and subsequently, their bending moment capacities increase.

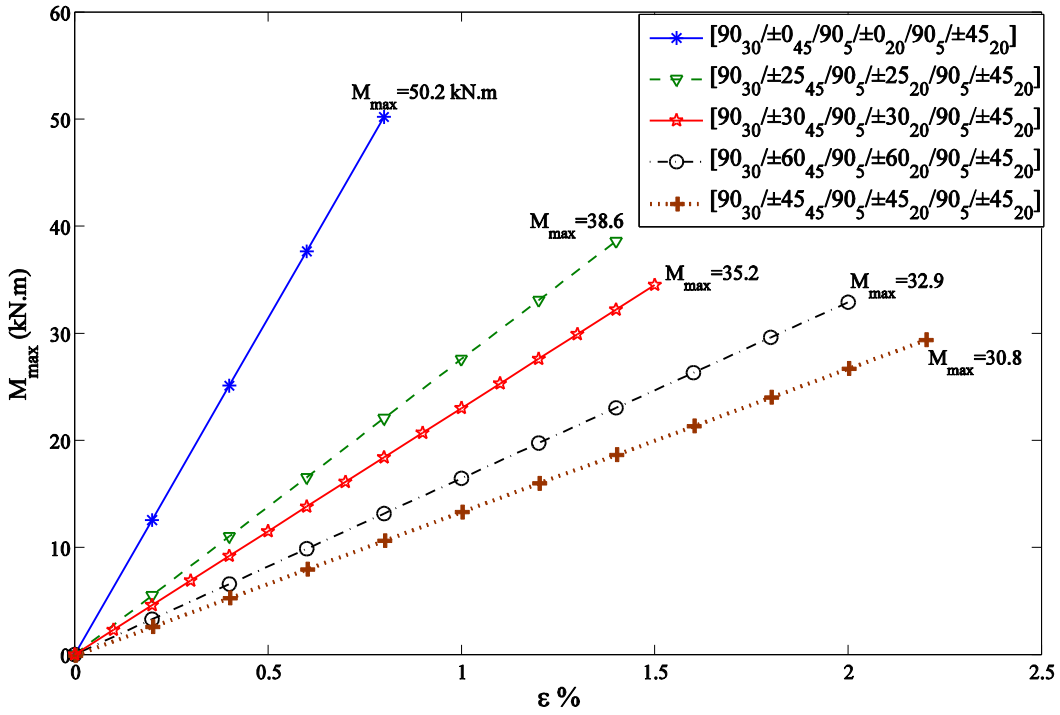

Figure 8.9: Maximum bending moment-axial strains at the mid-span of the composite curved tubes.

8.7.4. Observations

One of the composite toughening techniques is the lay-up sequence design. The lay-up sequence design for a composite tube is dependent on its application and manufacturing method. The obtained preliminary design guidelines contain the following:

1. Medium angle-plies such as 45° or 60° enhance the hoop strength of laminated composite curved tubes.
2. Low angle-plies such as 25° or 30° are extremely stiffer than medium angle-plies such as 45° or 60° along the fiber direction. Low angle-plies could help 0°-plies to be responsible for flexural and extensional stiffnesses of composite curved tubes. They increase load carrying capacity of composite tubes. Even at some points, they could be used as substitutes for 0°-plies.
3. The lay-up sequence of composite curved tubes could be affected by the necessity to maximize one or the other major bending stiffnesses, depending on loading directions and applications. However, the buckling resistance is maximized in most cases by placing the ±45°-plies on the outer surface. In addition, ±45°-plies in lay-up sequences of composite tubes would keep the integrity of tubes, provide large deformation and restrict the movement of layers that failed due to compression stresses.
4. There should be a group-layer of 90°-plies in the lay-up sequence as a foundation for laying up of thick composite curved tubes in order to improve the hoop and radial resistances.
5. Using 0°, 25° and 30°-plies in a lay-up sequence is improved the delamination resistance of thick composite curved tubes in comparison with using 45° and 60°-plies in the lay-up sequence.
6. Positive interlaminar stresses could cause delamination at composite curved tubes. One of interlaminar stresses is the radial stress where is positive at the compression zone of tube cross section. The location of the maximum interlaminar radial stress of different lay-up sequences along curved tube thickness occurs at the end of the largest 90° layer-group of the lay-up sequence.
7. Considering thick $[90°_{30}/\pm\alpha°_{45}/90°_{5}/\pm\alpha°_{20}/90°_{5}/\pm45°_{20}]$ composite curved tubes, with increasing α from 0°, the bending stiffness and strength of thick composite curved tubes decrease while the deflection of thick composite curved tubes under the loading condition increases. In addition, failure behavior becomes more gradual.
8. Thick composite curved tubes show different failure behavior compared to thin composite curved tubes. Moreover, failure behavior depends on the fiber orientation and lay-up sequence of thick laminated composite curved tubes.

8.8. Conclusion

With the focus on developing fast and computationally cost efficient methods, *e.g.* for thick composite structures, simple-input methods are becoming more important than FEM. The displacement-based approaches were used to study stresses and failure behavior in thick laminated composite curved tubes subjected to pure bending moment. The most general form of the displacement field of thick laminated composite curved tubes was derived using Toroidal Elasticity (TE) and layer-wise method. The accuracy of the results was examined by comparing the experimental results with those of the proposed method. The numerical results showed good agreement between the present method with the experimental results and FEM. A progressive failure analysis using Tsai-Wu criterion based on the results of the proposed method was done to obtain maximum bending moments, which thick composite curved tubes can carry up to the final failure. Effects of lay-up sequences on stress distributions and failure behavior were investigated. The key advantage of the developed method is its suitability for parametric study, enabling simple-inputs and being fast to run. In addition, the developed method proved the potential to perform failure analysis instead of using FEM especially for thick composite curved tubes with complex lay-up sequences.

Chapter 9

Conclusions, Contributions and Future works

9.1. Conclusions

Regarding the first part of this thesis, Chapters 3, 4 and 5, the following conclusions are summarized:

The displacement-based approach was developed to investigate stresses and strains in thick composite cantilever straight tubes subjected to transverse loading in Chapter 3. The most general form of the displacement field of thick laminated composite straight tubes was derived from the displacement-strain relations. Layer-wise method was then employed to analytically determine the displacement components. The equilibrium equations of composite straight tubes using layer-wise method were subsequently solved through a state-space approach. Moreover, the accuracy of stresses was assessed by comparing the results obtained from the proposed method with the experimental data. The numerical results showed good agreement between the present method with the experimental results, FEM and Lekhnitskii solution. Furthermore, the developed method was found to be more cost effective and accurate; therefore, it was employed to obtain stresses and strains instead of using FEM. In the numerical study, various thick composite tubes were studied to demonstrate the stress and strain distributions in the tube cross section. In addition, stresses and strains were investigated at different tube cross sections and for different applied transverse force values.

In Chapter 4, effects of lay-up sequences and orientations on stress distributions at tube cross sections in a thick composite straight tube under shearing load were studied. The lay-up sequences used to manufacture the straight part of helicopter landing gears were chosen to

study stress and strain distributions where were useful to develop practical design guidelines. The investigation was performed based on the new high-order simple-input displacement-based method developed in Chapter 3. The positive radial stress may cause delamination of some layers from the rest of the laminate. If such delamination occurs, the composite tube would fail prematurely by localized buckling. Since the radial stress affects delamination and the hoop stress affects buckling, the interlaminar radial and hoop stresses distributions were studied, in the majority of Chapter 4. In addition, locations for the maximum radial and hoop stresses in the thick laminated composite straight tube with different lay-up sequences were given.

In Chapter 5, the developed method was used to study thick laminated composite straight tubes subjected to axial force, torque and bending moment. The accuracy of the proposed method was verified by comparing the numerical results obtained using the proposed method with finite element method (FEM) and experimental data. The proposed method provided advantages in terms of computational time compared to FEM.

Regarding the second part of this thesis, Chapters 6, 7 and 8, conclusions are summarized as follows:

In Chapter 6, displacement-based Toroidal Elasticity, which was adapted for orthotropic materials, was proposed to address challenges within the study of stresses for single-layer composite curved tubes. The most general form of the displacement field in a composite curved tube with a single layer was derived using Toroidal Elasticity and successive approximation method. The contributions of different orders on stress distributions of composite curved tubes subjected to pure bending moments have been investigated. The accuracy of the results was examined by comparing the proposed method with FEM and Lekhnitskii solution. The numerical results showed good agreement. Furthermore, the present method could promise to be more cost effective and accurate; therefore, it is employed to obtain stresses instead of using FEM.

In Chapter 7, an investigation was performed on the study of thick laminated composite curved tubes by proposing the new displacement-based approach. The developed method was used to study stresses in thick composite curved tubes subjected to pure bending moment. The

most general form of the displacement field of thick laminated composite curved tubes was derived using displacement-based Toroidal Elasticity and layer-wise method. The accuracy of the results was verified by comparing the experimental and FEM results with those obtained from the proposed method. The numerical results showed good agreement between the present method with experimental results, FEM and a solution available in the literature. Furthermore, the developed method was found to be more precise in order to gain an in-depth and comprehensive understanding of the stress analysis of thick composite curved tubes; subsequently, it is employed to calculate stresses instead of using FEM.

Chapter 8 presented the failure analysis on thick laminated composite curved tubes subjected to pure bending moment by using the displacement-based method developed in Chapters 6 and 7. By employing the results of the proposed method, the progressive failure analysis was performed using Tsai-Wu criterion. In addition, effects of lay-up sequences of thick composite curved tubes on stress distributions and failure sequences were investigated.

9.2. Contributions

Each part of this thesis has produced contributions to knowledge, which all combine to allow for development of new practical methods to study the mechanical behavior of thick composite straight and curved tubes, which are structure can be found in helicopter landing gears. The contributions of this thesis are highlighted as follows:

1. The new high-order simple-input method has been proposed to analytically study the mechanical behavior of thick laminated composite straight tubes subjected to different types of mechanical loading conditions.
2. For the first time, the stress and strain fields of thick laminated composite straight tubes subjected to cantilever loading conditions have been developed.
3. The parametric study has been performed in order to provide some insight and knowledge into mechanical behavior of cantilever thick laminated composite straight tubes under shearing load. Systematic variations of lay-up sequences, orientations, number of layers and their effects on stress distributions have been examined at composite tube cross sections, for the purpose of design.

4. Formulations for locations of the maximum radial and hoop stresses within cantilever thick laminated composite straight tubes subjected to transverse loadings for different simple and complex lay-up sequences have been presented.
5. The developed simple-input method has been extended for analyzing thick laminated composite straight tubes subjected to different mechanical loadings such as axial force, torque and bending moment.
6. For the first time, a displacement-based Toroidal Elasticity has been adapted to analyze and design thick laminated composite curved tubes subjected to different types of mechanical loadings. The displacement field of single-layer composite curved tubes has been developed using a displacement-based Toroidal Elasticity and successive approximation method. The proposed displacement field has been employed to obtain stress distributions of single-layer composite curved tubes subjected to pure bending moments.
7. The displacement field of thick laminated composite curved tubes has been developed using displacement-based Toroidal Elasticity and layer-wise method. The proposed method is employed to study the mechanical behavior of thick composite curved tubes subjected to different loading conditions. In addition, stress distributions of thick laminated composite curved tubes under pure bending moments have been presented.
8. By using the proposed methods for composite straight and curved tubes, the more accurate solutions for structures have been obtained not only by using layer-wise method in the thickness direction (*i.e.,* the radial direction) as general case but also by using the theoretical approaches in other directions, including the longitudinal direction as well as the circumferential direction.
9. The failure analysis on thick laminated composite curved tubes subjected to pure bending moment has been conducted to provide the failure sequences in the cross section and study effects of lay-up sequences on failure behavior of thick composite curved tubes.

9.3. Future Works

As an extension to this research, the following future suggestions are recommended:

1. A method can be developed to do an analysis for the mechanical behavior of whole helicopter landing gears subjected to different mechanical loading conditions.

2. More experimental studies can be performed to assess theoretical studies on the behavior of entire and undivided helicopter landing gears under different mechanical loading conditions.
3. A dynamic analysis of thick laminated composite straight and curved tubes should be considered.
4. An analysis for helicopter landing gears under impact loading conditions should be conducted.
5. An optimization technique can be developed to propose proper lay-up sequences based on results of impact analyses.

9.4. List of Publications

1. H. Yazdani Sarvestani, S.V. Hoa, M. Hojjati. "Stress Analysis of Thick Orthotropic Cantilever Tubes under Transverse Loading". *Advanced Composite Materials,* 2016:1-28.
2. H. Yazdani Sarvestani, S.V. Hoa, M. Hojjati. "Effects of Shear Loading on Stress Distributions at Sections in Thick Composite Tubes". *Composite Structures,* 2016;140:433-445.
3. H. Yazdani Sarvestani, M. Hojjati. "A High-order Analytical Method for Thick Composite Tubes". *Steel & Composite Structures,* 2016;21(4):755-773.
4. H. Yazdani Sarvestani, M. Hojjati. "Effects of Lay-up Sequence in Thick Composite Tubes for Helicopter Landing Gears". *Journal of Aerospace Engineering: Proceedings of the Institution of Mechanical Engineers,* 2016.
5. H. Yazdani Sarvestani, S.V. Hoa, M. Hojjati. "Three-dimensional Stress Analysis of Orthotropic Curved Tubes-Part 1: Single-layer Solution". *European Journal of Mechanics-A/Solids,* 2016.
6. H. Yazdani Sarvestani, M. Hojjati. "Three-dimensional Stress Analysis of Orthotropic Curved Tubes-Part 2: Laminate Solution". *European Journal of Mechanics-A/Solids,* 2016.
7. H. Yazdani Sarvestani, M. Hojjati. "Failure Analysis of Thick Composite Curved Tubes". *Composite Structures,* 2016.

8. H. Yazdani Sarvestani, M. Hojjati. “Mechanical Behavior of Laminated Composite Curved Tubes”. *1st Int. Conference on Modern Research in Aerospace Engineering,* 2016.
9. H. Yazdani Sarvestani, S.V. Hoa, M. Hojjati. “Stress Analysis of an Orthotropic Cylindrical Beam under Shear Loadings”. *CANCOM 2015,* 2015.
10. H. Yazdani Sarvestani, S.V. Hoa, M. Hojjati. “Analysis of an Orthotropic Cylindrical Cantilever Beam under Transverse Loading”. *ICCS 18,* 2015.

REFERENCES

[1] B. Derisi, "Development of thermoplastic composite tubes for large deformation," PhD Thesis, Concordia University, Montreal, Canada, 2008.

[2] S. G. Lekhnitskii, Theory of elasticity of an anisotropic elastic body, San Francisco/Moscow: Holden Day/Mir Publishers, 1981.

[3] I. Sheinman, and S. Weissman, "Coupling between symmetric and antisymmetric modes in shells of revolution," *Journal Composite Materials,* vol. 21, no. 11, pp. 988-1007, 1987.

[4] L. Kollar, and G. S. Springer, "Stress analysis of anisotropic laminated cylinders and cylindrical segments," *International Journal of Solids and Structures,* vol. 29, no. 12, pp. 1499-1517, 1992.

[5] G. A. Kardomateas, "Buckling of thick orthotropic cylindrical shells under external pressure," *Journal of Applied Mechanics (ASME),* vol. 60, pp. 195-202, 1993.

[6] M. Miki, and Y. Sugiyama, "Optimum design of laminated composite plates using lamination parameters," *AIAA Journal,* vol. 31, no. 5, pp. 921-922, 1993.

[7] J. Ye, and K. P. Soldatos, "Three-dimensional stress analysis of orthotropic and cross-ply laminated hollow cylinders and cylindrical panels," *Computer Methods in Applied Mechanics and Engineering,* vol. 117, no. 3-4, pp. 331-351, 1994.

[8] N. N. Huang, "Influence of shear correction factors in the higher-order shear deformation laminated shell theory," *International Journal of Solids and Structures,* vol. 31, no. 9, pp. 1263-77, 1994.

[9] C. Jolicoeur, and A. Cardou, "Analytical solution for bending of coaxial orthotropic cylinders," *Journal of Engineering Mechanics,* vol. 120, no. 12, pp. 2556-2574, 1994.

[10] S. Di, and H. Rothert, "Solution of a laminated cylindrical shell using an unconstrained third-order theory," *Computers and Structures,* vol. 69, pp. 291-303, 1998.

[11] Y. Basar, and Y. Ding, "Interlaminar stress analysis of composites: layer-wise shell finite elements including transverse strains," *Composites Part B: Engineering,* vol. 5, no. 5, pp. 485-99, 1995.

[12] G. A. Kardomateas, "Benchmark three-dimensional elasticity solutions for the buckling of thick orthotropic cylindrical shells," *Composites Part B: Engineering,* vol. 278, pp. 569-580, 1996.

[13] B. Brank, and E. Carrera, "A family of shear-deformable shell finite elements for composite structures," *Computers and Structures,* vol. 76, no. 1-3, pp. 287-97, 2000.

[14] G. A. Kardomateas, "Elasticity solutions for a sandwich orthotropic cylindrical shell under external pressure, internal pressure and axial force," *AIAA Journal,* vol. 39, no. 4, pp. 713-719, 2001.

[15] R. K. Khare, T. Kant, and A. K. Garg, "Closed-form thermo-mechanical solutions of higher-order theories of cross-ply laminated shallow shells," *Computers and Structures,* vol. 59, pp. 313-40, 2003.

[16] J. H. Han, G. A. Kardomateas, and G. J. Simitses, "Elasticity, shell theory and finite element results for the buckling of long sandwich cylindrical shells under external pressure," *Composites Part B: Engineering,* vol. 35, no. 6, pp. 591-598, 2004.

[17] S. T. IJsselmuiden, M. M. Abdalla, and Z. Gurdal, "Implementation of strength based failure criteria in the lamination parameter design space," *AIAA Journal,* vol. 46, no. 9, pp. 1826-1834, 2008.

[18] N. Silvestre, "Non-classical effects in FRP composite tubes," *Composites Part B: Engineering,* vol. 40, no. 8, pp. 681-697, 2009.

[19] S. T. IJsselmuiden, M. M. Abdalla, O. Seresta, and Z. Gurdal, "Multi-step blended stacking sequence design of panel assemblies with buckling constraints," *Composites Part B: Engineering,* vol. 40, no. 4, pp. 329-336, 2009.

[20] B. Derisi, S. V. Hoa, D. Xu, M. Hojjati, and R. Fews, "Composite tube exhibiting large deformation under bending," *Journal of Composite Materials,* vol. 44, no. 16, pp. 2005-2020, 2010.

[21] B. Derisi, S. V. Hoa, D. Xu, M. Hojjati, and R. Fews, "Mechanical behavior of Carbon/ PEKK thermoplastic composite tube under bending load," *Journal of Thermoplastic Composite Materials,* vol. 24, no. 1, pp. 29-49, 2011.

[22] F. Shadmehri, B. Derisi, and S. V. Hoa, "On bending stiffness of composite tubes," *Composite Structures,* vol. 93, no. 9, pp. 2173-2179, 2011.

[23] L. Pickett, and V. Dayal, "Effect of tube geometry and ply-angle on energy absorption of a circular glass/epoxy crush tube-A numerical study," *Composites Part B: Engineering,* vol. 43, no. 8, pp. 2960-2967, 2012.

[24] C. Zhang, S. V. Hoa, and P. Liu, "A method to analyze the pure bending of tubes of cylindrically anisotropic layers with arbitrary angles including 0° or 90°," *Composite Structures,* vol. 109, pp. 57-67, 2014.

[25] X. S. Sun, V. B. C. Tan, Y. Chen, L. B. Tan, R. K. Jaiman, and T. E. Tay, "Stress analysis of multi-layered hollow anisotropic composite cylindrical structures using the homogenization method," *Acta Mechanica,* vol. 225, no. 6, pp. 1649-1672, 2014.

[26] M. Menshykova, and I. A. Guz, "Stress analysis of layered thick-walled composite pipes subjected to bending loading," *International Journal of Mechanical Sciences,* vol. 88, pp. 289-299, 2014.

[27] C. Capela, J. A. M. Ferreira, T. Febra, and J. D. Costa, "Fatigue strength of tubular carbon fiber composites under bending/torsion loading," *International Journal of Fatigue,* vol. 70, pp. 216-222, 2015.

[28] A. G. Arani, E. Haghparast, Z. K. Maraghi, and S. Amir, "Static stress analysis of carbon nano-tube reinforced composite (CNTRC) cylinder under non-axisymmetric thermo-mechanical loads and uniform electro-magnetic fields," *Composites Part B: Engineering,* vol. 68, pp. 136-145, 2015.

[29] T. Nowak, and J. Schmidt, "Theoretical, numerical and experimental analysis of thick walled fiber metal laminate tube under axisymmetric loads," *Composite Structures,* vol. 131, pp. 637-644, 2015.

[30] A. K. Jonnalagadda, A. S. Sawant, S. R. Rohde, B. V. Sankar, and P. G. Ifju, "An analytical model for composite tubes with bend-twist coupling," *Composite Structures,* vol. 131, pp. 578-584, 2015.

[31] J. Mackerle, "Finite elements in the analysis of pressure vessels and piping, an addendum: a bibliography (2001-2004)," *International Journal of Pressure Vessels and Piping,* vol. 82, pp. 571-592, 2005.

[32] R. L. Hinrichsen, and A. N. Palazotto, "Nonlinear finite element analysis of thick composite plates using a cubic spline function," *AIAA Journal,* vol. 24, no. 11, pp. 1836-1842, 1986.

[33] J. M. Hamdallah, and J. J. Engblom, "Finite element plate formulation including transverse shear effects for representing composite shell structures," *Journal of Reinforced Plastics and Composites,* vol. 9, no. 3, pp. 226-239, 1990.

[34] S. J. Hossain, "A finite element formulation for the analysis of laminated composite shells," *Computers and Structures,* vol. 82, no. 20-21, pp. 1623-38, 2004.

[35] G. Kress, R. Rooz, M. Barbezart, C. Dranfeld, and P. Ermanni, "Model for interlaminar normal stress in singly curved laminates," *Computers and Structures,* vol. 69, no. 4, pp. 458-69, 2005.

[36] C. M. C. Roque, and A. J. M. Ferreira, "New developments in the radial basis functions analysis of composite shells," *Composite Structures,* vol. 87, pp. 141-50, 2009.

[37] R. Salahifar, and M. Mohareb, "Finite element for cylindrical thin shells under harmonic forces," *Finite Elements in Analysis and Design,* vol. 52, pp. 83-92, 2012.

[38] C. Zhang, and S. V. Hoa, "A limit-based approach to the stress analysis of cylindrically orthotropic composite cylinders (0/90) subjected to pure bending," *Composite Structures,* vol. 94, no. 8, pp. 2610-2619, 2012.

[39] Y. Bai, W. Ruan, P. Cheng, B. Yu, and W. Xu, "Buckling of reinforced thermoplastic pipe (RTP) under combined bending and tension," *Ships and Offshore Structures,* vol. 9, no. 5, pp. 525-539, 2014.

[40] D. H. Roubins, and J. N. Reddy, "Modelling of thick composites using a layerwise laminate theory," *International Journal for Numerical Methods in Engineering,* vol. 36, pp. 655-677, 1993.

[41] S. Li, R. Wang, Z. Luo, and X. Hua, "An analytic solution for interlaminar stresses in a fiber reinforced double-layered circular cylindrical shell," *Acta Mechanica Sinica,* vol. 1, no. 2, pp. 352-64, 1985.

[42] X. Wang, and S. J. Li, "Analytic solution for interlaminar stresses in a multi laminated cylindrical shell under thermal and mechanical loads," *International Journal of Solids and Structures,* vol. 29, no. 10, pp. 1293-302, 1992.

[43] F. Fraternali, and J. N. Reddy, "A penalty model for the analysis of laminated composite shells," *International Journal of Solids and Structures,* vol. 30, no. 24, pp. 3337-55, 1993.

[44] M. Cho, and M-H. Kim, "A post process method using a displacement field of higher-order shell theory," *Computers and Structures,* vol. 34, no. 2, pp. 185-96, 1996.

[45] M. Cho, K-O. Kim, and M-H. Kim, "Efficient higher-order shell theory for laminated composites," *Computers and Structures,* vol. 34, no. 2, pp. 197-212, 1996.

[46] S. R. Rao, and N. Ganesan, "Interlaminar stresses in spherical shells," *Computers and Structures,* vol. 65, no. 4, pp. 575-83, 1997.

[47] C-Y. Lee, and C-H. Shu, "Layer reduction technique in the interlaminar shear stress analysis of laminated cylindrical shells," *Journal of the Chinese Society of Mechanical Engineers,* vol. 19, no. 4, pp. 433-439, 1998.

[48] C. P. Wu, and Y. W. Chi, "Asymptotic solutions of laminated composite shallow shells with various boundary conditions," *Acta Mechanica,* vol. 132, pp. 1-18, 1999.

[49] B. Brank, and E. Carrera, "A family of shear-deformable shell finite elements for composite structures," *Computers and Structures,* vol. 76, no. 1-3, pp. 287-97, 2000.

[50] R. Tanov, and A. Tabiei, "Adding transverse normal stresses to layered shell finite elements for the analysis of composite structures," *Computers and Structures,* vol. 76, no. 4, pp. 338-44, 2006.

[51] W. Zhen, and C. Wanji, "A global-local higher-order theory for multilayered shells and the analysis of laminated cylindrical shell panels," *Composite Structures,* vol. 84, pp. 350-61, 2008.

[52] H. Yazdani Sarvestani, and M. Yazdani Sarvestani, "Interlaminar stress analysis of general composite laminates," *International Journal of Mechanical Sciences,* vol. 53, no. 11, pp. 958-967, 2011.

[53] H. Yazdani Sarvestani, and M. Yazdani Sarvestani, "Free-edge stress analysis of general composite laminates under extension, torsion and bending," *Applied Mathematical Modelling,* vol. 36, no. 4, pp. 1570-1588, 2012.

[54] D. Mousanezhad V., H. Yazdani Sarvestani, and A. Nosier, "Stress analysis in symmetric composite laminates subjected to shearing loads," *International Journal of Mechanical Sciences,* vol. 75, pp. 16-25, 2013.

[55] M. S. Qatu, "Theories and analyses of thin and moderately thick laminated composite curved beams," *International Journal of Solids and Structures,* vol. 30, no. 20, pp. 2743-2756, 1993.

[56] C. Ossadzow, P. Muller, and M. Touratier, "A general doubly curved laminate shell theory," *Composite Structures,* vol. 32, no. 1-4, pp. 299-312, 1995.

[57] C. Zhang, L. B. Lessard, and J. A. Nemes, "A closed-form solution for stresses at curved free edges in composite laminates: A variational approach," *Composites Science and Technology,* vol. 57, no. 9-10, pp. 1341-1354, 1997.

[58] A. M. Yu, and G. H. Nie, "Explicit solutions for shearing and radial stresses in curved beams," *Mechanics Research Communications,* vol. 32, no. 3, pp. 323-331, 2005.

[59] J. Dryden, "Bending of inhomogeneous curved bars," *International Journal of Solids and Structures,* vol. 44, no. 11-12, pp. 4158-4166, 2007.

[60] A. S. Oktem, and R. A. Chaudhuri, "Fourier analysis of thick cross-ply Levy type clamped doubly-curved panels," *Composite Structures,* vol. 80, no. 4, pp. 489-503, 2007.

[61] R. Roos, G. Kress, M. Barbezat, and P. Ermanni, "Enhanced model for interlaminar normal stress in singly curved laminates," *Composite Structures,* vol. 80, no. 3, pp. 327-333, 2007.

[62] R. Roos, G. Kress, M. Barbezat, and P. Ermanni, "A post-processing method for interlaminar normal stresses in doubly curved laminates," *Composite Structures,* vol. 81, no. 3, pp. 463-470, 2007.

[63] M. T. Piovan, S. Domini, and J. M. Ramirez, "In-plane and out-of-plane dynamics and buckling of functionally graded circular curved beams," *Composite Structures,* vol. 94, no. 11, pp. 3194-3206, 2012.

[64] M. Hajianmaleki, and M. S. Qatu, "Static and vibration analyses of thick, generally laminated deep curved beams with different boundary conditions," *Composites Part B: Engineering,* vol. 43, no. 4, pp. 1767-1775, 2012.

[65] E. Arslan, and A. N. Eraslan, "Bending of graded curved bars at elastic limits and beyond," *International Journal of Solids and Structures,* vol. 50, no. 5, pp. 806-814, 2013.

[66] M. Wang, and Y. Liu, "Elasticity solutions for orthotropic functionally graded curved beams," *European Journal of Mechanics - A/Solids,* vol. 37, pp. 8-16, 2013.

[67] M. Z. Asik, E. Dural, M. Yetmez, and T. Uzhan, "A mathematical model for the behavior of laminated uniformly curved glass beams," *Composites Part B: Engineering,* vol. 58, pp. 593-604, 2014.

[68] M. Arefi, "Elastic solution of a curved beam made of functionally graded materials with different cross sections," *Steel and Composite Structures,* vol. 18, no. 3, pp. 659-672, 2015.

[69] V. R. Kar, and S. K. Panda, "Thermoelastic analysis of functionally graded doubly curved shell panels using nonlinear finite element method," *Composite Structures,* vol. 129, pp. 202-212, 2015.

[70] O. Gohner, "Schubspannungsverteilung im Querschnitt einer Schraubenfeder," *Archive of Applied Mechanics,* vol. 1, pp. 619-664, 1930.

[71] T. Von Karman, "Uber die Formanderung Dunnwandiger Rohre, insbesondere federnder Ausgleichsrochre," *VDI-Zeitdchriff,* vol. 55, 1911.

[72] A. Kornecki, "Stress distribution in a pressurized thick-walled toroidal shell- a three dimensional analysis," College of Aeronautics, Cranfield, England, Note 137, 1963.

[73] D. J. McGill, and I. H. Rapp, "Axismmetric stresses and displacements in thick-walled elastic torus," *Journal of the Engineering Mechanics Division,* vol. 99, no. 3, pp. 629-633, 1973.

[74] H. A. Lang, "The theory of toroidal elasticity," *International Journal of Structural Mechanics and Material Science,* vol. 26, pp. 289-357, 1989.

[75] H. A. Lang, "Stress analysis of pressurized elbow for nuclear components using toroidal elasticity," *Fourth International Conference on Pressure Vessel Technology,* London, vol. 2, pp. 251-261, 1980.

[76] H. A. Lang, "Toroidal elastic stress field for pressurized elbows and pipe bends," *International Journal of Pressure Vessels and Piping,* vol. 15, pp. 291-305, 1984.

[77] H. A. Lang, "In-plane bending of a curved pipe or toroidal tube acted on by end couples," *International Journal of Pressure Vessels and Piping,* vol. 15, pp. 27-35, 1984.

[78] H. A. Lang, "Stress field for a curved pipe subjected to in-plane end couples," *International Journal of Pressure Vessels and Piping,* vol. 15, pp. 93-104, 1984.

[79] H. A. Lang, "Stress field for an in-plane and shear forces acting on a 90° elbow or pipe bend," *International Journal of Pressure Vessels and Piping,* vol. 16, pp. 263-284, 1984.

[80] H. A. Lang, "Stress field for a normal forces acting on the end of a 90° elbow or pipe bend," *International Journal of Pressure Vessels and Piping,* vol. 17, pp. 163-172, 1984.

[81] H. A. Lang, "Toroidal elasticity stress state for an end shear force acting on an elbow," *International Journal of Pressure Vessels and Piping,* vol. 41, pp. 359-376, 1990.

[82] H. A. Lang, "Toroidal elasticity stress state for an end normal force acting on an elbow," *International Journal of Pressure Vessels and Piping,* vol. 48, pp. 209-227, 1991.

[83] H. A. Lang, "Out-of-plane bending of an elbow or pipe bend under an end loaded shear force," *International Journal of Pressure Vessels and Piping,* vol. 15, pp. 205-212, 1984.

[84] H. A. Lang, "Twist-bending of a 90° elbow or pipe bend," *International Journal of Pressure Vessels and Piping,* vol. 16, pp. 67-74, 1984.

[85] D. Redekop, "A displacement solution in toroidal elasticity," *International Journal of Pressure Vessels and Piping,* vol. 51, pp. 1-21, 1992.

[86] D. Redekop, and Y. Zhu, "A computer program for stresses in a thick-walled 90° elbow," *Computers and Structures,* vol. 45, no. 4, pp. 805-812, 1992.

[87] Y. Zhu, and D. Redekop, "An out-of-plane displacement solution in toroidal elasticity," *International Journal of Pressure Vessels and Piping,* vol. 58, no. 3, pp. 309-319, 1994.

[88] Y. Zhu, and D. Redekop, "Band loading of a thick-walled toroidal shell," *International Journal of Pressure Vessels and Piping,* vol. 61, no. 1, pp. 99-109, 1995.

[89] H. Reisman, Elasticity theory and applications, New York: John Wily & Sons, 1980.

[90] Y. C. Fung, and P. Tong, Classical and computational solid mechanics, New Jersey: World Scientific, 2001.

[91] C. T. Herakovich, Mechanics of fibrous composites, New York: John Wiley & Sons, 1998.

[92] H. Yazdani Sarvestani, S. V. Hoa, and M. Hojjati, "Stress analysis of thick orthotropic cantilever tubes under transverse loading," *Advanced Composite Materials,* 2016:1-28.

[93] F. Rooney, and M. Ferrari, "Tension, bending, and flexure of functionally graded cylinders," *International Journal of Solids and Structures,* vol. 38, no. 3, pp. 413-421, 2001.

[94] J. Tarn, "Exact solutions for functionally graded anisotropic cylinders subjected to thermal and mechanical loads," *International Journal of Solids and Structures,* vol. 38, no. 46-47, pp. 8189-8206, 2001.

[95] V. V. Zozulya, and C. Zhang, "A high order theory for functionally graded axisymmetric cylindrical shells," *International Journal of Mechanical Sciences,* vol. 60, no. 1, pp. 12-22, 2012.

[96] H. Yazdani Sarvestani, "Effects of layup sequences on stresses of thick composite cantilever tubes," *Advanced Composite Materials,* pp. 1:21, 2015.

[97] H. Yazdani Sarvestani, S. V. Hoa, and M. Hojjati, "Effects of shear loading on stress distributions at sections in thick composite tubes," *Composite Structures,* vol. 140, pp. 433-445, 2016.

[98] X. Ji, M. Zhang, H. Kang, J. Qian, and H. Hu, "Effect of cumulative seismic damage to steel tube-reinforced concrete composite columns," *Earthquakes and Structures,* vol. 7, no. 2, pp. 179-19, 2014.

[99] H. Yazdani Sarvestani, S. V. Hoa, and M. Hojjati, "Three-dimensional Stress Analysis of Orthotropic Curved Tubes-Part 1: Single-layer Solution," *European Journal of Mechanics - A/Solids,* 2016.

[100] L. Jodar, and E. Navarro, "Solving coupled systems of linear second-order differential equations knowing a part of the spectrum of the companion matrix," *Journal of Computational and Applied Mathematics,* vol. 39, no. 1, pp. 115-119, 1992.

[101] L. G. Brazier, "On the flexure of thin cylindrical shells and other thin sections," *Proceeding of the royal Society of London A,* vol. 116, no. 773, pp. 104–114, 1927.

[102] J. T. Boyle, "The finite bending of curved pipes," *International Journal of Solids and Structures,* vol. 17, pp. 515-529, 1981.

[103] F. A. Emmerling, "Flexible Shells," Springer Berlin Heidelberg, 1984.

[104] S. V. Levyakov, and V. N. Pavshok, "Buckling analysis of flanged curvilinear pipes in pure bending," *International Journal of Pressure Vessels and Piping,* vol. 85, no. 5, pp. 306-312, 2008.

[105] E. M. M. Fonseca, and F. J. M. Q. De Melo, "Numerical solution of curved pipes submitted to in-plane loading conditions," *Thin-Walled Structures,* vol. 48, no. 2, pp. 103-109, 2010.

[106] A. M. Kolesnikov, "Large bending deformations of pressurized curved tubes," *Archives of Mechanics,* vol. 63, no. 5-6, pp. 507-516, 2011.

[107] H. Yudo, and T. Yoshikawa, "Buckling phenomenon for straight and curved pipe under pure bending," *Journal of Marine Science and Technology,* vol. 20, no. 1, pp. 94-103, 2015.

[108] T. C. T. Ting, "New solution to pressuring, shearing, torsion and extension of cylindrically anisotropic elastic circular tube or bar," *Proceeding of the Royal Society of London A,* vol. 455, pp. 3527-3542, 1999.

[109] T. Chen, C. T. Chung, and W. L. Lin, "A revisit of a cylindrically anisotropic tube subjected to pressuring, shearing, torsion and extension and a uniform temperature change," *International Journal of Solids and Structures,* vol. 37, pp. 5143-5159, 2000.

[110] H. G. S. J. Thuis, and V. H. Metz, "The influence of trigger configurations and laminate lay-up on the failure mode of composite crush cylinders," *Composite Structures,* vol. 28, no. 2, pp. 131-137, 1994.

[111] N. O. Yokoyama, M. V. Donadon, and S. F. M. De Almeida, "A numerical study on the impact resistance of composite shells using an energy based failure model," *Composite Structures,* vol. 93, no. 1, pp. 142-152, 2010.

[112] S. M. R. Khalili, M. Soroush, A. Davar, and O. Rahmani, "Finite element modeling of low-velocity impact on laminated composite plates and cylindrical shells," *Composite Structures,* vol. 93, no. 5, pp. 1363-1375, 2011.

[113] M. S. Ismail, J. Purbolaksono, A. Andriyana, C. J. Tan, N. Muhammad, and H. L. Liew, "The use of initial imperfection approach in design process and buckling failure evaluation of axially compressed composite cylindrical shells," *Engineering Failure Analysis,* vol. 51, pp. 20-28, 2015.

[114] F. Romano, F. Di Caprio, B. Auriemma, and U. Mercurio, "Numerical investigation on the failure phenomena of stiffened composite panels in post-buckling regime with discrete damages," *Engineering Failure Analysis,* vol. 56, pp. 116-130, 2015.

[115] H. R. Mahdavi, G. H. Rahimi, and A. Farrokhabadi, "Failure analysis of $(\pm 55°)_9$ filament-wound GRE pipes using acoustic emission technique," *Engineering Failure Analysis,* vol. 62, pp. 178-187, 2015.

[116] R. A. Chaudhuri, "Effects of thickness and fiber misalignment on compression fracture in cross-ply (very) long cylindrical shells under external pressure," *Proceeding of the royal Society of London A,* vol. 471, pp. 2180, 2015.

[117] J. L. Y. Tan, V. S. Deshpande, and N. A. Fleck, "Failure mechanisms of a notched CFRP laminate under multi-axial loading," *Composites Part A: Applied Science and Manufacturing,* vol. 77, pp. 56-66, 2015.

[118] H. Yazdani Sarvestani, and M. Hojjati, "Three-dimensional stress analysis of orthotropic curved tubes-part 2: laminate solution," *European Journal of Mechanics - A/Solids,* 2016.

[119] D. O. Brush, and B. O. Almroth, "Buckling of bars, plates and shells," McGraw-Hill, Inc, 1975.

Appendix A

Constant coefficients of coupled ordinary differential equations presented in Section 3.4

The coefficient matrices [M], [K], $\{F_1\}$, $\{F_2\}$, $\{F_3\}$ and $\{F_4\}$ in Eq. (3.45) are:

$$[M]=\begin{bmatrix} -[H_{66}] & -[H_{26}] & -\left([H_{26}]+[B_{36}]-[B_{45}]^T\right) \\ -[H_{26}] & -[H_{22}] & -\left([H_{22}]+[B_{23}]-[B_{44}]^T+[H_{44}]\right) \\ [0] & [0] & -[H_{44}] \end{bmatrix},$$

$$[K]=\begin{bmatrix} [A_{55}] & -[B_{45}]^T & [0] \\ [A_{45}]-[B_{45}] & [A_{44}]-[B_{44}]-[B_{44}]^T+[H_{44}] & [0] \\ -[B_{45}]+[H_{26}]+[B_{36}]^T & [H_{44}]-[B_{44}]+[H_{22}]+[B_{23}]^T & [H_{22}]+[B_{23}]+[B_{23}]^T+[A_{33}] \end{bmatrix}$$

$$\{F_1\}=\begin{Bmatrix} -\{B_{16}\} \\ -\{B_{12}\} \\ -\left(\{\bar{B}_{13}\}+\{B_{12}\}\right) \end{Bmatrix}, \quad \{F_2\}=\begin{Bmatrix} \{0\} \\ \{0\} \\ \left(\{\bar{B}_{36}\}+\{B_{26}\}\right) \end{Bmatrix},$$

$$\{F_3\}=\begin{Bmatrix} \{0\} \\ \{0\} \\ -\left(\{A_{13}\}+\{F_{12}\}\right) \end{Bmatrix}, \quad \{F_4\}=\begin{Bmatrix} -\left(\{A_{55}\}+\{F_{66}\}\right) \\ -\left(\{A_{45}\}-\{F_{45}\}+\{F_{26}\}\right) \\ -\left(\{A_{36}\}+\{F_{26}\}-\{F_{45}\}\right) \end{Bmatrix} \qquad (A.1)$$

Appendix B

Boundary Conditions and Unknown Vector presented in Section 3.4

B.1. The First Group Boundary Condition

The boundary conditions (Eq. (3.38a)) in displacement form are obtained by substituting Eq. (3.41) into Eq. (3.38a):

$$
\begin{aligned}
R_\theta^k &= B_{45}^{kj}U_j + \left(B_{44}^{kj} - H_{44}^{kj}\right)V_j + H_{44}^{kj}W_j' + \mathrm{F}_{45}^k\left(C_1\sin\theta + C_2\cos\theta\right) = 0 \\
Q_x^k &= A_{55}^{kj}U_j + \left(A_{45}^{kj} - B_{45}^{jk}\right)V_j + B_{45}^{jk}W_j' + A_{55}^k\left(C_1\sin\theta + C_2\cos\theta\right) = 0 \\
N_z^k &= B_{36}^{jk}U_j' + B_{23}^{jk}V_j' + \left(B_{23}^{jk} + A_{33}^{kj}\right)W_j - \bar{B}_{36}^k C_3 + \bar{B}_{13}^k C_4\sin\theta + \bar{B}_{13}^k C_5\cos\theta + A_{13}^k C_6 \\
&\quad + A_{36}^k\left(C_1\cos\theta - C_2\sin\theta\right) = 0
\end{aligned}
\qquad (\mathrm{B.1})
$$

The system of Eqs. (B.1) is displayed in a matrix form as:

$$
\begin{aligned}
&\left[R_1\right]\{\eta''\} + \left[R_3\right]\{\eta\} + \left[R_4\right]C_3\theta + \left[R_5\right]C_4\cos\theta + \left[R_6\right]C_5\sin\theta \\
&\quad + \left[R_7\right]C_6\theta + \left[R_8\right]C_1\sin\theta + \left[R_9\right]C_2\cos\theta = 0
\end{aligned}
\qquad (\mathrm{B.2})
$$

where

$$
\left[R_1\right] = \begin{bmatrix} [0] & [0] & [H_{44}] \\ [0] & [0] & [B_{45}]^T \\ [0] & [0] & [0] \end{bmatrix}, \quad \left[R_3\right] = \begin{bmatrix} [B_{45}] & [B_{44}]-[H_{44}] & [0] \\ [A_{55}] & [A_{45}]-[B_{45}]^T & [0] \\ [B_{36}]^T & [B_{23}]^T & [B_{23}]^T + [A_{33}] \end{bmatrix},
$$

$$
\{R_4\} = \begin{Bmatrix} \{0\} \\ \{0\} \\ -\{\bar{B}_{36}\} \end{Bmatrix}, \quad \{R_5\} = \begin{Bmatrix} \{0\} \\ \{0\} \\ \{\bar{B}_{13}\} \end{Bmatrix}, \quad \{R_6\} = \begin{Bmatrix} \{0\} \\ \{0\} \\ -\{\bar{B}_{13}\} \end{Bmatrix},
$$

$$
\{R_7\} = \begin{Bmatrix} \{0\} \\ \{0\} \\ \{A_{13}\} \end{Bmatrix}, \quad \{R_8\} = \begin{Bmatrix} \{F_{45}\} \\ \{A_{55}\} \\ \{A_{36}\} \end{Bmatrix}, \quad \{R_9\} = \begin{Bmatrix} \{F_{45}\} \\ \{A_{55}\} \\ \{A_{36}\} \end{Bmatrix} \qquad (\mathrm{B.3})
$$

Finally, the unknown vector, {k}, is obtained by substituting Eq. (3.47) into Eq. (B.2):

$$
\{k_f\} = -\left[Z_1\right]^{-1}\left(\left[Z_2\right]C_3 + \left[Z_3\right]C_4 + \left[Z_4\right]C_5 + \left[Z_5\right]C_6 + \left[Z_{13}\right]C_1 + \left[Z_{14}\right]C_2\right) \qquad (\mathrm{B.4})
$$

where

$$[Z_1]=[R_1][\psi]\left[\lambda^2\sinh(\lambda\theta)\right]+[R_3][\psi]\left[\sinh(\lambda\theta)\right]$$

$$[Z_2]=[R_3][K]^{-1}\{F_2\}\theta+[R_4]\theta$$

$$[Z_3]=[R_1][K]^{-1}\{F_1\}\cos\theta-[R_3][K]^{-1}\{F_1\}\cos\theta+[R_5]\cos\theta$$

$$[Z_4]=-[R_1][K]^{-1}\{F_1\}\sin\theta+[R_3][K]^{-1}\{F_1\}\sin\theta+[R_6]\sin\theta$$

$$[Z_5]=[R_3][K]^{-1}\{F_3\}\theta+[R_7]\theta$$

$$[Z_{13}]=\left(([R_3]-[R_1])\sin\theta\right)[K]^{-1}\{F_4\}+[R_8]\sin\theta$$

$$[Z_{14}]=\left(([R_3]-[R_1])\cos\theta\right)[K]^{-1}\{F_4\}+[R_9]\cos\theta \qquad (B.5)$$

B.2. The Second Group Boundary Condition

The boundary conditions (Eq. (3.38b)) are:

$$\begin{aligned} u_1^{(k)}(x,\theta,z)=0 &\rightarrow U_k(\theta)=0 \\ u_2^{(k)}(x,\theta,z)=0 &\rightarrow V_k(\theta)=0 \rightarrow \{\eta\}=0 \\ u_3^{(k)}(x,\theta,z)=0 &\rightarrow W_k(\theta)=0 \end{aligned} \qquad (B.6)$$

The unknown vector, {k}, is obtained:

$$\{k_u\}=-\left([\psi]\left[\sinh(\lambda\theta)\right]\right)^{-1}\begin{pmatrix}[K]^{-1}\{F_1\}(C_5\sin\theta-C_4\cos\theta)+[K]^{-1}\{F_2\}C_3\theta \\ +[K]^{-1}\{F_3\}C_6\theta+[K]^{-1}\{F_4\}(C_1\sin\theta+C_2\cos\theta)\end{pmatrix} \qquad (B.7)$$

Appendix C

Unknown constants [C] presented in Section 3.4

For obtaining unknown constants (*Cj* (j=1, 2, 3, 4, 5 and 6)) in terms of the specific shear force F_0, after the integration of the global equilibrium conditions in Eq. (3.43), it is obtained:

$$\delta C_1 : \left[\frac{R}{\lambda_u^2+1}\left(2\{A_{55}\}-2\lambda_u^2\{F_{66}\}\right) \quad \frac{R}{\lambda_v^2+1}\left(2\{A_{45}\}-2\{F_{45}\}-2\lambda_v^2\{F_{26}\}\right) \quad \{0\}\right]\left([\psi]\left[\sinh(\lambda\pi)\right]\{k\}\right)+$$
$$\left[L_1+\bar{A}_{55} \quad L_2+\bar{A}_{66} \quad L_3 \quad L_4 \quad L_5+\bar{B}_{16} \quad L_6\right][C]R\pi=0$$

$$\delta C_2 : \left[\{0\} \quad \{0\} \quad \frac{R}{\lambda_w^2+1}\left(-2\lambda_w^2\{F_{45}\}-2\{F_{26}\}-2\{B_{36}\}\right)\right]\left([\psi]\left[\sinh(\lambda\pi)\right]\{k\}\right)+$$
$$\left[L_7-\bar{A}_{66} \quad L_8+\bar{A}_{55} \quad L_9 \quad L_{10}-\bar{B}_{16} \quad L_{11} \quad L_{12}\right][C]R\pi=0$$

$$\delta C_3 : \frac{R}{h}\left[2\{A_{66}\} \quad 2\{B_{26}\} \quad \{0\}\right]\left([\psi]\left[\sinh(\lambda\pi)\right]\{k\}\right)+$$
$$\frac{R}{h}\left[0 \quad 0 \quad 2\left(\{B_{26}\}+\{A_{66}\}\right)[K]^{-1}\{F_2\}-2\bar{D}_{66} \quad 0 \quad 0 \quad 2\left(\{B_{26}\}+\{A_{66}\}\right)[K]^{-1}\{F_3\}+2\bar{B}_{16}\right][C]\pi=-2F_0$$

$$\delta C_4 : \left[\{0\} \quad \{0\} \quad \frac{R}{\lambda_w^2+1}\left(2\{F_{13}\}+2\{B_{12}\}\right)\right]\left([\psi]\left[\sinh(\lambda\pi)\right]\{k\}\right)+$$
$$[A1 \quad A2 \quad A3 \quad A4 \quad A5 \quad A6][\mathrm{C}]R\pi=0$$

$$\delta C_5 : \left[-\frac{2R\lambda_u^2}{\lambda_u^2+1}\{B_{16}\} \quad -\frac{2R\lambda_v^2}{\lambda_v^2+1}\{B_{12}\} \quad \{0\}\right]\left([\psi]\left[\sinh(\lambda\pi)\right]\{k\}\right)+$$
$$[A7 \quad A8 \quad 0 \quad A10 \quad A11 \quad 0][\mathrm{C}]R\pi=0$$

$$\delta C_6 : \left[2R\{F_{16}\} \quad 2R\{F_{12}\} \quad \{0\}\right]\left([\psi]\left[\sinh(\lambda\pi)\right]\{k\}\right)+$$
$$\left[0 \quad 0 \quad 2\left(\{F_{12}\}+\{F_{16}\}\right)[K]^{-1}\{F_2\}-2\bar{B}_{16} \quad 0 \quad 0 \quad 2\left(\{F_{12}\}+\{F_{16}\}\right)[K]^{-1}\{F_3\}+2\bar{A}_{11}\right][\mathrm{C}]R\pi=0 \quad (\mathrm{C}.1)$$

where

$$[C]=[C_1 \quad C_2 \quad C_3 \quad C_4 \quad C_5 \quad C_6]^T$$

$$A1:\left(\{B_{12}\}+\{F_{13}\}\right)[K]^{-1}\{F_4\} \qquad A2:-\left(\{B_{12}\}+\{B_{16}\}\right)[K]^{-1}\{F_4\}-\bar{B}_{16}$$

$$A3:2\left(\{B_{12}\}+\{F_{13}\}\right)[K]^{-1}\{F_2\} \qquad A4:\left(\{B_{12}\}+\{B_{16}\}\right)[K]^{-1}\{F_1\}+\bar{D}_{11}$$

$$A5:\left(\{B_{12}\}+\{F_{13}\}\right)[K]^{-1}\{F_1\} \qquad A6:2\left(\{B_{12}\}+\{F_{13}\}\right)[K]^{-1}\{F_3\}$$

$$A7:\left(\{B_{12}\}+\{B_{16}\}\right)[K]^{-1}\{F_4\}-\bar{B}_{16} \qquad A8:\left(\{B_{12}\}+\{F_{13}\}\right)[K]^{-1}\{F_4\}$$

$$A10:-\left(\{B_{12}\}+\{F_{13}\}\right)[K]^{-1}\{F_1\} \qquad A11:\left(\{B_{12}\}+\{B_{16}\}\right)[K]^{-1}\{F_1\}+\bar{D}_{11}$$

$$L_1=\left(-\{F_{45}\}+\{A_{45}\}+\{A_{55}\}+\{F_{26}\}+\{F_{66}\}\right)[K]^{-1}\{F_4\}$$

$$L_2=\left(-\{F_{45}\}+\{F_{26}\}+\{B_{36}\}\right)[K]^{-1}\{F_4\}, L_4=\left(\{F_{45}\}-\{F_{26}\}-\{B_{36}\}\right)[K]^{-1}\{F_1\}$$

$$L_3=\left(-2\{F_{45}\}+2\{A_{45}\}+2\{A_{55}\}\right)[K]^{-1}\{F_2\}, L_5=\left(-\{F_{45}\}+\{A_{45}\}+\{A_{55}\}+\{F_{26}\}+\{F_{66}\}\right)[K]^{-1}\{F_1\}$$

$$L_6=\left(-2\{F_{45}\}+2\{A_{45}\}+2\{A_{55}\}\right)[K]^{-1}\{F_3\}, L_7=\left(\{F_{45}\}-\{F_{26}\}-\{B_{36}\}\right)[K]^{-1}\{F_4\}$$

$$L_8=\left(-\{A_{45}\}-\{A_{55}\}-\{F_{45}\}-\{F_{26}\}+\{F_{66}\}\right)[K]^{-1}\{F_4\}, L_9=\left(-2\{F_{26}\}-2\{B_{36}\}\right)[K]^{-1}\{F_2\}$$

$$L_{10}=\left(-\{A_{45}\}-\{A_{55}\}+\{F_{26}\}+\{F_{45}\}-\{F_{66}\}\right)[K]^{-1}\{F_1\}$$

$$L_{11}=\left(\{F_{45}\}-\{F_{26}\}-\{B_{36}\}\right)[K]^{-1}\{F_1\}, L_{12}=\left(-2\{F_{26}\}-2\{B_{36}\}\right)[K]^{-1}\{F_3\} \qquad (C.2)$$

which is displayed in a matrix form as:

$$[Z_{10}]\{k\}+[Z_9][C]=\begin{Bmatrix}0\\0\\-2F\\0\\0\\0\end{Bmatrix} \qquad (C.3)$$

where

$$[Z_9]=R\begin{bmatrix} \bar{A}_{55}\pi+L_1\pi & \bar{A}_{66}\pi+L_2\pi & L_3\pi & L_4\pi & \bar{B}_{16}\pi+L_5\pi & L_6\pi \\ \bar{A}_{55}\pi+L_7\pi & L_8\pi-\bar{A}_{66}\pi & L_9\pi & L_{10}\pi & -\bar{B}_{16}\pi+L_{11}\pi & L_{12}\pi \\ 0 & 0 & z_{33} & 0 & 0 & z_{36} \\ z_{41} & z_{42} & z_{43} & z_{44} & z_{45} & z_{46} \\ z_{51} & z_{52} & 0 & z_{54} & z_{55} & 0 \\ 0 & 0 & z_{63} & 0 & 0 & z_{66} \end{bmatrix}$$

$z_{41}:\left(\left\{B_{12}\right\}+\left\{F_{13}\right\}\right)\left[K\right]^{-1}\left\{F_4\right\}\pi$ $\quad$ $z_{51}:-\bar{B}_{16}\pi+\left(\left\{B_{12}\right\}+\left\{B_{16}\right\}\right)\left[K\right]^{-1}\left\{F_4\right\}\pi$

$z_{42}:-\left(\left\{B_{12}\right\}+\left\{B_{16}\right\}\right)\left[K\right]^{-1}\left\{F_4\right\}\pi-\pi\bar{B}_{16}$ $\quad$ $z_{52}:\left(\left\{B_{12}\right\}+\left\{F_{13}\right\}\right)\left[K\right]^{-1}\left\{F_4\right\}\pi$

$z_{43}:2\pi\left(\left\{B_{12}\right\}+\left\{F_{13}\right\}\right)\left[K\right]^{-1}\left\{F_2\right\}$

$z_{44}:\left(\left\{B_{12}\right\}+\left\{B_{16}\right\}\right)\left[K\right]^{-1}\left\{F_1\right\}\pi+\pi\bar{D}_{11}$ $\quad$ $z_{54}:-\left(\left\{B_{12}\right\}+\left\{F_{13}\right\}\right)\left[K\right]^{-1}\left\{F_1\right\}\pi$

$z_{45}:\left(\left\{B_{12}\right\}+\left\{F_{13}\right\}\right)\left[K\right]^{-1}\left\{F_1\right\}\pi$ $\quad$ $z_{55}:\pi\bar{D}_{11}+\left(\left\{B_{12}\right\}+\left\{B_{16}\right\}\right)\left[K\right]^{-1}\left\{F_1\right\}\pi$

$z_{46}:2\pi\left(\left\{B_{12}\right\}+\left\{F_{13}\right\}\right)\left[K\right]^{-1}\left\{F_3\right\}$

$z_{63}:-2\pi\bar{B}_{16}+2\pi\left(\left\{F_{12}\right\}+\left\{F_{16}\right\}\right)\left[K\right]^{-1}\left\{F_2\right\}$ $\quad$ $z_{33}:-\frac{2\pi}{h}\bar{D}_{66}+\frac{2\pi}{h}\left(\left\{B_{26}\right\}+\left\{A_{66}\right\}\right)\left[K\right]^{-1}\left\{F_2\right\}$

$z_{66}:2\pi\bar{A}_{11}+2\pi\left(\left\{F_{12}\right\}+\left\{F_{16}\right\}\right)\left[K\right]^{-1}\left\{F_3\right\}$ $\quad$ $z_{36}:\frac{2\pi}{h}\bar{B}_{16}+\frac{2\pi}{h}\left(\left\{B_{26}\right\}+\left\{A_{66}\right\}\right)\left[K\right]^{-1}\left\{F_3\right\}$

$$[Z_{10}]=R\begin{bmatrix} \left[2\left\{A_{55}\right\}-\frac{2\lambda_u^2}{\lambda_u^2+1}\left\{F_{66}\right\} \quad 2\left\{A_{45}\right\}-2\left\{F_{45}\right\}-\frac{2\lambda_v^2}{\lambda_v^2+1}\left\{F_{26}\right\} \quad \left\{0\right\}\right] \\ \left[2\left\{A_{55}\right\}-\frac{2\lambda_u^2}{\lambda_u^2+1}\left\{F_{66}\right\} \quad 2\left\{A_{45}\right\}-2\left\{F_{45}\right\}-\frac{2\lambda_v^2}{\lambda_v^2+1}\left\{F_{26}\right\} \quad \left\{0\right\}\right] \\ \frac{1}{h}\left[2\left\{A_{66}\right\} \quad 2\left\{B_{26}\right\} \quad \left\{0\right\}\right] \\ \left[\left\{0\right\} \quad \left\{0\right\} \quad 2\left\{F_{13}\right\}+2\left\{B_{12}\right\}\right] \\ \left[-\frac{2\lambda_u^2}{\lambda_u^2+1}\left\{B_{16}\right\} \quad -\frac{2\lambda_v^2}{\lambda_v^2+1}\left\{B_{12}\right\} \quad \left\{0\right\}\right] \\ \left[2\left\{F_{16}\right\} \quad 2\left\{F_{12}\right\} \quad \left\{0\right\}\right] \end{bmatrix}[\psi]\left[\sinh\left(\lambda\pi\right)\right] \quad \text{(C.4)}$$

Finally, unknown constants are obtained by substituting Eq. (C.4) into Eq. (C.3):

$$\begin{bmatrix} C_1 \\ C_2 \\ C_3 \\ C_4 \\ C_5 \\ C_6 \end{bmatrix} = \left([Z_{10}] \left(\frac{x}{2a} k_f + \frac{(2a-x)}{2a} k_u \right) + [Z_9] \right)^{-1} \begin{Bmatrix} 0 \\ 0 \\ -2F_0 \\ 0 \\ 0 \\ 0 \end{Bmatrix} \tag{C.5}$$

Appendix D

Global Lagrangian interpolation function in Section 5.3.2

The linear global interpolation function is defined as [52]:

$$\phi_k(z)=\begin{cases}0 & z \le z_{k-1}\\ \psi_{k-1}^{2}(z) & z_{k-1}\le z \le z_k\\ \psi_k^{1}(z) & z_k \le z \le z_{k+1}\\ 0 & z \ge z_{k+1}\end{cases} \quad (k=1,2,...,N+1) \qquad (D.1)$$

where $\psi_k^j\,(j=1,2)$ represent the local Lagrangian linear interpolation functions within the *k*th layer which are defined as:

$$\psi_k^1(z)=\frac{1}{h_k}(z_{k+1}-z) \quad \text{and} \quad \psi_k^2(z)=\frac{1}{h_k}(z-z_k) \qquad (D.2)$$

where h_k is the thickness of the *k*th layer.

Appendix E

Coefficient matrices [M], [K] and {F} in Section 5.4

The coefficient matrices [M], [K] and {F} in Eq. (5.17) are obtained as:

$$[M]=\begin{bmatrix} -[H_{66}] & -[H_{26}] & -\left([H_{26}]+[B_{36}]-[B_{45}]^T\right) \\ -[H_{26}] & -[H_{22}] & -\left([H_{22}]+[B_{23}]-[B_{44}]^T+[H_{44}]\right) \\ [0] & [0] & -[H_{44}] \end{bmatrix},$$

$$[K]=\begin{bmatrix} [A_{55}] & -[B_{45}]^T & [0] \\ [A_{45}]-[B_{45}] & [A_{44}]-[B_{44}]-[B_{44}]^T+[H_{44}] & [0] \\ -[B_{45}]+[H_{26}]+[B_{36}]^T & [H_{44}]-[B_{44}]+[H_{22}]+[B_{23}]^T & [H_{22}]+[B_{23}]+[B_{23}]^T+[A_{33}] \end{bmatrix},$$

$$\{F\}=\begin{Bmatrix} \{0\} & -\{B_{16}\}\sin\theta & \{0\} \\ \{0\} & -\{B_{12}\}\sin\theta & \{0\} \\ \left(\{\bar{B}_{36}\}+\{B_{26}\}\right)\theta & -\left(\{\bar{B}_{13}\}+\{B_{12}\}\right)\sin\theta & -\left(\{A_{13}\}+\{F_{12}\}\right)\theta \end{Bmatrix} \qquad (E.1)$$

Appendix F

Coefficients of Governing Equations in Toroidal Coordinates in Section 6.4

The coefficients of orders n=0, 1, 2 and 3 in Eqs. (6.5) and (6.7) are expressed as:

$$\begin{aligned} U_n = & \frac{1}{2}C_{11}\frac{\partial^2 u_n}{\partial r^2}+\frac{1}{2r}C_{11}\frac{\partial u_n}{\partial r}+\frac{C_{44}}{2r^2}\frac{\partial^2 u_n}{\partial \phi^2} \\ & +\left(\frac{1}{2}C_{11}-C_{22}\right)\frac{u_n}{r^2}+\left(C_{12}-C_{22}\right)\frac{1}{r^2}\frac{\partial v_n}{\partial \phi} \\ & +\frac{\partial}{\partial r}\left(\frac{1}{2}C_{11}\frac{u_n}{r}+\frac{1}{r}\left(\frac{C_{44}}{2}+C_{12}\right)\frac{\partial v_n}{\partial \phi}+\frac{1}{2}C_{11}\frac{\partial u_n}{\partial r}\right) \end{aligned} \qquad (F.1)$$

$$\begin{aligned} \bar{U}_n = & \cos\phi\frac{\partial u_n}{\partial r}\left(C_{11}-C_{13}\right)-\sin\phi\frac{\partial v_n}{\partial r}\frac{C_{44}}{2} \\ & -\sin\phi\frac{C_{44}}{2}\left(\frac{1}{r}\frac{\partial u_n}{\partial \phi}-\frac{v_n}{r}\right)+\cos\phi\left(C_{12}-C_{23}\right)\left(\frac{1}{r}\frac{\partial v_n}{\partial \phi}+\frac{u_n}{r}\right) \\ & +\frac{\partial}{\partial r}\left(\frac{C_{55}}{2}\frac{\partial w_n}{\partial \theta}+C_{13}\left(u_n\cos\phi-v_n\sin\phi+\frac{\partial w_n}{\partial \theta}\right)\right) \\ & +\frac{1}{r}\left(C_{13}-C_{23}\right)\left(u_n\cos\phi-v_n\sin\phi+\frac{\partial w_n}{\partial \theta}\right) \end{aligned} \qquad (F.2)$$

$$\begin{aligned} \hat{U}_n = & \frac{C_{55}}{2}\frac{\partial^2 u_n}{\partial \theta^2}-\frac{C_{55}}{2}\cos\phi\frac{\partial w_n}{\partial \theta} \\ & -C_{33}\cos\phi\left(u_n\cos\phi-v_n\sin\phi+\frac{\partial w_n}{\partial \theta}\right) \end{aligned} \qquad (F.3)$$

$$V_n = \frac{C_{44}}{2}\frac{\partial^2 v_n}{\partial r^2} + \frac{1}{2r}C_{44}\frac{\partial v_n}{\partial r} + \frac{C_{22}}{2r^2}\frac{\partial^2 v_n}{\partial \phi^2}$$
$$-\frac{1}{2}C_{44}\frac{v_n}{r^2} + \frac{1}{2}C_{44}\frac{1}{r^2}\frac{\partial u_n}{\partial \phi}$$
$$+\frac{1}{r}\frac{\partial}{\partial \phi}\left(C_{22}\frac{u_n}{r} + \left(\frac{C_{44}}{2} + C_{12}\right)\frac{\partial u_n}{\partial r} + \frac{1}{2r}C_{22}\frac{\partial v_n}{\partial \phi}\right) \qquad (F.4)$$

$$\bar{V_n} = \cos\phi\frac{C_{44}}{2}\frac{\partial v_n}{\partial r} - \sin\phi\left(C_{12} - C_{13}\right)\frac{\partial u_n}{\partial r}$$
$$-\sin\phi\left(C_{22} - C_{23}\right)\left(\frac{1}{r}\frac{\partial v_n}{\partial \phi} + \frac{u_n}{r}\right) + \cos\phi\frac{C_{44}}{2}\left(\frac{1}{r}\frac{\partial u_n}{\partial \phi} - \frac{v_n}{r}\right)$$
$$+\frac{1}{r}\frac{\partial}{\partial \phi}\left(\frac{C_{66}}{2}\frac{\partial w_n}{\partial \theta} + C_{23}\left(u_n\cos\phi - v_n\sin\phi + \frac{\partial w_n}{\partial \theta}\right)\right) \qquad (F.5)$$

$$\hat{V_n} = \frac{C_{66}}{2}\frac{\partial^2 v_n}{\partial \theta^2} + \frac{C_{66}}{2}\sin\phi\frac{\partial w_n}{\partial \theta}$$
$$-C_{33}\sin\phi\left(u_n\cos\phi - v_n\sin\phi + \frac{\partial w_n}{\partial \theta}\right) \qquad (F.6)$$

$$W_n = \frac{1}{2}C_{55}\frac{\partial^2 w_n}{\partial r^2} + \frac{1}{2r}C_{55}\frac{\partial w_n}{\partial r} + \frac{C_{66}}{2r^2}\frac{\partial^2 w_n}{\partial \phi^2} \qquad (F.7)$$

$$\bar{W_n} = \cos\phi\frac{C_{55}}{2}\frac{\partial w_n}{\partial r} - \frac{1}{r}\cos\phi\left(\frac{C_{55}}{2} - \frac{C_{66}}{2}\right)w_n - \frac{1}{r}\sin\phi\frac{C_{66}}{2}\frac{\partial w_n}{\partial \phi}$$
$$+\frac{\partial}{\partial \theta}\left(\left(\frac{C_{55}}{2} + C_{13}\right)\frac{\partial u_n}{\partial r} + \frac{1}{r}\left(\frac{C_{66}}{2} + C_{23}\right)\frac{\partial v_n}{\partial \phi} + \frac{1}{r}\left(\frac{C_{55}}{2} + C_{23}\right)u_n\right) \qquad (F.8)$$

$$\hat{W_n} = \frac{C_{33}}{2}\frac{\partial^2 w_n}{\partial \theta^2}$$
$$+\left(C_{55}\left(\frac{1}{2}\cos^2\phi - \cos\phi\right) + C_{66}\left(\frac{1}{2}\sin^2\phi - \sin\phi\right)\right)w_n$$
$$+\frac{\partial}{\partial \theta}\left(\left(C_{33} + \frac{C_{55}}{2}\right)u_n\cos\phi - \left(C_{33} + \frac{C_{55}}{2}\right)v_n\sin\phi + \frac{C_{33}}{2}\frac{\partial w_n}{\partial \theta}\right) \qquad (F.9)$$

Appendix G

Definition of functions Θ1, Θ2, Θ3, Θ4, Θ5 and Θ6 in Section 7.3

The functions Θ1, Θ2, Θ3, Θ4, Θ5 and Θ6 in Eqs. (7.13) are defined as:

$$\Theta 1 = \varepsilon^n \left(R_1 + z\right)^{m_n^{(k)}-1} \cos\theta \left(\left(\left(\begin{array}{l} \sigma_{zz}\left(m_n^{(k)} - 1\right) + \dfrac{\sigma_{\theta\theta}}{\rho}\left(R_1 + z\right) \\ +\sigma_{\phi\phi} - \dfrac{\sigma_{\theta z}}{\rho}\left(R_1 + z\right)\tan\theta \end{array} \right) B_{1,m_n^{(k)}} - \sigma_{\phi\phi} n A_{2,m_n^{(k)}} \right) \cos\left(n\phi\right) + \left(\left(\frac{\sigma_{\theta\theta}}{\rho}\left(R_1 + z\right) + m_n^{(k)}\sigma_{\phi z} + \sigma_{\phi\theta}\left(R_1 + z\right)\tan\theta \right) A_{2,m_n^{(k)}} - \sigma_{\phi z} n B_{1,m_n^{(k)}} \right) \sin\left(n\phi\right) \right)$$

$$\Theta 2 = \varepsilon^n \left(R_1 + z\right)^{m_n'^{(k)}-1} \cos\theta \left(\left(\left(\begin{array}{l} \sigma_{zz}\left(m_n'^{(k)} - 1\right) + \dfrac{\sigma_{\theta\theta}}{\rho}\left(R_1 + z\right) \\ +\sigma_{\phi\phi} - \dfrac{\sigma_{\theta z}}{\rho}\left(R_1 + z\right)\tan\theta \end{array} \right) B_{1,m_n'^{(k)}} - \sigma_{\phi\phi} n A_{2,m_n'^{(k)}} \right) \cos\left(n\phi\right) + \left(\left(\frac{\sigma_{\theta\theta}}{\rho}\left(R_1 + z\right) + m_n'^{(k)}\sigma_{\phi z} + \sigma_{\phi\theta}\left(R_1 + z\right)\tan\theta \right) A_{2,m_n'^{(k)}} - \sigma_{\phi z} n B_{1,m_n'^{(k)}} \right) \sin\left(n\phi\right) \right)$$

$$\Theta 3 = \varepsilon^n \left(R_1 + z\right)^{m_n^{(k)}-1} \cos\theta \left(\left(\left(\begin{array}{l} -\sigma_{zz}\left(m_n^{(k)} + 1\right) + \dfrac{\sigma_{\theta\theta}}{\rho}\left(R_1 + z\right) \\ +\sigma_{\phi\phi} - \dfrac{\sigma_{\theta z}}{\rho}\left(R_1 + z\right)\tan\theta \end{array} \right) B_{1,-m_n^{(k)}} - \sigma_{\phi} n A_{2,-m_n^{(k)}} \right) \cos\left(n\phi\right) + \left(\left(\frac{\sigma_{\theta\theta}}{\rho}\left(R_1 + z\right) - m_n^{(k)}\sigma_{\phi z} + \sigma_{\phi\theta}\left(R_1 + z\right)\tan\theta \right) A_{2,-m_n^{(k)}} - \sigma_{\phi z} n B_{1,-m_n^{(k)}} \right) \sin\left(n\phi\right) \right)$$

$$\Theta 4=\varepsilon^{n}\left(R_{1}+z\right)^{-m_{n}^{\prime}-1}\cos\theta\left(\begin{array}{l}\left(\left(\begin{array}{l}\left(\begin{array}{l}-\sigma_{zz}\left(m_{n}^{\prime(k)}+1\right)+\dfrac{\sigma_{\theta\theta}}{\rho}\left(R_{1}+z\right)\\ +\sigma_{\phi\phi}-\dfrac{\sigma_{\theta z}}{\rho}\left(R_{1}+z\right)\tan\theta\end{array}\right)B_{1,-m_{n}^{\prime(k)}}-\sigma_{\phi\phi}nA_{2,-m_{n}^{\prime(k)}}\end{array}\right)\cos\left(n\phi\right)\\ +\left(\left(\left(\dfrac{\sigma_{\theta\theta}}{\rho}\left(R_{1}+z\right)-m_{n}^{\prime(k)}\sigma_{\phi z}+\sigma_{\phi\theta}\left(R_{1}+z\right)\tan\theta\right)A_{2,-m_{n}^{\prime(k)}}-\sigma_{\phi z}nB_{1,-m_{n}^{\prime(k)}}\right)\right)\sin\left(n\phi\right)\end{array}\right)$$

$$\Theta 5=\varepsilon^{n}\left(R_{1}+z\right)^{\bar{m}_{n}^{(k)}-1}\sin\theta\left(\begin{array}{l}-\sigma_{\phi\theta}\left(n-1\right)\sin\left(\left(n-1\right)\phi\right)+\\ \left(\begin{array}{l}\sigma_{\phi\theta}\left(R_{1}+z\right)\dfrac{\sin\phi}{\rho}-\dfrac{\sigma_{\theta z}}{\rho}\cos\phi\left(R_{1}+z\right)\\ +\sigma_{\theta z}\bar{m}_{n}^{(k)}+\dfrac{\sigma_{\theta\theta}}{\rho}\left(R_{1}+z\right)\cot\theta\end{array}\right)\cos\left(\left(n-1\right)\phi\right)\end{array}\right)$$

$$\Theta 6=\varepsilon^{n}\left(R_{1}+z\right)^{-\bar{m}_{n}^{(k)}-1}\sin\theta\left(\begin{array}{l}-\sigma_{\phi\theta}\left(n-1\right)\sin\left(\left(n-1\right)\phi\right)+\\ \left(\begin{array}{l}\sigma_{\phi\theta}\left(R_{1}+z\right)\dfrac{\sin\phi}{\rho}-\dfrac{\sigma_{\theta z}}{\rho}\cos\phi\left(R_{1}+z\right)\\ -\sigma_{\theta z}\bar{m}_{n}^{(k)}+\dfrac{\sigma_{\theta\theta}}{\rho}\left(R_{1}+z\right)\cot\theta\end{array}\right)\cos\left(\left(n-1\right)\phi\right)\end{array}\right)$$

Appendix H

Definition of stress resultants based on displacement components in Section 7.3

The stress resultants in Eq. (7.14) based on displacement components are presented as:

$$
\begin{aligned}
\left(N_z^k, Q_\theta^k, Q_\phi^k\right) = & \left(A_{11}^{kj} + B_{12}^{jk} + E_{13}^{jk}\cos\phi, 0, 0\right)U_j + \left(0, B_{45}^{jk}, B_{44}^{jk}\right)U_j' \\
& + \left(-E_{13}^{jk}\sin\phi, A_{45}^{kj} - B_{45}^{jk}, A_{44}^{kj} - B_{44}^{jk}\right)V_j + \left(B_{12}^{jk}, 0, 0\right)V_j' \\
& + \left(E_{16}^{jk}\sin\phi, A_{55}^{kj} - E_{55}^{jk}\cos\phi, A_{45}^{kj} - E_{45}^{jk}\cos\phi\right)W_j + \left(B_{16}^{jk}, 0, 0\right)W_j' \\
& + \left(\hat{\bar{B}}_{11,n}^k + B_{12,n}^k + nA_{12,n}^k + H_{13,n}^k\cos\phi, 0, 0\right)\cos(n\phi)\cos\theta \\
& + \left(0, -H_{55,n}^k, -H_{45,n}^k\right)\cos(n\phi)\sin\theta \\
& + \left(F_{13,n}^k\sin\phi, -nB_{45,n}^k + \bar{A}_{45,n}^k - A_{45,n}^k, -nB_{44,n}^k + \bar{A}_{44,n}^k - A_{44,n}^k\right)\sin(n\phi)\cos\theta \\
& + \left(G_{13,n}^k, 0, 0\right)\cos\left((n-1)\phi\right)\cos\theta \\
& + \left(C_{16,n}^k(1-n), 0, 0\right)\sin\left((n-1)\phi\right)\sin\theta \\
& + \left(-F_{16,n}^k, 0, 0\right)\sin(n\phi)\sin\theta \\
& + \left(G_{16,n}^k\sin\phi, \bar{C}_{55,n}^k - G_{55,n}^k\cos\phi, \bar{C}_{45,n}^k - G_{45,n}^k\cos\phi\right)\cos\left((n-1)\phi\right)\sin\theta
\end{aligned}
\qquad (H.1)
$$

$$\left(M_{\theta}^{k},R_{\phi\theta}^{k}\right)=\left(E_{13}^{kj}+\hat{B}_{23}^{kj}+\hat{E}_{33}^{kj}\cos\phi,E_{16}^{kj}+\hat{B}_{26}^{kj}+\hat{E}_{36}^{kj}\cos\phi\right)U_{j}+$$
$$-\left(\hat{E}_{33}^{jk}\sin\phi,\hat{E}_{36}^{jk}\sin\phi\right)V_{j}+\left(\hat{B}_{23}^{k},\hat{B}_{26}^{k}\right)V_{j}'$$
$$+\left(\hat{E}_{36}^{kj}\sin\phi,\hat{E}_{66}^{kj}\sin\phi\right)W_{j}+\left(\hat{B}_{36}^{kj},\hat{B}_{66}^{kj}\right)W_{j}'$$
$$+\begin{pmatrix}\overline{H}_{13,n}^{k}+\hat{B}_{23,n}^{k}+n\hat{A}_{23,n}^{k}+\hat{H}_{33,n}^{k}\cos\phi,\\ \overline{H}_{16,n}^{k}+\hat{B}_{26,n}^{k}+n\hat{A}_{26,n}^{k}+\hat{H}_{36,n}^{k}\cos\phi\end{pmatrix}\cos(n\phi)\cos\theta$$
$$-\left(\hat{F}_{33,n}^{k}\sin\phi,\hat{F}_{36,n}^{k}\sin\phi\right)\sin(n\phi)\cos\theta$$
$$+\left(\hat{G}_{33,n}^{k},\hat{G}_{36,n}^{k}\right)\cos\left((n-1)\phi\right)\cos\theta$$
$$+\left(\hat{C}_{36,n}^{k}(1-n),\hat{C}_{66,n}^{k}(1-n)\right)\sin\left((n-1)\phi\right)\sin\theta$$
$$-\left(\hat{F}_{36,n}^{k},\hat{F}_{66,n}^{k}\right)\sin(n\phi)\sin\theta$$
$$+\left(\hat{G}_{36,n}^{k}\sin\phi,\hat{G}_{66,n}^{k}\sin\phi\right)\cos\left((n-1)\phi\right)\sin\theta \qquad (H.2)$$

$$\left(R_{\theta}^{k},M_{z\phi}^{k}\right)=\left(\hat{B}_{45}^{kj},\hat{B}_{44}^{kj}\right)U_{j}'+\left(E_{45}^{kj}-\hat{B}_{45}^{kj},E_{44}^{kj}-\hat{B}_{44}^{kj}\right)V_{j}$$
$$+\left(E_{55}^{kj}-\hat{E}_{55}^{kj}\cos\phi,E_{45}^{kj}-\hat{E}_{45}^{kj}\cos\phi\right)W_{j}$$
$$-\left(\hat{H}_{55,n}^{k},\hat{H}_{45,n}^{k}\right)\cos(n\phi)\sin\theta$$
$$+\left(-n\hat{B}_{45,n}^{k}+\overline{F}_{45,n}^{k}-\hat{A}_{45,n}^{k},-n\hat{B}_{44,n}^{k}+\overline{F}_{44,n}^{k}-\hat{A}_{44,n}^{k}\right)\sin(n\phi)\cos\theta$$
$$+\left(\overline{G}_{55,n}^{k}-\hat{G}_{55,n}^{k}\cos\phi,\overline{G}_{45,n}^{k}-\hat{G}_{45,n}^{k}\cos\phi\right)\cos\left((n-1)\phi\right)\sin\theta \qquad (H.3)$$

$$\left(M_{\phi}^{k},M_{\phi\theta}^{k}\right)=\left(B_{12}^{kj}+\overline{\overline{B}}_{22}^{kj}+\hat{B}_{23}^{kj}\cos\phi,B_{16}^{kj}+\overline{\overline{B}}_{26}^{kj}+\hat{B}_{36}^{kj}\cos\phi\right)U_{j}+$$
$$-\left(\hat{B}_{23}^{kj}\sin\phi,\hat{B}_{36}^{kj}\sin\phi\right)V_{j}+\left(\overline{\overline{B}}_{22}^{k},\overline{\overline{B}}_{26}^{k}\right)V_{j}'$$
$$+\left(\hat{B}_{26}^{kj}\sin\phi,\hat{B}_{66}^{kj}\sin\phi\right)W_{j}+\left(\overline{\overline{B}}_{26}^{kj},\overline{\overline{B}}_{66}^{kj}\right)W_{j}'$$
$$+\begin{pmatrix}\overline{B}_{12,n}^{k}+\overline{\overline{B}}_{22,n}^{k}+n\overline{\overline{A}}_{22,n}^{k}+\hat{B}_{23,n}^{k}\cos\phi,\\ \overline{B}_{16,n}^{k}+\overline{\overline{B}}_{26,n}^{k}+n\overline{\overline{A}}_{26,n}^{k}+\hat{B}_{36,n}^{k}\cos\phi\end{pmatrix}\cos(n\phi)\cos\theta$$
$$-\left(\hat{A}_{23,n}^{k}\sin\phi,\hat{A}_{36,n}^{k}\sin\phi\right)\sin(n\phi)\cos\theta$$
$$+\left(\hat{C}_{23,n}^{k},\hat{C}_{36,n}^{k}\right)\cos\left((n-1)\phi\right)\cos\theta$$
$$+\left(\overline{\overline{C}}_{26,n}^{k}(1-n),\overline{\overline{C}}_{66,n}^{k}(1-n)\right)\sin\left((n-1)\phi\right)\sin\theta$$
$$-\left(\hat{A}_{26,n}^{k},\hat{A}_{66,n}^{k}\right)\sin(n\phi)\sin\theta$$
$$+\left(\hat{C}_{26,n}^{k}\sin\phi,\hat{C}_{66,n}^{k}\sin\phi\right)\cos\left((n-1)\phi\right)\sin\theta \qquad (H.4)$$

$$
\begin{aligned}
R^{k}_{z\phi} = {} & \bar{\bar{B}}^{kj}_{44,n} U'_j + \left(B^{kj}_{44} - \bar{\bar{B}}^{kj}_{44} \right) V_j \\
& + \left(B^{kj}_{45} - \hat{B}^{kj}_{45} \cos\phi \right) W_j \\
& - \hat{B}^{k}_{45,n} \cos(n\phi) \sin\theta \\
& + \left(-n\bar{\bar{B}}^{k}_{44,n} + \bar{A}^{k}_{44,n} - \bar{\bar{A}}^{k}_{44,n} \right) \sin(n\phi) \cos\theta \\
& + \left(\bar{C}^{k}_{45,n} - \hat{C}^{k}_{45,n} \cos\phi \right) \cos\left((n-1)\phi \right) \sin\theta
\end{aligned} \qquad (H.5)
$$

where the laminate rigidities in Eqs. (H.1)-(H.5) are defined as:

$$
\left(A^{kj}_{pq}, \bar{B}^{kj}_{pq} \right) = \sum_{i=1}^{N} \int_{z_i}^{z_{i+1}} \bar{C}^{(i)}_{pq} \left(\phi'_k \phi'_j, \phi_k \phi'_j \right) \mathrm{dz}
$$

$$
\left(E^{kj}_{pq}, B^{kj}_{pq} \right) = \sum_{i=1}^{N} \int_{z_i}^{z_{i+1}} \bar{C}^{(i)}_{pq} \left(\frac{\phi_k \phi'_j}{\rho}, \frac{\phi_k \phi'_j}{R_1 + z} \right) \mathrm{dz}
$$

$$
\left(\hat{B}^{kj}_{pq}, \hat{E}^{kj}_{pq}, \bar{\bar{B}}^{kj}_{pq} \right) = \sum_{i=1}^{N} \int_{z_i}^{z_{i+1}} \bar{C}^{(i)}_{pq} \left(\frac{\phi_k \phi_j}{\rho(R_1 + z)}, \frac{\phi_k \phi_j}{\rho^2}, \frac{\phi_k \phi_j}{(R_1 + z)^2} \right) \mathrm{dz}
$$

$$
\left(A^{k}_{pq}, \bar{A}^{k}_{pq} \right) = \sum_{i=1}^{N} \int_{z_i}^{z_{i+1}} \bar{C}^{(i)}_{pq} \left(\phi'_k, \frac{\phi'_k}{\rho} \right) \mathrm{dz}
$$

$$
\left(\hat{\bar{B}}^{k}_{pq,n}, \hat{\bar{A}}^{k}_{pq,n}, \hat{\bar{C}}^{k}_{pq,n} \right) = \sum_{i=1}^{N} \int_{z_i}^{z_{i+1}} \bar{C}^{(i)}_{pq} \, \varepsilon^n \left(B'_n \phi'_k, A'_n \phi'_k, C'_n \phi'_k \right) \mathrm{dz}
$$

$$
\left(B^{k}_{pq,n}, A^{k}_{pq,n}, C^{k}_{pq,n} \right) = \sum_{i=1}^{N} \int_{z_i}^{z_{i+1}} \bar{C}^{(i)}_{pq} \, \varepsilon^n \left(\frac{B_n \phi'_k}{R_1 + z}, \frac{A_n \phi'_k}{R_1 + z}, \frac{C_n \phi'_k}{R_1 + z} \right) \mathrm{dz}
$$

$$
\left(H^{k}_{pq,n}, F^{k}_{pq,n}, G^{k}_{pq,n} \right) = \sum_{i=1}^{N} \int_{z_i}^{z_{i+1}} \bar{C}^{(i)}_{pq} \, \varepsilon^n \left(\frac{B_n \phi'_k}{\rho}, \frac{A_n \phi'_k}{\rho}, \frac{C_n \phi'_k}{\rho} \right) \mathrm{dz}
$$

$$
\left(\bar{H}^{k}_{pq,n}, \bar{F}^{k}_{pq,n}, \bar{G}^{k}_{pq,n} \right) = \sum_{i=1}^{N} \int_{z_i}^{z_{i+1}} \bar{C}^{(i)}_{pq} \, \varepsilon^n \left(\frac{B'_n \phi_k}{\rho}, \frac{A'_n \phi_k}{\rho}, \frac{C'_n \phi_k}{\rho} \right) \mathrm{dz}
$$

$$
\left(\hat{B}^{k}_{pq,n}, \hat{A}^{k}_{pq,n}, \hat{C}^{k}_{pq,n} \right) = \sum_{i=1}^{N} \int_{z_i}^{z_{i+1}} \bar{C}^{(i)}_{pq} \, \frac{\varepsilon^n}{\rho} \left(\frac{B_n \phi_k}{R_1 + z}, \frac{A_n \phi_k}{R_1 + z}, \frac{C_n \phi_k}{R_1 + z} \right) \mathrm{dz}
$$

$$
\left(\hat{H}^{k}_{pq,n}, \hat{F}^{k}_{pq,n}, \hat{G}^{k}_{pq,n} \right) = \sum_{i=1}^{N} \int_{z_i}^{z_{i+1}} \bar{C}^{(i)}_{pq} \varepsilon^n \left(\frac{B_n \phi_k}{\rho^2}, \frac{A_n \phi_k}{\rho^2}, \frac{C_n \phi_k}{\rho^2} \right) \mathrm{dz}
$$

$$
\left(\bar{B}^{k}_{pq,n}, \bar{A}^{k}_{pq,n}, \bar{C}^{k}_{pq,n} \right) = \sum_{i=1}^{N} \int_{z_i}^{z_{i+1}} \bar{C}^{(i)}_{pq} \varepsilon^n \left(\frac{B'_n \phi_k}{R_1 + z}, \frac{A'_n \phi_k}{R_1 + z}, \frac{C'_n \phi_k}{R_1 + z} \right) \mathrm{dz}
$$

$$
\left(\bar{\bar{B}}^{k}_{pq,n}, \bar{\bar{A}}^{k}_{pq,n}, \bar{\bar{C}}^{k}_{pq,n} \right) = \sum_{i=1}^{N} \int_{z_i}^{z_{i+1}} \bar{C}^{(i)}_{pq} \varepsilon^n \left(\frac{B_n \phi_k}{(R_1 + z)^2}, \frac{A_n \phi_k}{(R_1 + z)^2}, \frac{C_n \phi_k}{(R_1 + z)^2} \right) \mathrm{dz} \qquad (H.6)
$$

$$
\left(k, j = 1, 2, \ldots, N+1 \right)
$$

Appendix I

Definition coefficient matrices [M], [K_1], [K_2] and {F} in Section 7.4

The coefficient matrices [M], [K_1], [K_2] and {F} in Eq. (7.16) are presented as:

$$[M]=\begin{bmatrix} -\left[\bar{\bar{B}}_{44,n}\right] & [0] & [0] \\ [0] & -\left[\bar{\bar{B}}_{22}\right] & -\left[\bar{\bar{B}}_{26}\right] \\ [0] & -\left[\bar{\bar{B}}_{26}\right] & -\left[\bar{\bar{B}}_{66}\right] \end{bmatrix}$$

$$[K_1]=\begin{bmatrix} [0] & [B_{12}]^T+\left[\bar{\bar{B}}_{22}\right]+\left[\hat{B}_{23,n}\right]\cos\phi-[B_{44}]+\left[\bar{\bar{B}}_{44}\right] & [B_{16}]^T+\left[\bar{\bar{B}}_{26}\right]+\left[\hat{B}_{36}\right]\cos\phi-[B_{45}]+\left[\hat{B}_{45}\right]\cos\phi \\ -\left[\bar{\bar{B}}_{44,n}\right]-[B_{12}]-\left[\bar{\bar{B}}_{22}\right]+\left[\hat{B}_{23}\right]\cos\phi+[B_{44}]^T & \left[\hat{B}_{23,n}\right]\sin\phi+\left[\hat{B}_{23}\right]\sin\phi & \left[\hat{B}_{36}\right]\sin\phi-\left[\hat{B}_{26}\right]\sin\phi \\ [B_{45}]^T-\left[\bar{\bar{B}}_{26}\right]-\left[\hat{B}_{36}\right]\cos\phi-[B_{16}]-\left[\hat{B}_{45}\right]\cos\phi & \left[\hat{B}_{36}\right]\sin\phi+\left[\hat{B}_{26,n}\right]\sin\phi & [0] \end{bmatrix}$$

$$[K_2]=\begin{bmatrix} [1,1] & [1,2] & [1,3] \\ [2,1] & [2,2] & [2,3] \\ [3,1] & [3,2] & [3,3] \end{bmatrix}$$

$$[1,1]=\left[\hat{E}_{33}\right]\cos^2\phi+\left(\left[E_{13}\right]^T+\left[\hat{B}_{23}\right]+\left[E_{13}\right]+\left[\hat{B}_{23}\right]\right)\cos\phi+\left[A_{11}\right]+\left[B_{12}\right]^T+\left[B_{12}\right]+\left[\bar{\bar{B}}_{22}\right]$$

$$[1,2]=-\left(\left[E_{13}\right]^T+\left[\hat{B}_{23}\right]+\left[\hat{E}_{33}\right]\cos\phi\right)\sin\phi$$

$$[1,3]=\left(\left[E_{16}\right]^T+\left[\hat{B}_{26}\right]-\left[\hat{B}_{45}\right]+\left[\hat{E}_{36}\right]\cos\phi\right)\sin\phi$$

$$[2,1]=\left(\left[E_{13}\right]^T+2\left[\hat{B}_{23}\right]+\left[\hat{E}_{33}\right]\cos\phi\right)\sin\phi$$

$$[2,2]=-\left[\hat{E}_{33}\right]\sin^2\phi+\left[\hat{B}_{23}\right]\cos\phi-\left[B_{44}\right]-\left[B_{44}\right]^T+\left[A_{44}\right]+\left[\bar{\bar{B}}_{44}\right]$$

$$[2,3]=\left[\hat{E}_{36}\right]\sin^2\phi+\left(\left[\hat{B}_{45}\right]-\left[\hat{B}_{26}\right]-\left[E_{45}\right]^T\right)\cos\phi-\left[B_{45}\right]+\left[A_{45}\right]$$

$$[3,1] = \left(\left[E_{16} \right]^T + \left[\hat{B}_{26} \right] + \left[\hat{B}_{36} \right] + \left[\hat{E}_{36} \right] \cos\phi \right) \sin\phi$$

$$[3,2] = -\left[\hat{E}_{36} \right] \sin^2\phi + \left(\left[\hat{B}_{45} \right] + \left[\hat{B}_{36} \right] - \left[E_{45} \right] \right) \cos\phi - \left[B_{45} \right]^T + \left[A_{45} \right]$$

$$[3,3] = \left[\hat{E}_{66} \right] \sin^2\phi + \left[\hat{E}_{55} \right] \cos^2\phi - \left(\left[\hat{B}_{66} \right] + \left[E_{55} \right] + \left[E_{55} \right]^T \right) \cos\phi + \left[A_{55} \right]$$

$$\{F\} = \begin{Bmatrix} \{F_1\} \\ \{F_2\} \\ \{F_3\} \end{Bmatrix}$$

where

$$\{F_1\} = -\begin{pmatrix} \left\{ \hat{\bar{B}}_{11,n} \right\} + \left\{ B_{12,n} \right\} + \left\{ \bar{B}_{12,n} \right\} + \left\{ \bar{\bar{B}}_{22,n} \right\} + \left(\left\{ H_{13,n} \right\} + 2\left\{ \hat{B}_{23,n} \right\} + \left\{ \bar{H}_{13,n} \right\} + n\left\{ \hat{A}_{23,n} \right\} \right) \cos\phi \\ + \left\{ \hat{H}_{33,n} \right\} \cos^2\phi + n\left(\left\{ \bar{\bar{A}}_{22,n} \right\} - \left\{ \bar{A}_{44,n} \right\} + \left\{ \bar{\bar{A}}_{44,n} \right\} + \left\{ A_{12,n} \right\} \right) + n^2 \left\{ \bar{\bar{B}}_{44,n} \right\} \end{pmatrix} \cos(n\phi) \cos\theta$$

$$+ \left(\left\{ F_{13,n} \right\} + \left\{ \hat{A}_{23,n} \right\} + \left\{ \hat{F}_{33,n} \right\} \cos\phi \right) \sin\phi \sin(n\phi) \cos\theta$$

$$- \left(\left\{ G_{13,n} \right\} + \left\{ \hat{C}_{23,n} \right\} + \left\{ \hat{G}_{33,n} \right\} \cos\phi \right) \cos\left((n-1)\phi \right) \cos\theta$$

$$- (1-n) \left(\left\{ C_{16,n} \right\} + \left\{ \bar{\bar{C}}_{26,n} \right\} - \left\{ \bar{C}_{45,n} \right\} + \left(\left\{ \hat{C}_{36,n} \right\} + \left\{ \hat{C}_{45,n} \right\} \right) \cos\phi \right) \sin\left((n-1)\phi \right) \sin\theta$$

$$+ \left(\left\{ F_{16,n} \right\} + \left\{ \hat{A}_{26,n} \right\} + n\left\{ \hat{B}_{45,n} \right\} + \left\{ \hat{F}_{36,n} \right\} \cos\phi \right) \sin(n\phi) \sin\theta$$

$$- \left(\left\{ G_{16,n} \right\} + \left\{ \hat{C}_{26,n} \right\} - \left\{ \hat{C}_{45,n} \right\} + \left\{ \hat{G}_{36,n} \right\} \cos\phi \right) \sin\phi \cos\left((n-1)\phi \right) \sin\theta$$

$$\{F_2\} = -\left(\left\{\hat{B}_{45,n}\right\} - \left\{H_{45,n}\right\} + \left(\left\{\bar{H}_{13,n}\right\} + \left\{\hat{B}_{23,n}\right\} + n\left\{\hat{B}_{23,n}\right\} + \left\{\hat{H}_{33,n}\right\}\cos\phi + \left\{\hat{B}_{23,n}\right\} + n\left\{\hat{A}_{23,n}\right\}\right)\sin\phi\right)\cos(n\phi)\cos\theta$$

$$-\begin{pmatrix} n^2\left\{\bar{\bar{A}}_{22,n}\right\} + n\left(\left\{\bar{\bar{B}}_{44,n}\right\} - \left\{B_{44,n}\right\} + \left\{\bar{B}_{12,n}\right\} + \left\{\bar{\bar{B}}_{22,n}\right\} + \left\{\hat{B}_{23,n}\right\}\cos\phi\right) \\ -\left\{A_{44,n}\right\} + \left\{\bar{\bar{A}}_{44,n}\right\} + \left\{\hat{A}_{23,n}\right\}\cos\phi - \left\{\hat{F}_{33,n}\right\}\sin^2\phi \end{pmatrix}\sin(n\phi)\cos\theta$$

$$-\left\{\hat{G}_{33,n}\right\}\sin\phi\cos((n-1)\phi)\cos\theta$$

$$-(1-n)\left(\left\{\hat{C}_{36,n}\right\} - \left\{\hat{C}_{26,n}\right\}\right)\sin\phi\sin((n-1)\phi)\sin\theta$$

$$+\left\{\hat{F}_{36,n}\right\}\sin\phi\sin(n\phi)\sin\theta$$

$$-\left(\left\{\hat{\bar{C}}_{45,n}\right\} - \left(\left\{\hat{C}_{26,n}\right\} + \left\{G_{45,n}\right\}\right)\cos\phi + \left\{\hat{G}_{36,n}\right\}\sin^2\phi + (1-n)^2\left\{\bar{\bar{C}}_{26,n}\right\}\right)\cos((n-1)\phi)\sin\theta$$

$$-(n-1)\left\{\hat{C}_{23,n}\right\}\sin((n-1)\phi)\cos\theta$$

$$-n\left\{\hat{A}_{26,n}\right\}\cos(n\phi)\sin\theta$$

$$\{F_3\} = \frac{4}{\pi}\frac{M}{R_1+z}\{\Phi\}$$

$$-\left(\left\{\bar{H}_{16,n}\right\} + \left\{\hat{B}_{26,n}\right\} + \left\{\hat{B}_{36,n}\right\} + n\left\{\hat{A}_{26,n}\right\} + n\left\{\hat{A}_{36,n}\right\} + \left\{\hat{H}_{36,n}\right\}\cos\phi\right)\sin\phi\cos(n\phi)\cos\theta$$

$$-\begin{pmatrix} \left\{\bar{A}_{45,n}\right\} - \left\{A_{45,n}\right\} + n\left(\left\{\bar{B}_{16,n}\right\} + \left\{\bar{\bar{B}}_{26,n}\right\} - \left\{B_{45,n}\right\}\right) + n^2\left\{\bar{\bar{A}}_{26,n}\right\} \\ +\left(n\left\{\hat{B}_{45,n}\right\} + n\left\{\hat{B}_{36,n}\right\} - \left\{\bar{F}_{45,n}\right\} + \left\{\hat{A}_{45,n}\right\} + \left\{\hat{A}_{36,n}\right\}\right)\cos\phi - \left\{\hat{F}_{36,n}\right\}\sin^2\phi \end{pmatrix}\sin(n\phi)\cos\theta$$

$$+\left\{\hat{F}_{66,n}\right\}\sin\phi\sin(n\phi)\sin\theta$$

$$-\begin{pmatrix} \left\{\hat{\bar{C}}_{55,n}\right\} - \left(\left\{G_{55,n}\right\} + \left\{\bar{G}_{55,n}\right\} + \left\{\hat{C}_{66,n}\right\}\right)\cos\phi + \left\{\hat{G}_{36,n}\right\}\sin\phi + \left\{\hat{G}_{55,n}\right\}\cos^2\phi \\ +\left\{\hat{G}_{66,n}\right\}\sin^2\phi + (1-n)^2\left\{\bar{\bar{C}}_{66,n}\right\} \end{pmatrix}\cos((n-1)\phi)\sin\theta$$

$$-(n-1)\left\{\hat{C}_{36,n}\right\}\sin((n-1)\phi)\cos\theta$$

$$-\left(\left\{\hat{H}_{55,n}\right\}\cos\phi - \left\{H_{55,n}\right\} + n\left\{\hat{A}_{66,n}\right\}\right)\cos(n\phi)\sin\theta$$